0 0 0 0 4 4 0 2 0 7 4

LBL-4288
C.1

RECEIVED
LAWRENCE
BERKELEY LABORATORY

APR 26 1976

LIBRARY AND
DOCUMENTS SECTION

For Reference

Not to be taken from this room

CONCEPTUAL DESIGN REPORT

LBL-4288
C.1

Cover Designed By

Walter Zawojski

LEGAL NOTICE

This report was prepared as an account of work sponsored by the United States Government. Neither the United States nor the United States Energy Research and Development Administration, nor any of their employees, nor any of their contractors, subcontractors, or their employees, makes any warranty, express or implied, or assumes any legal liability or responsibility for the accuracy, completeness or usefulness of any information, apparatus, product or process disclosed, or represents that its use would not infringe privately owned rights.

0 0 0 0 4 4 0 2 8 9 5

LBL-4288
SLAC-189
(T/E/A)
UC-28

PEP

CONCEPTUAL DESIGN REPORT

STANFORD LINEAR ACCELERATOR CENTER
STANFORD UNIVERSITY
Stanford, California 94305

and

LAWRENCE BERKELEY LABORATORY
UNIVERSITY OF CALIFORNIA
Berkeley, California 94720

PREPARED FOR THE U.S. ENERGY RESEARCH AND
DEVELOPMENT ADMINISTRATION UNDER CONTRACTS NO. E(04-3)-515
AND NO. W-7405-ENG-48

February 1976

28178

PREFACE

In preparing this design for a large colliding beam facility, the Lawrence Berkeley Laboratory (LBL) and the Stanford Linear Accelerator Center (SLAC) have responded to the great importance of the colliding-beam technique for reaching otherwise unattainable reaction energies. The physics possibilities offered by colliding beams are attracting growing enthusiasm from both experimental and theoretical physicists. The successes already posted by colliding-beam storage rings in the U.S., in Europe and in the USSR, and especially by the SPEAR electron-positron project at SLAC have established at once the feasibility of designing and building such machines on a large scale and the practicality of doing physics experiments with them.

The proposed storage ring (PEP), operating at beam energies of up to 18 GeV, will make collisions yielding an interaction energy of 36 GeV in the center of mass. This is greater than the interaction energy achievable with 400 GeV protons from either the CERN II or Fermilab accelerators, the two largest scientific instruments ever constructed. By comparison, the effectiveness per dollar of cost of colliding-beam facilities is most impressive.

This would be the third storage ring project to be constructed at Stanford. The first, the 500-MeV Princeton-Stanford electron-electron storage rings, performed the first high-energy experiment with colliding beams. The second, the SPEAR facility, now upgraded to a beam energy of 4.2 GeV, is providing new results with profound implications for elementary particle theory. Many of the design details of the facility proposed here are based on SPEAR designs and experience, the success of which establishes the technical feasibility of the proposed facility and also provides a strong basis for confidence in the cost estimates.

The SLAC and LBL accelerator groups together comprise a highly complementary group with technical expertise and capability that is well-matched to the requirements of the PEP project. A successful joint study has been under way for the past three years, and early in 1974 a formal agreement for the continued collaborative effort in the construction and operational stages of PEP was negotiated. The Regents of the University of California and the Trustees of Stanford University have given approval for this cooperative venture.

The facility described in this report is designed to allow readily for the later addition of a superconducting proton storage ring to be capable of storing 200-GeV protons for collision with the electrons or positrons. The design also permits the installation of a second electron-positron storage ring to furnish the capability of electron-electron collisions and positron-positron collisions if that should prove desirable. Neither of these additional rings precludes the other; i.e., both could occupy the tunnel at once. The physics potential of these improvement programs fully warrants providing this compatibility now.

In proposing to construct this storage ring at SLAC, advantage is being taken of the availability already there of the very high energy, high-power electron accelerator with its attendant high-current positron beam. The two-mile accelerator is a uniquely suitable facility for meeting the filling requirements of a high energy electron-positron storage ring like PEP.

0 0 0 0 4 4 0 2 8 9 7

TABLE OF CONTENTS

Page

I. INTRODUCTION 1

A. History of the Project 1

B. High Energy Physics with Electron-Positron Colliding Beams 3

C. Description of the PEP Facility 7

D. Other Electron-Positron Colliding-Beam Facilities 10

E. Cost Estimate and Time Schedule 12

II. DESCRIPTION OF THE ELECTRON-POSITRON STORAGE RING 13

A. General Parameters and Beam Dynamics 13

1. Tables of Parameters 13

2. Choice of General Parameters 13

3. Selection of Lattice Parameters and Design Luminosity 20

4. Control of Beam Size and Polarization Time with the Beam Wiggler 31

5. Apertures 37

6. Transverse Beam Instabilities 39

7. Correction of Chromaticities 41

8. Beam Lifetime and Average Luminosity 42

9. Reduction of Synchrotron Radiation in the Interaction Region ... 44

B. The Magnet System 48

1. Introduction 48

2. Dipole Design and Models 49

3. Quadrupole Design and Models 53

4. Correction Magnets 65

5. Construction 75

6. Survey and Alignment 78

7. Power Supplies 79

C. RF System 89

1. Layout and General Parameters 89

2. Choice of Frequency 95

3. Structure Design 96

4. Klystrons 100

5. Klystron Power Supplies 104

6. Phasing and Tuning 106

Page

7. Control of Longitudinal Instabilities 108

8. Loss to Parasitic Modes 109

D. Vacuum System 112

1. Introduction 112

2. Vacuum Chamber Construction 112

3. Synchrotron Radiation 115

4. Vacuum Pumps 117

5. Instrumentation, Valves, Controls, etc. 120

6. Cooling Water 120

7. Insertions 122

8. Bakeout 124

E. Injection System 125

1. Requirements 125

2. Transport System 125

3. Pulsed Inflection System 128

4. Injection Rates 131

5. Major Components in the Injection System 133

F. Data System for Monitoring and Control 138

1. Introduction 138

2. Control System 138

3. Timing 139

4. Magnet and Guidance Controls 139

5. RF System Control 139

6. Interlocks and Miscellaneous 140

7. Beam Monitoring 140

G. Beam Parameters 142

III. PHYSICAL PLANT 154

A. General Features of the Terrain and Their Effects on Construction Techniques 154

1. Tunnel Design and Construction 154

2. Roads 159

3. Earthwork and Erosion Control 159

4. Drainage 160

5. Landscaping 160

0 0 0 0 4 4 0 2 8 9 8

Page

6. Sanitary Sewers 161
7. Surface Buildings 161

B. Utilities 170
1. Electrical Facilities 170
2. Cooling Water Systems and Piped Utilities 175
3. Fire Protection Systems 180
4. Ventilation 181

C. Shielding Requirements and Provisions 182
1. Introduction 182
2. Shielding for Curved Sections 183
3. Shielding for Experimental Areas 184

IV. EXPERIMENTAL AREAS 185
A. Introduction 185
B. Characteristics of the PEP Detectors 185
C. Design Requirements for the Experimental Areas 186
D. Description of the Experimental Areas 193
E. High Luminosity Option 206

V. COST ESTIMATES AND SCHEDULES 210
A. Introduction 210
B. Construction Cost Estimate 211
C. Cost Schedules 212
D. Time Schedules 217

VI. APPENDICES 221
A. The Proton-Electron System 221
1. Introduction 221
2. Physics Potential 221
3. The Total PEP Concept 226
4. Lattice System and Operating Parameters 229
5. Machine Components 234

B. Summary of Soil Studies to Date 240

C. Cooperative Basic Agreement between the Board of Trustees of the Leland Stanford Junior University and the Regents of the University of California 243

D. PEP Reports 251

E. References 265

F. Storage Ring Parameters 268

TABLES

Page

I. Center-of-mass energy from various high energy machines..... 5

II. General and lattice parameters of the PEP e^+-e^- storage ring 14

III. Typical beam parameters for different lattice configurations.....15

IV. Comparison of phase advance per cell and betatron functions.....29

V. PEP main ring bend parameters 52

VI. PEP standard quadrupole parameters (low impedance design).....58

VII. PEP standard quadrupole parameters (high impedance design) 64

VIII. PEP insertion region quadrupole parameters.....67

IX. PEP standard sextupole parameters.....70

X. PEP wiggler magnet.....73

XI. Low field bend magnet.....74

XII. PEP magnet power supplies 82

XIII. Typical RF system parameters at 15 GeV.....94

XIV. PEP power requirements at 18 GeV (kW) 171

XV. PEP power requirements (18 GeV) by area.....174

XVI. Summary of experimental requirements for the 1974 Summer Study detectors from PEP Note 177.....187

XVII. Summary of experimental requirements for the 1975 Summer Study detectors from PEP Note 205.....188

XIX. Operating parameters 233

XX. A breakdown of the 4.4°K refrigeration required for one-sixth of the PEP proton ring 237

0 0 0 0 4 4 0 2 8 9 9

FIGURES

Page

1. PEP site 8
2. Electron-positron colliding-beam facilities of the world 11
3. PEP nomenclature by areas 18
4. PEP nomenclature by components 19
5. Schematic layout of a typical arc 24
6. Schematic layout of insertion regions 25
7. Luminosity capability of the PEP lattice 27
8. Design luminosity 30
9. Wiggler magnet triplet 33
10. Wiggler parameters for pure beam size control 36
11. Wiggler parameters for optimum beam polarization time 38
12. Beam-stay-clear 40
13. Average luminosity 43
14. Photon spectrum for the main bending magnets and the low-field magnets at 15 GeV 45
15. Arrangement of low-field magnets and synchrotron radiation into interaction area 46
16. PEP main ring bend magnet 51
17. Photograph of prototype main ring bend magnet 54
18. PEP standard quadrupole assembly (low impedance design) 57
19. Photograph of prototype standard quadrupole 59
20. Multipole content of the prototype standard quadrupole 60
21. Effect on the tune due to the multipole content in the standard quadrupole 61
22. PEP standard quadrupole assembly (high impedance design) 63
23. PEP interaction region quadrupole 66
24. Photograph of prototype insertion region quadrupole 68
25. PEP sextupole assembly 69
26. PEP wiggler magnet assembly 72
27. Photograph of prototype chopper 86
28. RF cavity layout for Region 12 90
29. Klystron housing in Region 12 92
30. RF penetration between klystron housing and tunnel 93

Page

31. Cutaway view of the SPEAR II accelerating structure 98
32. Photograph of the SPEAR II accelerating structure 99
33. Schematic diagram of the experimental PEP klystron 102
34. Photograph of PEP prototype klystron 103
35. Klystron power supply block diagram 105
36. Block diagram of the drive, phasing, and cavity-tuning system 107
37. Stored current per beam for several lengths of RF structure 111
38. Standard cell bend vacuum chamber module 113
39. Cross section of bend magnet vacuum chamber 114
40. Photon and power spectrum of the synchrotron radiation at 15 GeV .. 116
41. Synchrotron radiation power distribution in a cell at 15 GeV 118
42. Synchrotron radiation power distribution in the wiggler magnets 119
43. Gas pressure distribution in a cell at 15 GeV 121
44. Conceptual design of the instrument module 123
45. Injection beam lines from SLAC to PEP 127
46. PEP injection system (schematic) 129
47. Radiation damping of beam envelope after injection of several beam pulses 130
48. Filling time into PEP 132
49. Betatron and eta function in the standard configurations 143
50. Beam emittance vs energy 144
51. Betatron damping time vs energy 145
52. Design current vs energy 146
53. RF peak voltage and synchronous phase vs energy 148
54. RF bucket height, energy spread in the beam, and bunch length vs energy 149
55. Synchrotron oscillation tune and momentum compaction factor vs energy 150
56. RF power distribution vs energy 151
57. Beam lifetime vs energy 152
58. PEP region numbering system 155
59. Tunnel cross section 158
60. Region 12 surface buildings and utilities 162
61. Region 2 surface buildings and utilities 163
62. Region 4 surface buildings and utilities 164

Page

63. Region 6 surface buildings and utilities 165
64. Region 8 surface buildings and utilities 166
65. Region 10 surface buildings and utilities 167
66. Sector 30 surface buildings and utilities 168
67. Floor layout for Region 8 surface buildings 169
68. Electrical research area 172
69. Cooling tower water system 177
70. PEP detectors from the 1974 and 1975 Summer Studies 191
71. Topographical profile of the PEP site 194
72. Architectural view of Region 12 196
73. Isometric view of Region 12 197
74. Possible experimental setup 198
75. Architectural view of Region 2 200
76. Isometric view of Region 2 201
77. Architectural view of Region 4 202
78. Isometric view of Region 4 203
79. Architectural view of Region 6 204
80. Isometric view of Region 6 205
81. Architectural view of Region 8 207
82. Isometric view of Region 8 208
83. Schematic view of the PEP electron-proton ring configuration 228
84. Schematic side view of insertion and cell structure for the proton-electron system 230
85. Tunnel cross sections with electron and proton magnets in alternate arcs of the ring 236

I. INTRODUCTION

A. History of the Project

In the summer of 1971 a group of physicists, including visitors from CERN and Frascati, Italy, working at LBL and SLAC, began to examine the feasibility of a new and powerful colliding-beam complex which could be capable of producing collisions at higher energies than hitherto envisaged between electrons and positrons and also between electrons and protons and between positrons and protons. They concluded that such a facility was quite feasible and that no known physical limitation of the behavior of stored beams would prevent the achievement of luminosities sufficient to yield useful reaction rates for many important high-energy-physics processes. The facility, then, would consist of an electron storage ring and a proton storage ring. To illustrate these conclusions, a conceptual design example was described and analyzed.[1]

The collaborative study between LBL and SLAC continued and grew, involving more people as more refined concepts and designs were devised, and a combination of an electron-positron ring capable of beam energies up to 15 GeV together with a superconducting proton ring emerged as the preferred design. It was dubbed PEP.[2,3] In the meantime, other laboratories in both the U.S. and Europe began studying similar or related ideas, and their representatives came together at SLAC and LBL in the summer of 1973 to exchange and compare ideas.

By this time there was a consensus that the electron-positron storage ring component of the system, operated at beam energies up to 15 or 20 GeV and capable of yielding high luminosity in electron-positron collisions, was but a straightforward extension of techniques already successfully used in several laboratories and that such a ring could confidently be designed and built

immediately. For the proton ring, superconducting-magnet technology offered the promise of achieving high beam energy with economical size and with low power consumption; however, there were some technical uncertainties yet to be resolved.

In the meantime, electron-positron rings operating in Europe and the U.S. had revealed that a wealth of new and previously unexpected information concerning the structure of elementary particles, both leptons and hadrons, could be gained from electron-positron collisions. These experiments made it clear that it was urgent to move to higher energies than those available from existing machines.

With these facts in mind, LBL and SLAC jointly decided to propose the immediate design and construction of the 15-GeV electron-positron storage ring. The proton storage ring was deferred pending further development of superconducting technology. The two laboratories agreed to locate the facility at SLAC and to design the electron-positron ring and its housing to be suitable for the addition later of a 200-GeV proton ring. Such a ring is briefly described in Appendix A of this report. Usage had established the name PEP, so it was retained for the e^+-e^- ring. The two universities signed an agreement in February 1974 outlining joint financial and management arrangements for the project. The text of that agreement appears in Appendix C of this report.

The PEP Proposal[4] was published in April 1974. Since then steady progress has been made in the design of PEP to improve its performance potential, especially at higher energies. Component systems have been optimized to reduce their costs where possible and the facility has been tailored for ready and flexible experimental utility. This joint LBL-SLAC research and development program has produced several tangible results, including models of bending magnets

and quadrupole magnets, a working test model of the 500-kilowatt klystron (in itself an accomplishment unparalleled elsewhere), test sections of vacuum chamber and a new highly compact and economical injection beam line design. All this has been accompanied by the successful operation of SPEAR II, which embodies many of the principles used in the design of PEP, and is therefore an ideal prototype. For example, the performance of the two-mile accelerator as a positron source for PEP has been verified. As another example, a rather good theoretical understanding of energy loss to electromagnetic modes in the RF cavities and other discontinuities in the vacuum chamber has been attained, and measurements of these losses have been carried out on SPEAR II, the results of which have been used to establish the criteria for PEP. Furthermore, experiments, detectors, and interaction-area requirements have been reviewed by many physicists from other laboratories throughout the world in the Summer Studies of 1974 and 1975. Suggestions and improvements resulting from these studies have been incorporated into the PEP design.

Those aspects and components which have been worked out in greater detail than can be presented in this report are described in PEP Notes, a list of which can be found in Appendix D.

B. High-Energy Physics with Electron-Positron Colliding Beams

High-energy electron-positron colliding-beam storage rings have opened a new window on the physical world, where elementary particles of matter and their interactions can be studied in a particularly simple and convenient manner. When an electron and its antiparticle, a positron, collide they can annihilate into a state of pure energy, losing their former identity. This energy then re-materializes into combinations of elementary particles which, in turn, can be observed in experimental detection apparatus. In conventional accelerators

where primary beams strike material targets, this simple annihilation state does not occur, nor does it when beams of protons collide in a proton-proton storage ring. Thus electron-positron storage rings provide data about the structure and interactions of elementary particles in a new experimental regime.

The view provided by present and past generations of electron-positron storage rings has added significantly to our picture of the subnuclear world. As new higher energy storage rings have been built and the energy of existing rings increased, surprising new information has been uncovered at every step. The most dramatic example occurred in November 1974 with the completely unexpected discovery of an entirely new family of relatively heavy and long-lived subnuclear particles. The first of these new particles was discovered simultaneously at the SPEAR[5] electron-positron colliding-beam facility at SLAC and at the Brookhaven National Laboratory[6] using very different techniques. Within days of the discovery of the first particle, a second, heavier one was found at SPEAR.[7] Further studies at SPEAR[8,9,10] and at the German storage ring DORIS[11] (located at the DESY Laboratory in Hamburg) have revealed still more new particles related to the first two. These results are among the most exciting events in the recent annals of physics. It is now clear that higher energy storage rings can greatly enlarge our view into the annihilation region.

With the PEP storage ring, we extend the center-of-mass energy in electron-positron collisions to 36 GeV, more than a fourfold increase over that available at SPEAR. The available reaction energy will be larger than that obtainable at the world's highest energy accelerators, even though the energy of the PEP circulating beams is very much lower. This is true because, when two oppositely directed antiparticles of the same momentum collide, the total energy, i.e., the sum of their energies, is available to the reaction. In contrast, when

a beam particle from a conventional accelerator strikes a stationary target particle most of its energy is necessarily tied up in the continuing forward motion of the reaction products, as required by the law of conservation of momentum. Only a small fraction is, therefore, available to the reaction. Table I compares the available reaction energy for the PEP electron-positron ring and for the four highest energy machines now operating or under construction, including the world's only proton-proton colliding-beam device, the CERN Intersecting Storage Rings (ISR). The most important conclusion to be drawn from the table is that the PEP facility will provide available reaction energies spanning almost the entire range now covered by other machines, and will do it by a process inaccessible through the other machines.

It should be noted that an electron accelerator capable of producing the same available reaction energy as PEP by striking stationary-target electrons with high-energy positrons would have to accelerate the positrons to more than a million GeV, about fifty thousand times the energy of the SLAC two-mile accelerator, by far the most energetic electron accelerator in existence.

TABLE I

Center-of-mass energy from various high energy machines

Machine	Available Reaction Energy (GeV)
PEP (18-GeV e^+-e^- storage ring)	36
SLAC (23-GeV electron linear accelerator)	6.6
NAL (400-GeV proton accelerator)	27
CERN II (400-GeV proton accelerator)	27
ISR (30-GeV p-p storage ring)	60

The range of experimental studies opened up by PEP is extremely rich and varied. It spans the entire field of elementary-particle interactions: strong interactions, electromagnetic interactions, and weak interactions.

Reactions leading to mesons and nucleons in the final state will reveal new and vital information about the strong interactions and the structure of the elementary particles. For example, a conceptually simple experiment, the measurement of the total reaction probability to produce strongly interacting particles from electron-positron collisions, tests very basic hypotheses about the structure of the particles produced.

Thus far the theory of quantum electrodynamics is the only successful field theory in particle physics in the sense that all experimental tests to date agree with the predictions of this theory. Through the study of processes with only electrons, mu-mesons, and gamma rays as reaction products we can probe the electromagnetic interactions to smaller distances than hitherto possible.

PEP will open wide new vistas for the study of weak interactions via electron-positron collisions. For example, the colliding electron-positron pair can transform itself into a mu-meson pair either by the weak interactions or by the electromagnetic interactions. The energy-dependences of these two processes are very different, so that the weak interaction, which is negligible at low energies, becomes more and more competitive with the electromagnetic as the interaction energy is increased. At PEP energies, the interference between the two processes is expected to become observable. Particle physicists are now seeking a unified picture of the weak and electromagnetic interactions and PEP offers the possibility of testing these concepts from a new experimental vantage point.

In summary, the proposed high-energy electron-positron colliding-beam facility PEP offers the possibility of the study of a very broad range of fundamental questions in particle physics in a new and presently inaccessible energy region. The profound discoveries made with the present generation of electron-positron colliding-beam facilities lead us to expect new phenomena to be uncovered with this device. These experiments, together with the complementary experiments with protons, neutrinos, and mesons at the highest-energy proton accelerators, offer great promise of leading to a new depth of understanding of elementary particles and the fundamental laws of physics.

More detailed summaries of PEP physics expectations have been published previously in references 4 and 26 and in the proceedings of the 1974 and 1975 PEP Summer Studies (PEP-137 and PEP-178).

C. Description of the PEP Facility

The main component of the proposed facility is a storage ring in which beams of positrons and electrons circulate in opposite directions in a vacuum chamber embedded in a magnetic guide field having six bending arcs and six long straight sections. The major diameter of the ring is about 710 m and the radius of the arcs is about 240 m. The facility is shown in Fig. 1. The electrons and positrons to be stored in it are produced in the SLAC linac and are introduced into the storage ring via two beam transport paths emanating from the end of the two-mile accelerator. One path joins the storage ring in the northwest straight section and the other in the southwest straight section. Beams of energies up to 18 GeV can be stored, and, at a future date, components could be added to permit energies as high as 22 GeV. Provisions are also made in the design of the ring housing so that a synchrotron-radiation research facility could be added in the future.

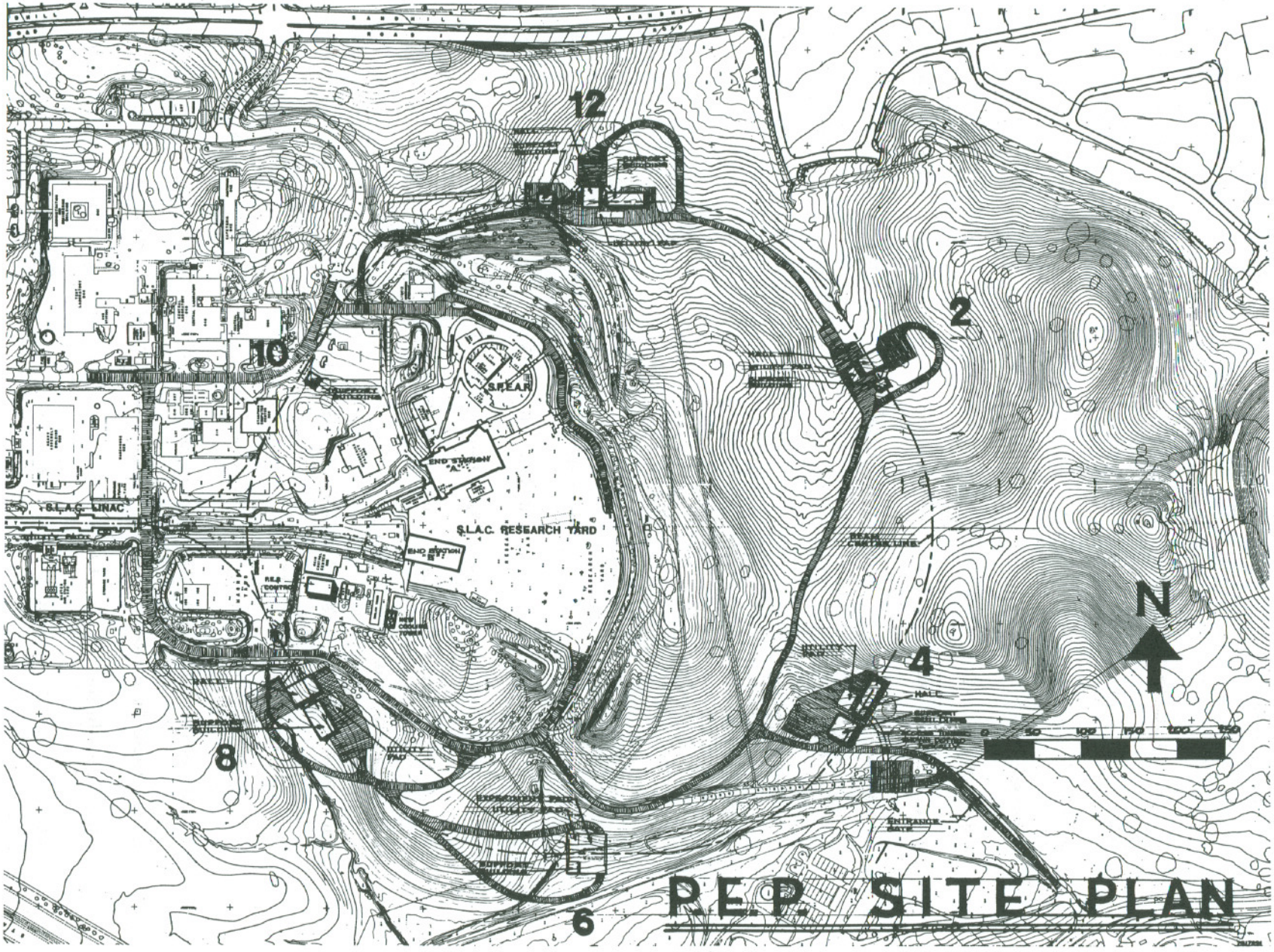

Fig. 1--PEP colliding-beam storage-ring site plan.

The energy lost from the beams by synchrotron radiation is restored by a high-power radio frequency accelerating system which employs klystrons to drive the accelerating structure at a frequency of 353 MHz. The system is capable of delivering five megawatts of power to the beams. Since much of this power appears as synchrotron radiation which strikes the outer wall of the vacuum chamber, that wall must be water-cooled. Moreover, the radiation causes the evolution of gases from the vacuum chamber surface and these gases must be pumped away very rapidly, because low pressures (about 10^{-8} Torr) must be maintained in the vacuum chamber both to achieve adequate beam lifetimes (several hours) and to attain low experimental background counting rates. These low pressures will be sustained by means of long, narrow sputter-ion pumps located in the vacuum chamber in the bending magnets directly alongside the beams.

The proposed storage ring is designed to generate a luminosity (reaction rate per unit reaction cross section) of more than $10^{31}\,cm^{-2}sec^{-1}$ per interaction region at beam energies between 5 GeV and 18 GeV and a maximum luminosity of $10^{32}cm^{-2}sec^{-1}$ per interaction region at a beam energy of 15 GeV. This luminosity is adequate to support a vigorous experimental program. To achieve this performance, it is necessary to store a particle current of up to 92 milliamperes in each beam. Based on the performance of the SLAC two-mile accelerator in filling SPEAR II, the filling time for PEP will be a few minutes, which is a comfortably short period compared to the storage time of several hours and ensures that storage ring operations will consume only a small fraction of the linear accelerator beam time.

The fundamental limitation on the performance of existing electron-positron storage rings is the so-called "incoherent beam-beam instability" which

imposes an upper limit on the current density of the beams where they collide. The magnetic guide field of PEP is designed to attain the specified performance, as described in Section II, within the limitations established by this instability. Other instabilities have been observed in operating storage rings affecting both single stored beams and colliding beams, but techniques have been found to cure or to avoid them and these techniques are incorporated into the PEP design. For these reasons, the high luminosity planned should be attainable.

Each counterrotating beam will be concentrated into three bunches, each a few centimeters long. They will be equally spaced around the ring, with the result that the bunches will collide at only six places. We will control the filling process such that the collisions will take place only at the centers of the six long straight sections, called interaction regions. Five of these interaction regions will be housed in experimental halls of various designs where the high-energy-physics experiments will be carried out. The designs for these halls and the rationales for them are presented in Section IV. The sixth interaction region (northwest) will be reserved for accelerator physics measurements and compatible particle physics experiments on a modest scale.

D. Other Electron-Positron Colliding-Beam Facilities

It was over a decade ago, in 1963, that a joint Italian-French group observed the first definite colliding-beam reactions in a small electron-positron ring at Orsay, France. Two years later, in 1965, the first colliding-beam high-energy-physics experiment was completed with the Princeton-Stanford 500-MeV storage rings at Stanford. Since then a substantial number of colliding beam facilities have been built.

The capabilities of the world's principal electron-positron storage rings are characterized in Fig. 2, in which their maximum center-of-mass energy

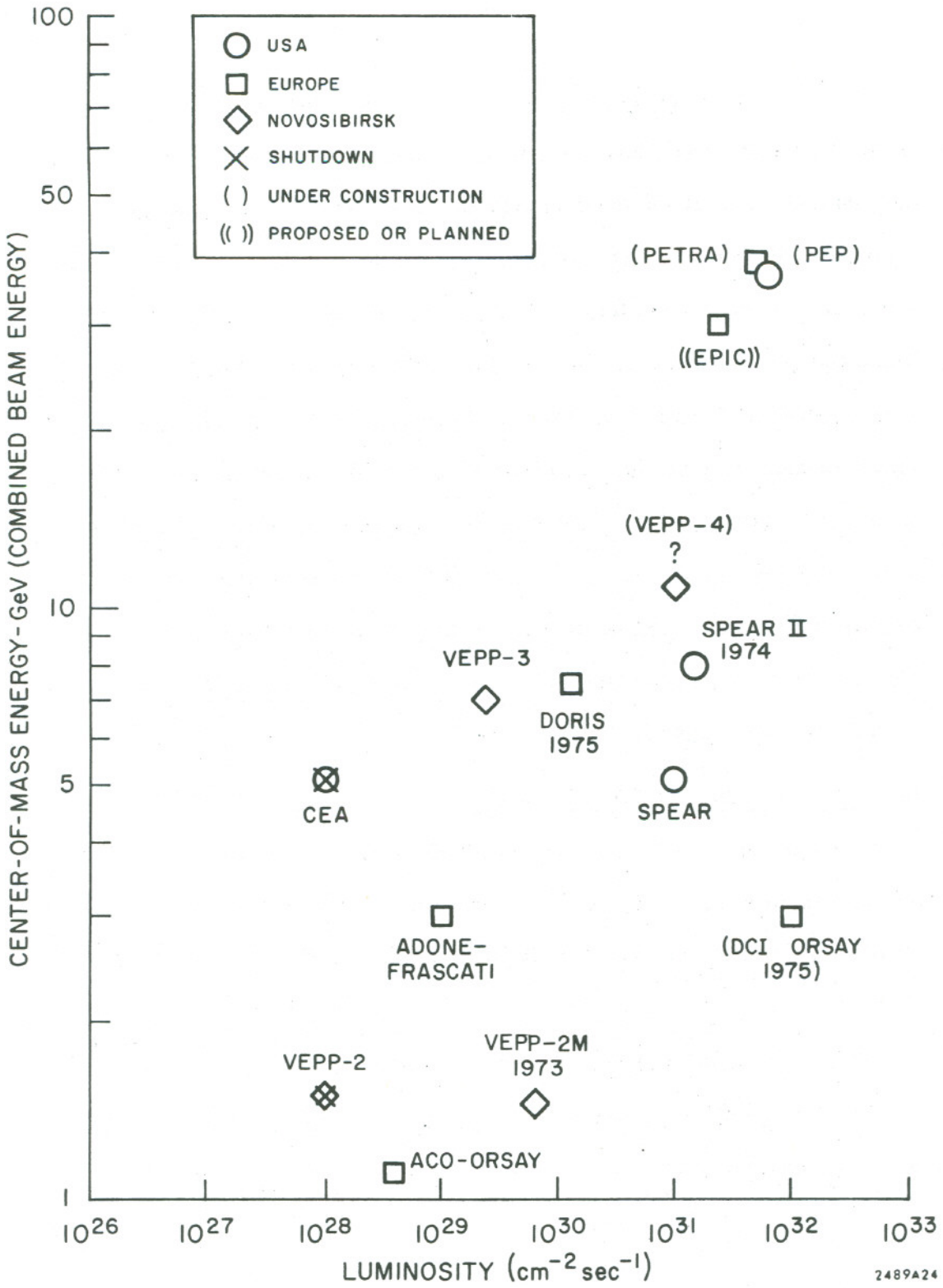

Fig. 2--Electron-positron colliding-beam facilities of the world.

(available reaction energy) is plotted against their maximum luminosity. It should be emphasized, however, that the maximum luminosity does not occur at the maximum center-of-mass energy but at somewhat lower energies (see, for example, Fig. 8). Concerning the Novosibirsk, USSR, storage rings, there are uncertainties as to when they will begin to function or when they will be built; hence the question marks. Neither the early Stanford-Princeton rings nor the very successful Intersecting Storage Rings at CERN in Geneva appear on the graph because they produce electron-electron and proton-proton collisions, respectively. Design studies of electron-positron storage rings having maximum beam energies in the range 14 GeV to 19 GeV have been under way for some time in the United Kingdom (EPIC) and in Germany (PETRA), as well as in Japan (TRISTAN). Construction of PETRA was authorized in October 1975 and excavation work began in January 1976.

E. Cost Estimate and Time Schedule

The estimated cost of the PEP storage-ring facility is $61.9 million (expressed in June 1975 dollars). We estimate 4 years to construct and bring the facility into operation, based on the schedule of availability of funds given in Section V.

Since both labor and materials costs continue to rise, an escalation allowance of $16.1 million has been made over the 4-year construction period; thus the total required project funding is estimated at $78.0 million.

Details of the estimated costs and construction schedules will be found in Section V.

II. DESCRIPTION OF THE ELECTRON-POSITRON STORAGE RING

A. General Parameters and Beam Dynamics

1. Tables of Parameters

Table II summarizes many of the important parameters of the PEP e^+-e^- storage ring, including general parameters and lattice parameters, worked out with the use of the computer codes TRANSPORT,[12] SYNCH,[13] and MAGIC.[14] Table III gives typical beam parameters for different operating energies and configurations. More detailed parameters are discussed in Section II. G. A compilation of most of the storage ring parameters can be found in Appendix F for fast reference.

2. Choice of General Parameters

Four primary goals were set for this storage ring: (1) to cover the range of beam energies from 4 GeV up to 18 GeV in order to provide a range of center-of-mass energies extending from that available at other smaller e^+-e^- colliding-beam machines up to that available at the largest proton accelerators; (2) to maintain luminosities $10^{31}cm^{-2}sec^{-1}$ to $10^{32}cm^{-2}sec^{-1}$ over this range so as to provide experimentally useful reaction rates; (3) to furnish an adequate number and variety of experimental halls (interaction regions) to accommodate a vigorous and varied national program of experimentation; and (4) to ensure that the housings and experimental halls will be compatible with the possible future addition of a superconducting 200-GeV proton storage ring for e-p collisions, or with another 18-GeV electron ring for e^--e^- or e^+-e^+ collisions, or both.

These goals, together with the size, shape, and geological characteristics of potential locations at SLAC, led to the choice of the six-sided storage ring shown in the site plan of Fig. 1, Section I.C. With a radiofrequency power of

TABLE II

General Parameters		
Beam Energy, E		
Nominal Maximum	18	GeV
Minimum	4	GeV
Design Luminosity per Interaction Region, $\mathscr{L}_{max}$		
At 15 GeV	$1 \times 10^{32} cm^{-2} sec^{-1}$	
Below 15 GeV	$10^{32} (E/15)^2 \ cm^{-2} sec^{-1}$	
At 18 GeV	$1.5 \times 10^{31} cm^{-2} sec^{-1}$	
Nominal Crossing Angle, 2δ	0	radians
Number of Interaction Regions		
Total (superperiodicity)	6	
Available for High-Energy Physics	5	
Reserved for Machine Physics Studies	1	
Number of Stored Bunches, N_b	3	
Available Length at Each Interaction Region for Experiments	19.0	m

Lattice Parameters		
Straight Section Length	117.086	m
Gross Radius of Arcs	238.330	m
Magnetic Bending Radius	165.518	m
Maximum Diameter of Ring	710.843	m
Circumference of Ring	2200.000	m
Normal Bending Cell Length	14.350	m
Total Number of Cells	96	
Effective Length of Bending Magnets	5.40	m
Effective Length of Cell Quadrupoles	0.64	m
Bending Field at 15 GeV	3.023	kG
Linear Tune Shift per Interaction Point ($\Delta\nu_x = \Delta\nu_y$)	$\leq$ 0.06	

TABLE III

Typical Beam Parameters for Different Lattice Configurations

		5 GeV	10 GeV	15 GeV*	18 GeV	
Total Betatron Tunes						
Horizontal	ν_x	12.75	15.75	18.75	27.75	
Vertical	ν_y	15.75	18.75	19.25	18.75	
Momentum Compaction	α	0.01530	0.00690	0.00423	0.00164	
Transverse Damping Time	τ_x, τ_y	0.220	0.0275	0.0082	0.00472	sec
x-y Coupling Coefficient	κ	0.250	0.275	0.274	0.105	
Horizontal Emittance ($\epsilon_x = \sigma_x^2/\beta_x$)	ϵ_x	0.168	0.245	0.234	0.087	mm-mrad
Vertical Emittance ($\epsilon_y = \sigma_y^2/\beta_y$)	ϵ_y	0.0105	0.0155	0.0163	0.0010	mm-mrad
Number of Stored Particles (each beam)	N	1.23×10^{12}	2.68×10^{12}	4.15×10^{12}	0.59×10^{12}	
Synchrotron Radiation Power (each beam)	P_{rad}	0.0089	0.312	2.443	0.72	MW
Linear Tune Shifts per Interaction Point						
Horizontal	$\Delta\nu_x$	0.06	0.06	0.06	0.03	
Vertical	$\Delta\nu_y$	0.06	0.06	0.06	0.06	
Luminosity (each interaction point)		0.11×10^{32}	0.44×10^{32}	1.00×10^{32}	0.15×10^{32}	$cm^{-2}sec^{-1}$
Normal Cell Parameters						
Horizontal Phase Advance	ψ_x	24.4^o	36.2^o	47.0^o	72.4^o	
Vertical Phase Advance	ψ_y	24.6^o	35.4^o	35.7^o	33.3^o	
Maximum Horizontal Beta	$\beta_{x\,max}$	42.0	31.5	25.6	20.9	m
Maximum Vertical Beta	$\beta_{y\,max}$	41.6	32.2	32.9	40.0	m
Maximum Momentum Dispersion	η_{max}	6.21	2.84	1.86	0.81	m
Interaction Region Parameters						
Horizontal Beta	β_x^*	4.600	3.800	3.800	4.00	m
Vertical Beta	β_y^*	0.160	0.180	0.185	0.20	m
Momentum Dispersion	η^*	-2.360	-1.020	-0.672	0.00	m
Horizontal Beam Size (betatron)	$\sigma_{x\beta}^*$	0.878	0.882	0.910	0.59	mm
Horizontal Beam Size (dispersion)	σ_{xE}^*	0.786	0.679	0.672	0.00	mm
Horizontal Beam Size (total)	σ_x^*	1.178	1.113	1.130	0.59	mm
Vertical Beam Size	σ_y^*	0.0410	0.0527	0.055	0.014	mm
Energy Width	σ_E/E	3.33×10^{-4}	6.66×10^{-4}	1.00×10^{-3}	1.20×10^{-3}	

* Standard configuration

2817896

0 0 0 0 4 0 2 7 0 8

about 5 MW available to the beams and with the arrangements for controlling the beam cross-sectional area as described further on, the storage ring should achieve a peak luminosity of $10^{32} cm^{-2} sec^{-1}$ at a beam energy E of 15 GeV, with a variation of luminosity approximately proportional to E^2 below 15 GeV and a luminosity of more than $10^{31} cm^{-2} sec^{-1}$ between 15 and 18 GeV.

The two most influential parameters in determining the ring's performance are the arc radius and the straight-section length. The arc radius is made as large as possible to minimize synchrotron radiation power with its attendant energy losses. Component-free drift spaces 19 m long centered at the interaction regions are reserved for experimental purposes. The rest of the space in the straight section is used for injection systems, RF cavities and various beam control elements. The straight sections are also designed to be long enough to accommodate the modifications which will be required for the proton-electron-positron option described in Appendix A.

It is well to introduce here the nomenclature peculiar to the PEP design. This terminology will be used throughout the report in referring to major divisions of the storage ring and the numbering systems, as well as components and their positions both above and below ground. The nomenclature will be found in the remainder of this subsection and may be skipped over at this point for uninterrupted reading and referred to only as needed.

General Nomenclature. The proposed system utilizes the clockwise numbering system originally proposed, with each region being numbered 1 through 12, as in a clock. The twelve o'clock position is the northernmost portion of the ring. The odd-numbered regions are called arcs because they form the bending portions of the ring and the even-numbered regions are called insertions because they are straight sections inserted between the arcs for the purpose of

performing experiments. Both arcs and insertions are divided into A and B halves with the A half located on the counterclockwise side and the B half on the clockwise side. The division point in the arcs is the symmetry straight section and in the insertions it is the interaction point. The PEP ring then appears as is shown in Fig. 3.

Arc Nomenclature. Each arc is subdivided into 19 cells as is shown in Fig. 4. The cells are numbered from 0 to 8 towards the symmetry cell in both the A and B halves. The symmetry cell, Cell 9, then separates the two halves. The elements within an arc will be designated both by cell location and by type and function. Thus the designator 7A1QF defines first the A half of Arc 7 and then the focusing quadrupole in the first cell. Similarly, "callouts" have been selected for other magnetic, vacuum, and RF components and are also given in Fig. 4. The magnetic elements are presented above the arc drawing and the vacuum components are given below it.

Insertion Nomenclature. Unlike the arcs, the insertions are not cellular or periodic in structure. Further, the equipment between Q1 and Q3 is machine-related, whereas that between Q1 and Q1 is experiment-related. Figure 4 also shows the selected nomenclature for a typical insertion. Once again, the magnetic elements are given above the diagram and the vacuum components below it.

For the magnetic components within an insertion, the callout will contain the distance from the interaction point to the center of the component as well as the name of the component. Thus the callout 8A152Q2 refers to the Q2 quadrupole in the A half of Insertion 8, which has its center 152 decimeters from the interaction points.

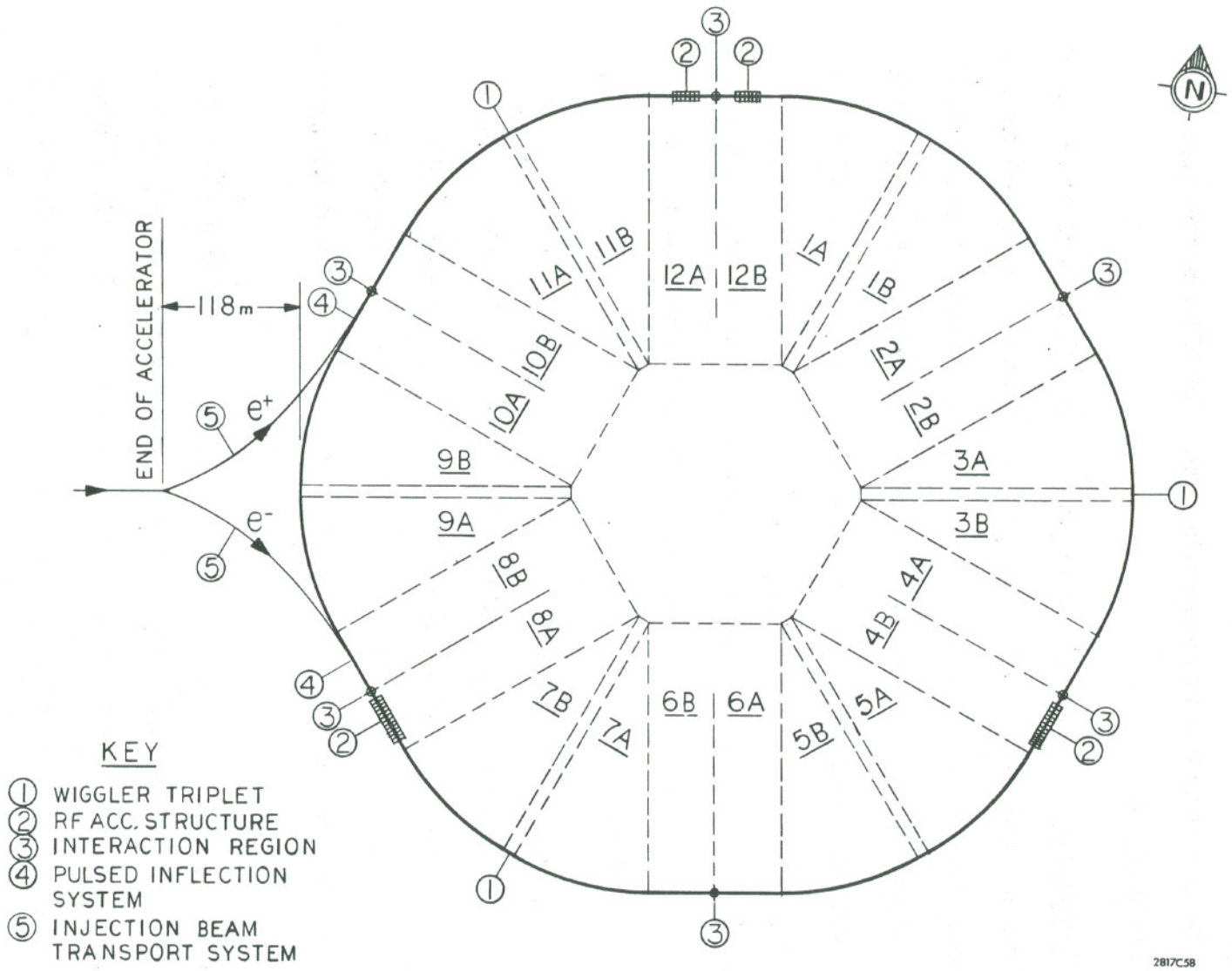

Fig. 3--PEP nomenclature by areas.

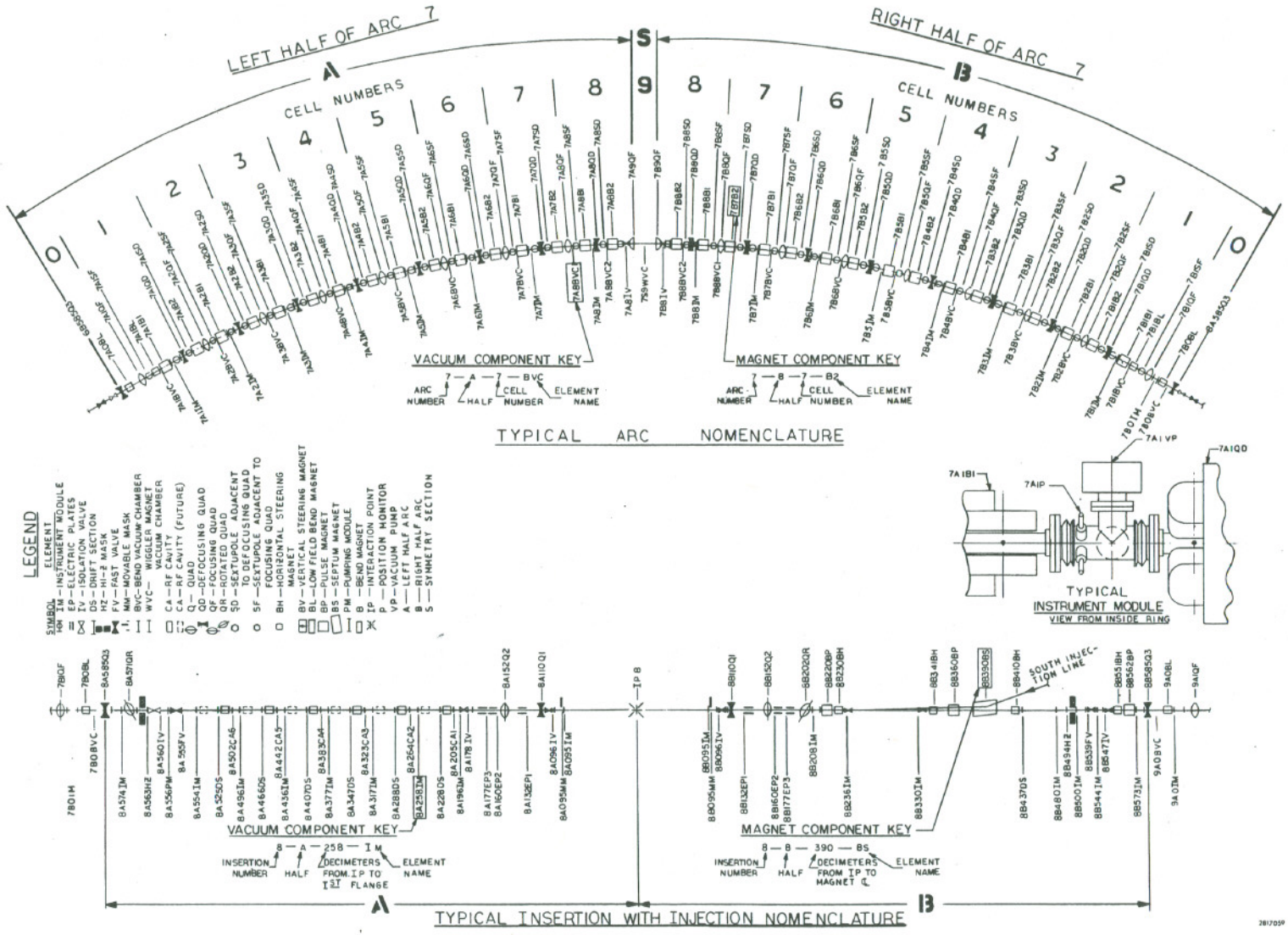

Fig. 4--PEP nomenclature by components.

0 0 0 0 4 0 2 9 1 0

Vacuum components are similarly located, except that the distance measurement is made to the flange closest to the interaction point. Thus the callout 8B330IM refers to the instrument module in the B half of Insertion 8 which measures 330 decimeters from the flange closest to the interaction point to the point itself. This system has the advantage that, given two adjacent vacuum component designators, the length of the vacuum chamber between them can be found to the nearest decimeter by subtraction.

Injection Line Nomenclature. Those elements of the injection system which are common to both the ring and injection lines will carry the insertion region nomenclature described above, and, more than likely, another defined by those concerned with the design of this system. Figure 4 again shows these components using ring nomenclature in the B half of Insertion 8.

Surface Nomenclature. In order to differentiate between those elements on the surface and those in the tunnel, the nomenclature proposed is the same with the exception that the A, B half designators are changed to C, D. The C half is above A and the D half is above B. In general, this will not affect magnet and vacuum components but will deal mainly with I&C and Power Supply Groups.

3. Selection of Lattice Parameters and Design Luminosity

To attain high luminosity intense beams must be made to collide within a small cross-sectional area. The number of particles which can be collided within a given area is limited by the incoherent beam-beam interaction. When beam currents are limited by the beam-beam interaction, the maximum theoretical luminosity, $\mathscr{L}_{max}$, is attained when the transverse beam size is made as large as the vacuum chamber permits. If one operates a storage ring at different energies with exactly the same disposition of magnets and their fields

scaled with energy, the transverse beam dimensions vary directly as energy, and the maximum (beam-beam-interaction-limited) number of stored particles varies as E^3; thus the luminosity varies as E^4 and drops off very rapidly at lower energies. If, however, by some technique, the beam size is held constant as the energy is lowered, then the maximum number of stored particles varies as E and the luminosity as E^2. This E^2 dependence is quite acceptable; most reaction cross sections increase at lower energies.

The PEP design provides several different methods for horizontal beam size control. They include (1) variation of the betatron tune, (2) variation of the momentum dispersion function at the interaction point, (3) unmatching the momentum dispersion function so that it does not repeat periodically from cell to cell but oscillates with amplitudes large compared to its matched value, and (4) additional radiation excitation of betatron oscillations with the help of the "wiggler magnet system". Vertical size can be adjusted by means of variable horizontal-vertical betatron-oscillation coupling. Using combinations of these techniques, it should be possible to approach closely the design luminosity which is given by the solid curve in Fig. 8.

Variation of the betatron tune gives a contribution to $\mathscr{L}_{max}$ which varies approximately as ν_{xA}^{-3}, where ν_{xA} is that part of the radial tune which comes from the bending arcs. Momentum dispersion gives a contribution proportional to η^{*2}/β_x^*, where η^* and β_x^* are, respectively, the momentum dispersion function and the betatron amplitude function at the interaction point. An unmatched dispersion function η gives a luminosity increment proportional to η_1^2/β_x^*, where η_1 is a measure of the mismatch in the bending cells. The wiggler magnet system is described in more detail later in this section. It causes the particles to emit more higher energy synchrotron radiation photons and, as a consequence, the

betatron oscillation amplitude, and therefore the beam size, is increased.

In order to implement techniques (1), (2), and (3), the values of β_x^*, β_y^*, η^*, and the radial tune ν_x are independently adjustable.[12] In addition, the vertical tune ν_y is adjustable in order to maintain stable beam confinement. Symmetry of the ring requires that the slopes of the betatron and dispersion functions vanish at the interaction region; i.e., $\beta_x'^* = \beta_y'^* = \eta'^* = 0$. Thus, eight mathematical constraints are imposed on the focusing strengths, requiring at least eight sets of quadrupoles with independently variable strengths. A number of other important constraints must also be considered. There must be nineteen meters of drift space kept free for experiments at the interaction regions. The maximum values of the β-functions and η-function must everywhere be kept within reasonable bounds in order to minimize aperture requirements and to reduce chromaticity and other aberrations. Magnetic-field values must be kept within conservative limits. Furthermore space must be reserved for various components such as RF cavities, injection components (septum magnets and kickers), vacuum equipment, rotated quadrupoles, sextupoles, beam monitors and control devices, electrostatic plates for separating the beams, and other miscellaneous instrumentation. (Many of these components are described in more detail in other parts of this report.)

From the considerations mentioned above, we have evolved a lattice design which is basically rather simple. The six bending arcs are composed of conventional separated-function bending cells which provide independent control of the total betatron tunes ν_x and ν_y by means of the independently controllable focusing and defocusing quadrupoles (QF and QD). Spaces between the quadrupoles and bending magnets in these cells provide space for the sextupoles, which are necessary to control chromaticity, beam monitors, vacuum bellows,

and other devices.

Two major changes in the lattice design have been made since the PEP Proposal[4] was written:

1. At the symmetry point, halfway between any two interaction points, a straight section of 5.66 m has been introduced. It is here that the separation in time between the passage of two bunches in either direction is the longest, making it easier to control each bunch individually. This place is, therefore, especially suited for beam control devices, e.g., feedback systems to control coherent beam oscillations and RF cavities to split the synchrotron frequencies.
2. The number of FODO cells has been doubled to 96 while the tunes and circumference of the storage ring have been kept approximately constant.[16]

The second change has been accomplished by doubling the number of quadrupoles while keeping the strength of each about the same. The betatron phase-shift-per-cell is thus reduced to about 45° at 15 GeV, resulting in a "smoother" beam envelope. The maximum values for the betatron functions in the cells are thereby reduced relative to the values at the interaction regions, so that the beam size in the cells is reduced and with it the required apertures. Another attractive consequence is the possibility of extending the maximum operating energy well beyond 15 GeV, as explained in the next paragraph. The details of the new magnet structure are shown in Fig. 5. The insertion, where few changes have been made, is shown in Fig. 6. Although doubling the number of cells did not change the luminosity expectations for energies below 15 GeV, the 96-cell lattice will make it possible, by adding to the RF cavity system, to go to energies well above 20 GeV with a luminosity which drops off only as $\mathscr{L} \sim E^{-3}$. To achieve this it is necessary to continue the variable-tune capabilities to

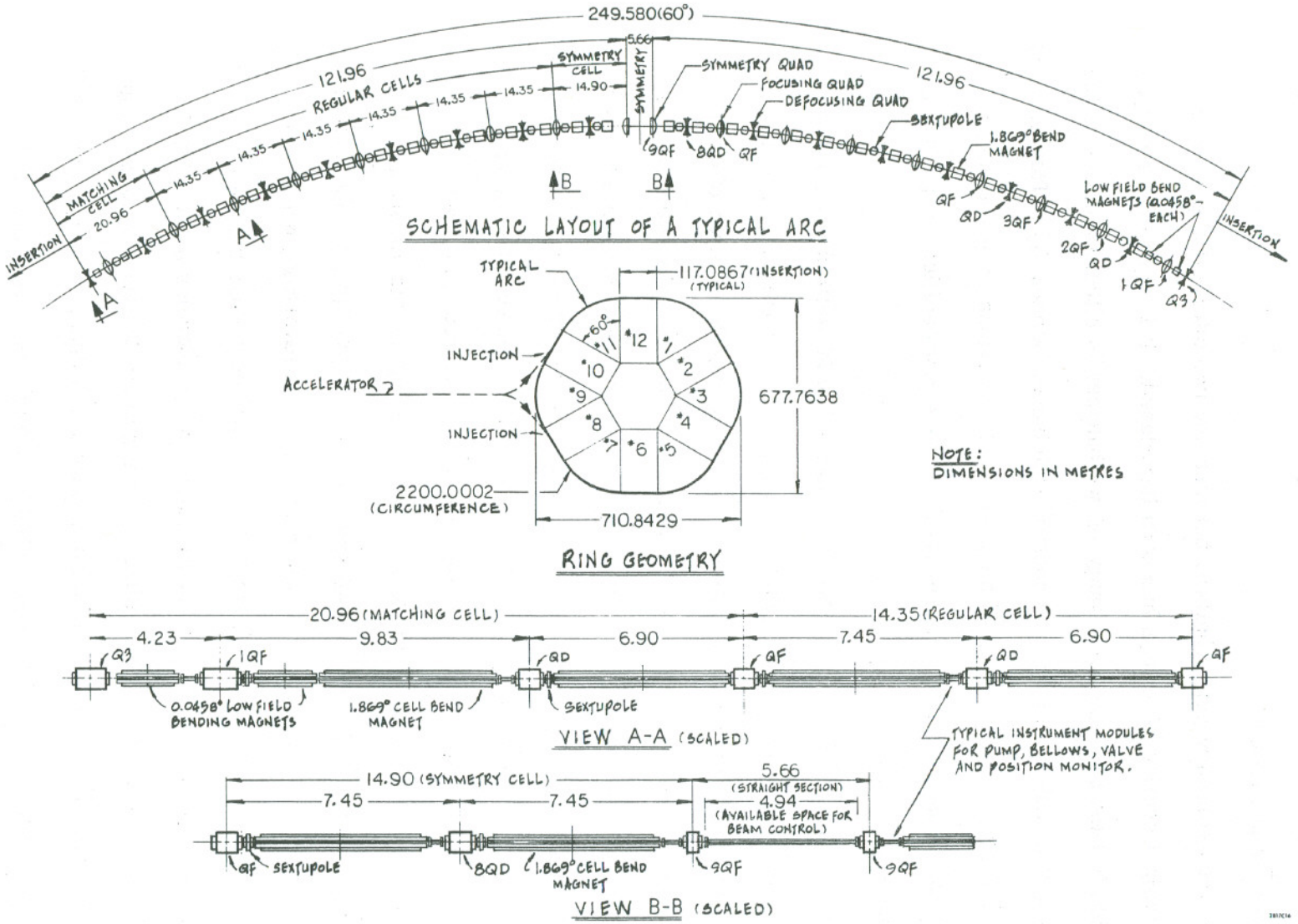

Fig. 5--Schematic layout of a typical arc.

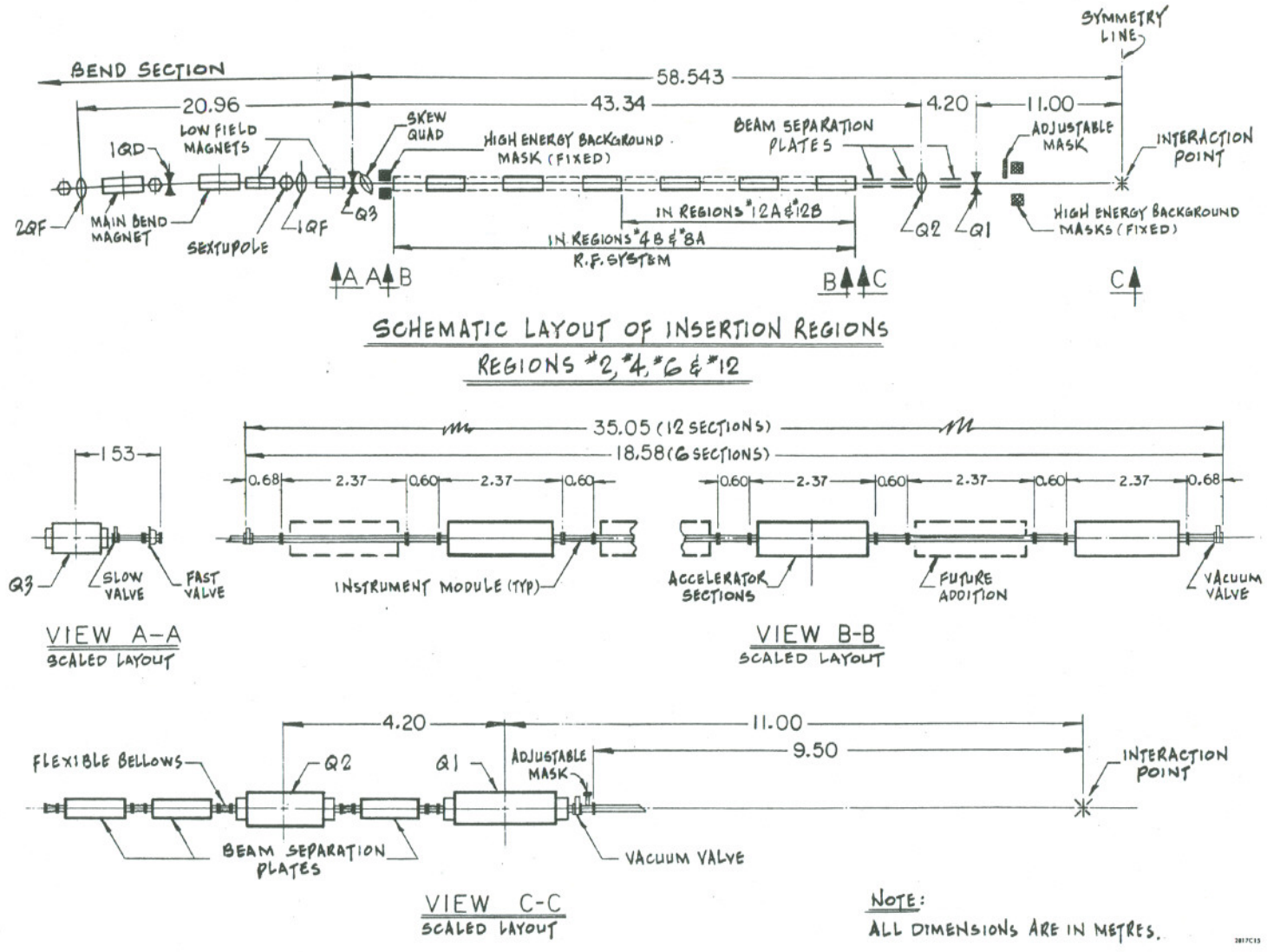

Fig. 6--Schematic layout of insertion regions.

0 0 0 0 4 0 2 9 1 3

energies above 15 GeV.

As we move up from lower energies, where the storage ring operates in the aperture-limited regime, the RF limit is reached at 15 GeV. If the tune were kept constant as we went above 15 GeV, the luminosity would scale as $\mathscr{L} \sim E^{-10}/(B \cdot \mu)$, where μ is the natural horizontal beam emittance normalized to 1 GeV and B is the number of bunches per beam.* At the same time, the incoherent beam-beam tune shift scales like $\Delta\nu \sim E^{-7}/(B \cdot \mu)$. The tune shift must be held constant to optimize luminosity. Since the normalized beam emittance is controllable by the focusing configuration, it is proposed to keep $(B \cdot \mu)$ proportional to E^{-7} for energies above 15 GeV in order to hold $\Delta\nu$ constant. This way we shall stay simultaneously at the RF limit and the beam-beam tune-shift limit so that the luminosity scales as $\mathscr{L} \sim E^{-3}$. This procedure permits luminosities as plotted in Fig. 7, taking no account of RF power limitations.

Varying μ as E^{-7} calls for a fast increase of focusing power with energy above 15 GeV. Consequently, at some energy, the maximum strength of the quadrupoles will be reached. If, then, the number of bunches is lowered from three to one, the quadrupole focusing can be reduced, and it is possible to continue on the $\mathscr{L} \sim E^{-3}$ curve to somewhat higher energies. However, with one bunch per beam, only two interaction points can be served with luminosity. If this is not done and three bunches are retained, the luminosity falls off like $\mathscr{L} \sim E^{-14}$ to E^{-15}, since then the quadrupole strength cannot be increased.

The luminosity curves for a maximum quadrupole field of 1T at the pole tip are shown for three-bunch and one-bunch operations in Fig. 7. Both curves end at 28 GeV, where the aperture is no longer large enough to contain the strongly scalloped beam. We assume a quadrupole field that is still of adequate

*The actual emittance at energy E in GeV is $\epsilon_x = \mu E^2$.

0 0 0 0 4 4 0 2 9 1 4

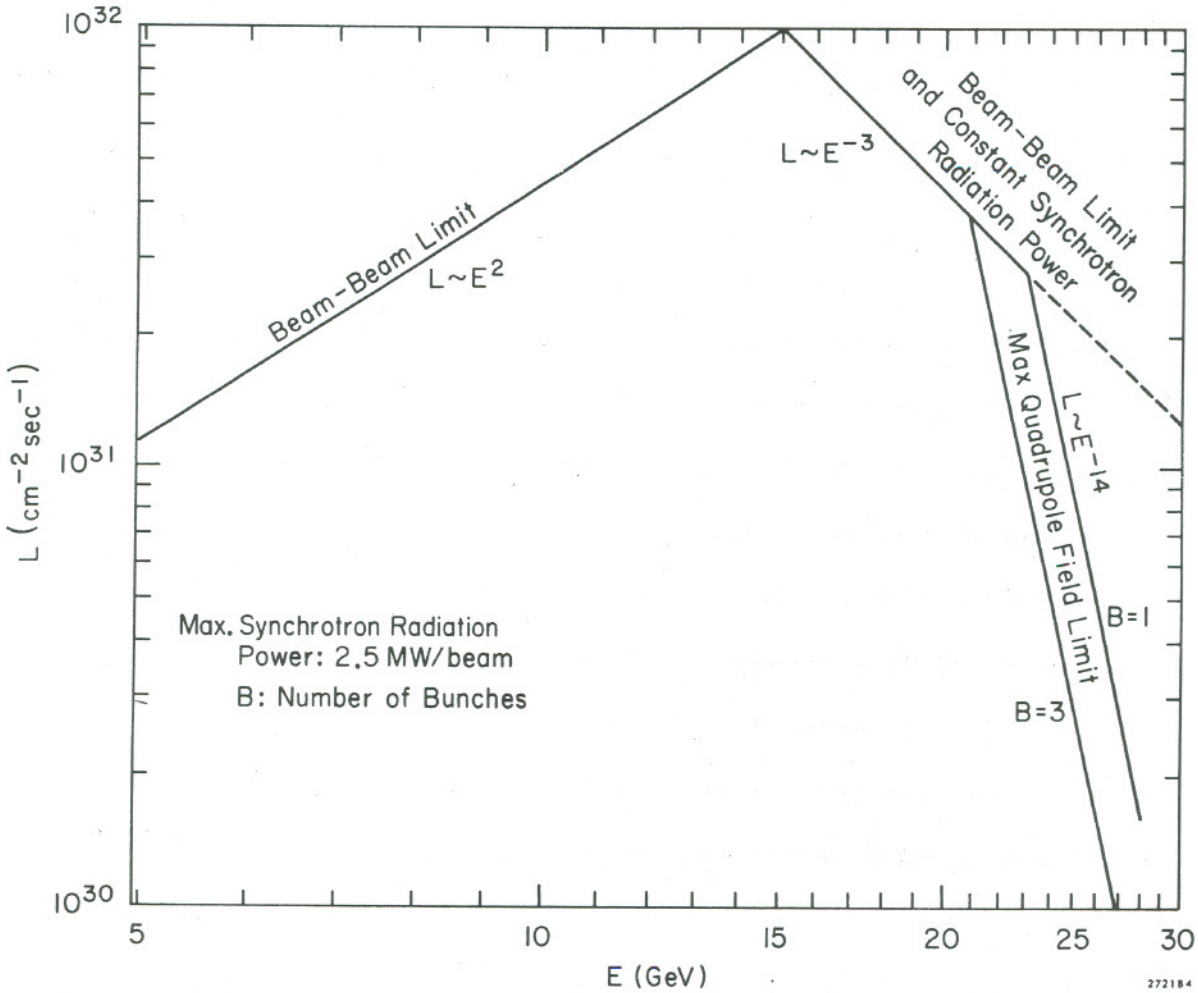

Fig. 7--Luminosity capability of the PEP lattice.

quality over the whole beam-stay-clear region at such high pole-tip fields. This appears to be realistic for the proposed PEP quadrupoles, since magnetic measurements of the first model quadrupole have shown no significant increase of the multipole content within the beam-stay-clear region up to pole-tip fields of 1.2 T. For higher energies, superconducting quadrupoles and sextupoles would be needed.

The aperture limit referred to above is reached when the phase advance per cell, and together with that, the maxima of the betatron functions, get too large. For comparison, the range of phase advance per cell ($\psi = \psi_x = \psi_y$) and betatron functions ($\beta = \beta_x = \beta_y$) between 5 GeV and maximum energy are shown in Table IV for both the new 96-cell lattice and the original 48-cell lattice.[4] Ideal FODO channels are assumed and minor deviations due to matching conditions to the insertions have been neglected. It can be seen that, for the original 48-cell lattice or any such 90°-per-cell lattice, the focusing cannot be increased very much before the betatron function gets very large.

The luminosity curves in Fig. 7 take into account only the lattice capabilities and depend on the postulate that at all energies a constant rf power of 2.5 MW is available to each beam if needed. (Less is required below 15 GeV.) RF cavity losses, which rise rapidly with beam energy, are not taken into account. The actual luminosity at high energies, on the other hand, is severely restricted by these losses. In Fig. 8 the design luminosity with the proposed 38-m aluminum cavity structure is shown as a solid line. Taking account of the cavity losses plus the estimated higher-order-mode losses, the maximum energy in PEP is limited to 18 GeV at a luminosity of $1.5 \times 10^{31} \mathrm{cm}^{-2} \mathrm{sec}^{-1}$. Typical beam parameters for the variable-tune mode of operation in the energy region between 5 and 18 GeV are shown in Table III. Enough space has been allowed in

TABLE IV

Comparison of Phase Advance per Cell (ψ) and Maximum Betatron Function (β_{max}) in the 96-cell and 48-cell Configuration

Energy (GeV)		5	15	18	21	25	30
96-cell Configuration:							
ψ (^{o})	(B = 3)	20.6	45.0	67.5	87.2	138.3	166.5
	(B = 1)	-	-	-	60.0	100.6	144.5
β_{max} (m)	(B = 3)	48.1	28.6	24.2	24.3	41.7	173.0
	(B = 1)	-	-	-	24.8	25.8	48.2
48-cell Configuration							
ψ (^{o})	(B = 3)	41.8	90.0	130.8	160.9	-	-
	(B = 1)	-	-	95.6	131.4	-	-
β_{max} (m)	(B = 3)	58.6	48.5	72.3	174.0	-	-
	(B = 1)	-	-	50.4	73.9	-	-

B = number of bunches per beam

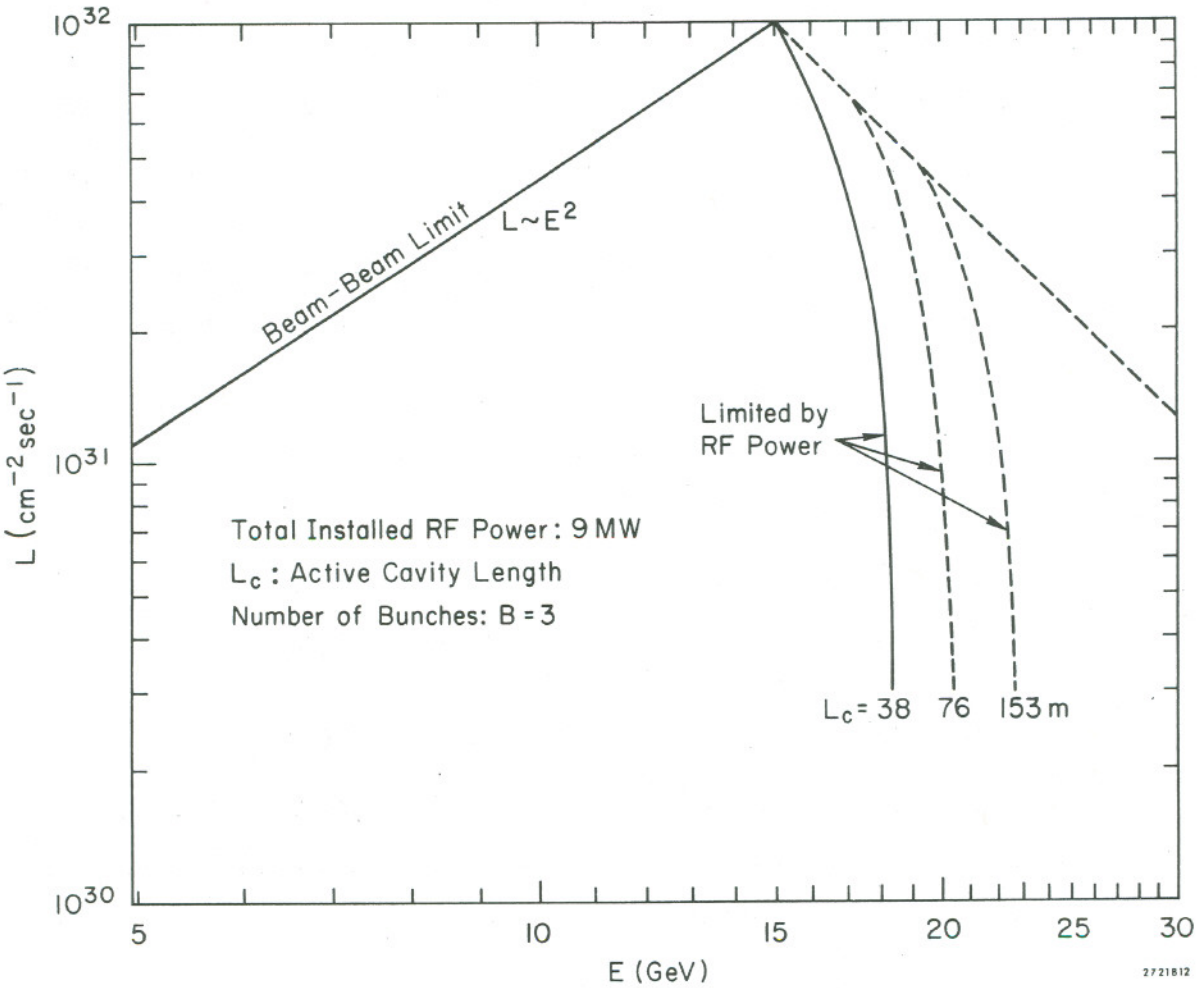

Fig. 8--Design luminosity.

the PEP design to increase the total cavity length at a later time to 76 m or even 153 m, so that the maximum PEP energy could be increased to 20 or 22 GeV, respectively, at a luminosity of $10^{31} cm^{-2} sec^{-1}$. Superconducting cavities would be needed to avoid excessive cavity losses at still higher energies.

The short 5.66 m straight sections at the middle of the arcs impose new matching requirements. The quadrupoles designated 8QD and 9QF (Fig. 5) are adjusted to match the β_x and β_y functions to accomplish this. The dispersion function is then only slightly mismatched, and there seems to be insufficient reason for varying an additional quadrupole to obtain an exact match.

4. Control of Beam Size and Polarization Time with the Beam Wiggler[17]

Of the methods of beam size control enumerated in the preceding section (Section II. A. 3), the first three impose severe penalties in filling rate at low energies, because they all result in momentum acceptances which decrease with decreasing energy. This would lead to rather long injection times below 10 GeV, since the damping times vary as E^{-3}. In order to avoid this difficulty, a system has been devised to control the beam size without changing the lattice configuration, the tune, or the momentum acceptance. In this scheme high-field wiggler magnets are used to increase the quantum excitation of the beam and concomitantly the damping rates with only a trivial effect on the focusing. As the strength of the wigglers is increased the excitation increases faster than the damping and the natural beam size increases.

The horizontal beam emittance is determined by equilibrium between the quantum excitation of betatron oscillations and the damping, both due to synchrotron radiation. The emittance can be written

$$\epsilon_x = C_q \frac{\gamma^2}{J_x} \frac{\oint \mathscr{H} \frac{1}{\rho^3} ds}{\oint \frac{1}{\rho^2} ds} ,$$

where $C_q = \frac{55}{32\sqrt{3}} \frac{\hbar}{mc} = 3.84 \cdot 10^{-13}$m, J_x is the damping partition number (in PEP, $J_x = 1.0$), γ the beam energy in units of the rest energy, ρ is the local bending radius and $\mathscr{H}$ is a characteristic (optical) function of the lattice configuration. $\mathscr{H}$ and ρ are functions of the azimuthal variable, s, and the integration is carried around the circumference of the central orbit. The variable-tune mode of operation controls the beam emittance by adjusting the characteristic function $\mathscr{H}$. By contrast the wiggler modulates the local curvature $1/\rho$ in a few places around the ring, keeping $\mathscr{H}$ approximately constant. Since the local curvature appears with different exponents in the numerator and denominator of the emittance equation, varying the strength of the wiggler varies the horizontal emittance.

The wiggler unit proposed for PEP is shown in Fig. 9 and consists of three rectangular flat-field bending magnets closely adjacent to one another. The two outboard magnets are powered with half the strength of the central magnet, so the net displacement and deflection of the orbit is null. The magnets are placed close together to minimize their optical effects. Three such triplets, located in three of the six symmetry straight sections (Fig. 5), are needed to obtain the desired variation of beam size at all energies below 15 GeV.

The physical effect of increasing the strength of the wiggler system is to increase the mean energy of the synchrotron radiation photons. This in turn enhances the perturbing effect of the emission of a photon on the betatron oscillation of the emitting particle. Since the photon emission is random, the

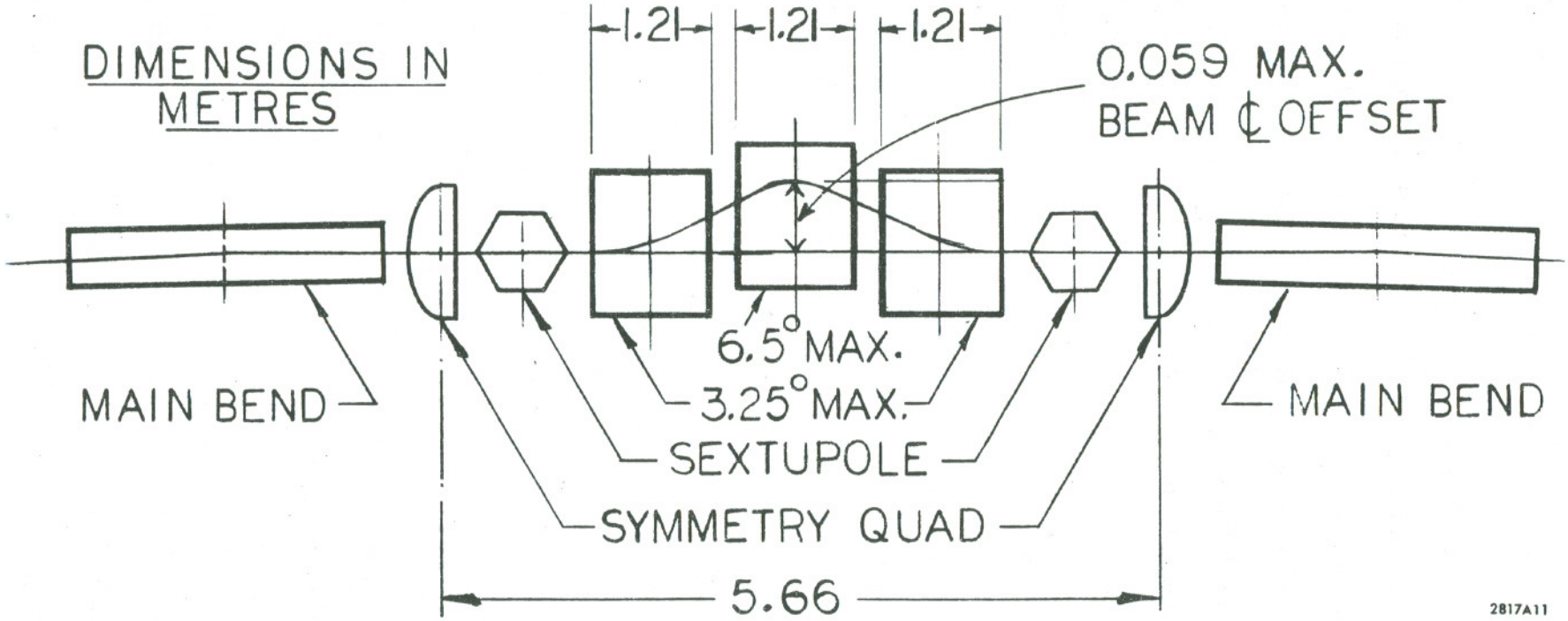

Fig. 9--Wiggler magnet triplet.

0 0 0 0 4 4 0 2 9 1 7

increase of the beam size is completely incoherent. The amount of the blowup of the beam can be smoothly adjusted by adjusting the strength of the wiggler system. Calculations show that the effects on beam dynamics (tune, betatron, and dispersion function) are negligible. The wiggler therefore appears to be an ideal means to control the beam size to maximize the luminosity. Only the horizontal beam emittance is directly affected by the wigglers. The vertical beam emittance and hence the vertical beam size will be increased by coupling the horizontal and vertical betatron motions by means of coupling elements such as rotated quadrupoles.

The beam wiggler can also be used to maximize the average luminosity on a minute-by-minute basis in operation as the stored beam decays. In a constant configuration, the luminosity decays as the square of the beam current. With the beam wiggler, the beam size can be adjusted continuously to stay at the beam-beam limit with the consequence that the luminosity decays only linearly with the beam current.

No increase in the installed RFpower is necessary to make up the losses due to the additional synchrotron radiation caused by the wiggler. It is turned off at energies of 15 GeV and above. Below 15 GeV, where it is turned on, the RF demand decreases rapidly with energy and is always less than the total installed RF power. The local synchrotron radiation power produced by the wiggler, however, is larger than that produced anywhere else and requires some special absorbers in the vacuum system.

As mentioned near the beginning of this subsection, the wigglers increase the radiation damping rates. This effect is an additional benefit. Not only do the wigglers permit us to maintain constant momentum acceptance with decreasing energy, but they also gentle the increase in damping time so that

injection can occur at higher pulse rates. At 5 GeV, for example, the damping times are reduced by about a factor of 2.5, resulting in a much shorter filling time than could be achieved without the beam wiggler. Alternatively, since the tune remains constant with varying energy, we could inject always at 15 GeV and then ramp the energy to the desired operating value.

Another happy feature of the PEP wiggler system is its capacity to reduce the beam polarization time. The contribution to the rate of polarization buildup due to a single magnet of field B is proportional to $(B^3E^5\ell)$ where ℓ is the central orbit length in the magnet.[18] If the field is in the same direction as that of the main bending magnets, the magnet in question increases the rate of polarization buildup and vice versa. For example a wiggler in which the sum of $(B^3\ell)$'s, with the sign of B taken into account, was equal to zero would have no net effect on the polarization rate.

In the PEP wiggler unit design, on the other hand, the lengths of the three magnets are the same and the central magnet has a field twice that of the outboard magnets and lying in the same direction as the main bending field of the storage ring. The central magnet contributes positively to the polarization rate. The outboard magnets have fields in the opposite direction and they each cancel one-eighth of the polarizing effect of the central magnet. The result is that the whole wiggler unit contributes to the rate of polarization by three-fourths of the effect of the central magnet alone.

Figure 10 refers to the case in which the wiggler system is operated so as to maintain constant beam size below 15 GeV as discussed above. The variation of the field strength B_c of the central wiggler magnet, the incremental synchrotron-radiation power ΔP_{RF} per wiggler per beam, the synchrotron-oscillation damping time τ_ϵ and the polarization time τ_{pol} are plotted against beam energy.

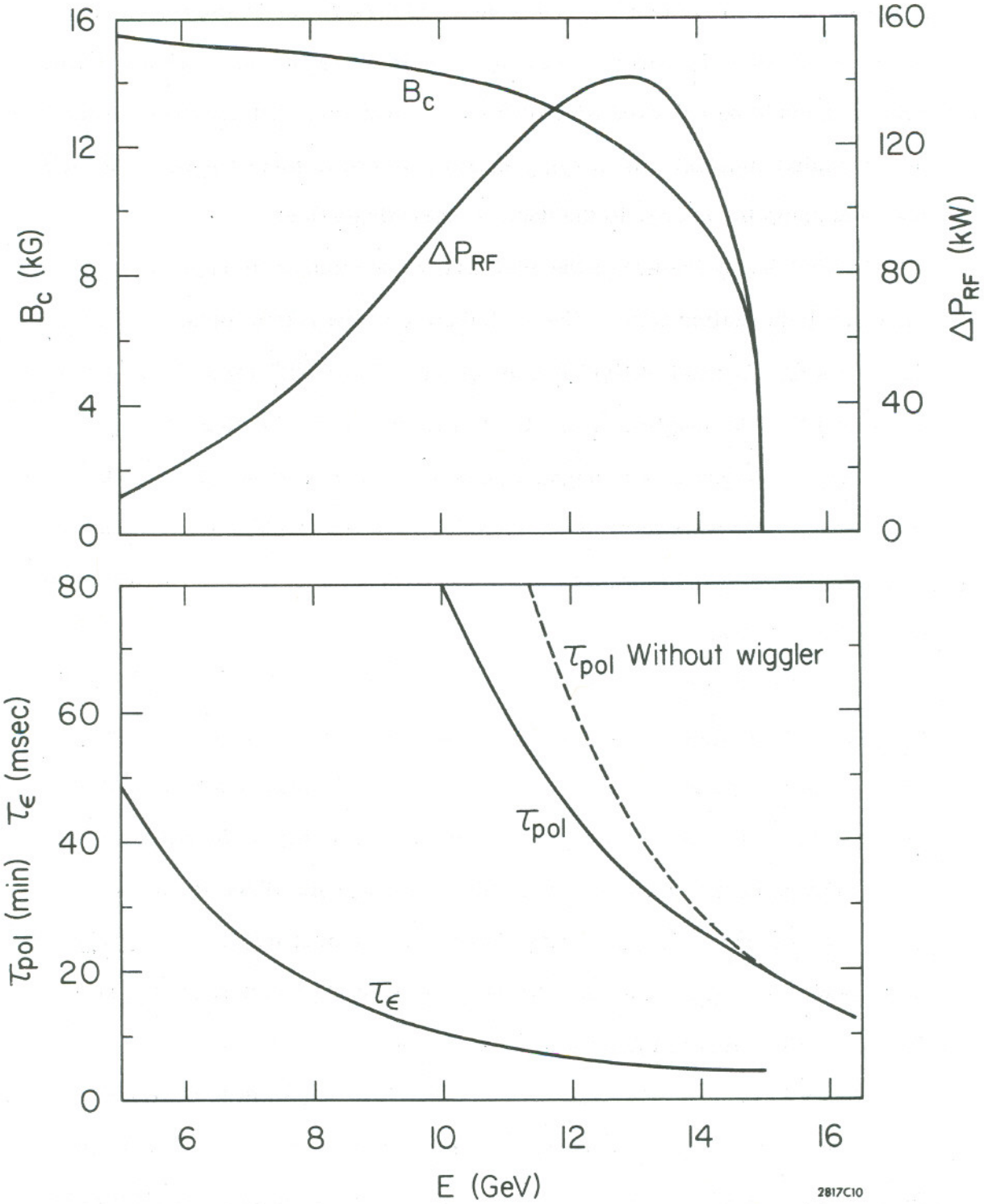

Fig. 10--Wiggler parameters for pure beam size control.

The wiggler system could also be used primarily to shorten the polarization time. Without the wigglers, the polarization time varies as E^{-5} and, as the beam energy is lowered, it quickly exceeds the beam lifetime, thus precluding the experimental use of polarized colliding beams. If the wiggler system strength is increased very rapidly with decreasing beam energy, the polarization time can be held constant at 20 minutes down to an energy of 12.7 GeV, at which point the maximum field strength of the wiggler (2T) is reached. From here on down, the polarization time increases, however, more like E^{-3} than E^{-5}. Graphs of B_c, ΔP_{RF}, τ_ϵ, and τ_{pol} for this mode of operation are shown in Fig. 11. To extend this technique to lower energies would require superconducting wiggler magnets.

If the wiggler magnets are turned on as strongly as just described, the blowup of the beam is larger than can be tolerated by the beam-stay-clear. Therefore, the size of the beam will have to be reduced by increasing the tune of the storage ring so that, in order to get the prescribed reduction in polarization time, a combination of the wiggler system and a variable-tune mode of operation must be used.

5. Apertures

The "beam-stay-clear", or minimum unobstructed lateral region all around the design orbit, has been defined by the formulae:

$$a_{xi} = 20\,\sigma_{x\ tot\ i} + 20\ \text{mm}$$

$$a_{yi} = 20\,\sigma_{yi} + 10\ \text{mm}\ ,$$

where a_{xi} and a_{yi} are the horizontal and vertical aperture diameters, respectively, at a particular location i on the circumference. $\sigma_{x\ tot}$ is the horizontal rms beam width defined by $\sigma_{x\ tot\ i} = \left[\sigma^2_{x\beta i} + \eta_i^2(\sigma_\epsilon/E_0)^2\right]^{\frac{1}{2}}$, where $\sigma_{x\beta i}$ is the

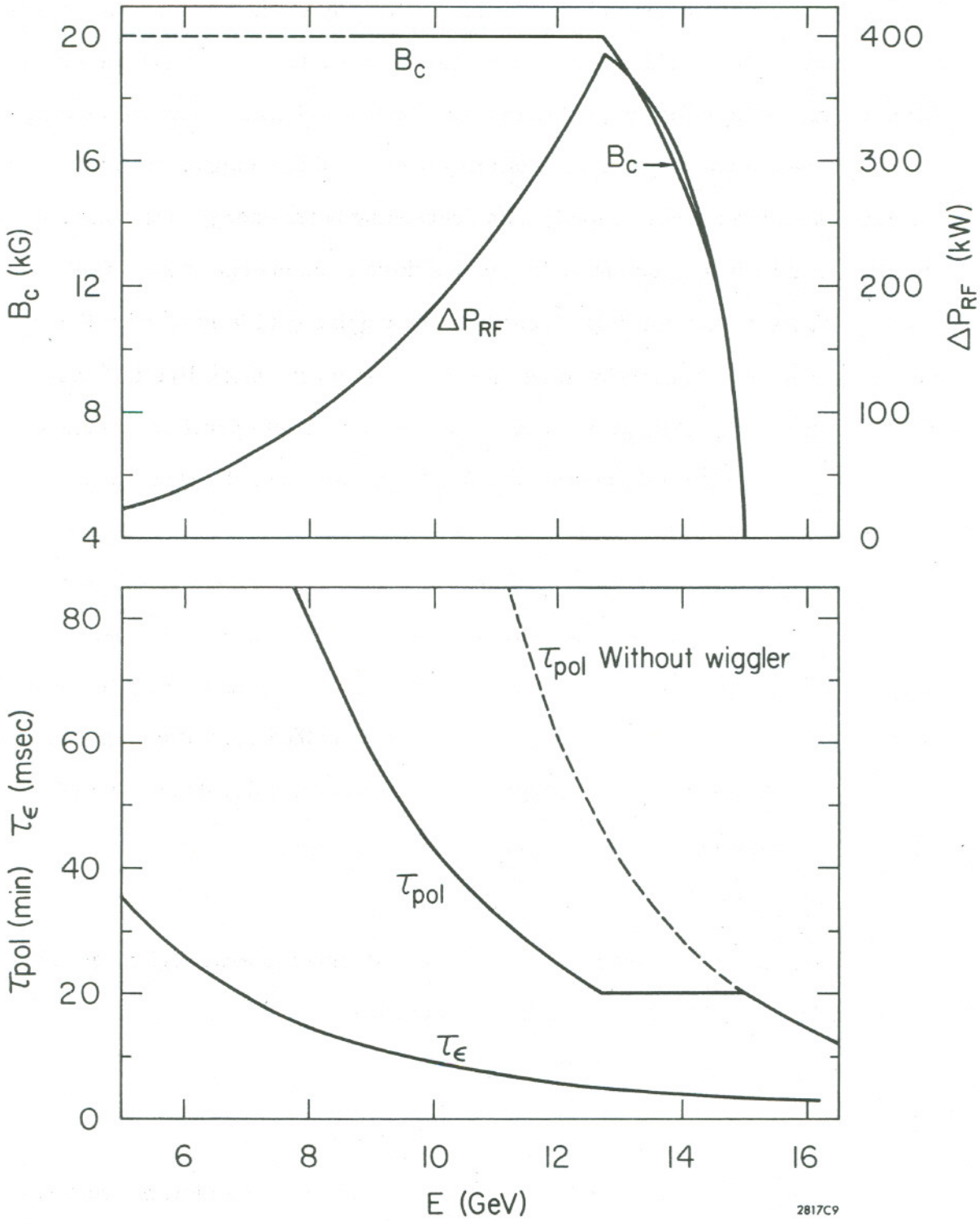

Fig. 11--Wiggler parameters for optimum beam polarization time.

rms horizontal betatron oscillation amplitude, η_i the dispersion function, and σ_ϵ the rms energy spread in the beam. σ_{yi} is the rms vertical betatron oscillation amplitude in the case of full coupling between horizontal and vertical betatron oscillations. SPEAR experience indicates that this large vertical beam-stay-clear would be necessary to avoid beam losses during changes of energy and beam-dynamics parameters. The additional 20 or 10 mm is a margin for orbit distortions and misalignments. The actual bore clearance of the magnets must also include an additional allowance for vacuum chamber walls, installation tolerances and a possible bake-out mantle. Figure 12 shows the beam-stay-clear regions in PEP, considering the above requirements.

6. Transverse Beam Instabilities

The design of this storage ring assumes that the maximum luminosity obtainable is determined by the beam-beam incoherent limit and that it is possible to store beams of sufficient intensity to reach this limit. The various transverse instabilities that can occur with large bunched beams and which might jeopardize the storage of such beams are generally thought to be of three types: those that are determined by the average circulating current, those that are present because there are multiple bunches in the ring, and those that depend upon the peak current in a single bunch.

The present PEP design is rather conservative in requiring an average single-beam current of 92 mA in three bunches. Many electron storage rings have stored such currents at much lower energies where the transverse instabilities are generally far more troublesome. While multiple-bunch transverse instabilities have been predicted, they have not been a problem for rings with only a few widely spaced bunches and have been troublesome only for the storage rings with many bunches, such as CEA and DORIS. In SPEAR it has been

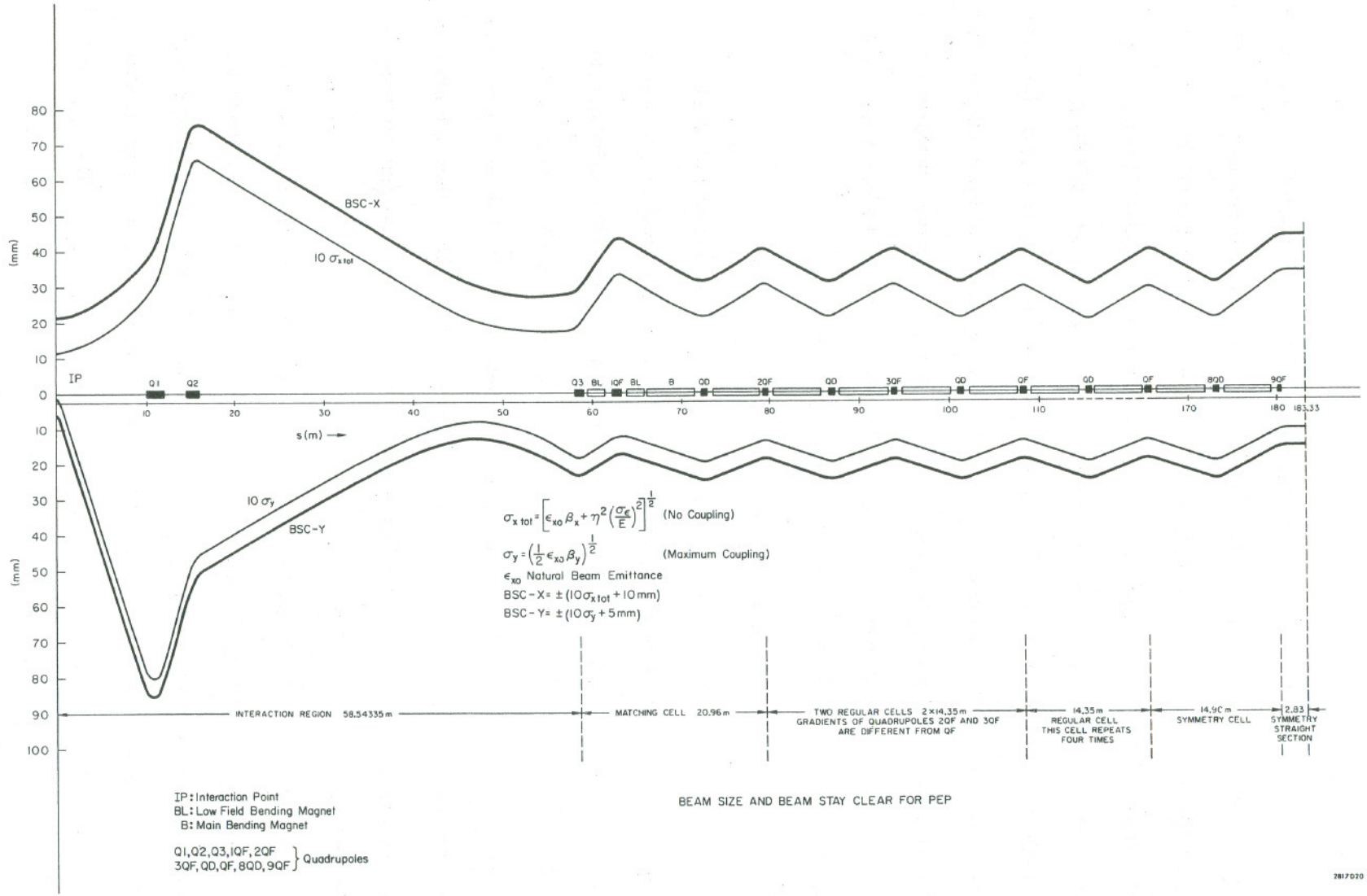

Fig. 12--Beam-stay-clear.

possible to store total currents of 100 mA in several bunches of a single beam without any indication of transverse multibunch instability. Also, because the bunch spacing in PEP is so large and the revolution frequency is fixed, it is entirely feasible to build a feedback system to damp each bunch individually. The only multiple-bunch motion that has been observed in SPEAR is the coherent motion between two colliding beams and it has not been of major concern.

The head-tail instability has been the most important single-beam transverse instability observed in electron storage rings and it can be controlled by the appropriate choice of the chromaticity. In the PEP design it will be possible to vary the value of the chromaticity, without producing destructive nonlinear resonances, by means of the sextupole fields which are distributed throughout the lattice. Considering the fact that transverse instabilities usually scale inversely with energy the PEP design may be considered conservative inasmuch as it is presently possible to store single-bunch currents in SPEAR at 1.5 GeV that exceed those necessary to reach the maximum luminosity in PEP at 15 GeV as determined from the beam-beam limit.

7. Correction of Chromaticities

The machine chromaticities, defined as $\xi = \Delta\nu \frac{p_0}{\Delta p}$, where $\Delta\nu$ is the change in either radial or vertical tune, measure the changes in the tunes with momentum. They are measures of the chromatic perturbations of beam dynamics due to the energy deviations of particles in the beam. These perturbations occur even in a perfectly linear machine. The uncorrected chromaticities in PEP are very large ($\xi_x \approx -34$ and $\xi_y \approx -100$) and must be corrected by the use of sextupoles which are fairly strong and represent a major nonlinear perturbation of the linear beam dynamics. To avoid nonlinear structural resonances due to the sextupoles, it is necessary to go beyond merely compensating for the

chromaticities. The azimuthal distribution and relative strengths of the sextupoles are also crucial to the stability of the beam.

A particle tracking program has been developed to simulate the trajectories of particles around PEP under the influence of the nonlinear sextupole fields. This computer simulation, together with theoretical studies on the beam-perturbing effects of sextupoles in storage rings, resulted in a satisfactory sextupole distribution for the standard beam dynamics configuration (Table III) in PEP. Twenty-eight out of the possible 36 sextupole locations in each arc are used for this sextupole distribution. These 28 have to be grouped into seven different circuits to meet the requirements for stable particle trajectories. Particle trajectories with all possible amplitudes for betatron and synchrotron oscillations within the acceptance of PEP have been simulated and found to be stable.

Further studies are necessary, however, to develop an algorithm which would define a procedure to find the best sextupole distribution for lattice configurations differing from the standard one.

8. Beam Lifetime and Average Luminosity

The lifetime of two stable colliding beams in PEP is determined mainly by bremsstrahlung energy loss occurring in beam-beam interaction and in the interaction of the beam with the residual gas. This is discussed in detail in Section II. G. The luminosity decreases as the beam decays; therefore the average luminosity is lower than the maximum shown in Fig. 8. Assuming a time span of one-half hour for storing both beams, adjusting the storage ring to the collision configuration, and preparing the experimental counters to start again, the average luminosity is shown in Fig. 13 versus the time between two fillings. The dashed curve is valid if additional pumps at the focusing quadrupoles (QF)

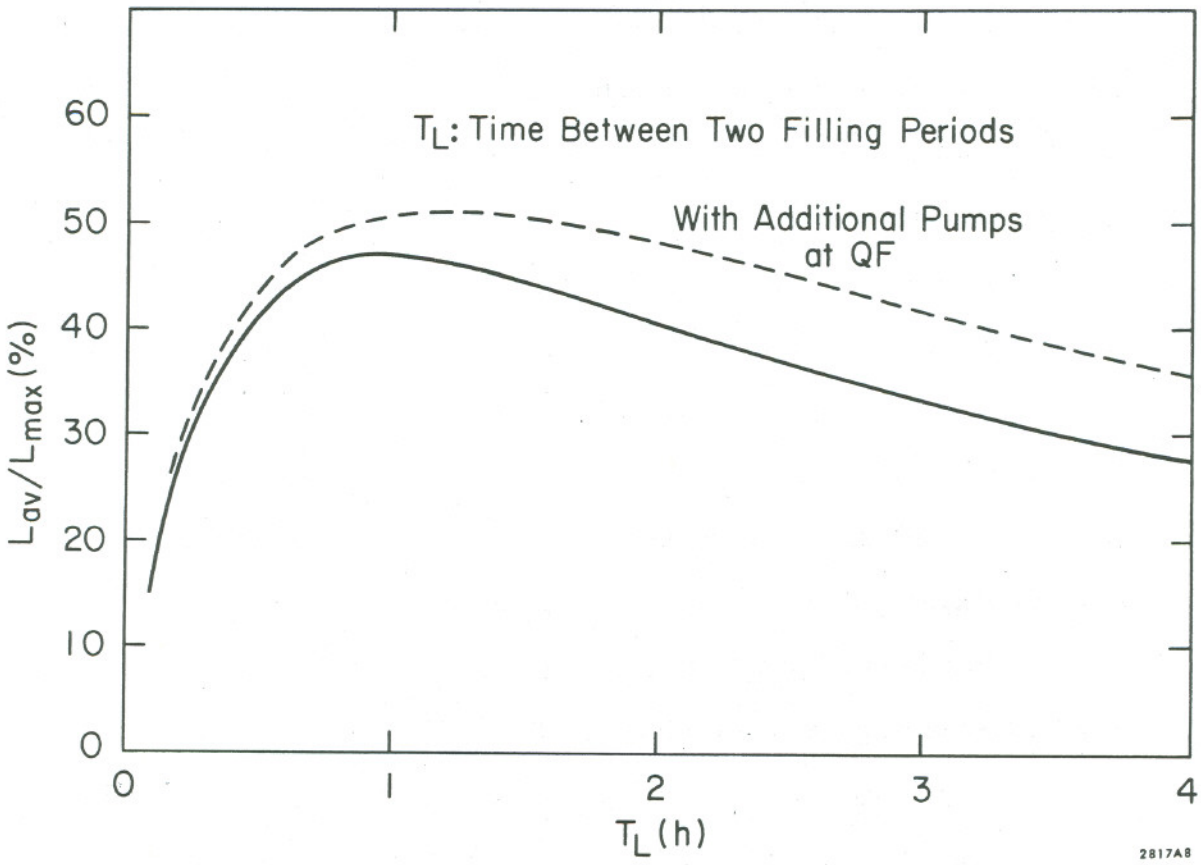

Fig. 13--Average luminosity.

are installed at a later time. Figure 13 is conservative in representing a pessimistic view of the average luminosity, since it assumes that the luminosity decays like the product of the beam currents. In SPEAR, however, it has been observed that the luminosity decays somewhat more slowly.

9. Reduction of Synchrotron Radiation in the Interaction Region

The synchrotron radiation generated by the last main bending magnet and emitted into the long interaction straight sections can be a source of high background rates in the experimental detectors. To reduce this background in PEP, the last two bends are very low field magnets with a bending radius of 2500 m as compared to 165 m in the main bending magnet (Fig. 5).

Although the critical energy ϵ_c of the synchrotron radiation from the main bending magnet at 15 GeV is only 45.3 keV, the spectral density of these photons is high. Consequently, the number of photons with energies ten or twenty times the critical energy is still very large. In Fig. 14 the number per second of photons per unit photon energy into a cone of 1 mrad is plotted for both the main bending magnet and the low-field bending magnets.

The low-field magnet arrangement is shown in Fig. 15. The deflection angle of these magnets was designed so that all the synchrotron radiation from the last magnet (between quadrupoles Q3 and 1QF) passes through the whole interaction region without hitting the vacuum chamber.

The second low-field bending magnet is used to lower the energy of the radiation striking the absorber at Q1 and to prevent the high-energy synchrotron radiation from the main bending fields from entering the long straight section. This radiation is absorbed by the thick mask at quadrupole Q3, which absorbs not only the synchrotron radiation from the main bending magnet but also those high-energy particles which have been lost from the beam but still form a halo

0 0 0 0 4 4 0 2 9 2 3

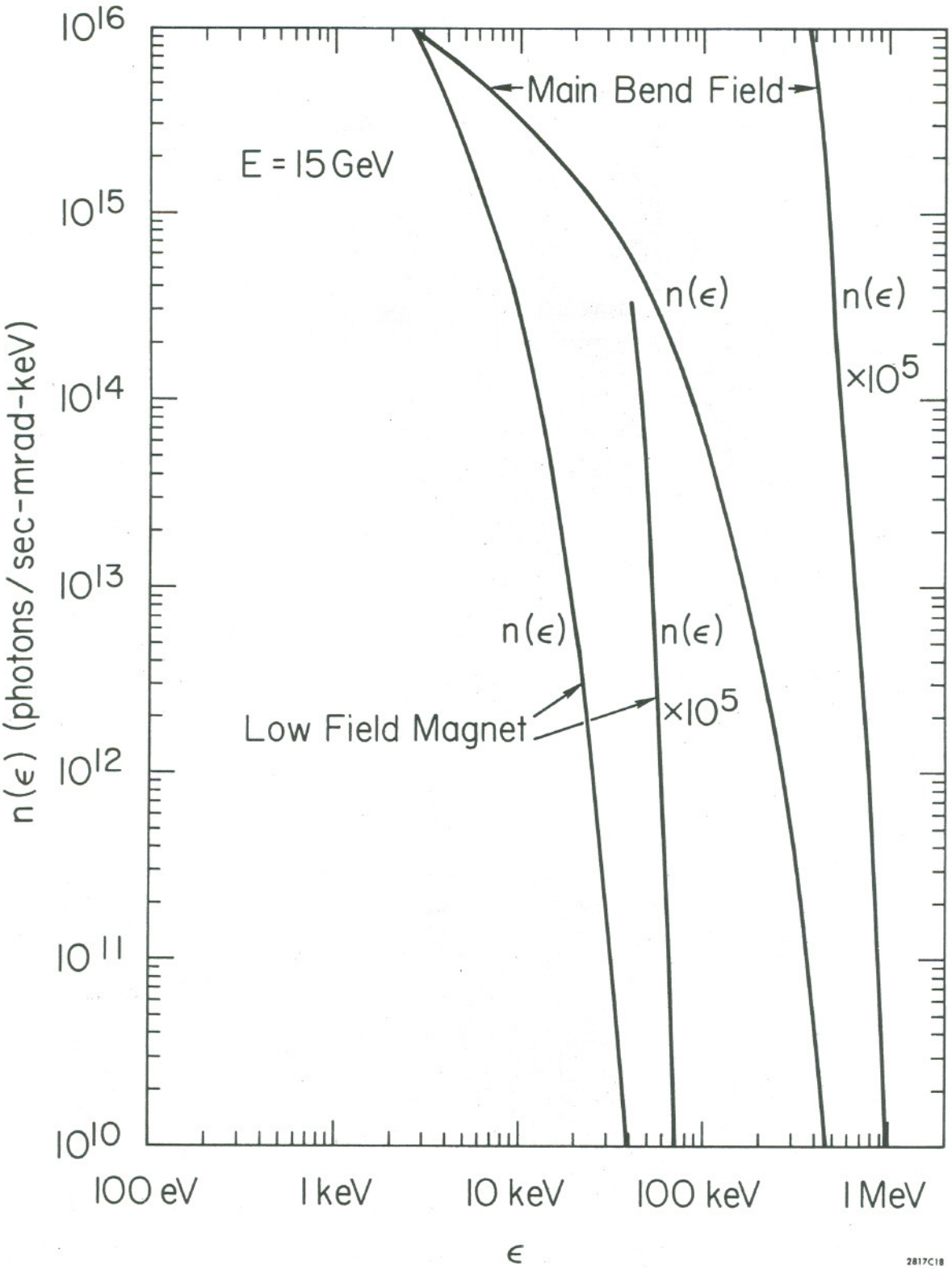

Fig. 14--Photon spectrum for the main bending magnets and the low-field magnets at 15 GeV.

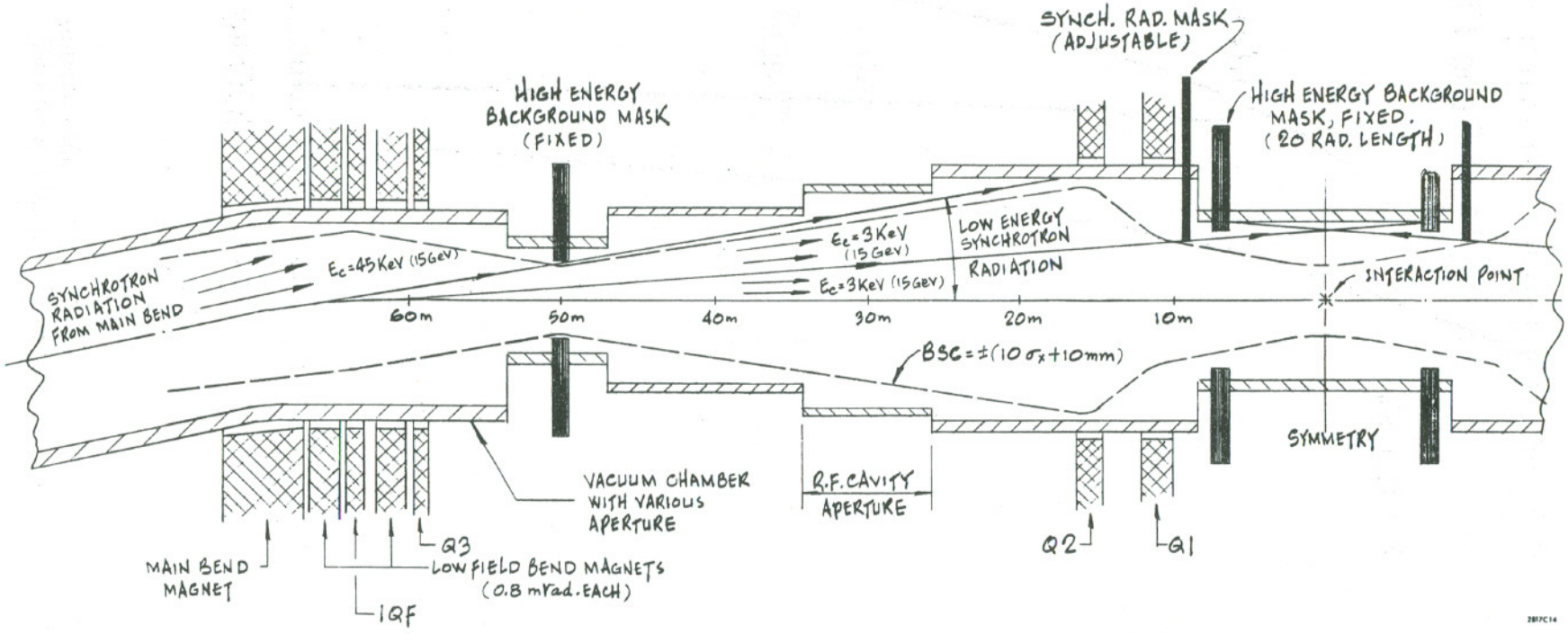

Fig. 15--Arrangement of low-field magnets and synchrotron radiation into interaction area.

around it. The mask is 20 radiation lengths thick and surrounds the beam. The synchrotron radiation mask at Q1 is a thin (0.5 cm) scraper on the outer side of the beam where the synchrotron light occurs. Since it is movable it can be adjusted to the minimum of the synchrotron radiation power between the two radiation cones from the two low-field magnets in order to reduce scattering from the edge of the scraper.

SPEAR experience indicates this should reduce the synchrotron-radiation background sufficiently. The remaining background from synchrotron radiation due to edge-scattering on scrapers or multiple scattering along the vacuum pipe, etc., should be small enough to be handled by the detectors.

B. The Magnet System

1. Introduction

The function of the magnet system in the PEP storage ring is to provide the guide field that bends the electrons and positrons in their circular paths and also to focus these particles so that they remain within the machine throughout their many orbits. The system selected for PEP is a separated-function system, meaning that the bending and focusing is accomplished by different magnets. Dipoles provide the bending field while quadrupoles provide the focusing field. A number of correction magnets, such as sextupoles, rotated quadrupoles, wiggler magnets, and low-field bending magnets, are interspersed among the main ring bending and quadrupole magnets, performing beam correction functions as needed.

The design of the different types of magnets in the magnet system is optimized by minimizing the installed capital cost plus ten years' operating cost at 15 GeV. In this way prudent attention is paid to reducing power consumption. Laminated magnets were selected for the main-ring elements both to reduce capital costs and to insure uniformity magnet to magnet by shuffling as explained later in this section.

The main bending system consists of 192 C-type uniform-field magnets, each approximately $5\frac{1}{2}$ m long. Each steel core contains nearly 3,500 $1\frac{1}{2}$-mm-thick laminations having outside dimensions of about $\frac{1}{2}$ m. These laminations are sandwiched between two thick end plates and are held in place by welding straps to both the end plates and the individual laminations. The completed core weighs 9.5 tons. The coils located above and below the beam aperture are of water-cooled aluminum having a conductor cross section of 9×65 mm^2.

There are 240 quadrupoles in the ring. Two styles of quadrupoles having two different apertures will be used: the 216 main-ring quadrupoles have the smaller bore; the 24 insertion-region quadrupoles have the larger bore. The 640-mm long main-ring quadrupoles are of four-piece construction. Each piece contains 430 $1\frac{1}{2}$-mm thick laminations (nearly 1700 per magnet) sandwiched between thick end plates and held together by welding an angle to both the end plates and the laminations. Four core blocks are fitted with water-cooled aluminum coils and bolted together to form one two-ton quadrupole. Two types of insertion region quadrupoles, one of 2 and one of 1.5 m length, are required. These magnets are of two-piece construction, each piece containing two poles. Again, $1\frac{1}{2}$-mm thick laminations are sandwiched between thick end plates and held in place by welding straps to both the laminations and end plates. Half-cores are then fitted with water-cooled aluminum coils and bolted together to form the completed quadrupole. The different lengths are produced by varying the number of laminations stacked for different quadrupoles.

The sextupoles, low-field bending magnets, wiggler magnets, and rotated quadrupoles, unlike the main ring elements, are of solid-core design. All have aluminum coils.

2. Dipole Design and Models

C-magnets were selected for use as the main-ring (flat-field) bending magnets because they afford easy access to the vacuum chamber for infield repair and also because they allow construction and installation of the magnet system independent of the vacuum system. H-magnets would result in smaller magnet cores and consequently a lower capital cost; however, the easy accessibility to the vacuum chamber and the independent construction schedules offered by the C-magnets more than outweigh the slight reduction in capital costs.

The vertical aperture was determined by adding space for the vacuum chamber and clearance to the pole tip to the vertical beam-stay-clear region described in Section II.A.5. For reasons of economy, the apertures of all bending magnets are the same. The horizontal aperture, or good-field region, was determined by adding 20 mm to the maximum beam width to allow for orbit distortions, misalignments, and the sagitta of the curved beam orbit over the total length of the straight magnet. Once the vertical aperture and the horizontal good-field region were determined, the pole width required to produce this field was defined for the dipoles as that region in which $\Delta B/B \leq 0.001$.

The coil-slot area is determined by the optimum current density which for PEP is close to 1 A/mm^2. Since the packaged coils must pass through the magnet gap, the maximum height of the individual coil packages is determined by the gap. Further, analysis has shown that a magnet having single wide coil packages above and below is less expensive to fabricate than one with two or more narrow packages.

The dimensions of the vertical return yoke were determined from structural limitations. Back-leg thicknesses of greater than 100 mm are required so that gap deflections at 18 GeV operation are less than 0.025 mm. The widths of the horizontal yokes were made equal to that of the vertical yoke. The resulting magnet cross section is shown in Fig. 16. Table V presents the important design information.

A computer model of the above design was run using the POISSON program of LBL. Comparative calculations were made for the cross section shown and another cross section with a narrower pole having shims. The narrower, shimmed pole resulted in a slightly increased operating cost since its gap had to be larger than that of the flat pole to accommodate the insertion of the vacuum

0 0 0 0 4 4 0 2 9 2 6

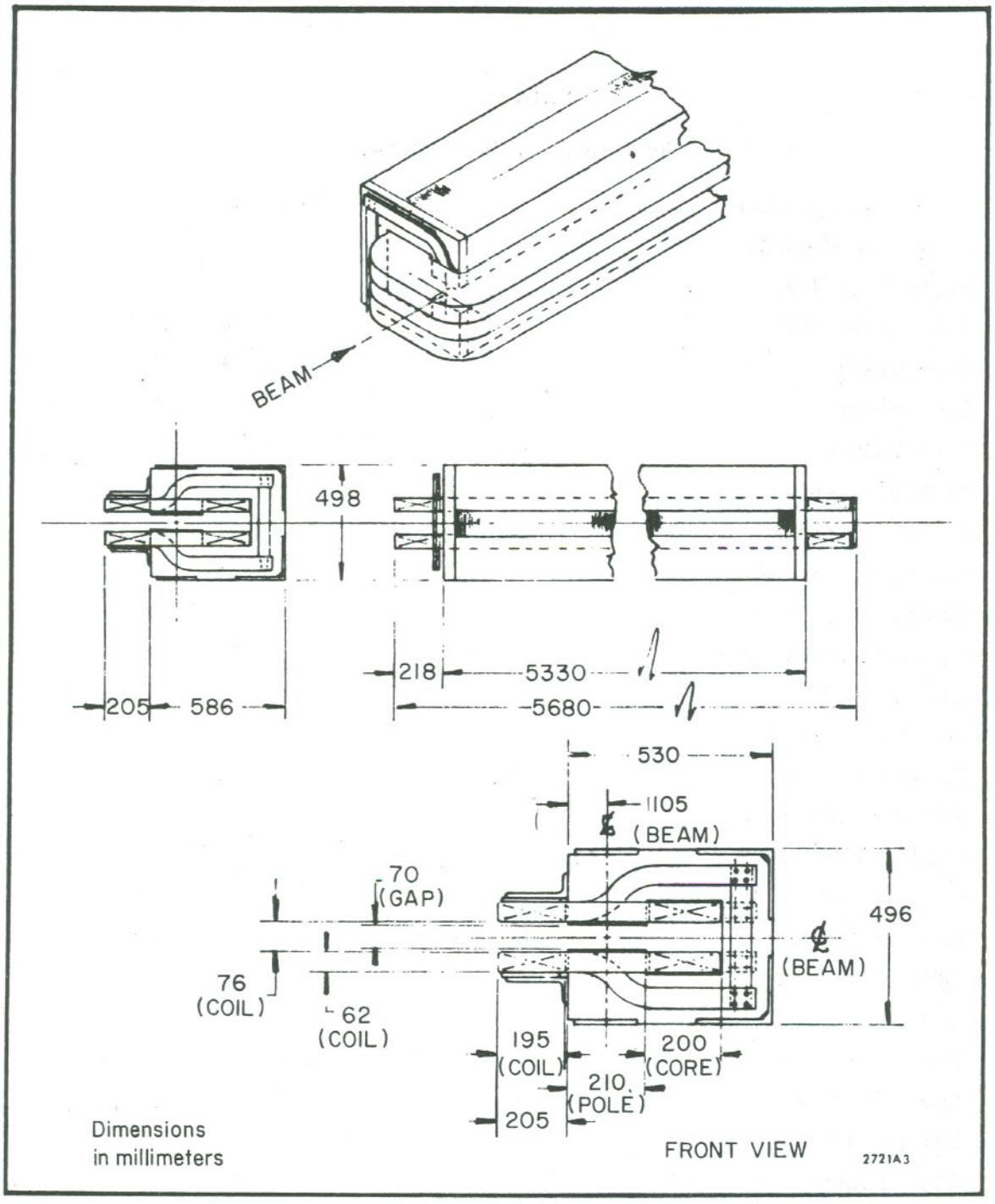

Fig. 16--PEP main ring bend magnet.

TABLE V

PEP Main Ring Bend Parameters

Magnet Designation	70C5400	
Number of Magnets	192	
Field @ 18 GeV	0.3625	T
$\int B d\ell$ @ 18 GeV	1.957	T-m
Pole Width	0.21	m
Gap Height	70	mm
Core Length	5.33	m
Magnetic Length	5.40	m
Width of Useful Field (0.1%)	100	mm
Lamination Height	0.496	m
Lamination Width	0.53	m
Packing Factor (min)	96	%
Core Weight	8580	kg
Amp Turns per Pole @ 18 GeV	10409	A-turns
Turns per Pole	16	
Pancakes per Pole	1	
Conductor Cross Section	65 x 9	mm^2
Cooling Hole Diameter	2 @ 5	mm
Conductor Cross-Sectional Area	546	mm^2
Current @ 18 GeV	650.6	A
Inductance	19.6	mH
Resistance @ 40^oC	17.9	mΩ
Power @ 18 GeV	7.58	kW
Voltage Drop @ 18 GeV	11.6	V
Stored Energy @ 18 GeV	4.15	kJ
Coil Weight	242	kg
Number of Water Circuits	2	
Water Flow Rate	9.45×10^{-5}	m^3/sec
Water Pressure Drop	1.38	MPa
Temperature Rise	19	^oC

tank between the bumps. This increased operating cost was offset by a reduced capital cost. No final choice has been made; however, the flat-pole version is favored for its support system for the vacuum tank.

A full-size mechanical model of a 60-mm gap, flat-pole main ring bending magnet has been constructed, as shown in Fig. 17. Mechanical and electrical tests are currently in progress and preliminary results indicate good agreement with theory.

After the model was constructed, the gap-height specification was increased from 60 to 70 mm in order to accommodate full coupling between the vertical and horizontal betatron oscillations in the beam. Also the number of turns in the half-coil was increased from 12 to 31 to decrease the size of the current bus in the ring. A further improvement was the winding in of an additional half-turn so that the magnet can act as part of its own bus. Another model, incorporating the above changes as well as improvements in fabrication techniques, is presently being constructed.

3. Quadrupole Design and Models

The best quadrupole field is produced by a magnet having four hyperbolic poles symmetrically arranged about a circular aperture. Four coils, one for each pole, are used to energize the magnet. In the separated-function design, the focusing is done primarily by the quadrupoles. To achieve different tunes, quadrupole (focusing) strengths must be controlled independently, and thus powered independently, of the bending magnets.

The bore, or aperture, of the quadrupoles was determined by the height of the bending magnet vacuum tank for the main ring quadrupoles and by the beam-stay-clear for the insertion-region quadrupoles. The vacuum tank in the arc sections of the ring is common to two bending magnets and two quadrupoles.

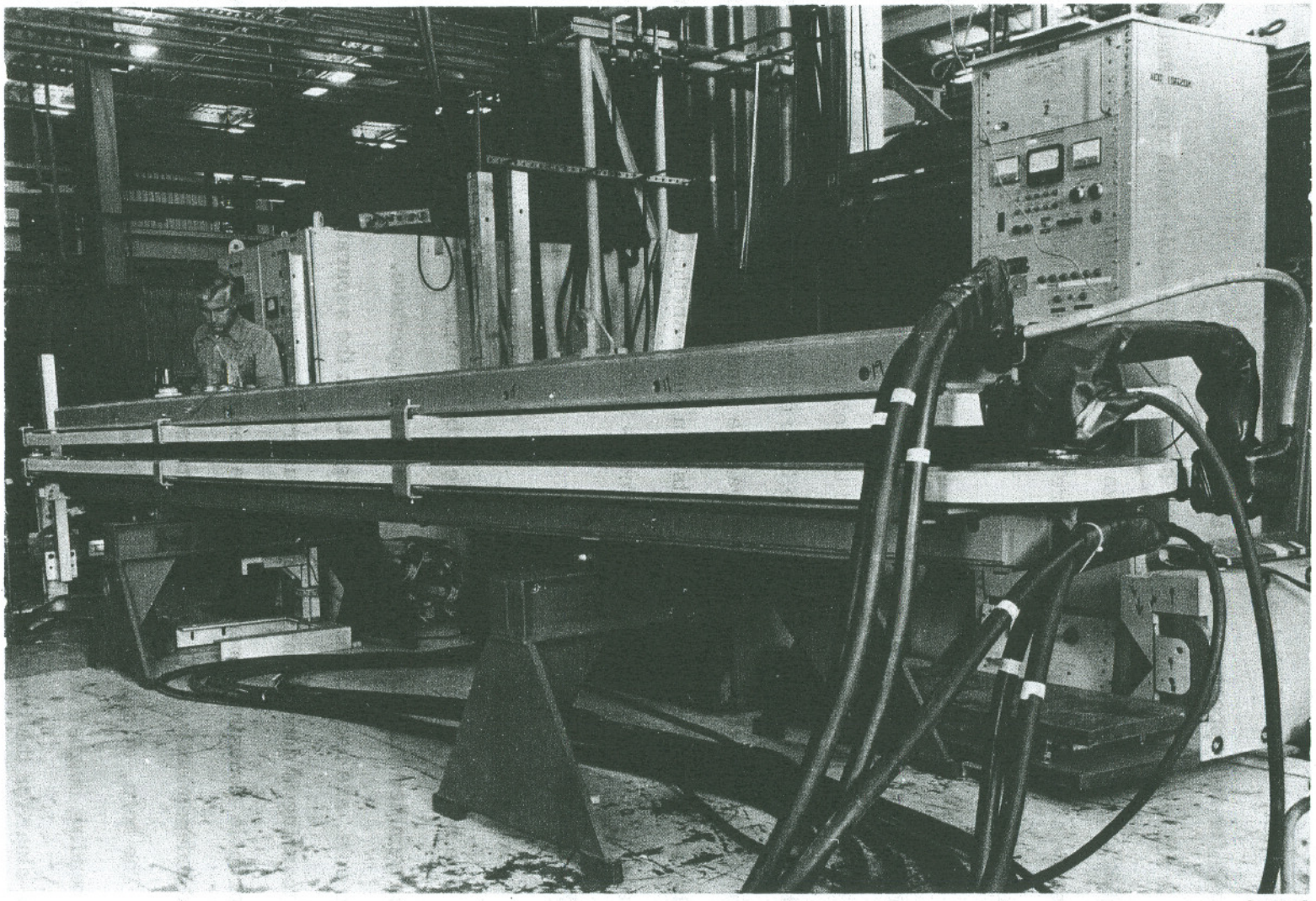

2017A15

Fig. 17--Photograph of prototype main ring bend magnet.

The bore of the 216 main-ring quadrupoles was determined by minimizing the circular aperture to allow adequate clearance for the vacuum chamber. A 120-mm bore was found to be sufficient. A further reduction in quadrupole bore, and consequently a reduced capital and operating cost for the magnets, could be made if the vacuum chamber at the quadrupoles could be "upset", or made to conform more closely to the quadrupole pole shape. Attempts to effect this configuration have resulted in a loss of vacuum integrity. Further study continues; however, the present design is based on the 120-mm bore.

The bore of the insertion-region quadrupole was determined by the beam-stay-clear requirements in the area of Q2. Using the beam-stay-clear numbers shown in Fig. 12 and providing adequate clearance resulted in a bore of 160 mm. Twenty-four such quadrupoles are required, twelve 2 m long and twelve 1.5 m long.

The field of any magnet can be described as the superposition of the fields of many pure multipole magnets, each having different strengths and numbers of poles. A pure quadrupole would be one in which the field is 100% four-pole. One measure of the field quality of a magnet is the list of ratios of the other multipole strengths present to the strength of the desired multipole. This list is called the multipole content, and is usually expressed in terms of percentages of the fundamental multipole strength. For the main-ring quadrupole, the design multipole content criterion was that all multipoles were to be less than 0.1%. SPEAR experience has shown that insertion-region quadrupoles must have all multipole contents less than 0.01%.

The original main-ring quadrupole design was a scaled-down version of the highly successful SPEAR quadrupole with an increased coil slot to reduce the energy consumption. Four laminated coil blocks were fitted with four 12-turn

water-cooled aluminum coils having a current density of 1.74 A/mm^2 at 15 GeV operation. Figure 18 shows the cross section and Table VI gives the magnet's design parameters.

Computer models of this magnet were analyzed using the POISSON program. At low field strengths, the iron in the yoke has essentially infinite permeability and the hyperbolic portion of the pole determines the desired linear dependence of the field. The termination of the hyperbolic poles at the coil slots causes the field to deviate from the optimum linear dependence, but proper shaping of the pole in this area and proper positioning of the coils can compensate for this effect. POISSON was used to determine the required pole shaping.

A full-sized, 127-mm bore model of this magnet was constructed, as shown in Fig. 19. The iron core was found to be within 0.1 mm of the ideal dimensions. After coils were fitted, magnetic measurements were made which indicated that the model more than met the design specification of having all multipoles less than 0.1%. The results of the magnetic measurements are given in Fig. 20. Although the results shown are for a modest excitation, no significant degradation of field quality was observed up to pole-tip fields in excess of 1.25 T, the power supply limit.

The dependence of betatron frequency upon the particle energy, $E = E_0 + \epsilon$, and betatron amplitude, x_β, were calculated for the case where the magnetic multipole field of the model quadrupole was present in all the main-ring quadrupoles. The results are summarized in Fig. 21, where lines of constant tune are plotted in the (ϵ, x_β) space. This quadrupole design is acceptable, and care will be taken to insure that the sextupole and octupole terms of the final magnets do not exceed those of the model.

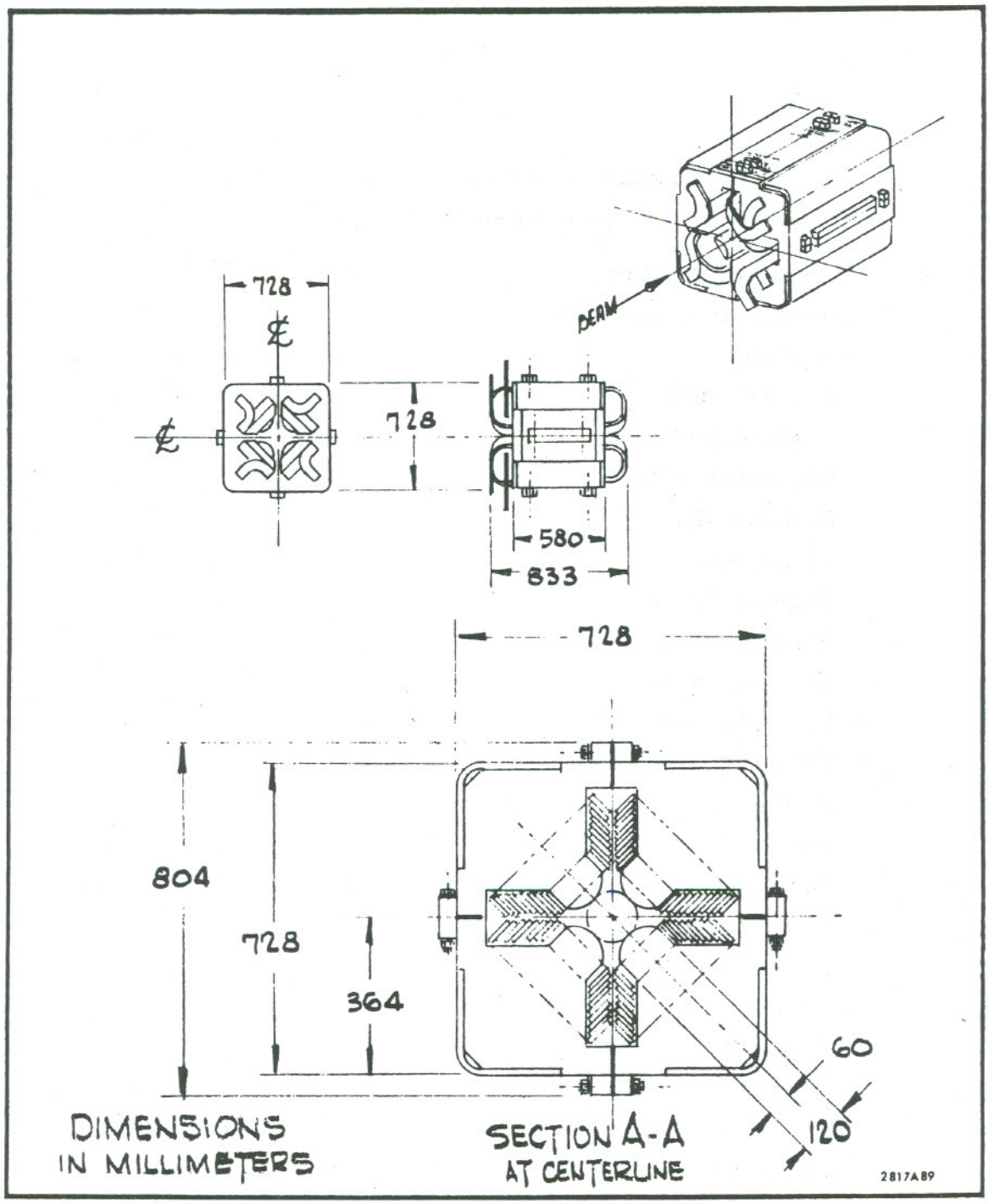

Fig. 18--PEP standard quadrupole assembly (low impedance design).

TABLE VI

PEP Standard Quadrupole Parameters (18 GeV)

(Low Impedance Design)

Magnet Designation	120Q640	
Nominal Peak Gradient	20	T/m
Gradient	12.61	T/m
Pole Tip Field	0.757	T
Gradient Length Product	8.07	T
Inscribed Radius	60	mm
Minimum Gap	34.4	mm
Core Length	0.580	m
Magnetic Length	0.64	m
Width of Useful Field	120	mm
Laminate Height	365	mm
Laminate Width	402	mm
Packing Factor (min)	96%	
Core Weight	1700	kg
Amp Turns per Pole	18062	A-turns
Turns per Pole	12	
Pancakes per Pole	1	
Conductor Cross Section	9×72	mm^2
Cooling Hole(s) Diameter	2 @ 5	mm
Conductor Cross-sectional Area	609	mm^2
Current	1505	A
Current Density	2.47	A/mm^2
Inductance	5.14	mH
Resistance @ 40^oC	4.47	$m\Omega$
Power	10.1	kW
Voltage Drop	6.73	V
Stored Energy	5.82	kJ
Aluminum Weight	150	kg
Number of Water Circuits	1	
Temperature Rise	35.4	^oC
Water Flow Rate	6.85×10^{-5}	m^3/sec
Water Pressure Drop	1.034	MPa

0 0 0 0 4 4 0 2 9 3 0

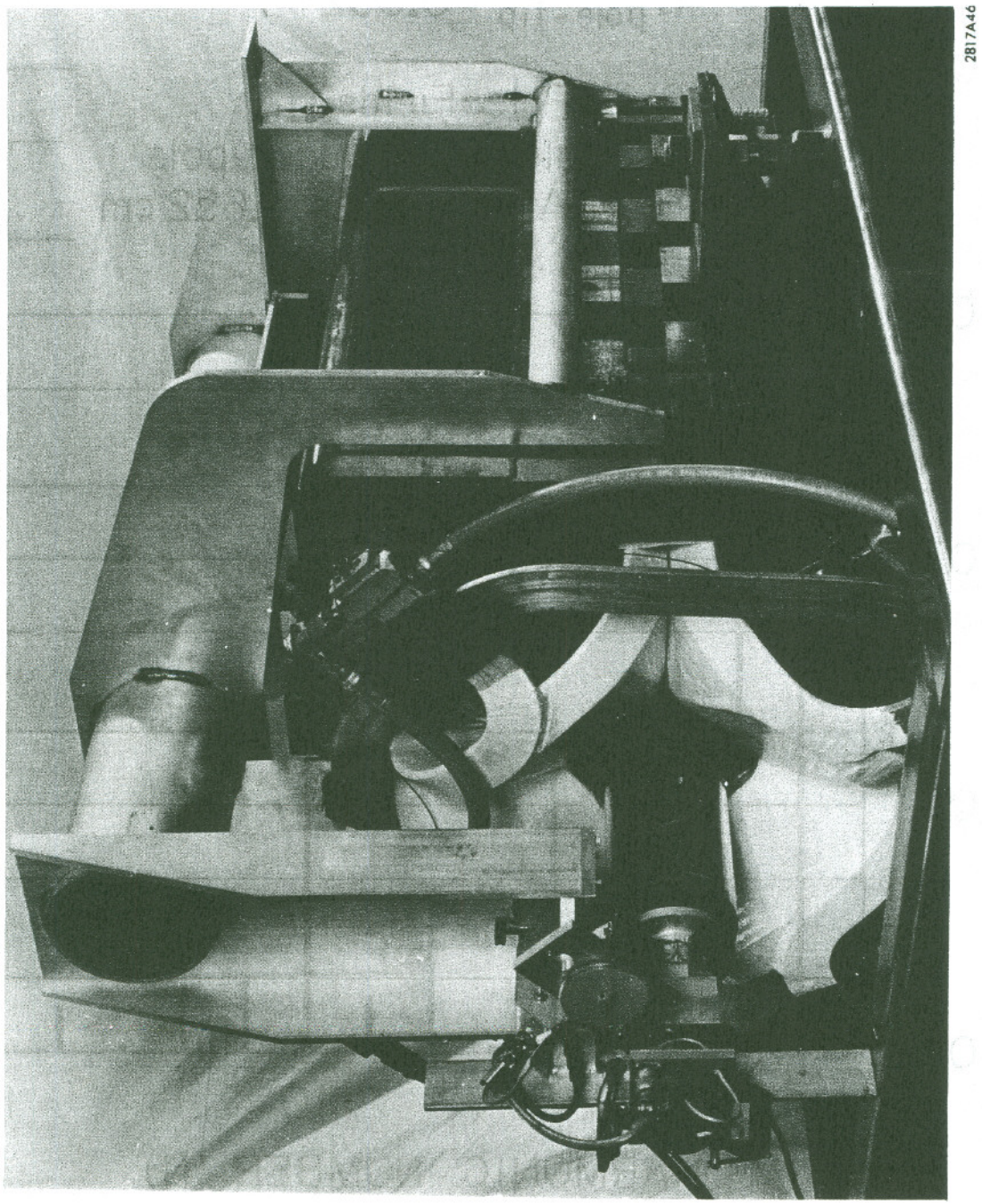

Fig. 19--Photograph of prototype standard quadrupole.

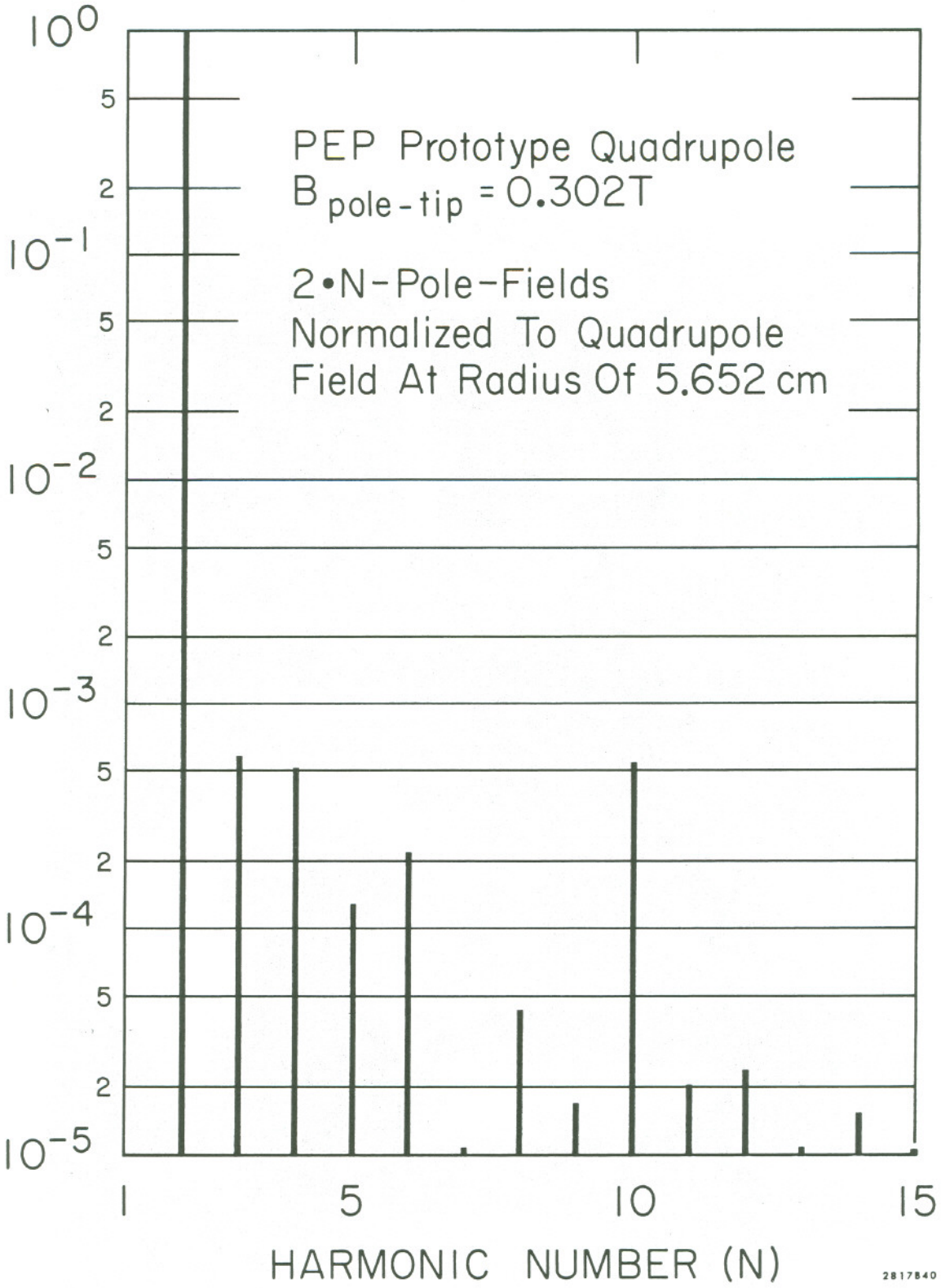

Fig. 20--Multipole content of the prototype standard quadrupole.

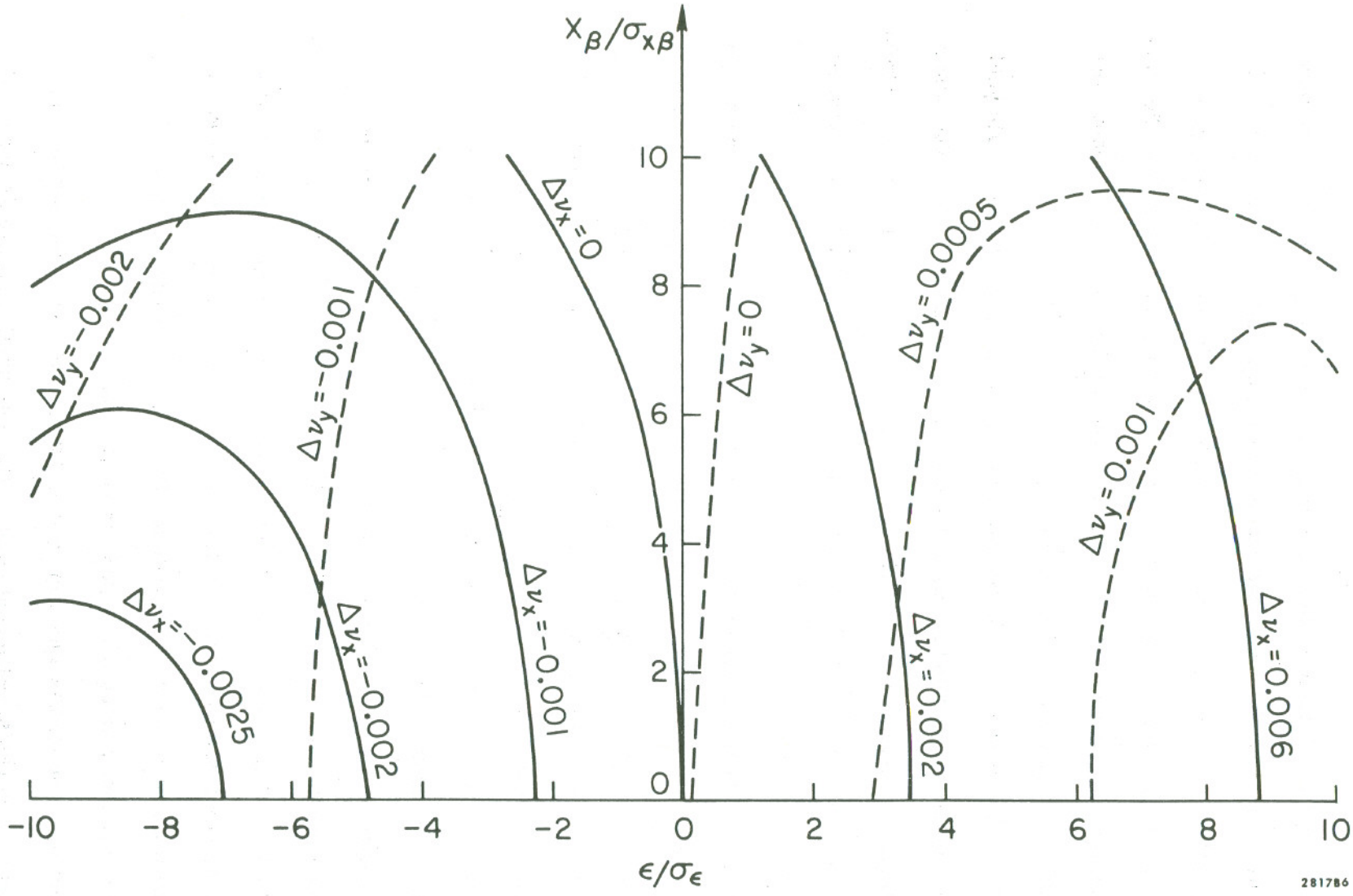

Fig. 21--Effect on the tune due to the multipole content in the standard quadrupole.

Two other quadrupole models utilizing the same strap-coil configurations were built. The second was a two-piece core design with an asymmetric pole configuration. The two-part core was selected for economy in punching and core assembly, and the asymmetric poles were necessary to introduce the wide coil packages into the coil slots. Magnetic and mechanical measurements are currently in progress on these models.

The third model is exactly the same as the first except that the angle holding the laminations and end plates to form a core block is inverted. The assembled magnet resembles a cross, giving the model the name "iron cross". Great difficulties encountered in fabricating straight core blocks have caused this design to be dropped.

To reduce busing costs in the ring, efforts were made to reduce the current of the ring magnets. The number of turns in the bending-magnet coils was doubled, but it was found that increasing the number of turns while retaining the strap-wound coil configuration in the quadrupole was impractical. Thus a fourth design, the high-impedance quadrupole, evolved. This design differs from the original in that it contains nearly five times the number of turns, resulting in a fivefold reduction in current and a corresponding increase in voltage. Figure 22 and Table VII present the main features of this design. Power supplies distributed around the ring would maintain the voltage-to-ground of any one magnet string below 600 V, and the reduced current requirement results in a smaller bus size and hence in lower bus costs. The increase in cost of the coil due to a larger number of turns is offset by the savings in bus cost. This model is presently being fabricated for evaluation.

The insertion-region quadrupole is of two-piece core construction with symmetric hyperbolic optimized poles. The pole profiles were designed and

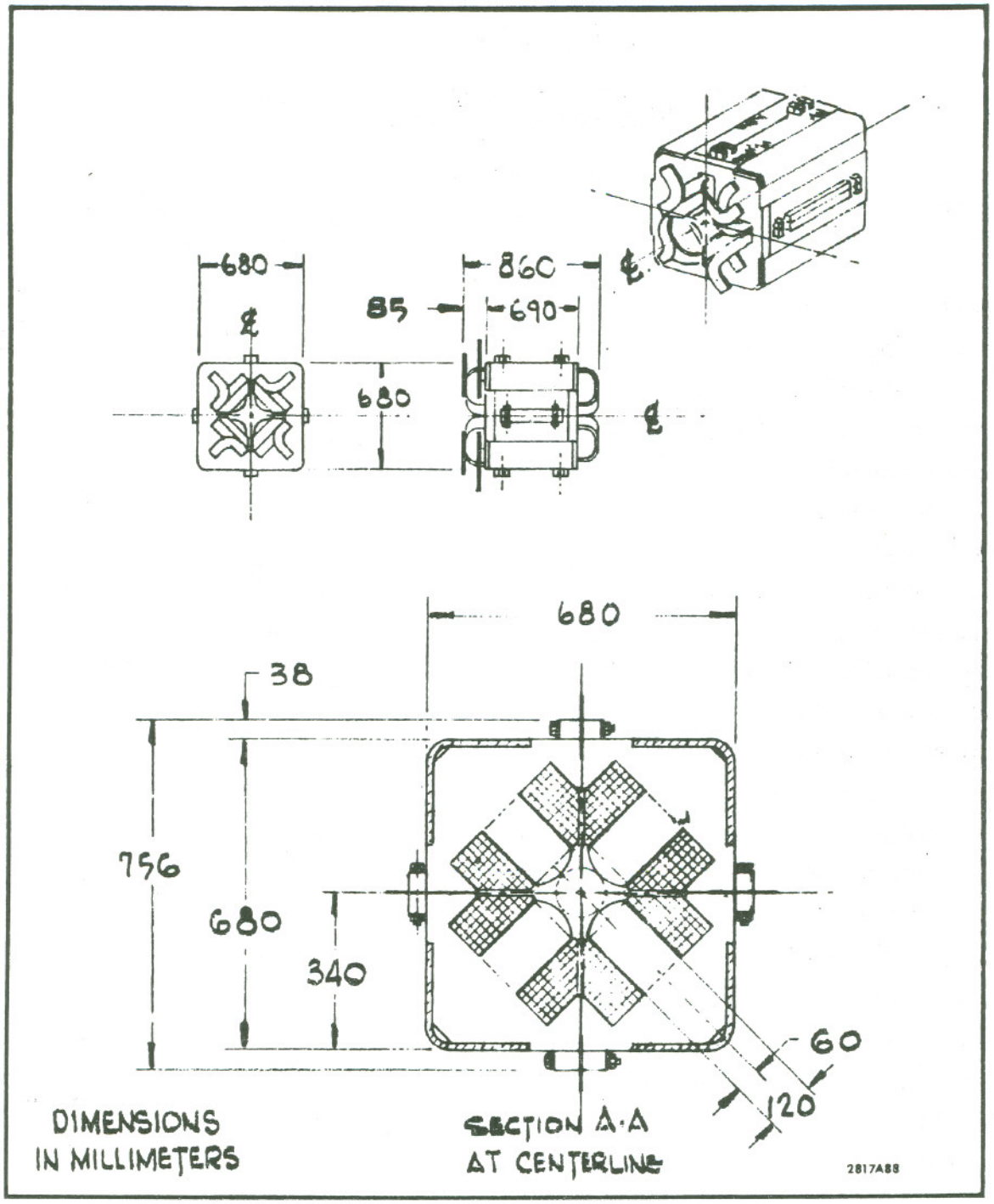

Fig. 22--PEP standard quadrupole assembly (high impedance design).

TABLE VII

PEP Standard Quadrupole Parameters (18 GeV)
(High-impedance Design)

Magnet Designation		120Q750	120Q1000	120Q380
Used for		QF, QD, 2QF, 3QF, 8QF, 8QD, 1QD	Q3, 1QF	9QF
Number of Magnets		180	24	12
Nominal Peak Gradient	T/m	20	20	20
Operating Gradient	T/m	10.76	10.76	10.76
Pole Tip Field @ Operating Gradient	T	0.646	0.646	0.646
Gradient Length Product	T	8.07	10.76	4.09
Inscribed Radius	mm	60	60	60
Minimum Gap	mm	34.4	34.4	34.4
Core Length	m	0.690	0.940	0.32
Magnetic Length	m	0.750	1.00	0.38
Width of Useful Field	mm	120	120	120
Lamination Height	mm	340	340	340
Lamination Width	mm	378	378	378
Packing Factor (min)	%	96	96	96
Core Weight	kg	1700	2316	788
Amp Turns per Pole	A-turns	15412	15412	15412
Turns per Pole		57	57	57
Pancakes per Pole		1	1	1
Conductor Cross Section	mm^2	12.7 sq.	12.7 sq.	12.7 sq.
Cooling Hole Diameter	mm	6.3	6.3	6.3
Conductor Cross-Sectional Area	mm^2	121.3	121.3	121.3
Current	A	270.4	270.4	270.4
Current Density	A/mm^2	2.23	2.23	2.23
Inductance	mH	56.4	75.2	28.6
Resistance @ 40^oC	mΩ	112	140	68.4
Power @ 18 GeV	kW	8.17	10.2	5.0
Voltage Drop @ 18 GeV	V	30.2	37.9	18.5
Stored Energy	kJ	2.06	2.74	1.04
Aluminum Weight	kg	150	187.5	91.6
Number of Water Circuits		2	4	2
Temperature Rise	^oC	24.6	10.2	11.4
Water Flow Rate	$10^{-5}m^3/sec$	7.95	18.4	10.5
Water Pressure Drop	MPa	1.034	1.034	1.034

optimized using the computer program POISSON. To reduce core costs and improve high-field performance, the pole widths were minimized while maintaining the proper good-field region. The core blocks are constructed of $1\frac{1}{2}$-mm thick laminations sandwiched between 50-mm end plates and welded in a manner similar to the bending magnets. The vertical return yokes are narrower than the horizontal yokes to minimize the horizontal angle subtended by the magnet from the interaction point. Figure 23 shows a cross section of the proposed design and Table VIII gives the design parameters. Three separate aluminum coil packages surround each of the four poles. Two of these packages comprise the main winding and are tied electrically in series with the main ring bending magnet circuit. The third package is a trim winding which enables the individual quadrupoles to be set at their proper operating point.

A model of the insertion-region quadrupole has been built, a photograph of which is shown in Fig. 24. Preliminary mechanical and magnetic measurements have been made which indicate some problems with core assembly. Work is currently under way to rectify these problems.

4. Correction Magnets

Sextupoles. Sextupoles are required to compensate the momentum dependence of betatron oscillation frequency. Space has been allocated for 192 such magnets, one adjacent to each of the main-ring quadrupoles. The criterion for determining the 140-mm aperture was that the magnet must be capable of passing the bending magnet vacuum chamber. Experience at SPEAR has shown that cast-core sextupoles produce sextupole fields of sufficient quality, so this construction will also be used for PEP. The SPEAR sextupoles may be regarded as models. Figure 25 presents the preliminary design and Table IX gives the design parameters. Unlike the other magnetic elements, the coils for these

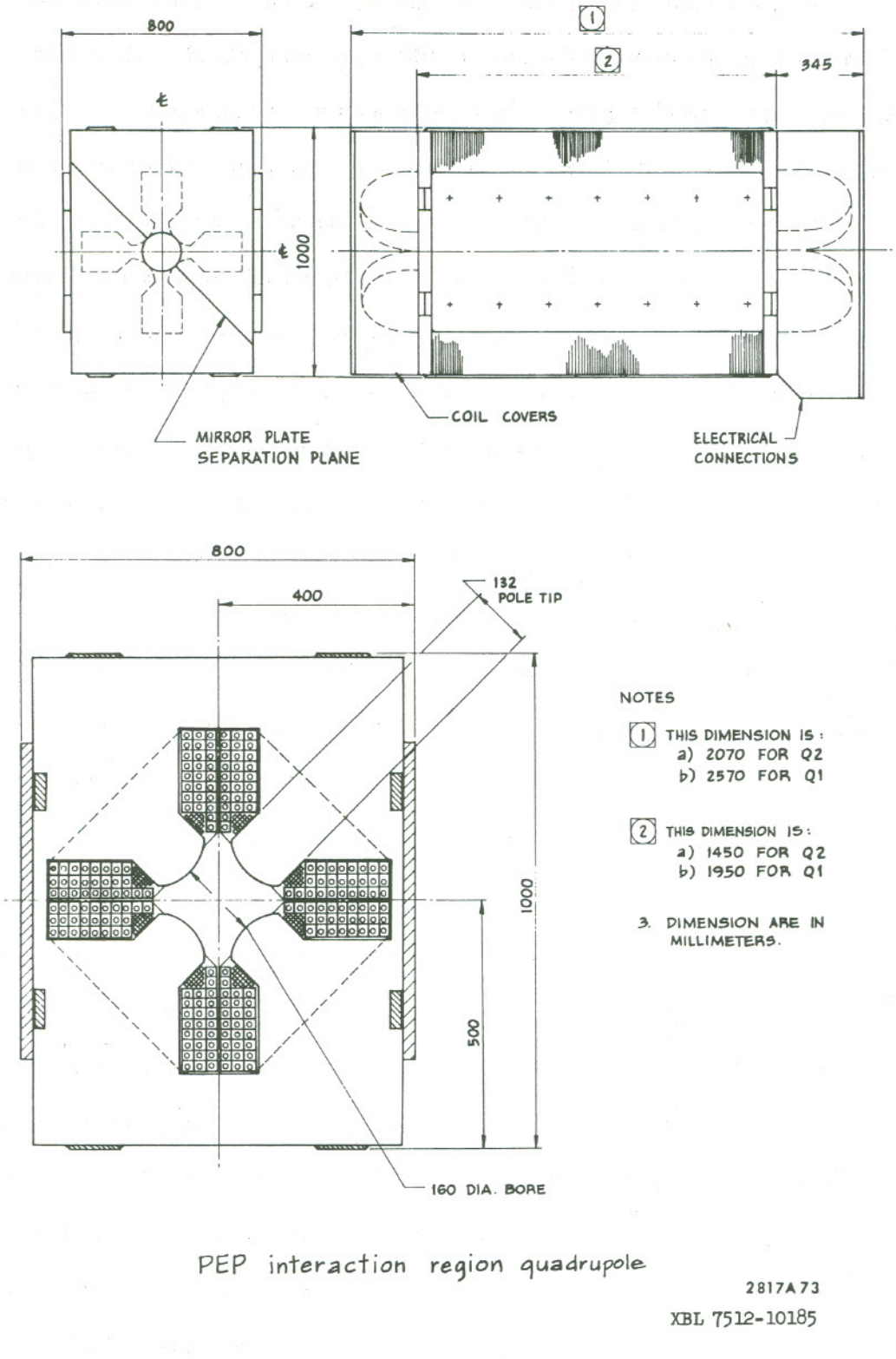

Fig. 23--PEP interaction region quadrupole.

TABLE VIII

PEP Insertion Region Quadrupole Parameters

Magnet Designation		160Q2000 (Q1)	160Q1500 (Q2)
Number of Quadrupoles		12	12
Rated Gradient	T/m	6.6 (±0.4)	6.6 (±0.4)
Rated Pole-tip Field @ 18 GeV	T	0.53 (±0.03)	0.53 (±0.03)
Inscribed Aperture Radius	mm	80	80
Minimum Gap Between Poles	mm	53	53
Core Length	m	1.95	1.45
Magnetic Length	m	2.0	1.5
Useful Field Width ($\Delta B/B \leq 10^{-4}$)	mm	168	168
Turns per Pole		26 (16)	26 (16)
Rated Current	A	660 (±65)	660 (±65)
Current @ 15 GeV	A	542 (-16)	542 (+9)
Current @ 18 GeV	A	651 (-5)	651 (+22)
Coil Sections per Pole		2 (1)	2 (1)
Conductor Cross Section	mm^2	23 x 20 (6.5 x 6.5)	23 x 20 (6.5 x 6.5)
Cooling Hole Diameter	mm	6.5 (3.5)	6.5 (3.5)
Conductor Area	mm^2	426 (32)	426 (32)
Rated Current Density @ 18 GeV	A/mm^2	1.54 (2.0)	1.54 (2.0)
Resistance @ 40^oC	mΩ	36.5 (260)	29.1 (200)
Rated Voltage (max.)	V	24.1 (16.9)	19.2 (13.0)
Rated Power (max.)	kW	15.9 (1.1)	12.7 (0.9)
Stored Energy @ 18 GeV	kJ	9 (∿0)	7 (∿0)
Inductance @ 18 GeV	mH	42 (16)	32 (12)
Core Weight	kg	9000	6700
Aluminum Coil Weight	kg	594	474
Number of Water Circuits		4 (2)	4 (2)
Water Temperature Rise	^oC	20	20
Water Flow Rate	m^3/sec	1.90×10^{-4} (1.3×10^{-5})	1.52×10^{-4} (1.0×10^{-5})
Water Pressure Drop	MPa	0.82 (0.60)	0.46 (0.30)

Values in parentheses are for auxiliary windings.

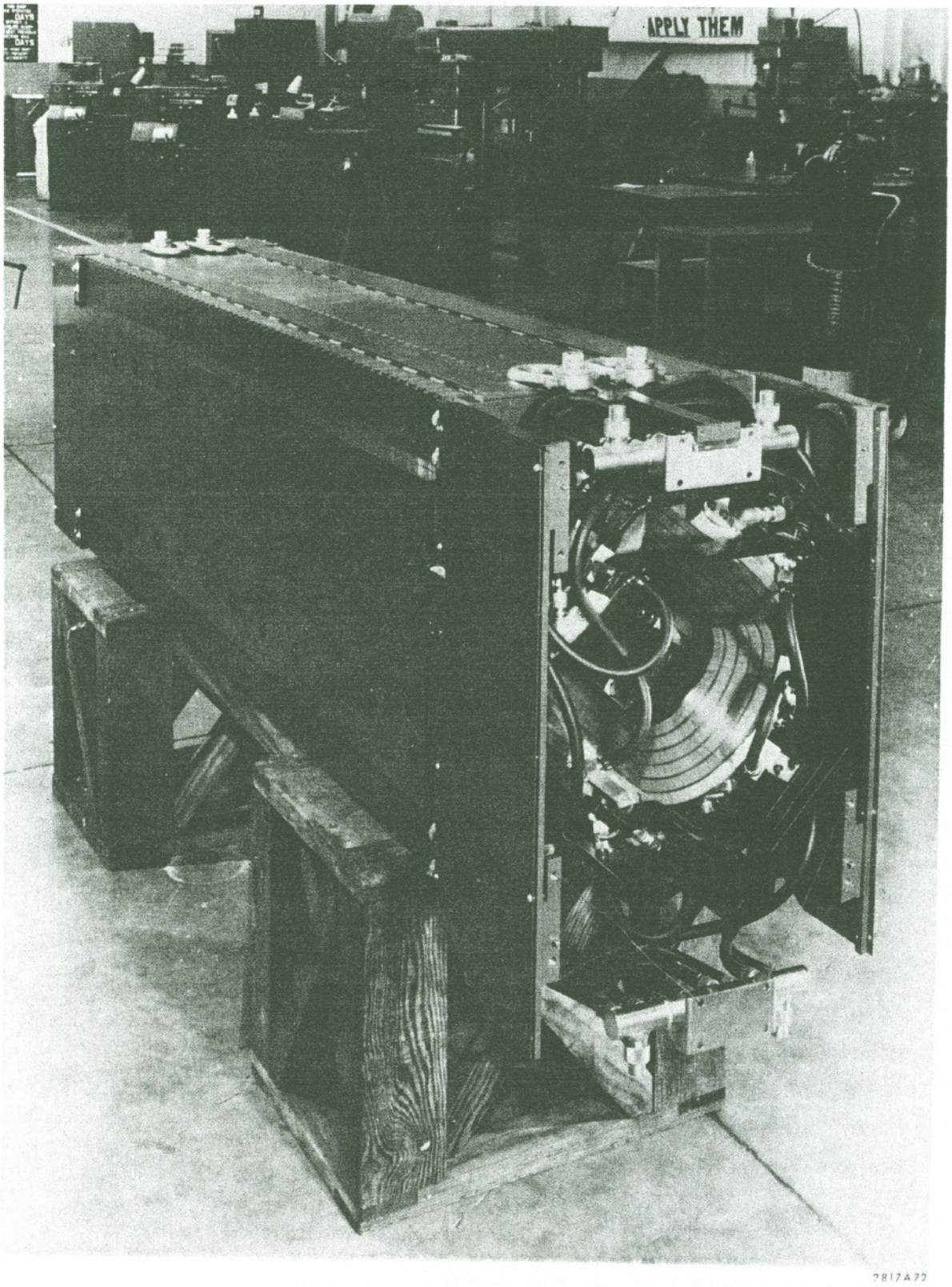

Fig. 24--Photograph of prototype insertion region quadrupole.

0 0 0 0 4 4 0 2 9 3 5

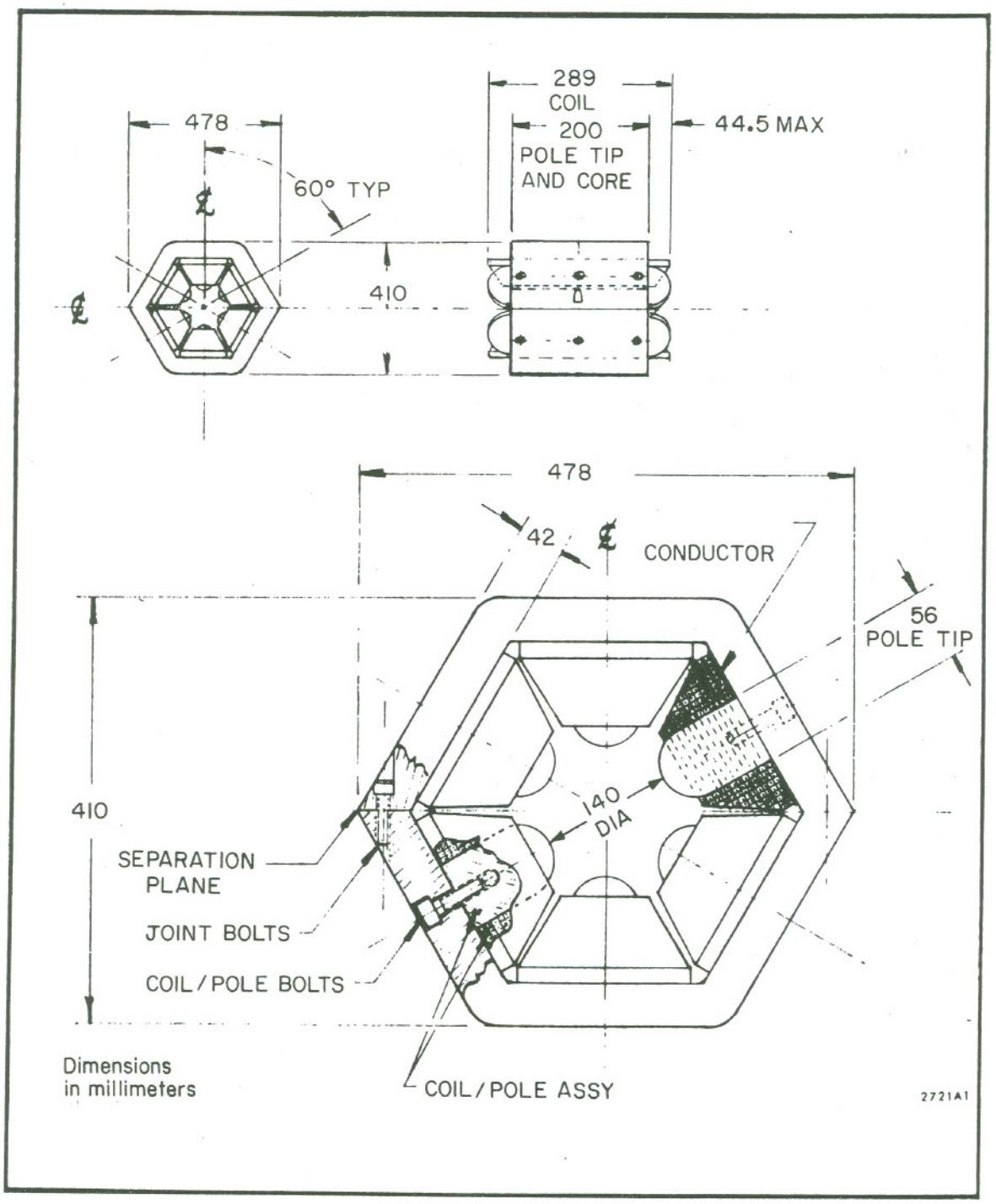

Fig. 25--PEP sextupole assembly.

TABLE IX

PEP Standard Sextupole Parameters

Magnet Designation	140S250	
Number of Sextupoles	162	
Peak Design Gradient	15.0	T/m
Design Gradient at Pole Tip	7.91	T/m
Pole Tip Field @ Design Gradient	0.277	T
Inscribed Radius	70	mm
Core Length	0.20	m
Magnetic Length	0.25	m
Weight of Iron	205	kg
Amp Turns per Pole	5655	A-turns
Turns per Pole	49	
Design Current	115	A
Conductor Size (square copper)	5.8 x 5.8	mm^2
Conductor Area	24.7	mm^2
Current Density	4.7	A/mm^2
Resistance @ 40^oC	91.6	mΩ
Power	1.22	kW
Number of Water Circuits	2	
Temperature Rise	9	^oC
Water Flow Rate	$1.6 \times 10^{-5} m^3/sec$	
Water Pressure Drop	1.03	MPa

magnets will be made of water-cooled copper. The conductor size is small enough to insure single-length conductors in each coil package, keeping labor costs for fabrication comparable to coils made of aluminum.

Wiggler Magnets. The wiggler magnets, used for control of beam size and beam polarization time, will be of solid-core construction. Their apertures are determined by the beam-stay-clear in the symmetry straight sections in the arcs. The vertical apertures are 50 mm. The horizontal aperture was found by adding the 75-mm beam offset at peak bending power to the good-field region of 70 mm and using the computer to calculate the pole-width required to produce this field. The coil slots were determined by the space available between magnets, the height of the slot being close to half the space available. The width of the slot was found by reducing the power consumption to an acceptable level.

Three identical magnets are required for each wiggler unit. Two of the magnets operate at half the field of the third magnet in the center. All three are connected electrically to produce a net bend of zero. Fields in the central magnet are as high as 2T. Computer optimization of this design is in progress. The preliminary design cross section is given in Fig. 26 and the design data in Table X. Models are planned upon completion of the computer study.

Low-field Bending Magnets. Two low-field bending magnets located in the cells closest to the insertions and having bend angles of 0.8 milliradians are planned to reduce the backgrounds in the interaction areas. The apertures of these magnets are similar to those of the main-ring bending magnets except that the fields required are an order of magnitude less. Table XI gives the design data. Air-cooled copper conductors are foreseen for these magnets.

Other Correcting Elements. Horizontal and vertical steering will be accomplished through the use of trim windings on the sextupoles and bending

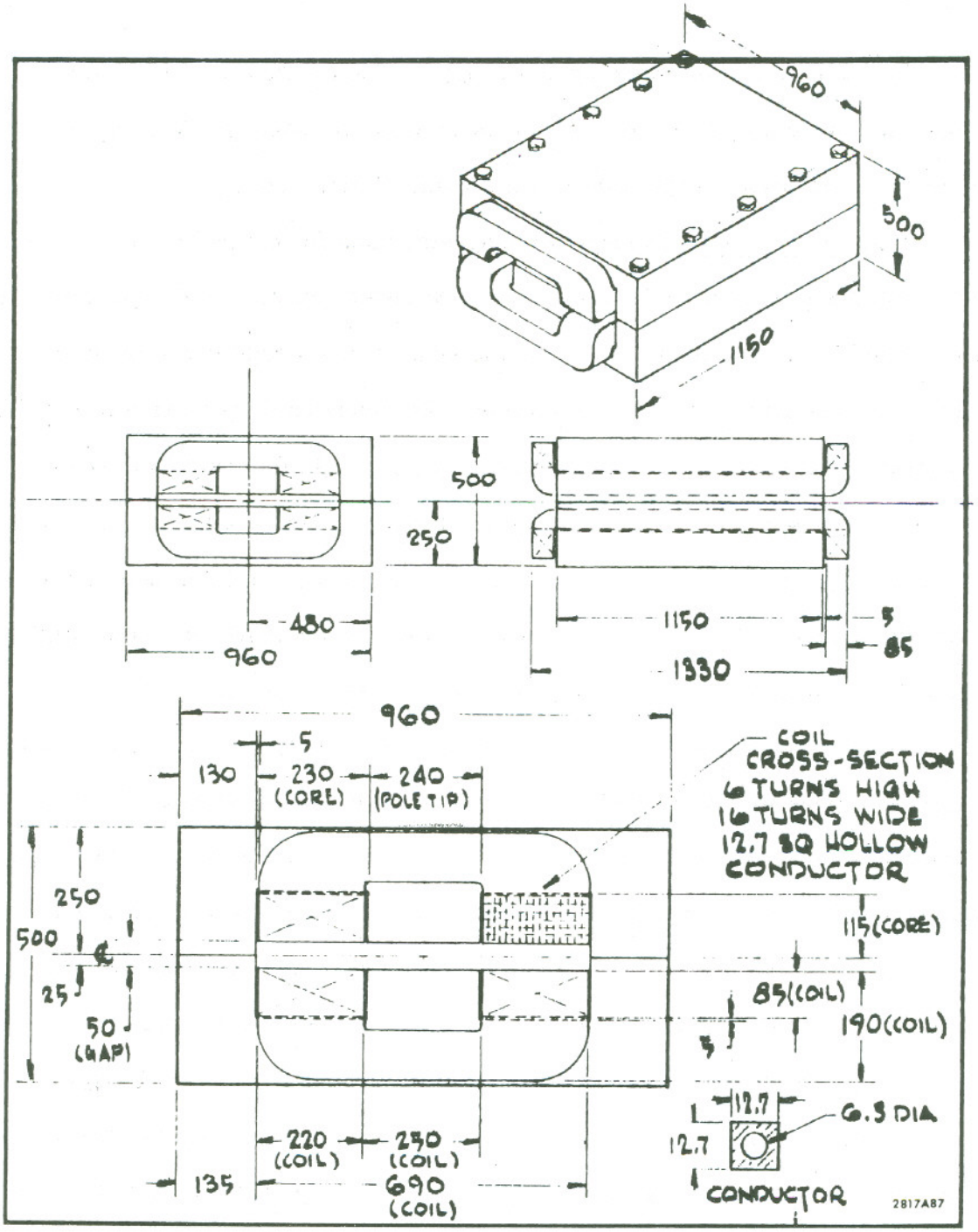

Fig. 26--PEP wiggler magnet assembly.

TABLE X

PEP Wiggler Magnet

Magnet Designation	50H1200	
Number of Magnets	9	
Peak Field	2	T
$\int B d\ell$ @ 2T	2.40	T-m
Gap Height	50	mm
Pole Width	240	mm
Core Length	1.15	m
Magnetic Length	1.20	m
Width of Useful Field ($\Delta B/B < 0.1\%$)	130	mm
Magnet Height	500	mm
Magnet Width	960	mm
Core Weight	3360	kg
Amp Turns per Pole @ 2T	44210	A-turns
Turns per Pole	96	
Pancakes per Pole	3	
Conductor Cross Section (sq. aluminum)	12.7 x 12.7	mm^2
Cooling Hole Diameter	6.3	mm
Conductor Cross-Sectional Area	121.3	mm^2
Current @ 2T	460.5	A
Inductance	968	mH
Resistance @ 40^oC	184	mΩ
Power @ 2T	39.1	kW
Voltage Drop	84.7	V
Stored Energy	102.7	kJ
Coil Weight	123.4	kg
Number of Water Circuits	6	
Water Flow Rate	3.26×10^{-4}	m^3/sec
Water Pressure Drop	1.38	mPa
Temperature Rise	28.8	^oC

TABLE XI

Low Field Bend Magnet

Magnet designation	70C2000	
Number of magnets	24	
Field @ 18 GeV	240	G
$\int B d\ell$ @ 18 GeV	480	G-m
Pole width	0.19	m
Gap height	0.07	m
Core length	1.93	m
Magnetic length	2.0	m
Width of the useful field	.080	m
Amp-turns/pole @ 18 GeV	690	A-turns
Turns/pole	23	
Conductor cross section	26.7	mm^2
Cooling	Air	
Current @ 18 GeV	30	A
Resistance	0.172	Ω
Power @ 18 GeV	154	W
Voltage drop	5.13	V

magnets. Tests have been made on the vertical steering capacity of a SPEAR sextupole. The results were published in Ref. 20 and were in general favorable.

Small rotated quadrupoles will be provided for control of the horizontal-vertical betatron oscillation coupling. The bore of these quadrupoles is similar to that of the main ring quadrupole. Depending upon the strength specified and beam-line space available, spare main-ring quadrupoles may be used.

5. Construction

Core Construction

Steel. The cores for the main ring bending magnets, main ring quadrupoles and insertion region quadrupoles are of laminated construction, selected as a result of experience with the solid-core magnets used in SPEAR. There, difficulty was encountered in making one magnet track another at high fields. Because the steel in different cores turned out to have different permeabilities, the magnets had to be relocated around the ring. In PEP the low-field properties as well as high-field excitation must be considered. To maintain high-field uniformity over the broadest range of excitation, a high-permeability at high fields and a low coercivity are required. The best saturation characteristics are obtained in steel sheets having a low carbon content. Subjecting such a sheet to an open-coil anneal in a controlled atmosphere will produce a low coercivity with a variation in properties sufficiently small that with proper mixing an average magnet can be constructed. Steel similar to that supplied FNAL will be used for the PEP magnets in 1.5-mm thick sheets. A thickness of 1.5 mm was selected since the fully decarburized sheet is available in thicknesses of 1.5 mm or less.

Punching and Shuffling. Approximately 700,000 laminations are required to fabricate the main-ring bending magnets and 370,000 for the main-ring

quadrupoles. Steel will be supplied to the vendors in sheet or coil, depending upon availability and the vendor's ability to handle coils. Experience with the models has shown that only one punching operation is necessary to produce laminations of sufficient quality.

In order to achieve uniform magnetic properties, it is anticipated that random shuffling of a half store of laminations similar to that used on the CERN ISR will be required. This, together with a random magnetic sampling of magnet steel, will produce the desired uniformity. Magnetic quality assurance measurements will be made on each magnet prior to installation in the ring.

Core Assembly. The laminations for both bending magnets and quadrupoles are stacked between thick end plates on reference surfaces in an appropriate stacking fixture. When enough laminations have been stacked, they are compressed to the desired length at a given pressure. Straps in the form of angles or straight bars are then welded to both the laminations and the end plates, after which the pressure is released. Uniformity in stacking is extremely important to insure constant magnetic properties at high fields, magnet-to-magnet.

The bending magnets are removed from the fixture and supported on an assembly table where the coil-support angles are installed.

Four quadrupole blocks are required to make one magnet. These blocks are assembled and doweled to prevent lateral motion. A V-groove punched in the laminations simplifies this assembly.

Coil Construction

Economic considerations have shown that aluminum-coil magnets are less expensive to fabricate than their copper-coil equivalent. For this reason, both bending magnets and quadrupoles have all-aluminum coils. Further advantages in using aluminum are that it is available in sufficient lengths that no joints are

necessary in any of the coils and that, unlike copper, it does not work-harden.

The insulation system proposed for the PEP magnets is the same as that used so successfully in SPEAR. In four years of operation, SPEAR has not lost a single magnet to insulation failure. The system consists of a 0.003-in. thick, 1-in. wide, adhesive-backed mylar tape half-lapped on the conductor, followed by a 0.007-in. thick, 1-in. wide, fiberglass tape butt-lapped over the mylar tape. The entire coil is ground-wrapped using a 0.007-in. thick half-lapped glass tape, after which it is impregnated in a mold under vacuum with a suitable epoxy resin.

The resin system employed in SPEAR may not be sufficiently radiation-resistant for the PEP magnets, but it can be made harder through the addition of alumina. Studies are currently under way to determine the radiation levels in the areas of the coils. PEP-109 indicated levels of 10^7 rads if a 1/8-in. thick lead shield were placed adjacent to the vacuum tank. If such a shield is used, radiation-hardened coils will not be necessary; otherwise, a hardened epoxy system will be required.

Power and Water Distribution

The main ring bending magnets and the main windings of the insertion-region quadrupoles are connected electrically in series. By winding an extra half-turn into the bending magnet coils, the bending magnets can be made to act as their own bus. Jumper cables are provided to connect the top coil of one bending magnet to the top coil of the next. After going entirely around the ring, a jump is made to the bottom coil and the circle is retraced, connecting bottom coil to bottom coil. In this manner, the net ampere turn for the bus circuit is zero.

There are nine independent series bus circuits for the quadrupoles. Air-cooled 600-V cables mounted in trays adjacent to the magnets will be used. The sextupole and wiggler circuits are handled similarly. The circuits for the steering coils are not continuous around the ring but terminate at the nearest insertion region where the power supplies are located.

The proposed magnet low-conductivity water (LCW) cooling system consists of three stainless steel pipes, one supply and a return doubled back on itself to insure that all magnets see the same pressure drop. The cooling water holes on the magnets will be sized so that at 15 GeV there will be a 20°C temperature rise and a 13.6-atm pressure drop. Each arc has its own closed LCW system with the distribution point located at the insertion utility building. The total flow capacity of each arc is 130 gpm, resulting in a heat capacity of 685 kW for a 20°C temperature rise.

Support

The magnet support system is still in the design stage. The supports must provide adjustments of three translations and three rotations, and these six adjustments will be uncoupled as much as possible. The bending magnets will be supported on stands at their points of minimum deflection.

6. Survey and Alignment

Magnet alignment errors in the PEP ring, especially quadrupole magnet offsets, can produce substantial closed orbit distortions. The purpose of the survey and alignment system is to minimize these errors so that very little beam steering will be required to store circulating beam. The long range surveying, over distances greater than about 200 meters, will be performed separately from the short range surveying.

The long range horizontal alignment will be based upon 12 survey monuments to be located by the U.S. Coast and Geodetic Survey at the ends of each long straight section. The survey will take place above ground, and the locations will be transferred down vertical shafts to monuments on the tunnel floor. The long range vertical alignment will be based upon reference levels provided by a hydrostatic level permanently installed in the tunnel.

The short range survey and alignment task consists of locating every ring magnet relative to the two nearest survey monuments. Although several short range survey methods are being considered, one method has received the most attention. This method consists of performing an optical survey using alignment lasers. First, a series of instrument stations will be located at 30 meter intervals between adjacent survey monuments. Then, since a straight line of sight will be available between adjacent instrument stations, it will be a straightforward task to locate ring magnets relative to the instrument stations. The primary advantages of using alignment lasers are high speed and low labor costs. Wherever possible, the radial survey errors will be minimized by measuring offsets to lines of sight rather than measuring small angles.

A conventional optical survey using tapes, theodolites, and alignment telescopes has also been considered, primarily as a backup to the alignment lasers. The conventional method is straightforward but its use will incur higher labor costs. Lastly, automatic surveying systems, including the use of inertial guidance, are being investigated. Such automatic systems would provide extremely high speed surveys and would drastically reduce labor requirements.

7. Power Supplies

Size of Supplies. Groups of magnets are separately powered according to their function in the ring lattice. A listing of these separate circuits is shown

in Table XII. In terms of the number of magnets and total power the largest circuit is that of the Bend Magnets and Insertion Region Quadrupoles with a total of 216 elements and 1850 kW of losses. Ten of the remaining thirteen major circuits are various quadrupole circuits; of those only the QF and QD contain more than 12 magnets around the ring. The wigglers and focusing and defocusing sextupole circuits comprise the rest of the major ring circuits.

The circuits discussed above are all independent series circuits with single or multiple power supplies inserted around the ring as necessary to make up the required loop voltage at the maximum current defined for 18 GeV operation. The number of supplies necessary is determined by the choice of 600 V dc as the maximum for each individual supply. Reasons for choosing this maximum voltage are as follows:

1. The maximum voltage to ground is then 600V, which is the standard insulation level for conductors.
2. Supplies can be powered from standard 480V distribution transformers and switchgear.
3. Thyristor and diode voltage ratings of 1500V are available and satisfy the standard 2.5X operating voltage criterion.
4. The current in the circuits will be as low as reasonable (concurrent with good magnet design practice) to reduce the conductor losses around the ring.

The number of 600V supplies to be used in each of the magnet circuits is shown in column 3 of Table XII, and their locations in column 5. For the Bend Magnet circuit the two supplies at each location are plus and minus 600V symmetrically with respect to their common midpoint. The large supplies are located only in regions 4, 8, and 12, with by far the greatest number in region 8,

in order to concentrate the control and maintenance functions to a minimum number of locations. Region 8 is the most logical for the heaviest concentration because of its nearness to the Main Control Room. The Ring power supplies will be placed in buildings along with the RF klystrons and their power supplies and the Instrumentation and Control equipment. These buildings will be above ground in the interaction regions. The ac power will come from the 13 kV ring feed system. The cooling water for the power supplies will be on the same system as that for the klystrons and their power supplies.

In addition to the basic design decisions already mentioned, i.e., minimizing the current in the buses around the ring concurrent with a maximum voltage to ground of 600 volts, another goal has been to keep to a minimum the number of different types of power supply circuitry. To this end the Injection System magnet circuits are also designed for a 600V dc maximum level. These large supplies are listed in Table XII, beneath the ring supplies already described, and the magnet systems they power are described in Section II.E. The supplies will be located at the end of the SLAC building in Sector 30. There is adequate 13 kV feeder power already in existence in the area to satisfy the injection needs.

Type of Supplies. Three possible types of Power Supply Controllers have been evaluated for the requirements described above. They are:

1. 6 or 12 pulse, phase-back, thyristor-controlled, three-phase supplies with appropriate filtering on the dc output.
2. Same as 1, plus a transistor bank in series with, or shunted across, the magnet load.
3. Chopper control by a series thyristor from a dc source, where the average output is determined by pulse-width modulation at a fixed repetition rate of at least 1 kHz.

TABLE XII

PEP Magnet Power Supplies

Ring and Injection Choppers

Magnet Circuits	Total Power Required (kW)	No. of 600V dc Choppers	Current Rating (A)	Locations	No. of Magnets per Circuit
B+Q1+Q2	1850	6	700	4, 8, 12	192+12+12
Q3	134	1	300	8	12
1QF	185	1	300	8	12
1QD	114	1	300	8	12
2QF	252	1	300	8	12
3QF	196	1	300	8	12
QF	430	3	300	4, 8, 12	48
QD	420	3	300	4, 8, 12	72
8QF	130	1	300	8	12
8QD	116	1	300	8	12
9QF	99	1	300	8	12
Wigglers	180	1	700	8	9
SD	53	1	300	8	48
SF	26	1	300	8	48
H1	160	1	200	Sector 30	15
H9S	80	1	200	Sector 30	8
H9N	80	1	200	Sector 30	8
Q1S	36	1	100	Sector 30	9
Q1N	36	1	100	Sector 30	9
Q18S	28	1	100	Sector 30	7
Q18N	28	1	100	Sector 30	7

Magnet	Total Power	No. of Circuits	Rating (V/A)	Location
Ring Corrective Elements (not choppers)				
Special Sextupoles	60	5		8
Q1, Q2 Trims	48	24	± 30/100	2, 4, 6, 8, 10, 12
Steering Coils (transitions)	160	48	± 30/100	2, 4, 6, 8, 10, 12
Steering Coils (arcs)	30	96	± 30/10	2, 4, 6, 8, 10, 12
Low Field Bends	7	24	± 30/10	2, 4, 6, 8, 10, 12
Rotated Quad	20	2	± 120/100	8
Remaining Injection Supply Requirements (not choppers)				
Q6N, S thru Q17N, S	64	16	+ 50/100	Sector 30
Bumps	40	8	+ 50/100	Sector 30
Trim T1	3	1	± 50/100	Sector 30
Vertical Bends	36	3	+ 120/100	Sector 30
Trims T2S, N thru T18S, N	12	10	± 120/10	Sector 30
V and H Steering	29	24	± 120/10	Sector 30

2817A98

It is predominantly because of the failings of phase-back thyristor control alone (1) that system 2 must be resorted to. The added transistors, with their wide bandwidth, are not so much needed because of the effects of fast ac line voltage perturbations on the magnet current as because of firing circuits imbalance and/or three-phase supply voltages imbalance. Without the transistors the attendant subharmonic ripple present in the output voltage, and therefore in the magnet current, would be out of specification. This ripple is 60 Hz, whether a 6-pulse or 12-pulse rectifier connection is used (normally 360 and 220 hertz ripple, respectively). There is also the problem of subharmonic oscillations caused by single or multiple power supplies interacting through the impedance of the ac feeder system and the firing circuits. An output voltage filter with a low enough corner frequency to reduce these effects to less than 0.01% in the current would have too slow a response to the ramp reference change in the PEP system to be satisfactory.

While the combination of transistors and phase-back thyristors solves the limitations of the individual use of either, it substantially complicates the system and increases the problems of maintenance. The cost of the combined system is also at least 30% more than the cost of the thyristor system alone.

The third choice of a chopper system retains the advantages of a phase-back thyristor system without its inherent disadvantages. Because the chopper controls the average value of the output voltage by acting as a switch in series with an unregulated dc supply, the efficiency is similar to the three-phase thyristor system. But the chopper is completely decoupled from the ac supply system by being powered from a filtered dc supply, and therefore the problem of subharmonics in the output is eliminated. Being decoupled also means that the feeder power factor remains constant over the range of operation of the chopper,

whereas in the phase-back, ac commutated system the power factor varies directly with the phase-back angle. Utilities usually start charging for reactive VARS when the power factor drops below 0.95, so the chopper will possibly save on future operating costs.

The filter on the dc supply feeding the chopper also means that high frequency noise associated with commutation will not be able to get back to the 13 kV distribution system and pollute other systems. To get the same result with an ac commutated phase-back system, the commutation spikes would have to be minimized by adding reactance, which again would result in an increased power factor and higher output regulation under load. In the output voltage of the chopper frequency components will be nominally filtered to prevent their coupling into other circuits around the ring. No filter beyond that provided by the magnet and the vacuum tank walls is actually necessary to bring the magnetic field ripple to within tolerance.

Because all the chopper circuits are designed for 600V dc operation a common power supply can be used to feed all the choppers in a given location. Thus all the choppers in region 8 will be fed from a 2.5 MW transformer-rectifier set, and those in regions 12 and 4 will each have a 1 MW set. There will be one common filter on each rectifier for all the choppers fed from it, and the rms current drawn from the capacitor will be held down by staggering the basic kilohertz repetition rate fed to the various choppers. This way there are significant savings in transformer costs over using separate units for each circuit. Ground fault detection on each individual circuit will be provided by sensing differential current between the two leads leaving each chopper.

The chopper operates by storing the energy required for commutating the series thyristor switch on a capacitor which is switched into the circuit by a

bridge of auxiliary thyristors. The schematic below shows one possible implementation among many of the basic chopper principle. The efficiency of the

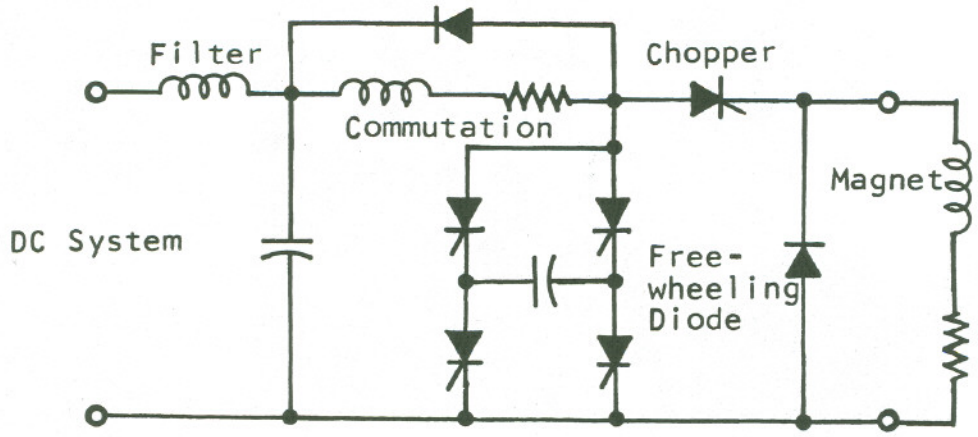

chopper system is then less (typically by 5-10%, depending on the thyristor turn-off time) than that of an ac voltage commutated system due to the losses incurred in charging the capacitor and turning off the series thyristor. A prototype chopper rated 0-300V dc, 0-1200 amps, is shown in Fig. 27.

The allowable band of tolerance about the set-point of the current reference is ± 0.01%. The maximum rate of change will be not more than 1% per second. An update every 10 milliseconds of a 14-bit DAC is then required for each reference. The currents will all be monitored with transductors capable of ±0.001% operation and with a separate calibration winding built into each of the transductors to provide the means for periodic calibration with respect to previous values and other units in the system. Feed-forward information from the unregulated dc supply voltage will be summed into the control circuit that determines the chopper turnoff time, so that ac line voltage changes will be sensed and corrected during the chopper period in which they occur.

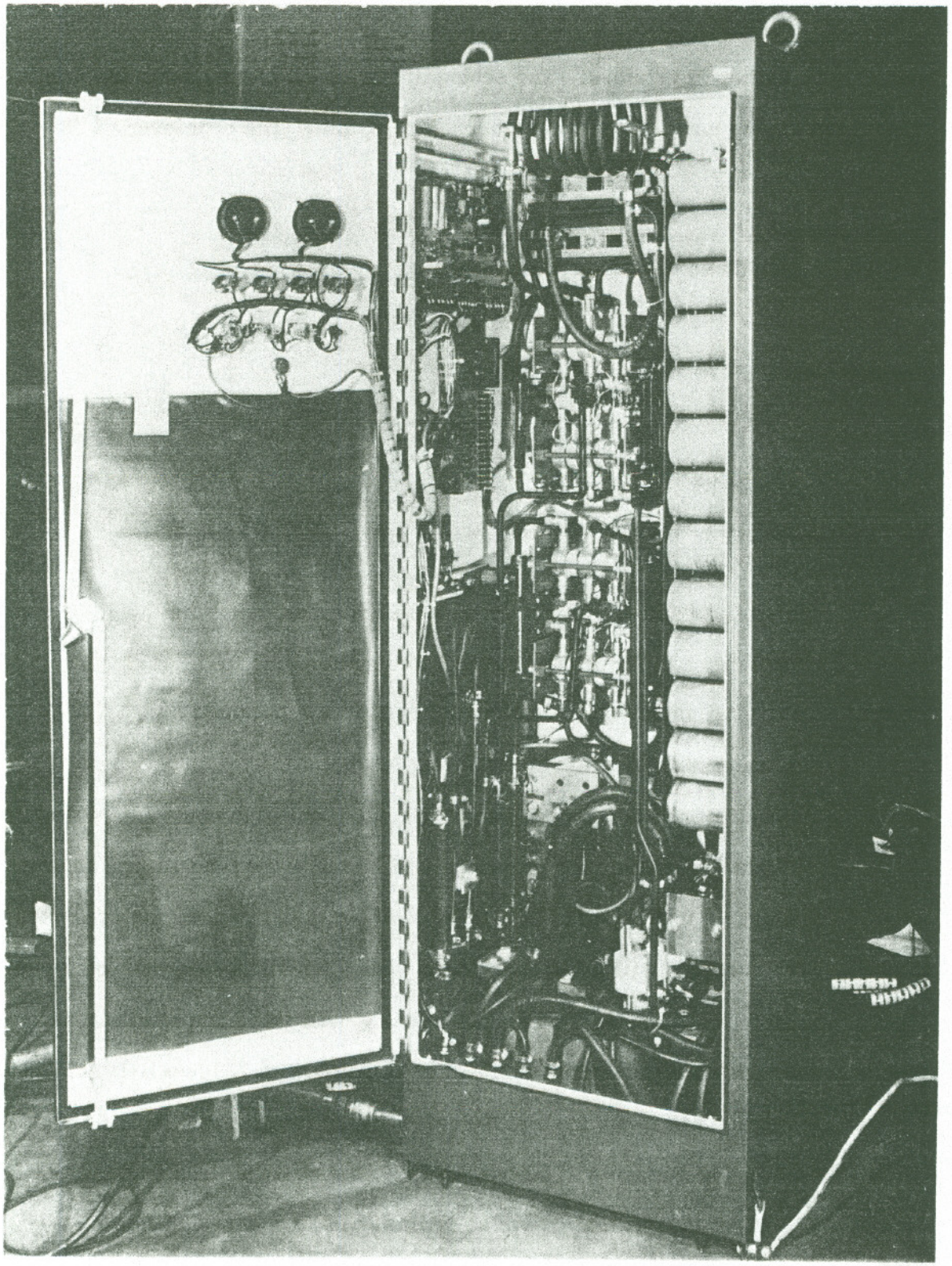

2917A71

Fig. 27--Prototype chopper for operation from a 300V dc bus at up to 1200A, with a repetition rate of 1 kHz. All the elements needed for ± 0.01% magnet current regulation are included in this package.

Small Supplies. A large number of small supplies are necessary in the Ring and Injection System for special functions such as steering, trimming, low-field bends, sextupoles, and rotated quadrupoles. The trim and steering functions are bipolar and must be adjustable through zero current. Because the loads are single windings, the requirements are well served by continuously controlled transistor actuators. Because of the trimming nature of these supplies the reversal of the polarity applied to the magnet does not have to occur rapidly and therefore a thyristor bridge in conjunction with single polarity supplies can be employed.

The various supplies and their ratings are shown in Table XII. As can be seen in column 4 there are two ranges of power supply voltages required: (1) the 30V and 50V and (2) the 120V. Again, as in the chopper systems, dc unregulated supplies will be used to supply the bulk power at the 30V and 120V level to each ring power supply location with feeders to each individual regulator supplying power as required. The 50V requirement for the injector will employ two of the 30V supplies in series (with transformer taps). Again the emphasis is on minimizing the number of different types of components used.

The transistor-actuator heat-sink and printed-circuit-board package will also be standardized. A Wakefield Heat Sink, Model 180-26 or equivalent, which holds twelve TO-3 transistors, will be used for all applications, with the possibility of "seriesing" or paralleling as necessary. This is an efficient and inexpensive heat sink which is widely available. All components other than the transistors will be mounted on a printed-circuit board which will also serve as a 100-amp emitter bus. The board is purchased with standard 2-ounce copper on one side, but with 7-ounce copper laminate on the other, and with appropriate artwork and with emitter and base pin sockets riveted directly to the

board the 100 amps can be brought to a connector at one end of the board. This system provides high reliability and ease of maintenance, along with allowing production line techniques for loading the components. Continually improving ratings in both continuous and switching transistors in the TO-3 package makes it advisable to postpone the transistor selection at this time. Opting for a standard heat-sink package, rather than a particular manufacturer's combination of heat-sink plus transistors, allows the possibility of changing transistors at some later date if an improved type comes on the market or an existing type is no longer available.

The small supplies can be set and will maintain the current setting to ±0.1%. The control and monitoring will be done with DAC's and ADC's located at each actuator.

All the large and small supplies will be fabricated from standard available hardware and mounted in standard racks. Subassemblies for protection, on-off control, monitoring, etc., will be standardized and fabricated for mounting in the racks. Water manifolds will run in trenches below the racks and hose connections will utilize quick disconnects wherever possible for easy maintenance. The 30V dc supplies available at each power supply location will also be used for control functions and conversion to 5V logic level and ± 15V operational amplifier level, making the racks free of 60 Hz ac power. Isolation of individual dc circuits will be by means of a contactor with a fuse for high-level fault conditions. Conductors coming from the bulk dc supplies and going to the magnets will be in trays located above the racks.

C. RF System

1. Layout and General Parameters

The synchrotron radiation energy radiated by a 15 GeV electron circulating once around the PEP ring is 27 MeV. Additional energy is lost due to the excitation of parasitic modes in the RF structure itself, in vacuum chamber boxes, and at vacuum chamber discontinuities around the circumference of the ring, and this energy loss is calculated to be 3.7 MeV at a circulating current of 92 mA, based on assumptions to be discussed in detail later. In addition to restoring these losses, the RF accelerating cavities must provide an overvoltage in order to insure a useful quantum lifetime. At the PEP radiofrequency of 353 MHz (chosen for reasons to be discussed in the following section), a peak RF voltage of 49 MV is required for operation at 15 GeV with 92 mA stored in each beam.

A total of 9 MW is required and it is proposed that it be supplied by 18 klystrons, each delivering a cw output power of 500 kW. In the initial installation, each klystron will feed a single accelerating section 2.1 m in length. Each section comprises five coupled π-mode cavities very similar in design to the SPEAR II cavities. Six such accelerating sections will be located initially in each of Regions 4, 8, and 12. Within each of these regions, the layout of the sections may vary. In Region 12, present plans are to install a group of three sections on either side of the interaction point. In Regions 4 and 8, all six sections will be located on the B and A sides, respectively, of the interaction point. As shown in the layout of Fig. 28, the installation will be compatible with a future expansion of the RF system.

The initial complement of accelerating sections and vacuum pumps will be installed as shown by the solid-line components in Fig. 28. The RF system may

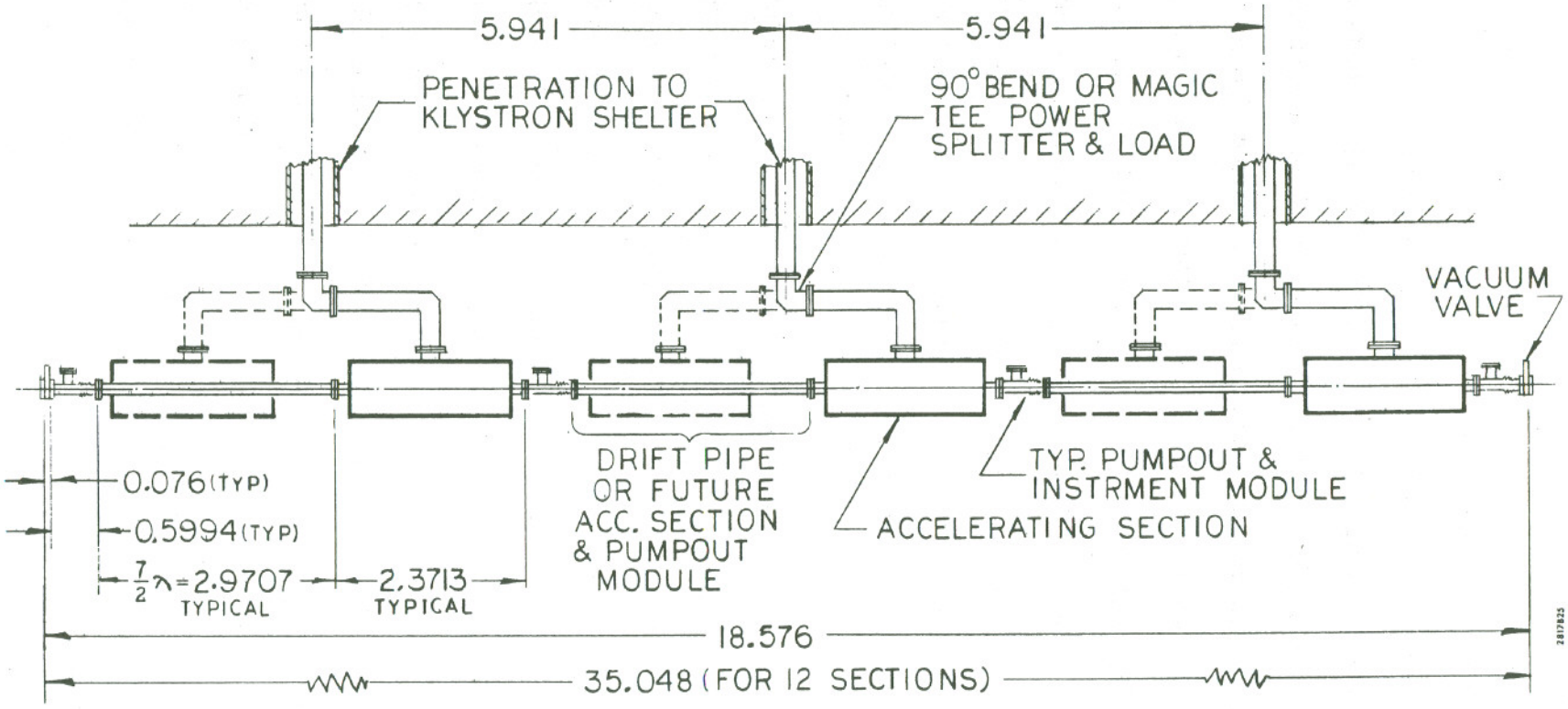

Fig. 28--RF cavity layout for Region 12. Cavity groups are twice as long in Regions 4 and 8.

be expanded at any time by increments of three additional accelerating sections so as to preserve symmetry around the ring. Orbit distortions due to either of these distributions of the RF cavities and synchrotron radiation loss have been calculated to be tolerable. As first constructed, drift pipes will occupy the spaces reserved for future accelerating sections. As these future sections are installed, a power splitter will replace the 90° bend at the foot of the waveguide penetration so that each klystron will power two accelerating sections.

The plan for providing the RF system with the capability for ready future expansion, as shown by the layout in Fig. 28, represents an improvement over the RF system as originally proposed. Although the greater flexibility provided by this plan will occasion some additional expense, such as the cost of longer RF alcoves in the tunnel, compensating cost reductions have been achieved elsewhere in the system which will permit the overall cost to remain essentially the same as in the present cost estimate.

The klystrons will be housed in shelters above ground as shown in plan view in Fig. 29. An important feature of the construction is that the klystron power supplies are located on concrete pads outside the buildings. As shown in Fig. 30, waveguides running through vertical penetrations connect the klystrons to the accelerating sections in the tunnel below.

Typical parameters for the RF system at 15 GeV are shown in Table XIII, assuming a shunt impedance given by the measured shunt impedance for the SPEAR II cavities. The attainable circulating current depends strongly on the assumptions made concerning parasitic-mode losses in the RF cavities and vacuum chamber components. As discussed later in Section II.B.8, it is estimated that a parasitic-mode loss impedance of 40 MΩ can be attained at a bunch length of 4.5 cm (twice the natural bunch length). An impedance of this order will

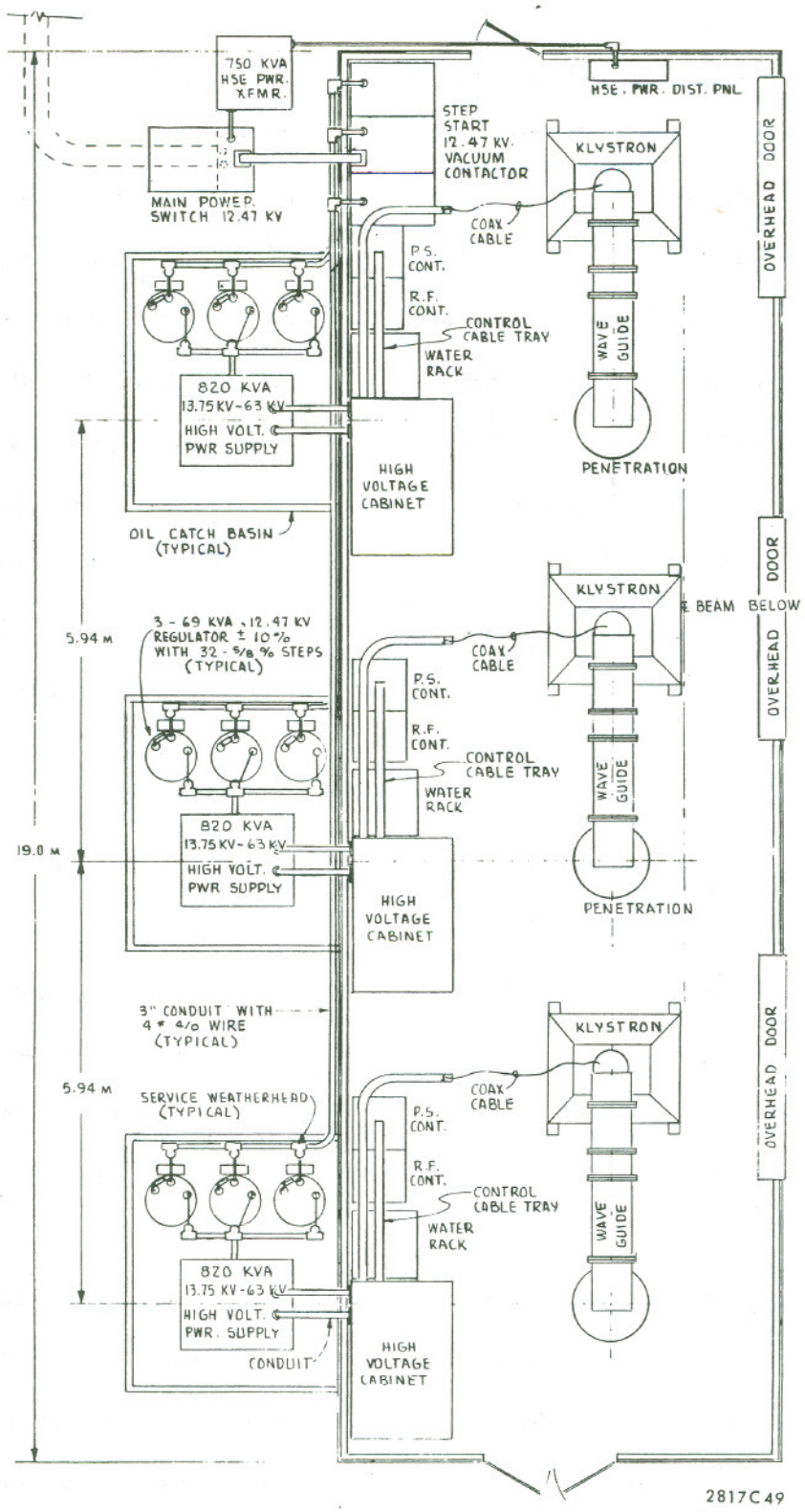

Fig. 29--Klystron housing in Region 12. In Regions 4 and 8 there are six klystrons per housing and each housing is twice as long.

0 0 0 0 4 4 0 2 9 4 7

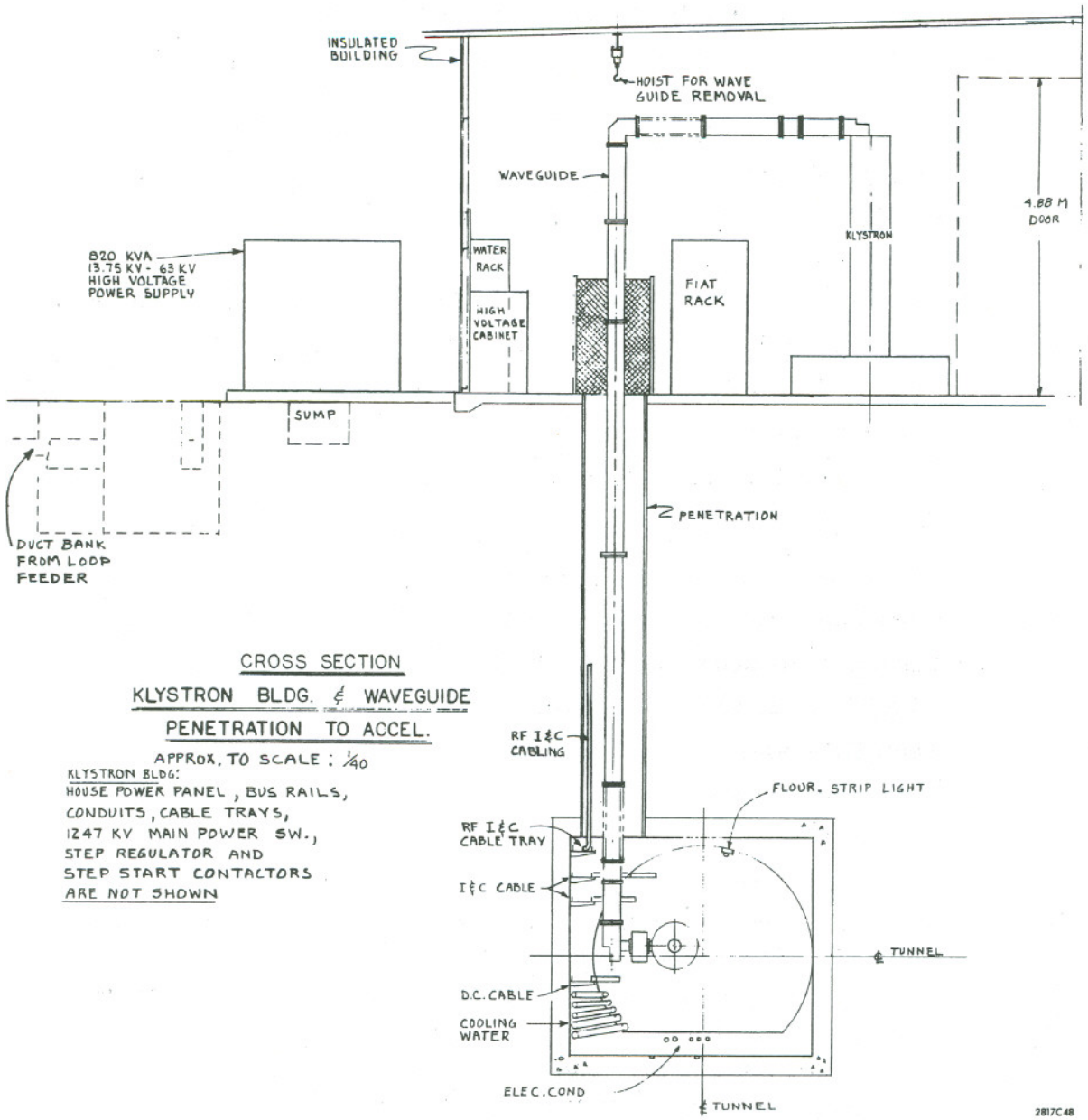

Fig. 30--RF penetration between klystron housing and tunnel.

TABLE XIII

Typical RF System Parameters at 15 GeV

Orbital Frequency	136.269	kHz
Harmonic Number	2592	
Frequency	353.209	MHz
Synchrotron Radiation Energy Loss per Turn	27.0	MeV
Higher-Mode Energy Loss per Turn[1]	3.7	MeV
Peak RF Voltage[2]	48.8	MV
Particles per Beam	4.2×10^{12}	
Circulating Current per Beam	92	mA
Synchrotron Radiation Power (both beams)	5.0	MW
Active Length of Accelerating Structure	38.2	m
Shunt Impedance for all Cavities Together[3]	715	MΩ
Fundamental-Mode Cavity Dissipation	3.3	MW
Power Loss to Parasitic Modes[1]	0.7	MW
Total RF Power	9.0	MW
Number of 500-kW Klystrons	18	
Total Power Input to RF Power Supplies	14	MW

[1] Estimated for a bunch length of 4.5 cm and a higher-mode loss impedance of 40 MΩ.

[2] For a quantum lifetime of 50 hours.

[3] The definition of shunt impedance used here is $R_s = V_p^2/P_c$, where R_s is shunt impedance, V_p is peak RF voltage and P_c is power dissipated in the cavity walls.

allow a circulating current of 92 mA per beam at 15 GeV. Since the parasitic-mode loss impedance depends on bunch length, the supportable circulating current will also depend on bunch length. There is no completely adequate theory which can give an exact prediction of the bunch lengthening to be expected in PEP. Consequently, bunch lengthening by a factor of two at 92 mA has been used in extrapolating SPEAR II results to the PEP case, using the potential-well-distortion model of bunch lengthening.[22] Should the bunch-lengthening factor be greater, the circulating current will be higher, and conversely.

2. Choice of Frequency

RF systems of early e^+-e^- storage rings operated at frequencies below 100 MHz; the SPEAR I RF system, for example, operated at a frequency of 51 MHz. Although operating at this low a frequency does have some important advantages, the shunt impedance per unit length of the cavities is on the order of only 1 MΩ/m. If the PEP RF operating frequency were chosen to be at such a low value, then the RF structure would need to be several hundred meters in length in order to attain the high peak voltage required. By using a higher frequency, as in SPEAR II, the geometric shape of the cavities can be optimized without introducing unduly large structures, and the shunt-impedance-per-unit-length can be increased significantly. The disadvantage in using a higher frequency is that the overvoltage ratio (peak voltage divided by the synchrotron radiation loss per turn) required to give a reasonable quantum lifetime also increases. Taking these two competing factors into account, it can be shown that there is a rather broad optimum for PEP in frequency region 100 to 400 MHz,[23] but biased toward the lower end of this range if parasitic-mode losses are also taken into account.

Given this optimum frequency region, then economic and engineering considerations dominate the choice of RF frequency. The structure diameter, weight, and cost increase as frequency decreases. The same is true of the available RF power sources. A careful study of the comparative advantages of klystrons vs gridded tubes was made in connection with the design of the RF system for SPEAR II.[24] It was concluded that klystrons were superior to available gridded tubes with respect to initial and annual operating costs, reliability, and expected life. Klystron size and cost are lowest at the upper end of the 100-400 MHz frequency range. These factors led to a choice of 358 MHz for the SPEAR II RF system, and similar reasoning leads to the conclusion that a frequency of 353 MHz is reasonable for PEP. This choice has the added significant advantage that the successful SPEAR II RF system becomes a model for the PEP system.

The 358-MHz SPEAR II RF system is described in Ref. 25. Installation was completed in November 1974, and operation is now routine. Colliding beams have been obtained up to 4 GeV, where the peak accelerating voltage is over 6 MV. Some of the problems encountered and the measures taken to resolve them are discussed in Ref. 25. So far they do not indicate any basic reason why this system cannot be extended to meet the PEP requirements. In summary, we feel that the experience obtained from the construction and operation of the SPEAR II RF system provides a firm basis for the design of the PEP system.

3. Structure Design

The requirement of cw operation at high energy gain, together with the need in a storage ring to minimize the space occupied by the RF system, demands an RF structure with high shunt-impedance-per-unit-length. Thus, many

of the same considerations entering into the design of the shaped-cavity LAMPF accelerating structure[26] also apply to the PEP structure. There are in addition some further special design considerations. These include the large aperture required to accommodate the storage-ring beam during injection, the need for tuning to compensate for reactive beam loading and for thermal detuning effects, and the requirement to mask some surfaces against intense synchrotron radiation. In addition, in a high-energy storage ring the RF power transferred to the beam per unit length of accelerating structure is typically much higher than in linacs. In the PEP case, for example, it may reach 100 kW/m. Taking these factors into consideration, the accelerating structure chosen for SPEAR II consists of five strongly coupled cavities operating in the π mode so as to accelerate both counterrotating beams. This structure is depicted schematically in Fig. 31 and a photograph of an accelerating section is shown in Fig. 32. The shape of the individual cavities has been adjusted to produce a high shunt impedance which, for a perfect copper surface, would be 30 MΩ/m. The coupling slots reduce this figure by about 10%. In addition, an aluminum alloy having a surface conductivity 75% that of copper was used in the fabrication of the SPEAR II cavities. Taking into account the fact that surface conductivity for real surfaces falls 5 to 10% below the theoretical predictions, a shunt-impedance-per-unit-length of about 19 MΩ/m was predicted for the SPEAR II structure. This value was confirmed both by cold test measurements and by performance in the SPEAR ring.

Modifications will be required to adapt the structure to PEP operating conditions. Of particular importance, the higher power density per unit length (a maximum of 100 kW per cavity) will require increased cooling. The nose cones, for example, will be shortened to provide shorter heat paths. Simplifications

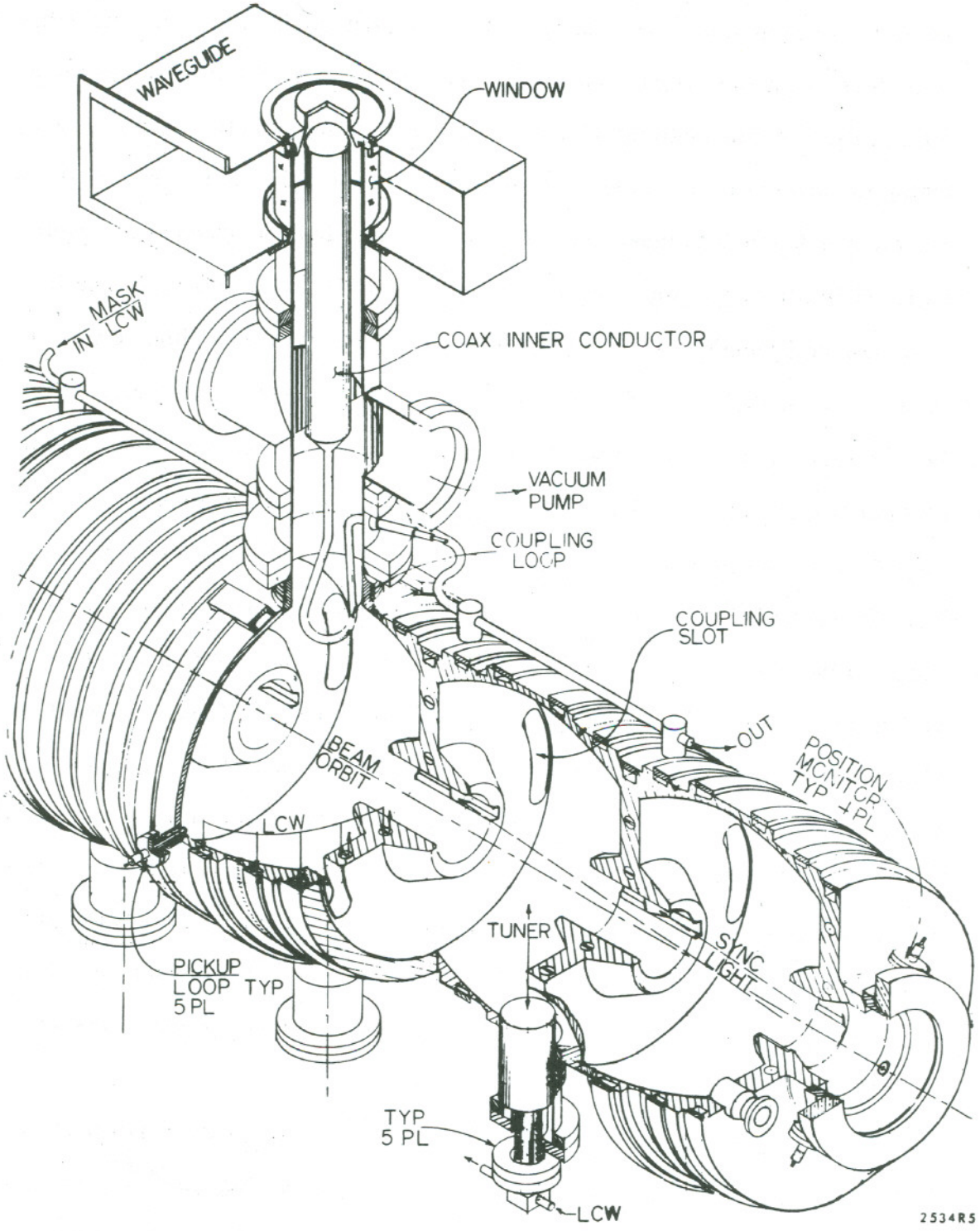

Fig. 31--Cutaway view of the SPEAR II accelerating structure.

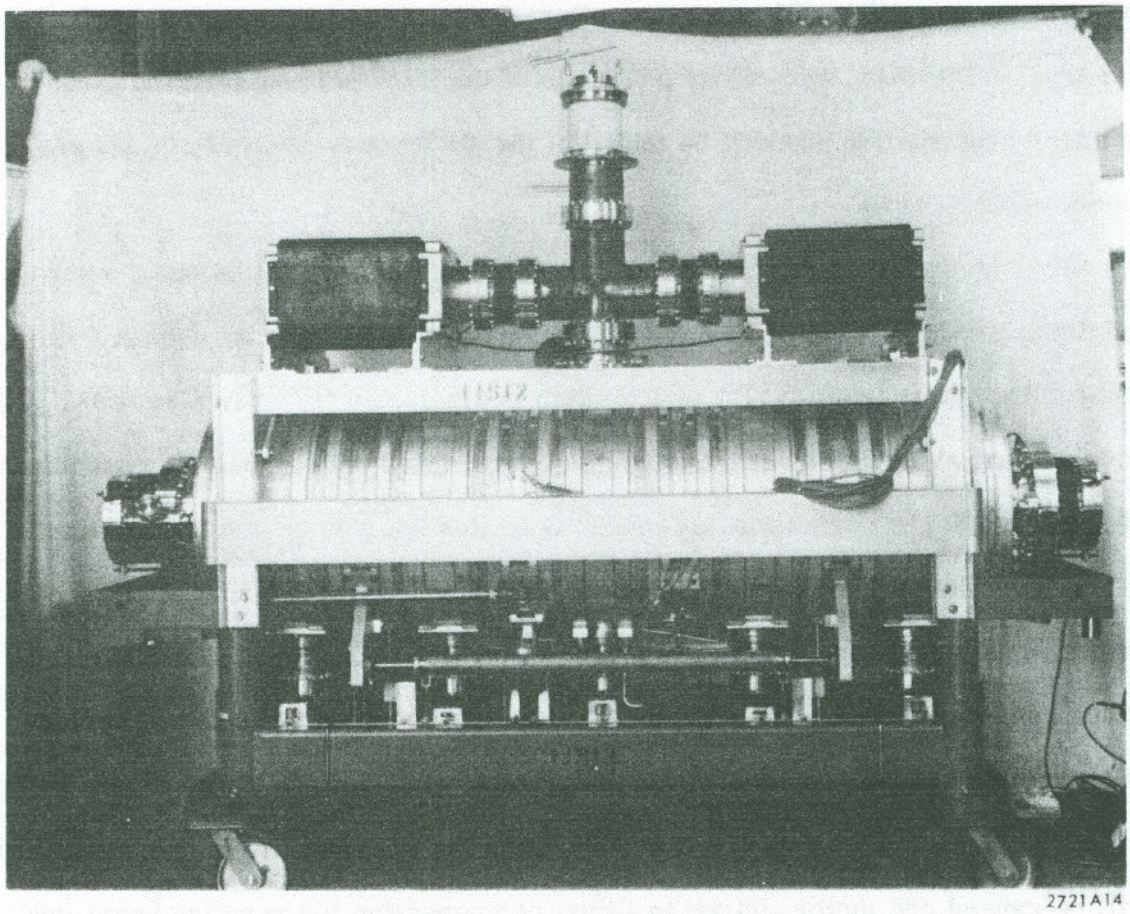

Fig. 32--Photograph of the SPEAR II accelerating structure.

will also be made in the cavity shape to permit easier fabrication. A 1/7-scale model has been built and measured as part of the PEP R&D program, and the results of these measurements indicate that there is a loss of about 13% in shunt impedance due to these modifications. On the other hand, a 1100-series aluminum alloy having higher thermal and electrical conductivities will be used in the fabrication of the PEP structure and the gain in RF conductivity (about 16%) in going to the new alloy will more than offset the loss due to changes in cavity geometry. A full size, two-cavity prototype of the modified accelerating structure is under construction and will be tested at the PEP power level of 100 kW per cavity early in 1976.

The unloaded Q of this structure will be about 30,000. At 15 GeV, where a maximum beam current of 92 mA (each beam) will be stored, the beams will extract more power from the RF source than is dissipated in the cavity walls. The accelerating structure must therefore be overcoupled with a coupling coefficient of about 2.5. The corresponding loaded Q is about 8,000 and the filling time is 7.5 μsec. The peak voltage which would be induced by the beam if all 18 accelerator structures were tuned to resonance would be about 37 MV for two circulating beams of 92 mA each. Each cell of the five coupled cells in an accelerating section will be provided with a separate tuner. Initially these tuners will be hand-adjusted to compensate for manufacturing tolerances. In operation they will be ganged and motor-driven to adjust compensation for reactive beam loading and provide stability against phase oscillations.

4. Klystrons

The need for klystrons capable of supplying 500 kW of cw RF power at 353 MHz can be met with several designs. It would be easiest simply to scale the SPEAR II klystrons, which have demonstrated an efficiency slightly greater than

55% at a power output of 125 kW. If this were done, the dc input power to each klystron would be close to 1 MW. However, in view of the scarcity and cost of power, both now and to be expected in the future, it is especially desirable to develop a very high efficiency klystron to reduce the total power consumption for the PEP RF system. Computer calculations indicate that an efficiency somewhat greater than 70% should be achievable in a 500-kW tube. The input power per tube would then be 715 kW instead of 910 kW, reducing by 3.5 MW the total installed capacity for the 18 stations. Such high efficiency is achieved by introducing a second-harmonic cavity which, at the fundamental frequency, produces sharper bunches having a greater component of RF current at the output cavity. This requires additional interaction length, and results in a klystron which is about four meters long.

An experimental tube has been built. A schematic diagram of it is shown in Fig. 33 and a photograph in Fig. 34. This experimental tube is at present being tested under pulsed conditions since it does not have a full-sized collector. In initial tests we have measured an efficiency of 63% with 60 kV on the anode. A power output of 500 kW was reached at 65 kV. The measured gain was within 1 dB of that predicted by the computer design program. By reshaping the profile of the magnetic focusing field along the tube axis, we expect that the efficiency can be increased further, approaching the design value. A full-scale klystron capable of cw operation at the 500-kW design level will be ready for testing in the spring of 1976.

Typical parameters of the PEP klystron operating into a matched load are:

Beam Voltage	62	kV	Drive Power	15	W
Beam Current	11.5	A	Output Power	500	kW
Beam Power (input)	713	kW	Electromagnet Focusing	50 at 25 A	V
Frequency	353	MHz			

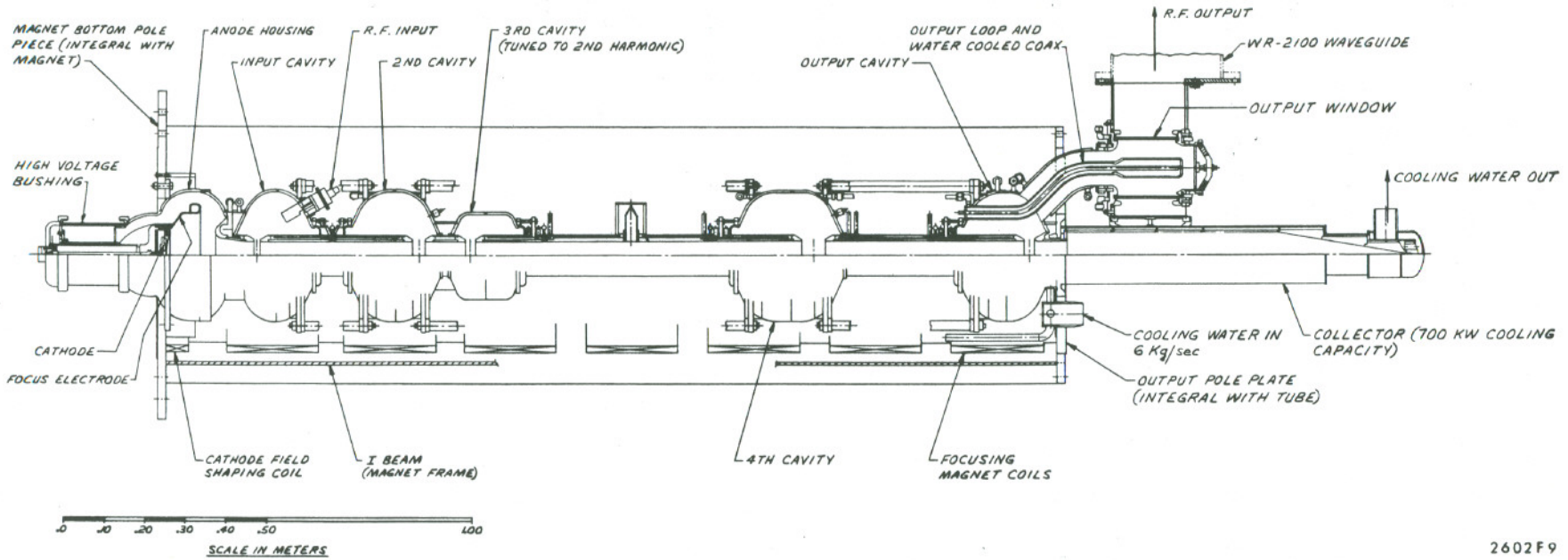

Fig. 33--Schematic diagram of the experimental PEP klystron.

0 0 0 0 4 4 0 2 9 5 1

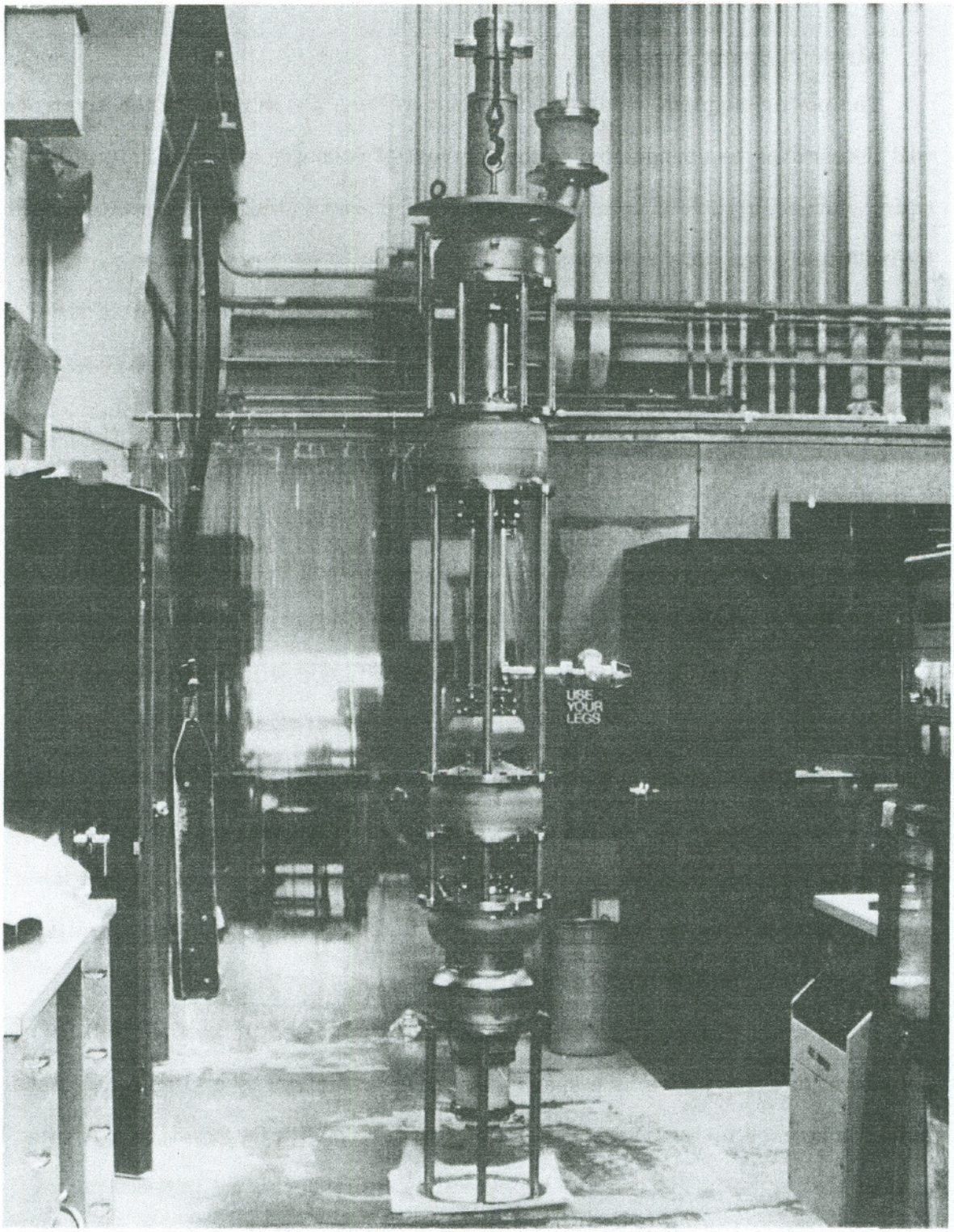

Fig. 34--Photograph of PEP prototype klystron.

5. Klystron Power Supplies

The power supplies which provide beam voltage and current to the klystrons will themselves be unregulated in the interest of economy and simplicity. However, slow regulation of voltage and adjustment over a limited range is afforded by induction regulators in series with the ac input to each power supply. These low-priced, commercially available units provide voltage control over a 20% range in 5/8% steps (Fig. 35). Fine control of the RF accelerating voltage can be obtained by varying the RF drive to the klystrons.

Since the characteristics of all klystrons will not necessarily be identical, taps on the primaries of the high-voltage transformers will permit the optimum operating voltage to be selected for each klystron when it is installed and as its characteristics change with aging. Each supply will have a maximum output of 756 kW at 63 kV and 12 A. They will be oil-filled units with a solid-state rectifier and a 6-henry filter choke contained in the same oil tank. They will be in weatherproofed housings located outdoors, as indicated in Fig. 30, minimizing the fire hazard and reducing the size of the klystron buildings. The output of each supply passes through the building wall to a high-voltage cabinet just inside, housing a one-microfarad filter capacitor, crowbar, interlock circuits, control circuits, and voltage and current metering circuits.

In the event of a klystron fault, the energy dissipated in the fault will be held down to a few joules by a spark-gap crowbar, driven by a simple thyratron pulser triggered by a current transformer in series with the klystron. A vacuum contactor at the input to the supply will simultaneously be tripped.

A prototype power supply has been delivered, installed, and tested. It will be used first in tests on a diode composed of the gun and collector from the 500-kW tube. These initial tests will, in addition to proving the capability of

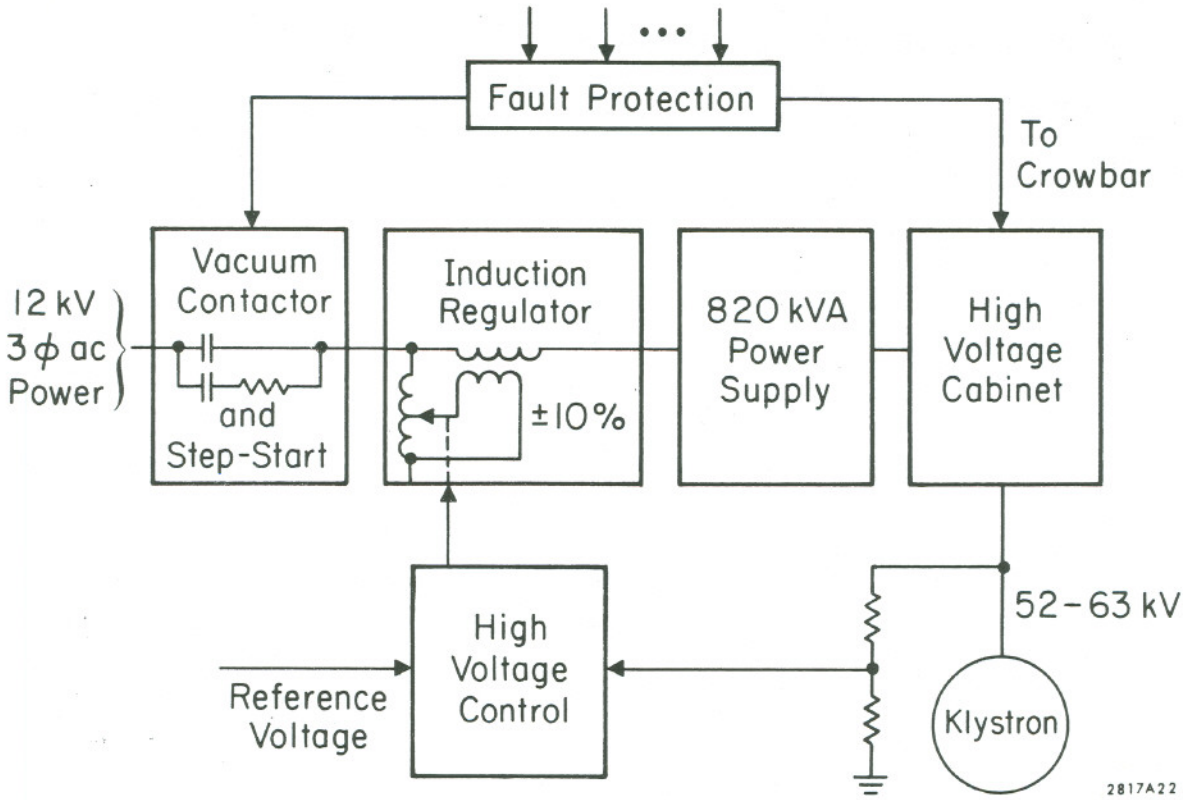

Fig. 35--Klystron power supply block diagram.

the power supply, provide a test of the gun and collector design for the full-scale tube. Tests on the first full-scale model klystron will follow.

6. Phasing and Tuning

A block diagram showing the drive, phasing, and cavity-tuning systems for the RF system is given in Fig. 36. Consider first the control system for accelerator section tuning which must be adjusted with increasing beam current. A phase bridge will accomplish this by comparing the phase of the RF power incident on the accelerator section with the phase of the field in the section. The output of the phase bridge activates the tuner drive, which moves the tuners either in or out to null the signal from the phase bridge.

Relative phasing of the accelerating sections will be carried out by first capturing a low-energy beam in the ring with a single RF cavity on. Then a second cavity will be turned on and phased relative to the first by maximizing the synchrotron oscillation frequency. This second cavity will then be turned off and a third one turned on and phased to the first in a similar manner and so on, until all the cavities have been successively phased.

In operation of the system the largest changes tending to degrade the phase alignment will be phase changes across the klystron as the beam voltage and klystron drive are varied. A phase-lock loop around the klystron will reduce these changes to acceptable levels. A stable phase reference cable will carry phase information from a pickup in each accelerator section back to a phase bridge near the RF source. At any time, the phase can be touched up to within an accuracy set by the stability of the phase reference cable by varying the input phase to each klystron until the phase of the signal from each cavity pickup agrees with a reference phase setting. The reference phase settings are those measured for each pickup immediately after the complete phase alignment has

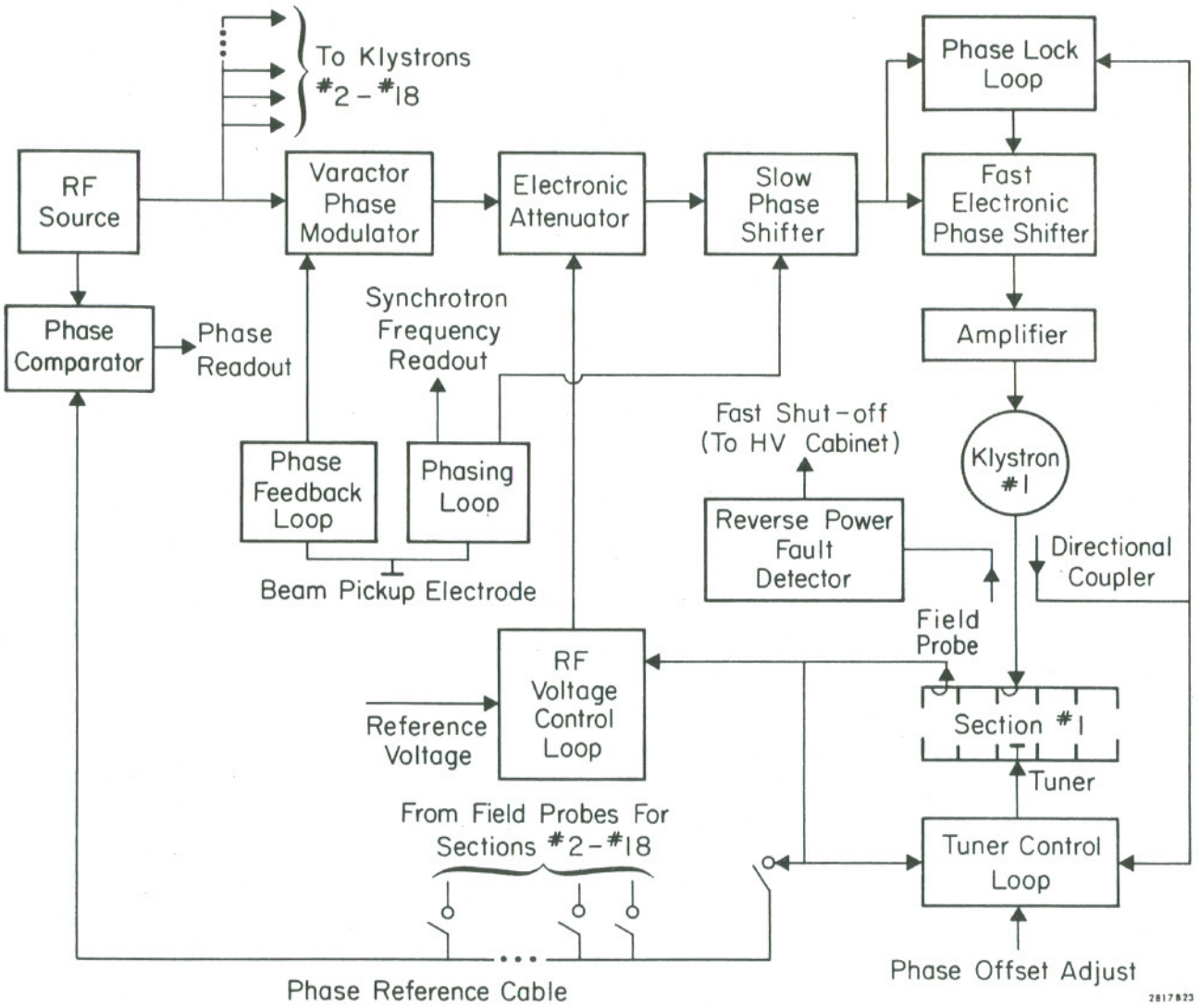

Fig. 36--Block diagram of the drive, phasing, and cavity-tuning system.

0 0 0 0 4 0 2 9 5 3

been made using the synchrotron-frequency technique described above.

7. Control of Longitudinal Instabilities

The six circulating bunches in PEP can be considered as six coupled harmonic oscillators with six normal modes. The inphase barycentric (zero-mode) phase oscillations of the bunches can probably be stabilized by appropriate tuning of the accelerator sections. Should this measure prove to be inadequate, this mode can be controlled by a feedback loop using a narrow-band phase signal picked up from the beam and fed back to phase modulators in the input drive lines to the klystrons. In order to damp the other five possible modes, one or more high-frequency cavities may be required. When such cavities are in operation, the time derivative of the voltage, and hence the synchrotron oscillation frequency, is different for each bunch. If this "splitting" of the synchrotron frequencies is sufficiently large, the bunches are effectively decoupled against longitudinal phase oscillations. This technique proved successful in SPEAR I and in other storage rings. In SPEAR II, however, no longitudinal phase oscillations of any kind are normally observed, leading us to expect that they may not occur in PEP. For this reason high-frequency cavities will not initially be installed in PEP, although provision will be made for them should the need be demonstrated.

Three potential longitudinal instabilities which can arise out of the beam-beam interaction have been suggested and studied.[27] They appear not to be significant for PEP. The first instability occurs only when the colliding beams cross at an angle, which is not the case in PEP. The second one is due to a nonzero value of η^*, the η-function at the interaction region. It places an upper limit on η^* which is higher than the value at which PEP will operate. The third instability occurs when the bunch length is large compared to the value of the β-function at the interaction region. This again will not be the case in PEP.

8. Loss to Parasitic Modes

As discussed previously, parasitic modes in the RF cavities and in vacuum chamber components lead to an additional loss of energy from the beam particles over and above that due to synchrotron radiation. Both theoretical and experimental approaches have been used to estimate the magnitude of this loss for the PEP design. Calculations are available which give the loss for the case of a closed cylindrical box, or for the case of a chain of such boxes coupled by holes on the beam center.[28] To the extent that such a disk-and-cylinder model can predict the higher mode losses for the PEP RF structure, these losses follow the relation $R(CAV) = 110 \exp(-0.43\,\sigma_z)M\Omega$ for the 90-cavity structure proposed for PEP, where R is the higher mode loss resistance and σ_z is the bunch length in cm.

An experimental measurement on SPEAR II gives an indication of the losses that might be expected for the "incidental" vacuum chamber cavities.[29] By subtracting the calculated higher mode losses for the RF cavities from the total measured loss for SPEAR II, an expression is obtained for the vacuum chamber loss alone. This loss, when scaled to the PEP circumference, assuming the same loss per unit length of vacuum chamber as in SPEAR II, gives $R(VAC) = 915 \exp(-0.3\,\sigma_z)M\Omega$. However, in designing the SPEAR vacuum chamber, no effort was made to reduce the number or magnitude of the discontinuities which determine the parasitic mode loss. After reviewing the construction of the SPEAR vacuum chamber, it was felt that it was not unreasonable to expect that these losses could be reduced by a factor of 10. Adopting this as a criterion, we add one-tenth of the vacuum-chamber loss obtained from the preceding expression to the calculated loss for the RF cavities and a total parasitic mode loss of $R(TOT) = 200 \exp(-0.36\,\sigma_z)M\Omega$ is obtained for PEP.

Using this expression for parasitic-mode loss, the circulating current for PEP can be calculated as a function of energy. The calculation is described in detail in Ref. 30 and uses parameters appropriate to the lattice described previously in Section II. A. Results are shown in Fig. 37 for three different lengths of RF structure. The solid line gives the stored current capability for the 38 m long structure proposed for initial installation. Results are also shown for RF structure lengths which are twice and four times as long. In all three cases the stored current capability is 92 mA or more at 15 GeV; the advantages of the longer systems lie in a savings in RF power at 15 GeV and below and a higher stored-current capability above 15 GeV. For a stored current of 10 mA per beam, the energies reached by the 38 m, 76 m, and 153 m systems are seen to be 18.0 GeV, 19.8 GeV, and 21.6 GeV, respectively.

All stored currents shown in Fig. 37 have been calculated for bunches which are lengthened by a fixed factor of two over the natural bunch length, which is the estimated bunch lengthening at the design current level. At lower currents, the actual bunch lengthening will probably be less, the parasitic-mode losses will be somewhat greater, and the stored currents will be slightly less than shown.

0 0 0 0 4 4 0 2 9 5 5

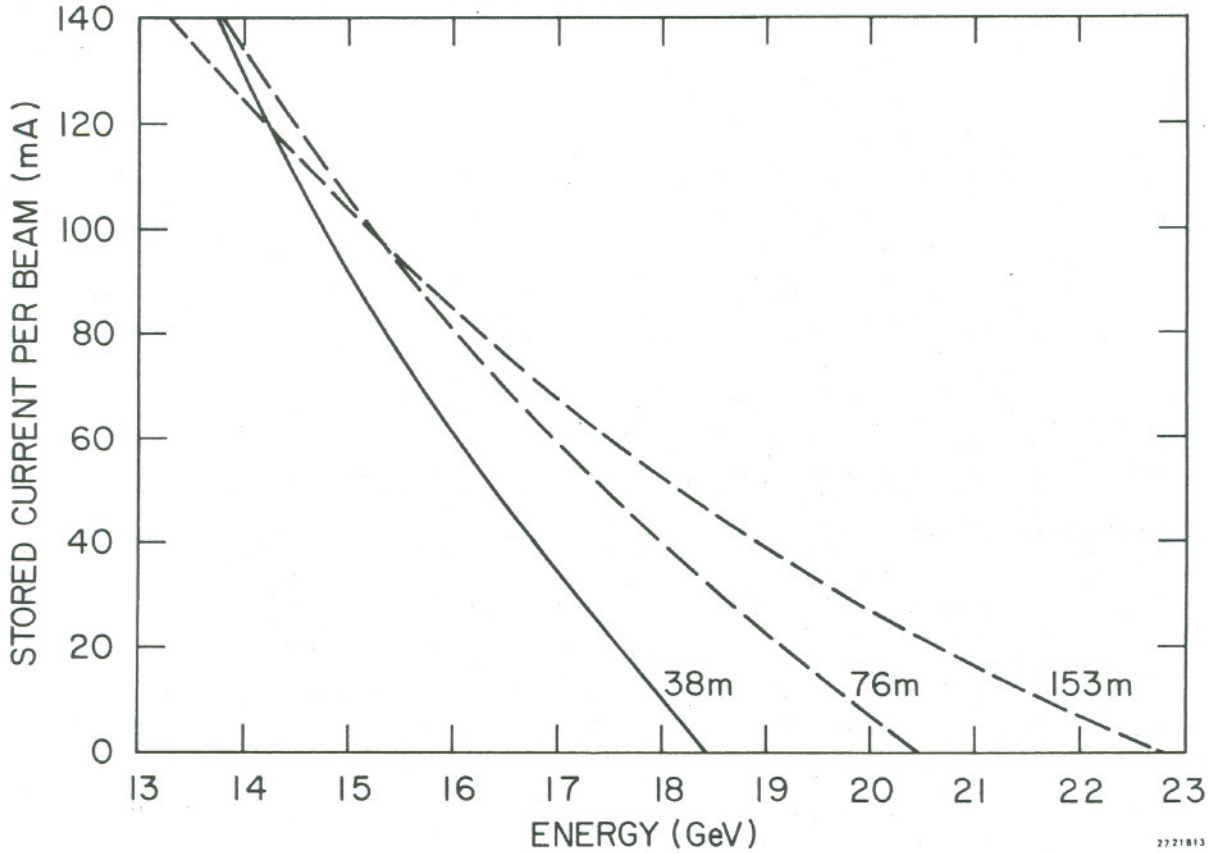

Fig. 37--Stored current per beam for several lengths of RF structure.

D. Vacuum System

1. Introduction

The vacuum system proposed for the PEP storage ring will be similar to the successful SPEAR design, which has proven so reliable and satisfactory, both in construction and operation.[31] Any modifications are due primarily to the increased synchrotron power radiated per unit length, which tends to increase radiation-induced gas desorption. All design parameters and system features are dictated by the pressures required to achieve adequate beam lifetimes and acceptable background rates in the interaction region areas.

2. Vacuum Chamber Construction

The vacuum chamber in the bending magnets will be 14 meters long (Fig. 38), of extruded 6061-T4 aluminum with an internal cross section as shown in Fig. 39. The inner cross-sectional area is designed to accommodate the beam-stay-clear region required by beam dynamics and to allow for unavoidable errors in mechanical positioning. The synchrotron-radiation-absorbing wall will be approximately 10 mm thick. As shown in Fig. 38, a regular cell contains one bent aluminum extrusion and one instrument module. The stainless steel instrument module will accommodate an expansion bellows, position monitors, vacuum gauges, synchrotron radiation masks, holding pumps, and other components.

The segments of the vacuum chamber are joined together with standard vacuum flanges, all of which will be of stainless steel with copper gaskets. The largest flanges are the holding pump flanges and the 250-mm flanges at the ends of the chambers. They will be attached to the aluminum chambers by means of transition sections made of the explosively bonded aluminum-stainless steel sandwich material used in SPEAR, where the system has reached base

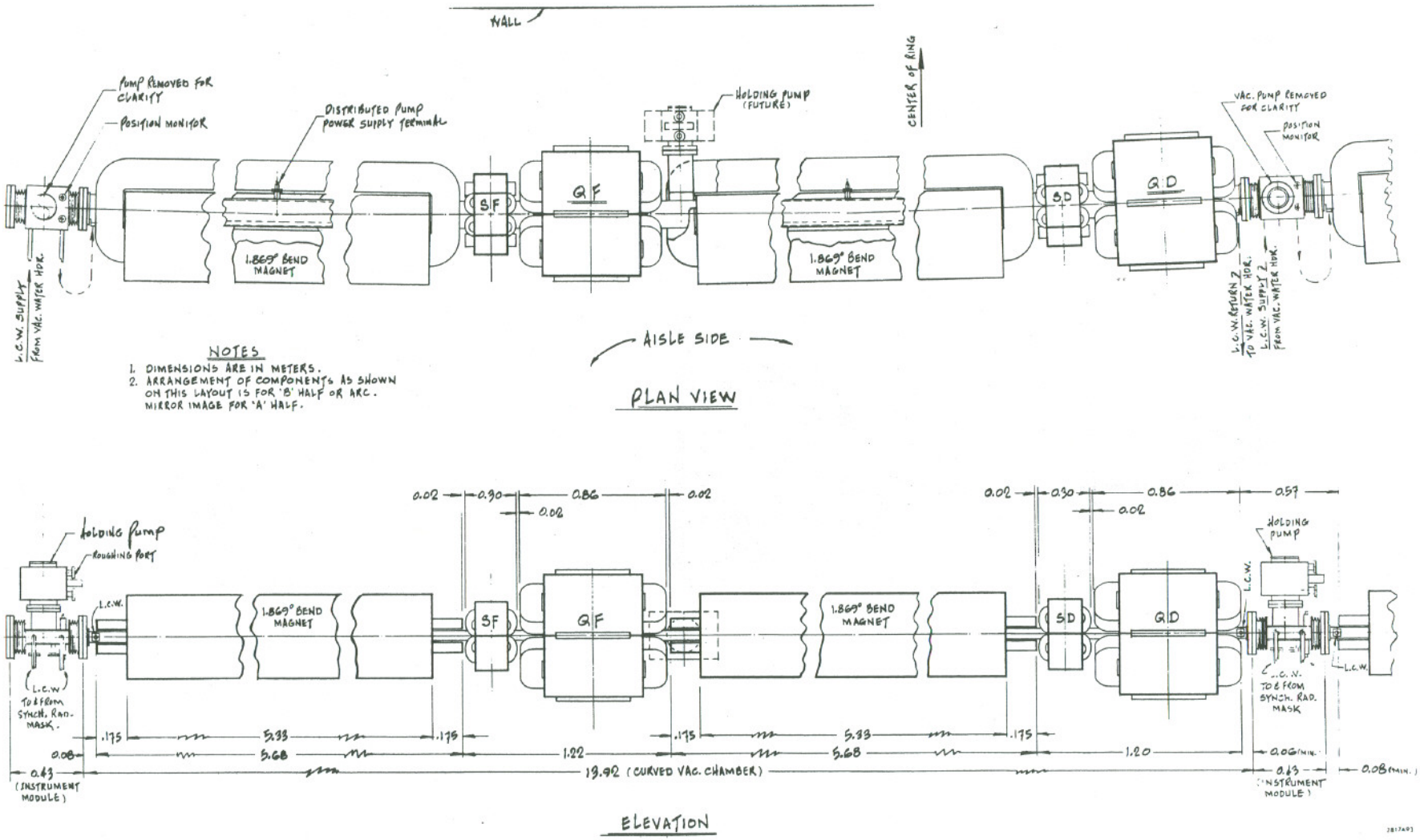

Fig. 38--Standard cell bend vacuum chamber module.

0 0 0 0 4 0 2 9 5 6

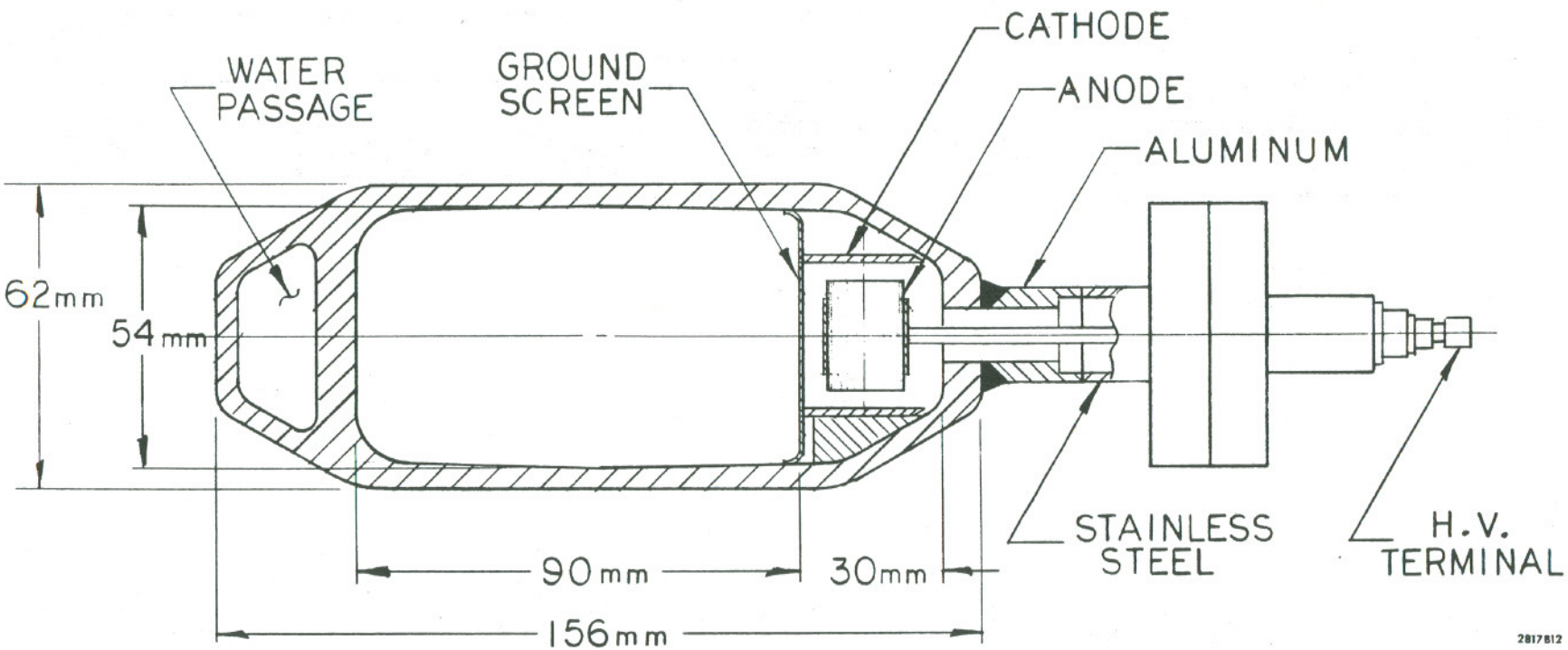

Fig. 39--Cross section of bend magnet vacuum chamber.

pressure levels lower than 2×10^{-10} Torr without any in-place bakeout and with no detectable leaks.

In view of the concern regarding the higher-order-mode losses evidenced at SPEAR,[29] changes and discontinuities in vacuum chamber cross section will be held to a minimum. The individual sections of vacuum chamber will be continuous through two bend magnets and two quadrupoles, and mesh screens will mask the beam from unavoidable abrupt changes in chamber cross section, caused, for example, by bellows and pump ports.

3. Synchrotron Radiation

The spectral energy distribution of the synchrotron radiation is shown in Fig. 40. The critical energy at 15 GeV is 45.4 keV with a considerable fraction of the photons having energies above 80 keV. In the region below 40 keV, the photoelectric process dominates the attenuation of photons in aluminum; hence almost all the power at these photon energies is absorbed in the chamber wall. Above this photon energy, attenuation by Compton scattering begins to dominate. Calculations show that many of these photons are scattered out of the chamber wall with energies above 3 keV carrying away about 40% of the radiated synchrotron power.

One of the major factors determining the vacuum system design is the thermal load which must be dissipated by surfaces subject to intense synchrotron radiation. Design criteria must be conservative to reduce the danger of a burnout, and a resulting water-to-vacuum leak. Therefore, for design purposes of the PEP vacuum system, we assume that all the synchrotron power is absorbed in the walls and masks even though some escapes the system.

At 15 GeV with 92 mA stored in each beam, the total power radiated per beam will be 2.5 MW. The design power distribution for the vacuum chamber

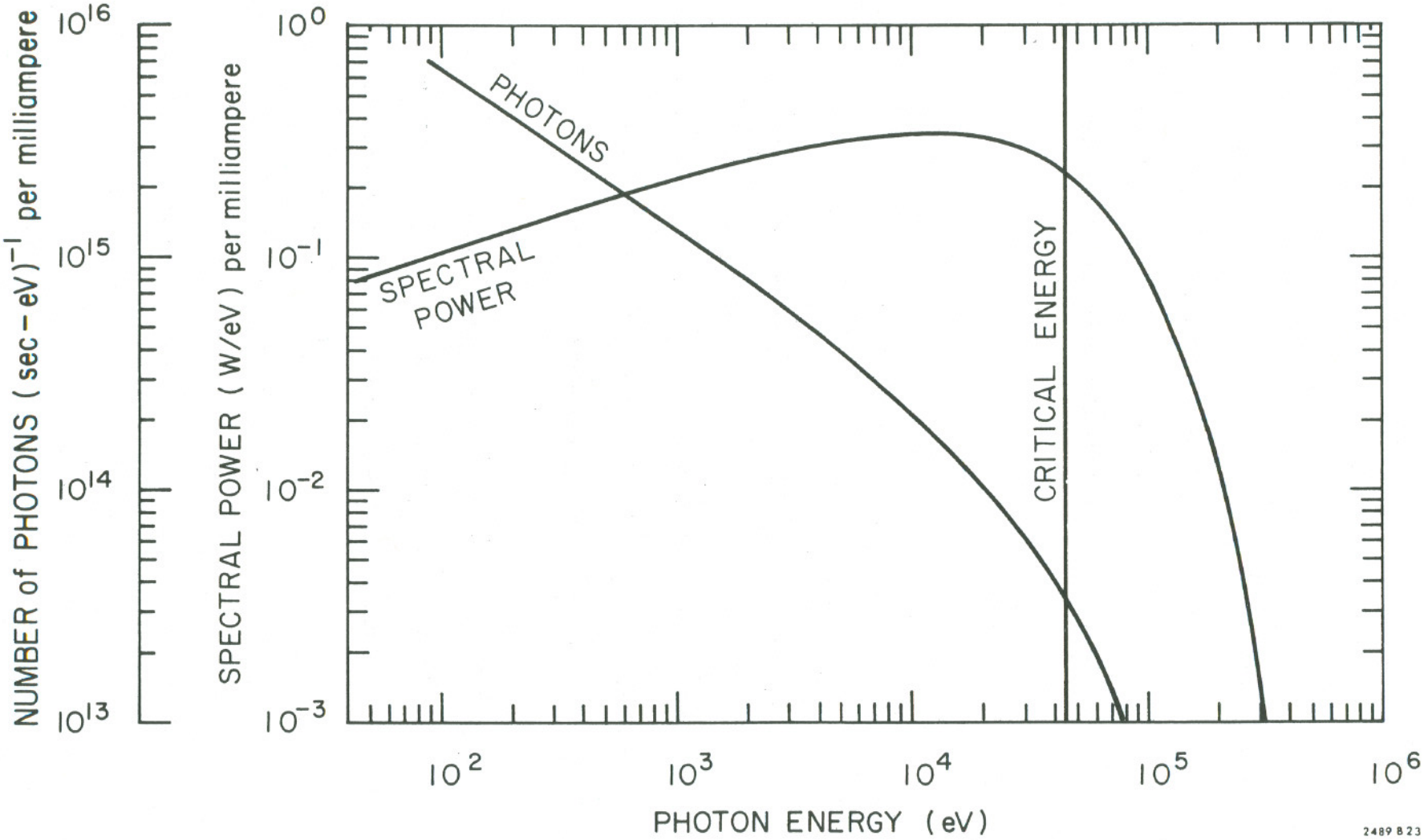

Fig. 40--Photon and power spectrum of the synchrotron radiation at 15 GeV.

geometry in a main bending cell is plotted in Fig. 41. The maximum linear heat flux for two counterrotating beams is about 46 W/cm. These values include a 10% margin for safety above the total radiated power.

Heat fluxes in the zones adjacent to the wiggler magnets will be particularly high, the maximum being 115 W/cm as shown on Fig. 42. This flux is based on a maximum synchrotron radiation power loss of 141 kW/beam, for each of the wiggler triplets required for beam size control. See Fig. 10. Special absorbers will be required in these regions.

The main gas load is due to synchrotron-radiation-induced desorption, which is a function not only of the machine energy and stored current, but also of the condition and history of the irradiated surface. The crucial measure of gas desorption is the pressure rise when beams are stored in the ring. When the first beams are stored, the initial rise will carry the pressure two or three orders of magnitude above the base pressure. Continuous exposure to synchrotron radiation will "condition" the surfaces and then the pressure rise will decrease. The total synchrotron-radiation-induced gas load for the storage ring is estimated by extrapolation from SPEAR to be on the order of 10^{-5} Torr ℓ/mA-sec at 15 GeV, after a reasonable period of conditioning.

4. Vacuum Pumps

The vacuum system is conductance-limited in the bending-magnet chambers, where most of the outgassing occurs. Here, we will use the same type of distributed sputter-ion pumps developed and used for SPEAR. These pumps are rated at 160 ℓ/sec per meter of pump length. Commercially available 100 ℓ/sec ion pumps will be mounted at every second quadrupole, and will maintain the system at a base pressure of 1×10^{-9} Torr without a stored beam.

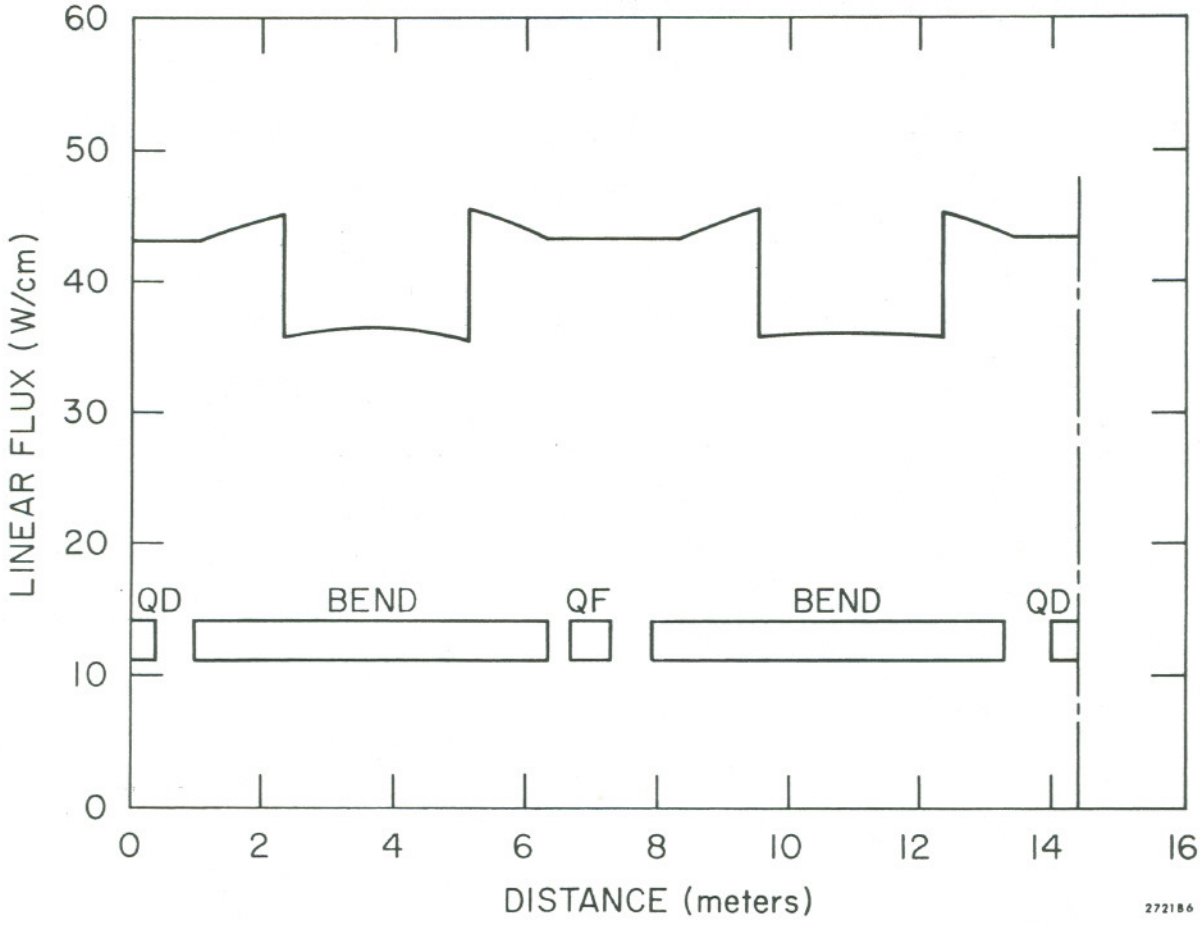

Fig. 41--Synchrotron radiation power distribution in a cell at 15 GeV.

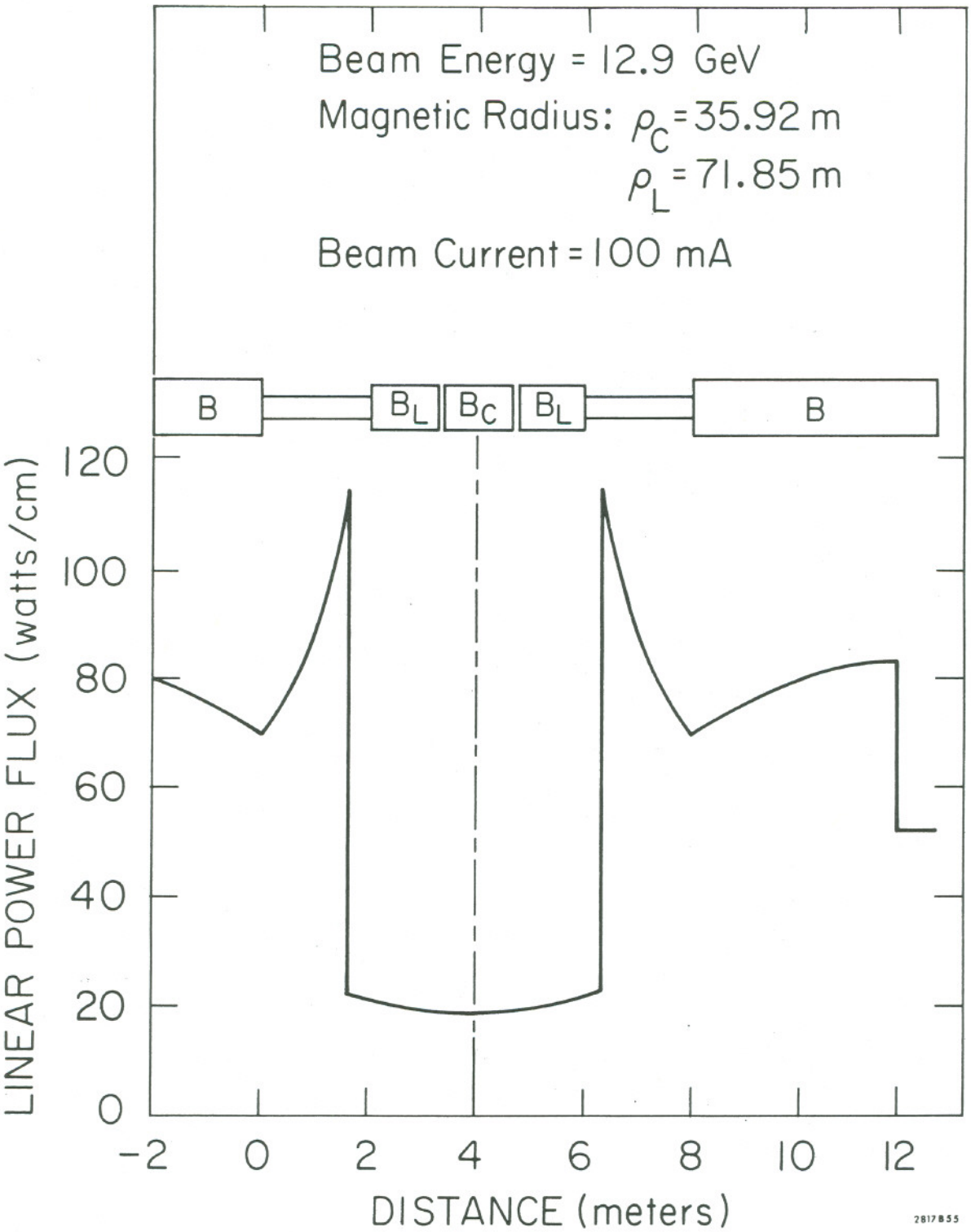

Fig. 42--Synchrotron radiation power distribution in the wiggler magnets.

With two 15-GeV, 92-mA beams circulating, the calculated pressure distribution is as shown in Fig. 43. Based on the above estimate for the total gas load, the average pressure will be on the order of 2.2×10^{-8} Torr. We are studying the possibility of future installation of additional 100 ℓ/sec pumps, to reduce the average pressure to 1.0×10^{-8} Torr. See Fig. 43.

5. Instrumentation, Valves, Controls, etc.

Isolation valves, vacuum gauges, and blanked-off pump ports are incorporated in the design to make pumpdown easier, to isolate sections as protection against accidental venting-to-air, and to facilitate diagnostics. There will be a nude pressure gauge in every fourth cell. Four inline, all-metal valves will be installed in each arc and can be actuated manually, either locally or from the Control Room, or automatically upon any indication from the vacuum gauges of abnormal pressure rise. Ports with all-metal right-angle valves will be installed in each instrument module. They will be used for pumpdown connections, installation of mechanical or thermocouple gauges, diagnostics, and venting. Pumpdown will be accomplished by a combination of trapped mechanical pumps and cryosorption pumps.

6. Cooling Water

Based upon the distribution of synchrotron radiation per cell as shown in Fig. 41, the maximum heat flux is 46 watts/cm. The temperature differential across the water-cooled wall of the chamber at this flux is approximately 45°C, and the temperature differential across the surface film in the water is 26°C. Water will be supplied at 30°C and the total water flow for the storage ring will be 220 ℓ/sec to hold the bulk temperature rise to 10°C.

The thermal conditions given above determine the thickness of the water-cooled web of the vacuum chamber and the area of the cooling water passage.

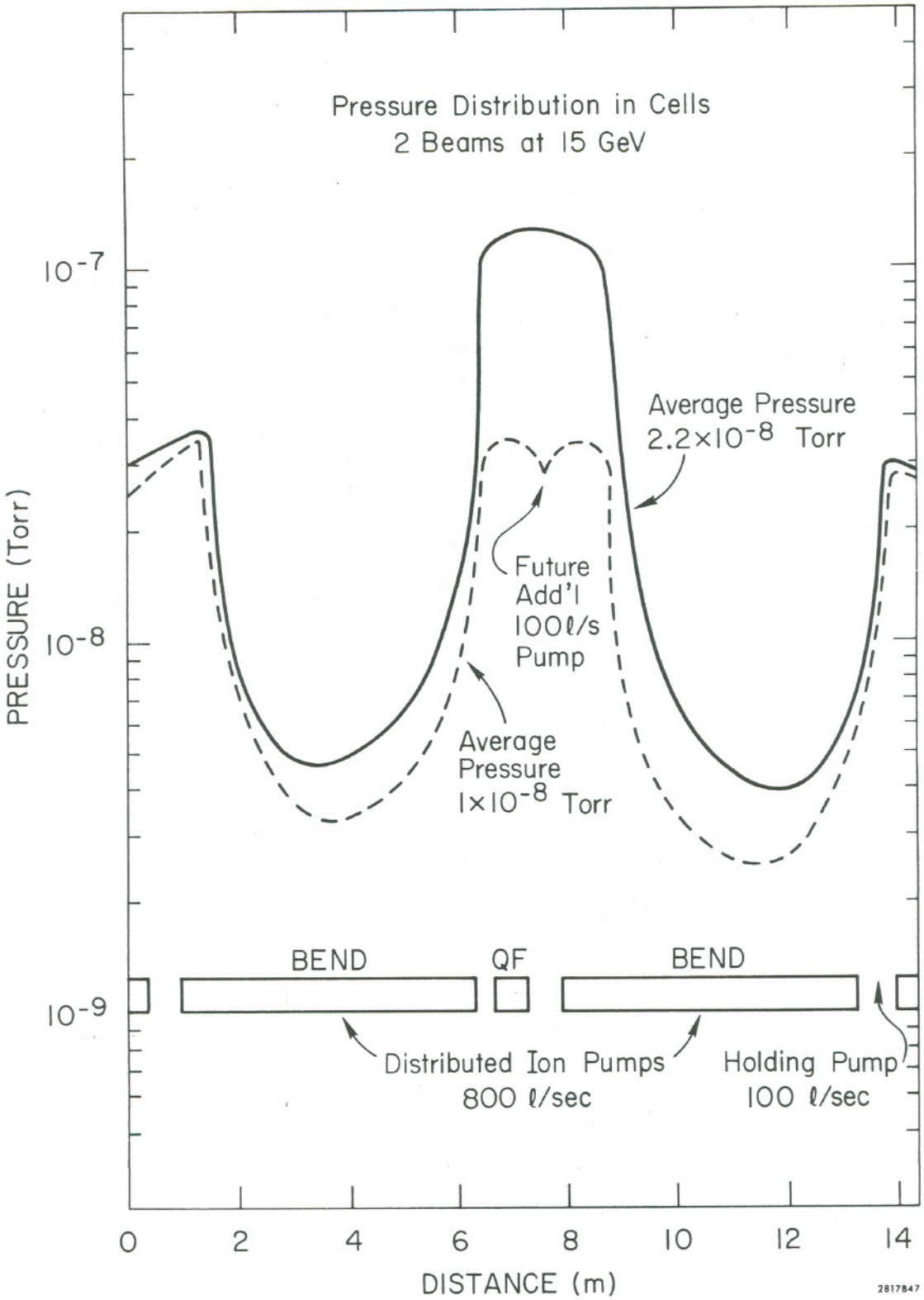

Fig. 43--Gas pressure distribution in a cell at 15 GeV.

A supply-water pressure of 17 atm, with a differential pressure drop of 13 atm through the fourteen meters of cooling water passage, will provide the flow without exceeding the allowable stress in the cooled web.

Figure 44 shows a conceptual design of the instrument module, which includes the pump port, position monitor, synchrotron-radiation mask, and ports for pumpdown and instrumentation. The copper mask, brazed to the stainless steel cooling tubes, will average 3 cm in thickness. For the configuration shown, the maximum local water temperature will be less than $100^{\circ}C$, and the maximum local metal temperature will be less than $250^{\circ}C$.

Due to the intense heat fluxes and the associated heat transfer problems, the vacuum chamber cooling water system must be an independent high-quality system.

7. Insertions

The vacuum chambers for the insertion regions will be fabricated mostly from 300-series stainless steel tubing. The initial design of the insertions, where, in contrast to the arcs, the main gas load is due to thermal outgassing, will provide for an average pressure of 5×10^{-9} Torr, primarily of gas with mass 28. The chambers will be provided with ports to simplify the addition of pumps adequate to maintain an average pressure of 5×10^{-10} Torr of mass 28 gas if experimental conditions require it.

Experience at SPEAR has shown that a large number of high-energy photons can be scattered or transmitted into the interaction areas requiring collimators to shield off extremely high backgrounds. To abet the low-field magnets and the bend magnets already mentioned in Section II. A. 9, a pair of high-Z masks, one movable and the other stationary, will be located at the entrance of each interaction region. These masks will be water-cooled.

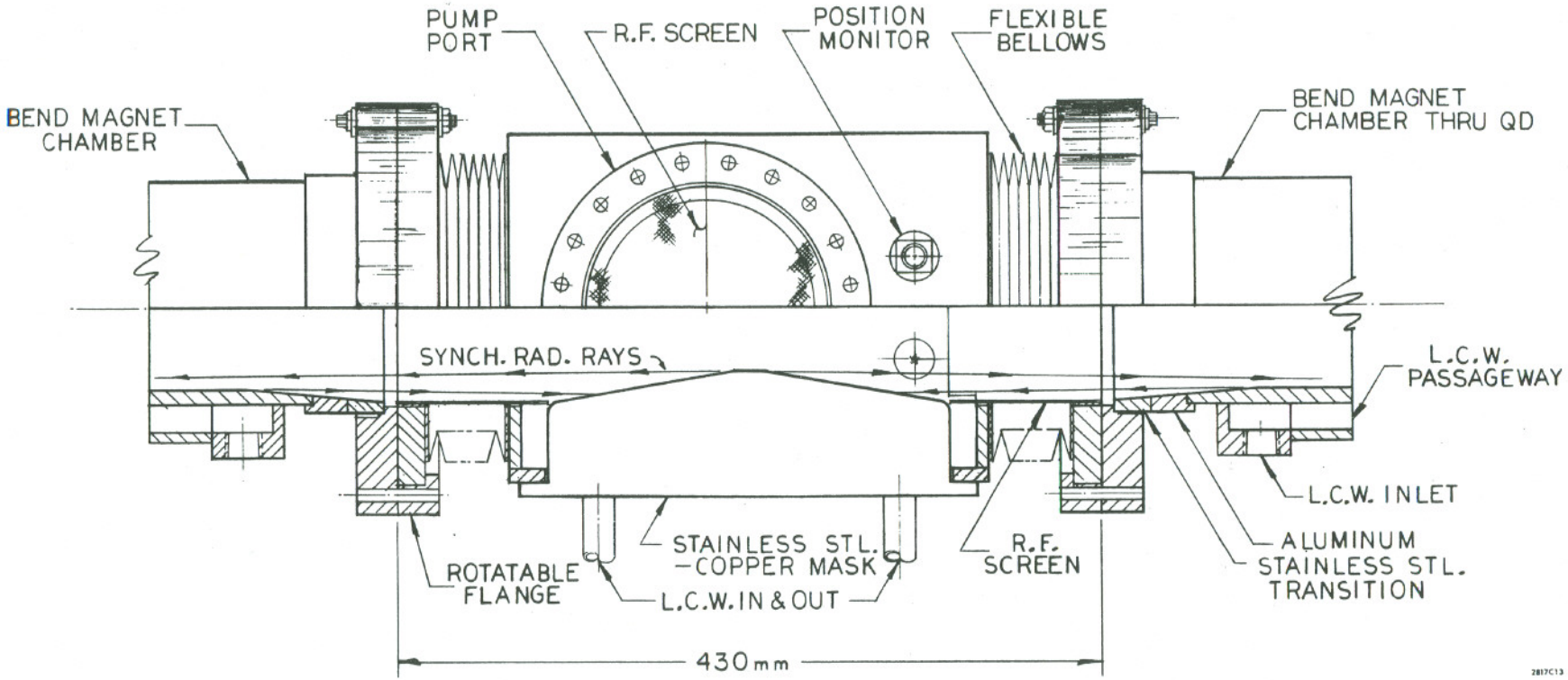

PLAN VIEW
INSTRUMENT MODULE

DJ-2030 | RO

12-15-75

Fig. 44--Conceptual design of the instrument module.

0 0 0 0 4 4 0 2 9 6 1

8. Bakeout

The extruded aluminum vacuum chambers in the arcs will be baked out by circulating hot water (185°C) through the cooling water passages. The bakeout mantle for the chambers will consist of 4 mm of insulating material covered with glass tape and insulating paint. Calculations show that the transverse temperature difference across the width of the chamber will be 18°C and the water flow required for the bakeout will be one ℓ/sec per chamber at 185°C and 18 atm. All chambers will be baked to a temperature of 185°C to 200°C prior to installation in the ring.

The instrument-module chambers and the chambers in the insertions will be wrapped with electrical heater tapes and sufficient insulation to achieve a bakeout temperature of 200°C. Bakeout temperatures will be monitored by the use of remotely read thermocouples.

E. Injection System

1. Requirements

The injection system transports the electron and positron beams from the two-mile linear accelerator and switches them onto stable orbits within the vacuum chamber of the PEP ring. The SLAC beams have the following parameters:

Energies	4 to 15 GeV
Momentum width	± 0.5%
Emittance, positrons	0.2 π (15 GeV/E) mm-mrad
Emittance, electrons	0.02 π (15 GeV/E) mm-mrad
Pulse length	1 ns
Particles per pulse	1.3×10^8 positrons, and 1.3×10^9 electrons
Repetition rate	up to 360 pps

2. Transport System

The transport system has been designed to transmit a momentum width of ± 0.8% with a resolution of at least ± 0.3%. The magnet apertures are determined largely by the momentum passband and resolution requirements. The monoenergetic emittance of the SLAC linac is easily transmitted and is only of secondary importance in determining the required apertures in the transport system.

For reasons of cost coupled with the relatively modest momentum resolution demanded of the system, a simple periodic FODO array of identical quadrupoles with interspersed bending magnets is selected as the design basis of the system. The horizontal aperture requirements are uniquely determined by the spacing ℓ between quadrupoles, the total angle of the bend, and the required momentum pass-band. For the vertical apertures the transmitted monoenergetic

emittance of the beam is determining. The required apertures are ± 25 mm for the "good" field region of the quadrupoles and 25 mm for the total bending-magnet gap.

For the periodic FODO quadrupole array, the phase shift per unit cell (length, 2ℓ) is chosen to be 90°. It follows, then, that the monoenergetic matrix transformation between any two positions separated by a distance of 4ℓ is $-I$ (the negative unit matrix). Because of this, each 360-degree-phase-shift segment of the system will be achromatic if, for every $\Delta\alpha$ of bend angle inserted at any position s there is an equal $\Delta\alpha$ of bend inserted at a position $(s + 4\ell)$.

The proposed design is illustrated in Fig. 45. The total system consists basically of three 360° achromatic segments,* the first two bending in an approximately horizontal plane and the last in the vertical plane. The plane of the nearly horizontal segments is rolled a few degrees about the initial linac beam axis so as to carry the beams down to the lower elevation of the storage ring.

The distribution of bending magnets has been selected for practical reasons consistent with the above rule for achromaticity. In the first two segments, the bending magnets are distributed as shown because of two dominant considerations: first, that there are "missing" magnets to simplify transporting the beam through existing SLAC concrete walls, and, second, that the first and second achromatic segments are placed in mirror symmetry so as to provide five quadrupoles (28Q6 through 28Q10) in the achromatic region between the two segments to adjust the monoenergetic beam phase ellipses to match the various possible PEP injection configurations. In addition, two appropriate quadrupoles (e.g., 28Q12 and 28Q16) in the second 360° segment, separated by a minus unity transformation, are varied in the opposing sense so as to vary $\eta' = dx'/d(\Delta p/p)$ at the injection point

*In this section the term 360° will refer to phase shift.

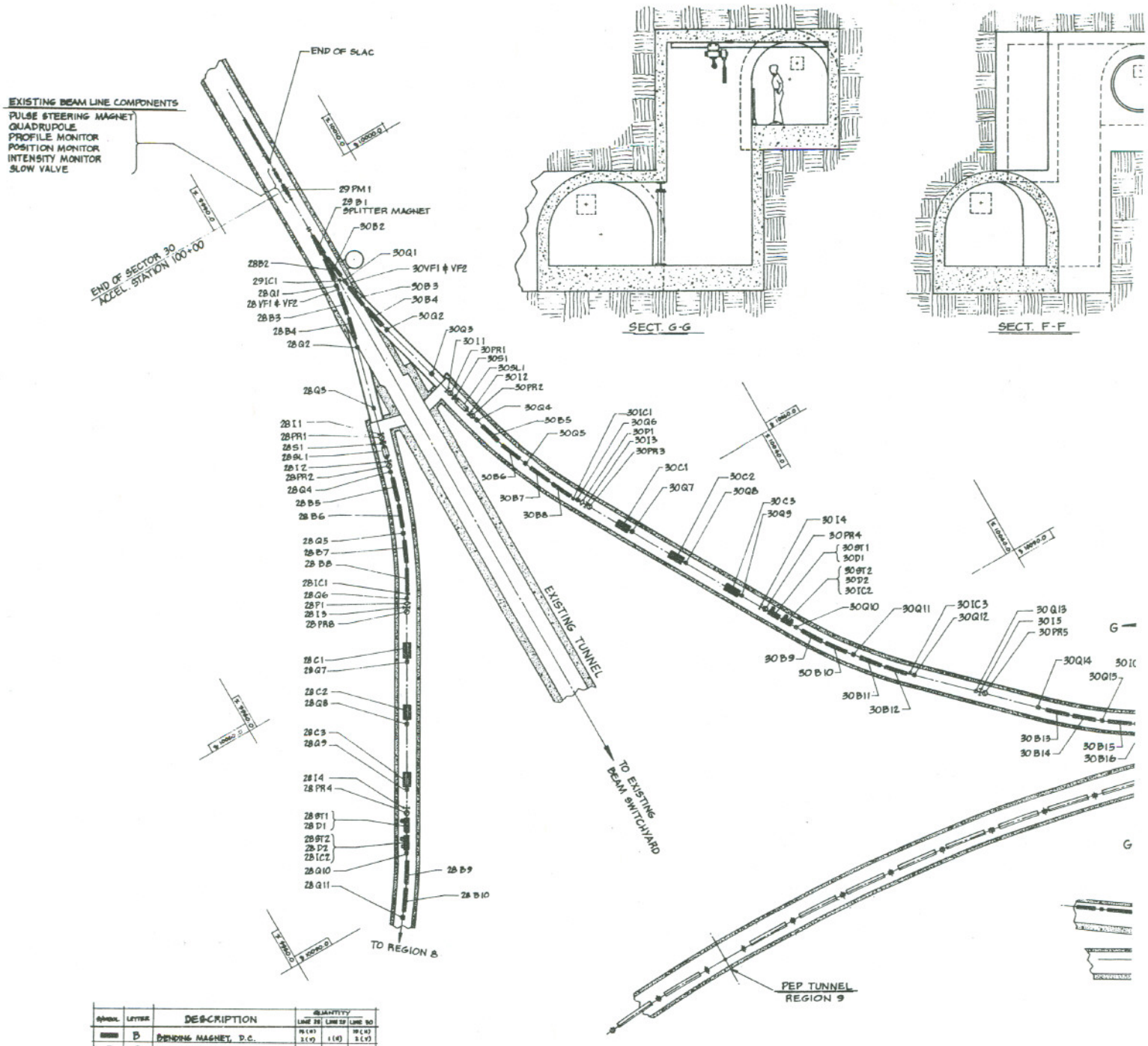

SYMBOL	LETTER	DESCRIPTION	QUANTITY LINE 28	QUANTITY LINE 29	QUANTITY LINE 30
	B	BENDING MAGNET, D.C.	25 (H) 2 (V)	1 (H)	28 (H) 2 (V)
	Q	QUAD MAGNET, D.C.	24	0	24
	PM	PULSE MAGNET	5 (H)	1 (V)	5 (H)
	A	"BUMP" STEERING MAGNET	4 (H)	0	4 (H)
	I	BEAM CURRENT INTENSITY MONITOR	8	0	8
	PR	BEAM PROFILE MONITOR (PROFILE SCREEN)	10	0	10
	P	BEAM POSITION MONITOR	4	0	4
	SL	ENERGY DEFINING SLIT	1	0	1
	S	BEAM ENERGY SPECTRUM INDICATOR	1	0	1
	ST	BEAM STOPPER	2	0	2
	DM	DISABTLE MONITOR	2	0	2
	IC	IONIZATION CHAMBER	5	1	5
	VF	VACUUM ISOLATION FOIL	4	0	4
	FC	FARADAY CUP	1	0	1
	C	COLLIMATOR	3	0	3
	DS	ELECTROSTATIC DEFLECTION PLATE	3	0	3

Fig. 45--Injection bean

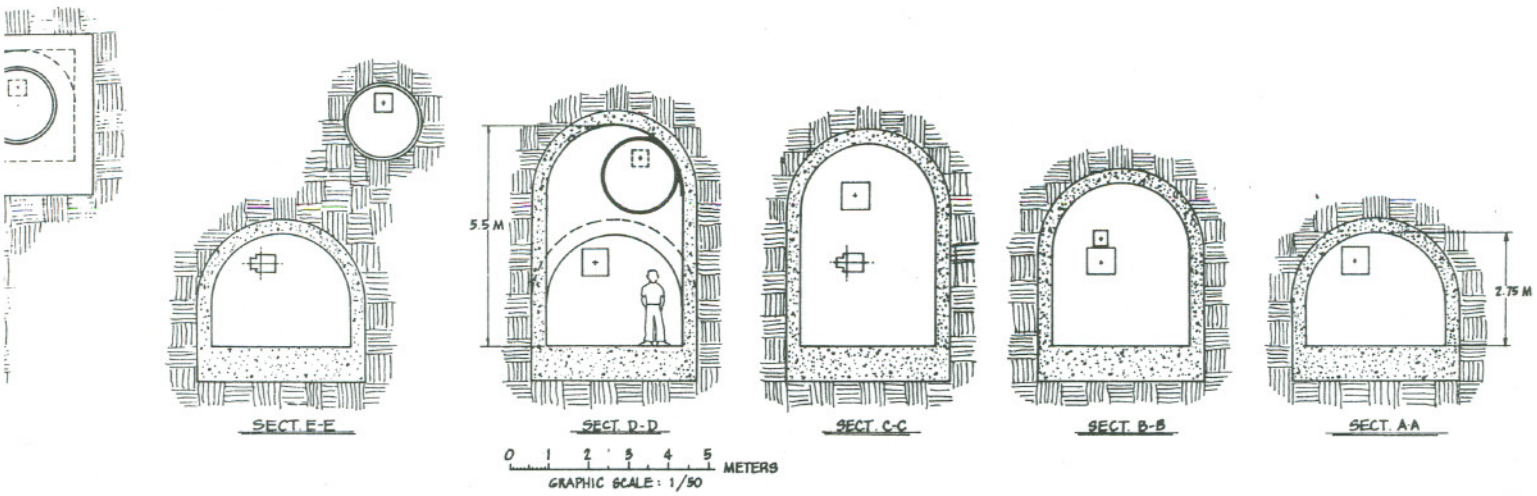

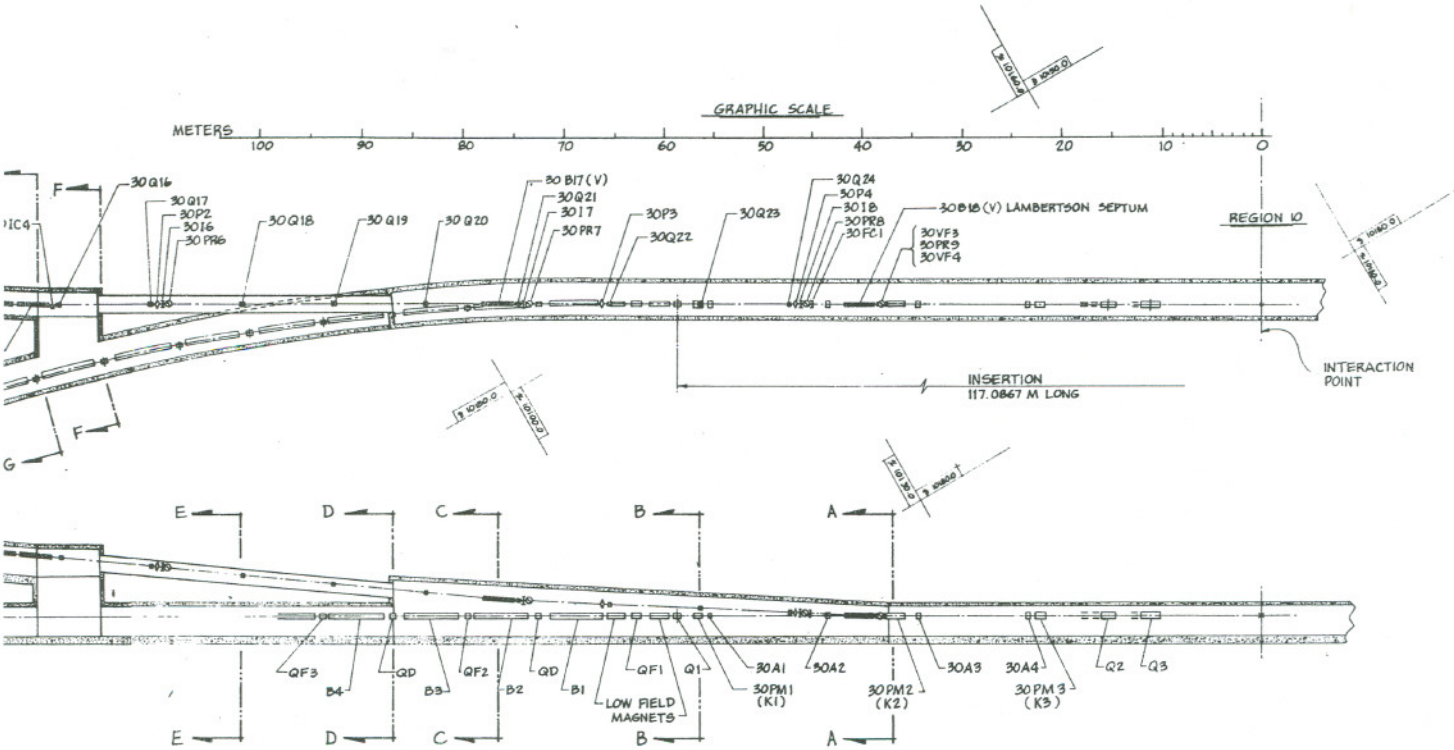

m lines from SLAC to PEP.

2817B26

without disturbing the monoenergetic phase-space configurations.

The last 360° achromatic segment bends the beam vertically a total of 88 milliradians and deposits it at the ring injection position via a Lambertson iron-septum magnet.

3. Pulsed Inflection System

The injection process whereby electrons or positrons from the linac are trapped in the PEP storage ring has two steps, as illustrated in Fig. 46 and 47: (1) a launch into a stable orbit in the ring, having large-amplitude betatron oscillation, followed by (2) a slow damping of that oscillation down into a small-amplitude equilibrium distribution.

The entering particles are deflected horizontally by a pulsed "kicker" magnet (Kicker Magnet 3) onto an orbit in which they can safely circulate within the vacuum chamber with a radial collective betatron oscillation of 2- or 3-cm amplitude, depending on the lattice configuration in use. To compensate the effect of this kicker magnet on the beam already stored in the ring, it is made part of a triad of pulsed magnets (Kickers 1, 2, and 3) whose function is to distort, or "bump," the local closed orbit at the time of injection as illustrated in Fig. 46. The amplitude of the bump required is the sum of the width of the injected envelope (including dispersion effects), the septum width, and a small allowance for clearance, the sum typically running 1 to 2 cm. In this system, the septum separating the external path of the entering beam from the internal orbits is the thin conductor which terminates the central field of Kicker Magnet 2.

In addition to the triad of pulsed kicker magnets, which produce the fast bump, a quartet of dc magnets is arranged in the injection area to produce a dc bump of variable amplitude and slope at the point of injection. This variable bump helps match the beam optics of the transport line to that of the wide range

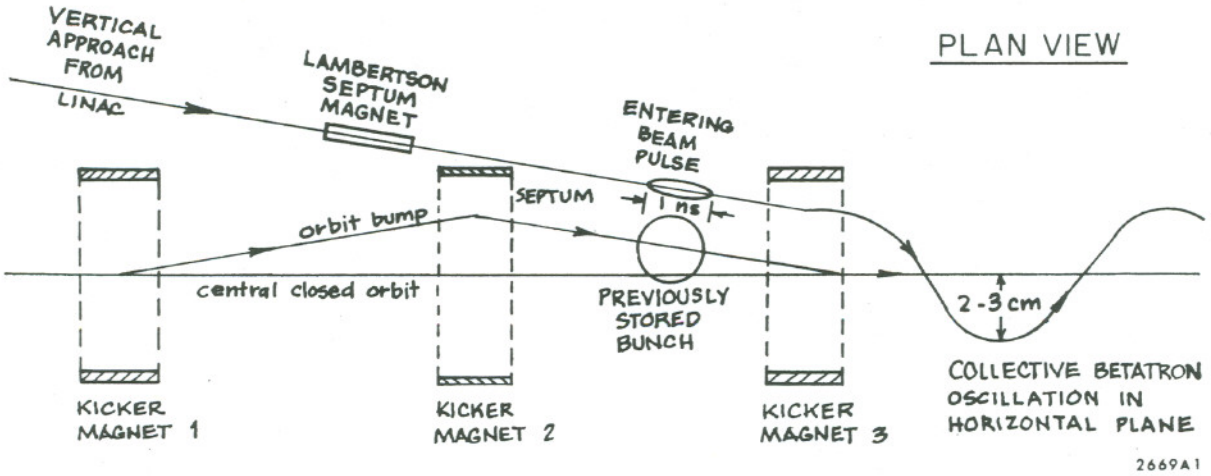

Fig. 46--PEP injection system (schematic).

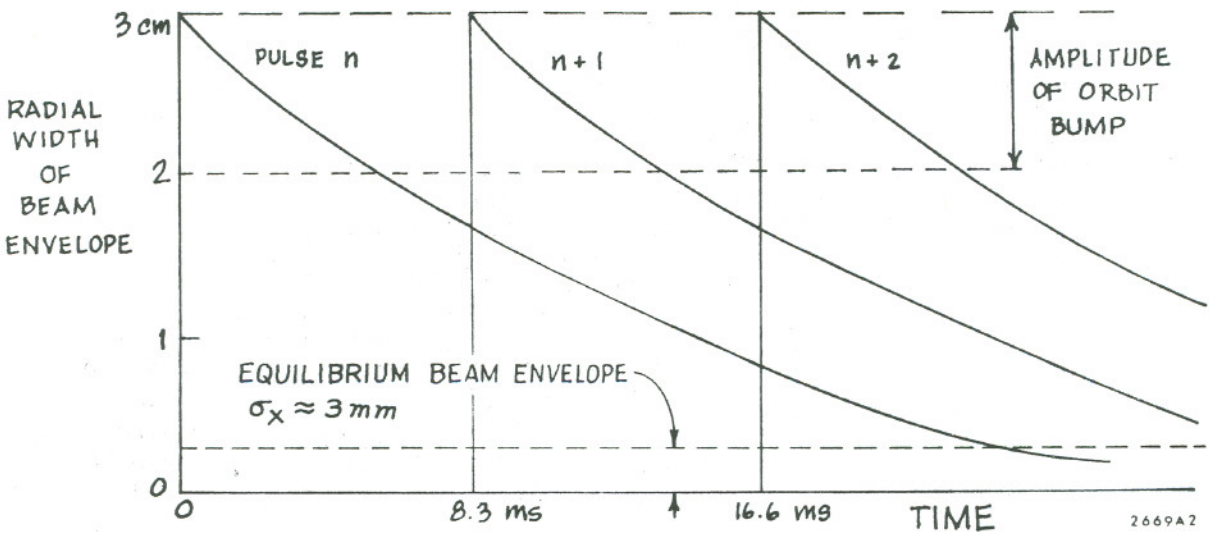

Fig. 47--Radiation damping of beam envelope after injection of several beam pulses.

of lattice configurations which can be used in the PEP ring. The beam exits the transport line through a foil window and enters the ring vacuum through another foil window that is on the inner radius of the ring in order to protect it from the intense synchrotron radiation. In the vertical plane, the beam is centered and phase space matched.

4. Injection Rates

While the beam circulates, the synchrotron-radiation process continuously damps the beam dimensions and also the energy spread toward an equilibrium distribution determined by quantum fluctuations. This radiation process allows each injected pulse of particles eventually to be deposited in a volume of phase space already occupied by previously stored bunches and thus avoids the limitation of constant phase-space density (Liouville's Theorem) common in proton machines. Also, it is a "forgiving and forgetting" process in the sense that deliberate or accidental variations in the injection procedure do not affect the final equilibrium beam distribution.

The loading time of the storage ring is short but not negligible. To load 92 mA of electrons and positrons into the ring at 15 GeV from the linear accelerator operating at 360 pps takes about 5 minutes. This maximum repetition rate of 360 pps is possible only at energies greater than 12.5 GeV, where the damping time in the storage ring is less than 8.33 milliseconds, the time needed to load three successive linac pulses into the three active RF buckets in a beam. At lower energies, the damping times in the normal lattice would increase as E^{-3}. However, the wiggler system serves to shorten the damping times so that the effective energy dependence is approximately E^{-2}. The required current in the ring varies as E, so that the overall filling time below 12.5 GeV varies approximately as E^{-1}, as shown in Fig. 48. Since the usable SLAC repetition rate is

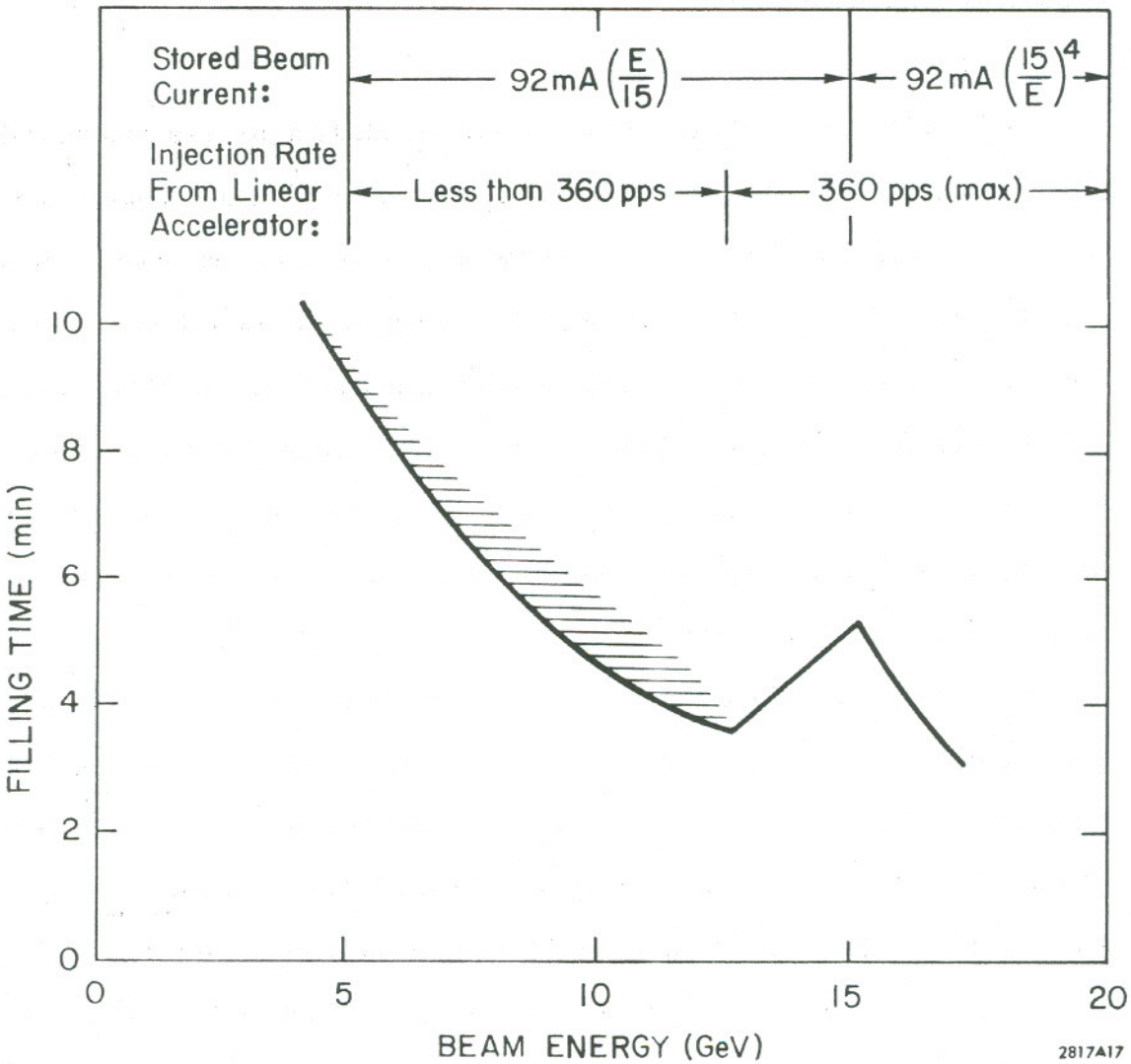

Fig. 48--Filling time into PEP.

quantized, the actual curve has small jogs where the ratio of beam-damping time to SLAC-interval times becomes an integral number; the dashed area on the curve of filling time represents this irregularity. Above 15 GeV, the filling time drops because the required current falls as E^{-4}. With the wiggler system, the filling time requirements below 15 GeV are reduced significantly from those in systems in which beam size is controlled by varying the betatron tunes and the dispersion function.

A special new electron gun, installed on the two-mile accelerator to provide the high peak currents and the short pulses necessary for injection into the SPEAR II storage ring, has been in use since October of 1974. It is now providing peak positron currents at the end of the accelerator in excess of 20 mA. This performance is adequate for the proposed PEP requirements, so that a further major gun development is not necessary. The filling time curve of Fig. 48 is based on the assumption that only 50% of the 20-mA positron current from the linac is transmitted and trapped in the PEP ring.

Precise timing and energy definition are required for successful injection. Each injected pulse contains 10^8 positrons or 10^9 electrons, is about 1 ns in length (consisting of four s-band pulses), and has ± 0.5% energy spread. These dimensions just fit within a typical RF bucket in the PEP ring. Furthermore, each injected pulse must be placed in a specific RF bucket, one of three in use (out of a total of 2592 in the ring). This requires precise timing, but the means of doing it are already in use on SPEAR.

5. Major Components in the Injection System

A description of the major components in the transport line and injection system and their principal characteristics at 15 GeV is as follows (see also Fig. 45):

(1) Pulsed Switching Magnet (29PM1)

Maximum Field	3.3 kG
Effective Length	0.96 m
Bend Angle (15 GeV)	6.3 mr
Clear Aperture	± 12.5 mm
Wave Form	Single 600-Hz sinusoid
Repetition Rate	360 Hz
Peak Voltage and Current	3.8 kV, 420 A
Average Power	3 kW
Weight	725 kg
Number Required	1

Comment: The design will probably be that of the SLAC switch magnet PM30 with the aperture increased by 25% to accommodate a ceramic vacuum chamber.

(2) Splitter Iron-Septum Magnet (29B1)

Maximum Field	10.9 kG
Effective Length	3.0 m
Beam Angle (15 GeV)	65 mr (3.75°)
Gap Height	30 mm
Clear Aperture	± 12.5 m (vert.), ± 115 mm (horiz.)
Ampere-turns	35,000 A-t, dc
Power	22 kW
Weight	9000 kg
Number Required	1

(3) Horizontal Bend Magnets (28B2 to 28B16, 30B2 to 30B16)

Maximum Field	12.6 kG
Effective Length	2.6 m
Bend Angle (15 GeV)	65 mr (3.75°)
Gap Height	30 mm
Clear Aperture	± 12.5 mm (vert.), ± 25 mm (horiz.)
Ampere-turns	32,000 A-t, dc
Power	12 kW
Weight	2700 kg
Number Required	30

Comment: Each magnet will have auxiliary windings for providing up to 0.65 mr horizontal steering.

(4) Quadrupoles (28Q1 to 28Q23, 30Q1 to 30Q23)

Maximum Gradient	3.0 kG/cm
Effective Length	0.4 m
Inscribed Radius	30 mm
Clear Aperture	25.0 mm radius
Ampere-turns/pole	12,000 A-t, dc
Power	7.9 kW, max.
Weight	225 kg
Number Required	46

Comment: Each quadrupole will have auxiliary windings for providing up to 0.4 mr horizontal and vertical steering.

(5) Vertical Bend Magnets (28B17, 30B17)

Maximum Field	7.3 kG
Effective Length	3.0 m
Bend Angle	44 mr (2.5^{o})
Gap Height	45 mm
Clear Aperture	± 20 mm (horiz.), ± 35 mm (vert.)
Ampere-turns	28,000 A-t, dc
Power	10 kW
Weight	2250 kg
Number Required	2

(6) Injection Iron-Septum Magnets (28B18, 30B18)

Maximum Field	7.3 kG
Effective Length	3.0 m
Bend Angle (15 GeV)	44 mr (2.5^{o})
Gap Height	35 mm
Clear Aperture	± 12.5 mm (horiz.), ± 25 mm (vert.)
Ampere-turns	21,500 A-t, dc
Power	8.2 kW
Weight	2250 kg
Number Required	2

(7) Pulsed Kicker Magnets (28PM1 to 28PM3, 30PM1 to 30PM3)

Maximum Field	~ 0.6 kG
Effective Length	1.0 m (PM1 and 3), 2.0 m (PM2)
Clear Aperture, Vert.	~ ± 40 mm
Clear Aperture, Horiz.	~ ± 40 to ± 80 mm
Wave Form	Half-sinusoid, damped, 3 μs long
Peak Voltage	12 to 19 kV
Peak Current	10 to 15 kA
Repetition Rate	360 Hz
Number Required	6

(8) D. C. Bump Magnets (28A1 to 28A4, 30A1 to 30A4)

Maximum Field	4.7 kG
Effective Length	0.5 m
Gap Height	140 mm
Clear Aperture, Vert.	± 25 to ± 40 mm
Clear Aperture, Horiz.	± 50 to ± 80 mm
Ampere-turns	23 to 50 kA-t
Maximum Power	2 to 5 kW
Weight	~ 225 kg
Number Required	8

(9) Instrumentation

The injection line instrumentation components to measure and/or to define the beam intensity, emittance, size, position and energy spectrum are indicated by symbols in Fig. 45. In general, the design of this equipment follows that already being used in the various beam transport lines at the SLAC-SPEAR complex. A listing of the types of instruments and the number required of each component is as follows:

Component	Number Required
Beam Intensity Monitor	17
Beam Profile Monitor	21
Beam Position Monitor	9
Energy Defining Slit	2
Energy Spectrum Monitor	2
Ionization Monitor	11
Beam Stopper	4
Emittance Collimators	6

(10) Vacuum

The vacuum requirements for the injection lines are modest. A pressure of 10^{-3} Torr is adequate, so that relatively crude vacuum hardware and pumping will be enough. This coarse vacuum in the injection line will be isolated from the high vacua in the SLAC linac and the PEP ring by pairs of thin foils or cold-trap sections.

F. Data System for Monitoring and Control

1. Introduction

The PEP storage ring system physically covers too wide an area for a single data-collection point to be practical. We will, therefore, collect data at a number of places. It will be edited and compressed as much as possible and then transmitted to the control room, located near one of the injection points, creating a short path for direct transmission of fast monitoring signals from the injection lines.

Data from magnet interlocks, vacuum pressure gauges, beam monitors, and small magnet-trim power supplies will be gathered at centers in Regions 2, 4, 6, 8, 10, and 12. In Regions 4, 8, and 12, the data center will also be adjacent to the RF system reducing the amount of control cabling. The bend-magnet power supplies are also in these same areas. This consolidation not only makes for efficient utilization of installed equipment, but also simplifies providing of the required utilities such as LCW and ac power. The surface buildings at Regions 8 and 10 will also house the power supplies and controls for the injection beam transport lines.

Signals generated within the bending arcs will, for the most part, be wired only to instrumentation racks in the nearest data center to further reduce the amount of cabling. Interlock signals will be summarized there and wired directly to the equipment they must control. The remaining signals will be edited by a small local computer and sent by serial link to the control room. The computer in the data-collection area will have provision for graphic displays, eliminating the need for extensive alarm and annunciator panels.

2. Control System

The control system will depend heavily upon several small computers. Fourteen of these will be connected by links to the Central Control Computer. These

small computers will be "real time" units, while the larger Central Control Computer will interface with the outside world. A link to the SLAC IBM Triplex computer system can supplement this computer. At each small computer a small control console will aid in checkout and maintenance of the equipment associated with that computer.

3. Timing

Much of the instrumentation will require timing signals at the circulation frequency of the ring for gating of beam monitors and feedback systems, for injection, for displays in the control room, and for experimenters. The timing system will divide the 353 MHz radio frequency to the 136 kHz revolution frequency and distribute a reference signal to each data area. Timing repeaters will then provide separate channels with individual delays for each instrument.

4. Magnet and Guidance Controls

The controllers for magnet power supplies will be standardized as much as possible, and will include a digital-to-analog converter attached to each power supply regulator. All of the converters are to be of the same design and the magnet power supply regulators will be designed to accept signals in the same voltage range, e.g., 0 - 10 V. Each power supply will have an individual controller. The ganging of controls for magnets which have identical currents, but which are physically too far apart to be in series, will be accomplished in the computer system software.

The high-voltage supplies for the electrostatic guidance plates will be remotely controlled, the controllers being similar to those of the magnet power supplies.

5. RF System Control

The RF system will be largely self-contained; for example, it will have the

internal logic for phasing on command. The control system will provide for operator's instructions for phasing and control of RF voltage amplitude, and it will monitor the general health of the RF system components.

6. Interlocks and Miscellaneous

All interlocks will be hard-wired to cross-connect racks located at each data-gathering center using relay logic wherever possible. If semi-conductor logic proves to be preferable, it will be designed to be at least twofold redundant and self-checking. The relay logic will be redundant with checking capabilities incorporated where personnel protection is involved.

Analog and status signals for vacuum gauges, pumps, vacuum-valve position, trim-magnet current and thermocouple signals will be read into the computer system at each data-gathering location and will also be available at each data-gathering point as an aid in maintenance of equipment when the local computer is down.

All the vacuum valves will be controlled by a hard-wire system. The fast valves will be controlled via vacuum gauges. The permissive signal to open the vacuum valves will be under the control of the control room operators via a hard-wire system.

For personnel protection, a system of gates and monitors to control access to the arcs and to the interaction areas will prevent the injection or circulation of beam if any area can be occupied.

7. Beam Monitoring

The synchrotron light monitor consists of optics and sensors to generate a TV image of the beam and provide beam-profile and bunch-length information. The light emitted from the two counter-rotating beams will be collected separately and photodiodes will be used to measure the current in each beam independently. These sensors will be calibrated from a single toroidal dc

transformer capable of measuring the total current ($e^+ + e^-$) in the ring to an accuracy of 0.1 mA. (Calibration is done with a single beam in the ring.)

The beam-position monitoring system is similar in design to that of SPEAR.[32] It measures the position of the beam in the ring at approximately 80 points. Each monitor consists of four buttons in the vacuum system which couple capacitively to the beam. Comparing the amplitudes of the signals produced by the buttons generates the beam position information.

Two luminosity monitors, one a small-angle, high-rate system and the other a large-angle (10° - 20°), low-rate system will be provided.

Fast strip-line monitors for the stored beam and injection beam monitors will also be provided.

G. Beam Parameters

For the sake of concreteness and to avoid confusion in this section, we choose two specific modes of operation of PEP from among those described in Chapter II.A: one for operation at beam energies from 15 GeV down and one for operation at higher energies. The modes chosen are those we consider most likely to be used.

For energies of 15 GeV and lower, we choose to control beam size by means of the wiggler magnets and to use at all energies the same "standard" lattice configuration (Table III). Figure 49 displays the characteristic functions of the standard configuration.

For energies above 15 GeV, we choose the method of variation of tune for the control of beam size.

The horizontal beam emittance in both regimes is shown in Fig. 50. The betatron-oscillation damping time τ_β and its reduction by the wiggler magnets are shown in Fig. 51. (Since the PEP lattice is a separated-function lattice, both the vertical and the horizontal damping times are the same and the longitudinal damping time is one-half of τ_β.) Figure 52 gives the design beam current as limited by the beam-beam limit and, above 15 GeV, by the total installed RF power. The currents above 15 GeV depend very much on the momentum compaction factor and therefore on the beam-dynamics configurations. The lattice parameters corresponding to Fig. 52 were scaled from the 15-GeV configuration and the actual configurations used may be somewhat different due to various matching requirements.

Some of the RF parameters are given in Fig. 53 - 56. Included in the calculation of RF and RF-related parameters are the higher-order-mode losses in the cavities and the vacuum chamber, as explained in Section II.C.8. We take the bunch-lengthening factor to be 2 and assume that the vacuum chamber meets the criterion

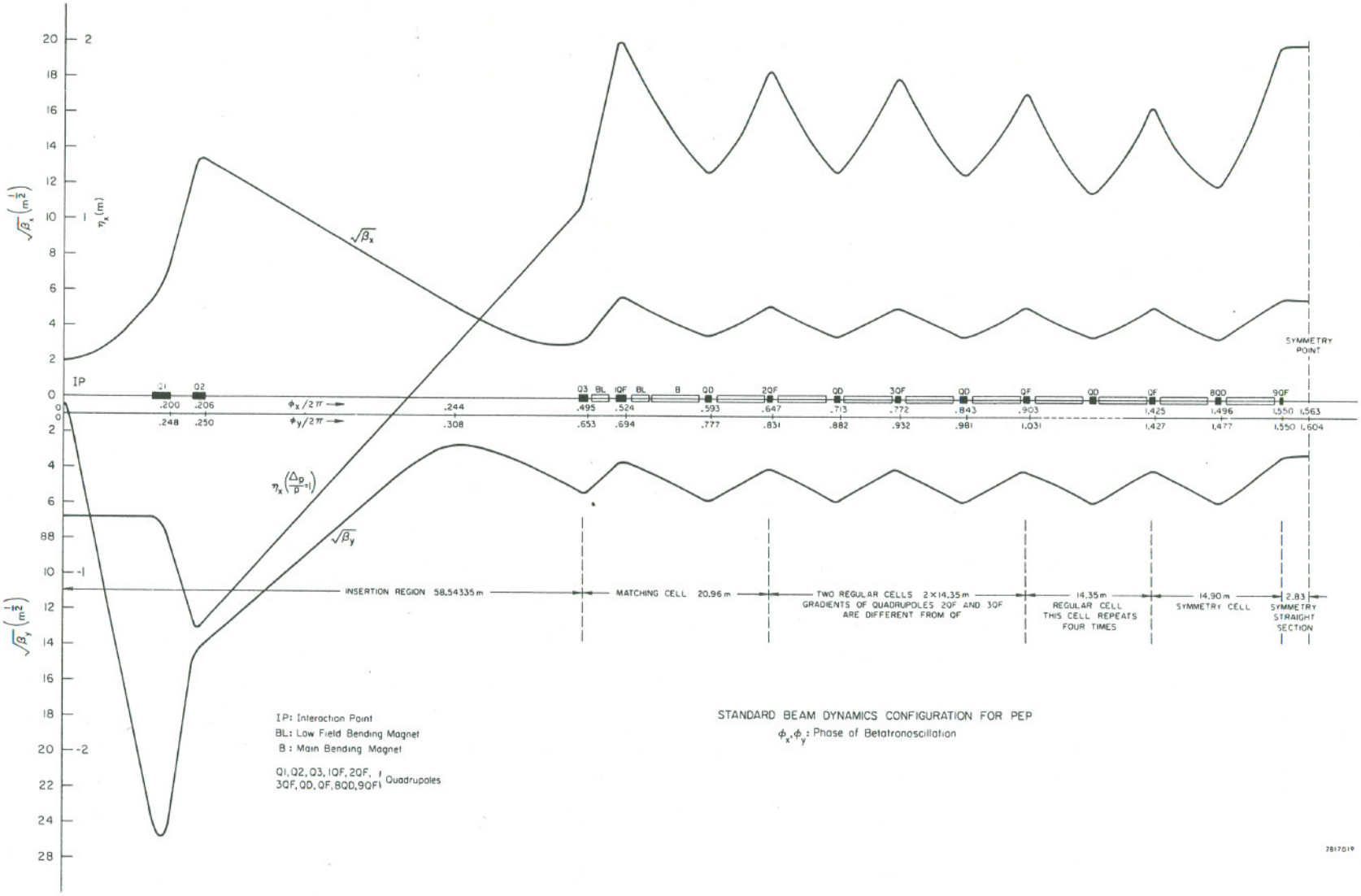

Fig. 49--Betatron and eta function in the standard configurations.

0 0 0 0 4 0 2 9 7 2

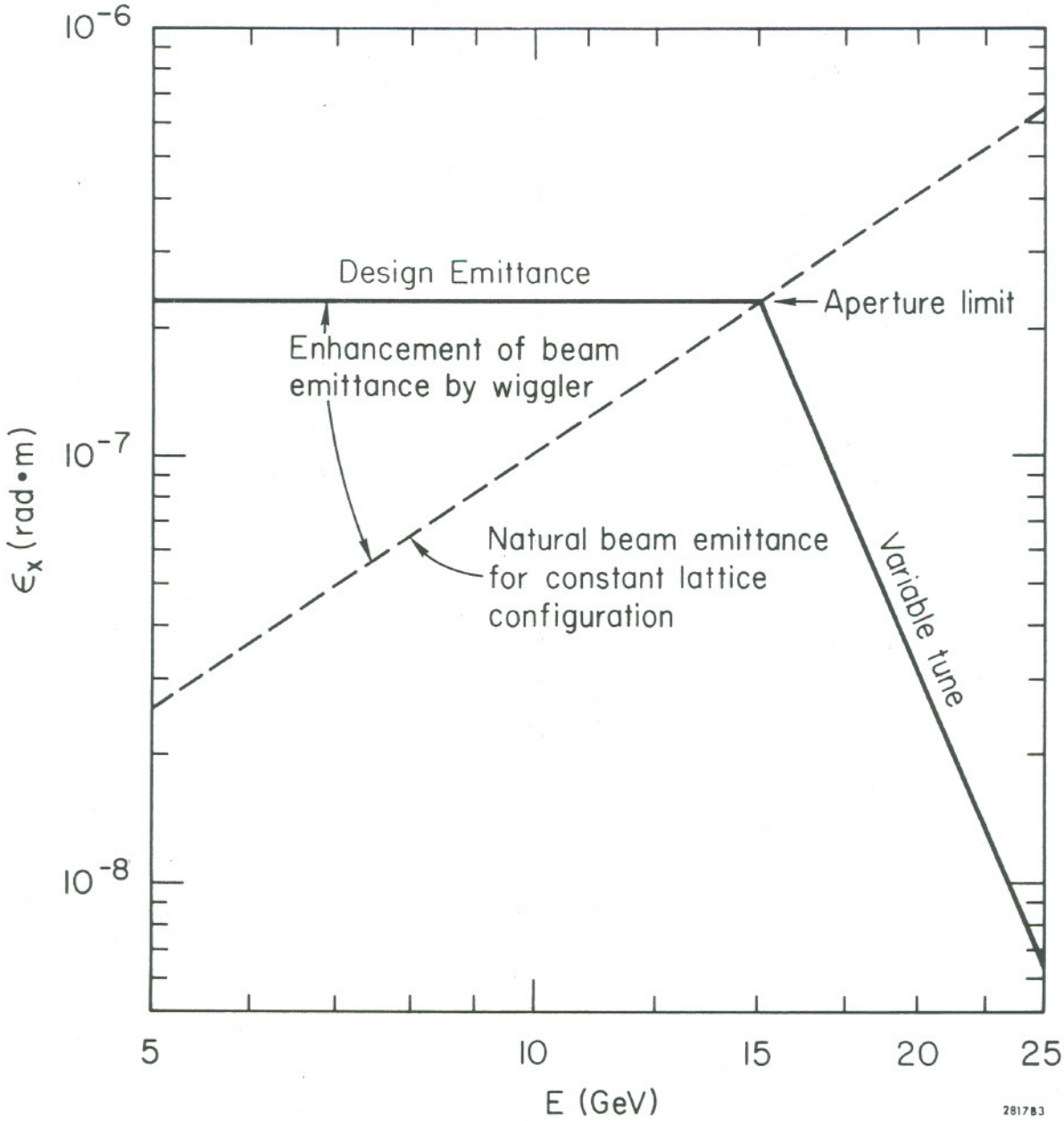

Fig. 50--Beam emittance vs energy.

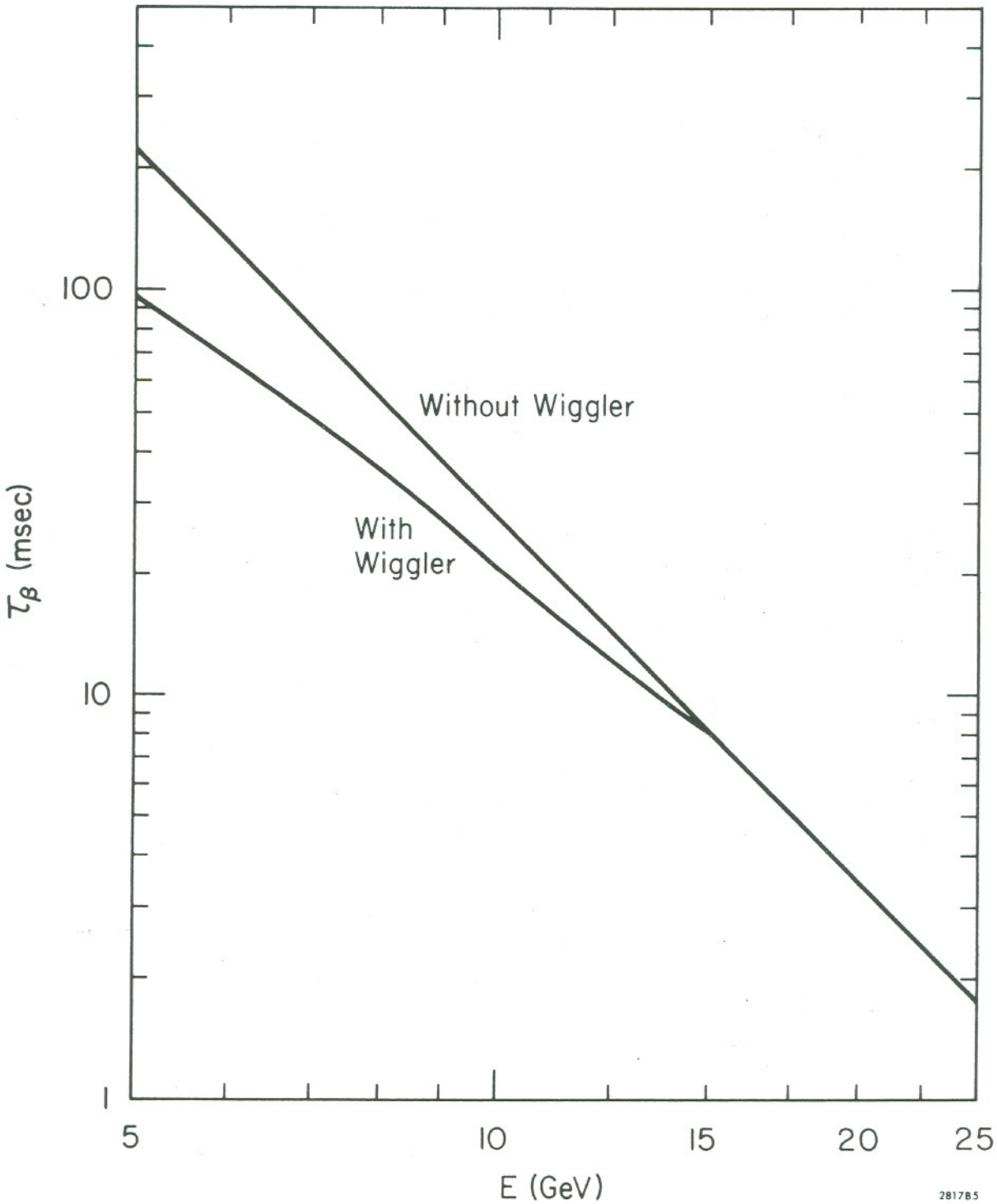

Fig. 51--Betatron damping time vs energy.

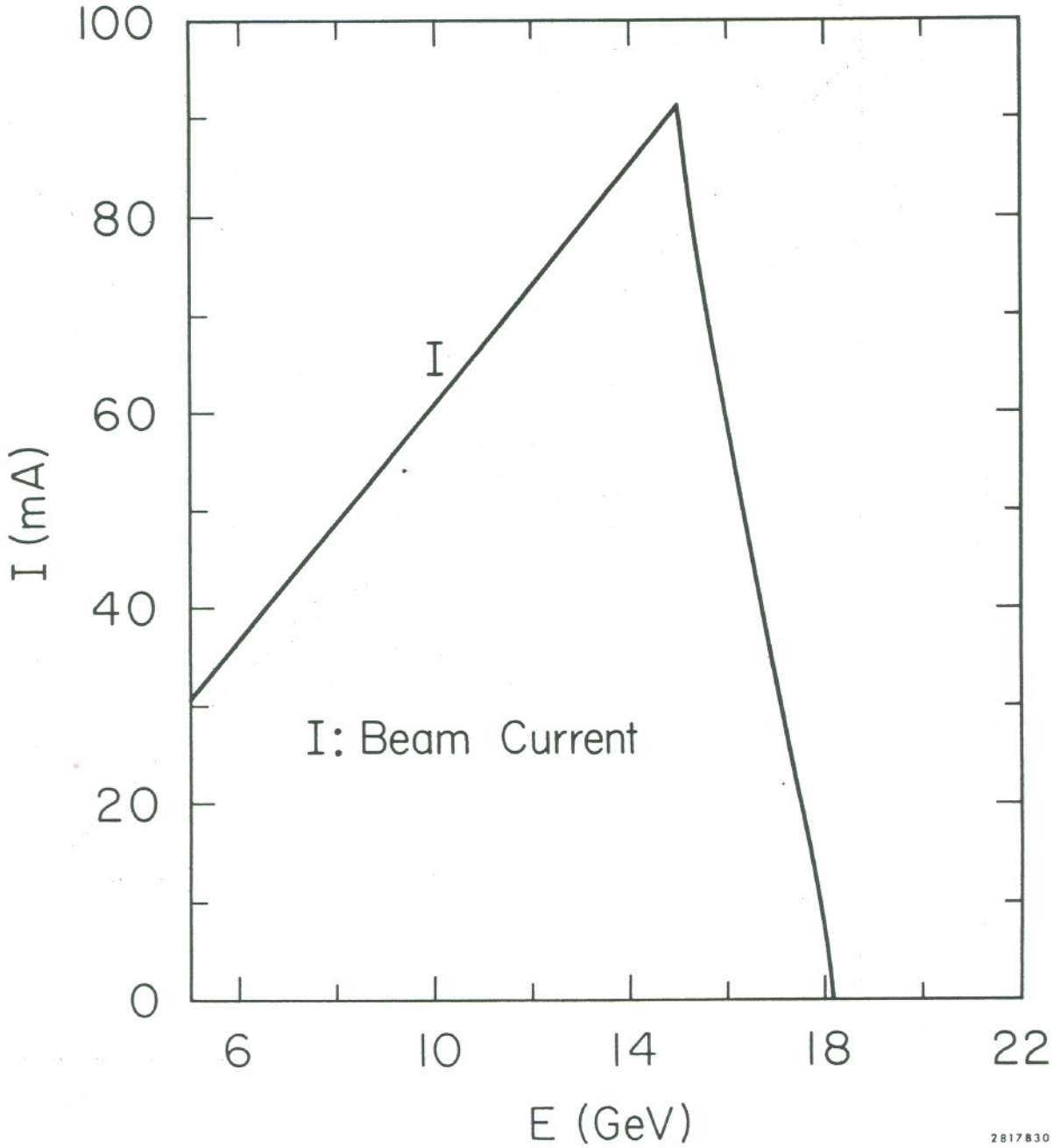

Fig. 52--Design current vs energy.

of being a factor of 10 better with respect to higher-order-mode losses per unit length than the SPEAR chamber.

In the operation of the RF system, there are three principal energy regimes with differing limiting conditions. See Fig. 53.

In the highest regime, above 15 GeV, the storable beam current is limited solely by the available RF power. The peak voltage required to maintain adequate quantum lifetime (50 hours) rises rapidly and, with it, the power deposited in the cavity walls, with the result that the power available to the beam drops off with rising energy. With the power rising and the voltage-per-turn demand rising, the storable current falls dramatically. This fact is reflected in Fig. 52.

In the intermediate regime just below 15 GeV, the storable current is limited by the aperture and the beam-beam limit. As the energy is reduced, less and less RF power is required by the beam so that more is made available for cavity losses.

In the lowest energy regime, below about 14 GeV, the dominating consideration is maintaining the energy aperture at ± 1% for good injection rate.

The energy spread (σ_ϵ/E_0) in the beam stays constant up to 15 GeV and increases above 15 GeV. See Fig. 54. A bunch-lengthening factor of 2 is assumed in calculating the bunch length σ_z. This factor of 2 is a guess at the real bunch lengthening with energy and current based on a rough extrapolation from SPEAR. The synchrotron oscillation tune and the momentum compaction factor are shown in Fig. 55. In Fig. 56, the total RF power consumption by both beams and its composition in terms of synchrotron radiation power, fundamental-mode cavity losses and the higher-order-mode losses are shown.

Figure 57 shows the calculated total beam lifetime and several of the most significant partial lifetimes. The total lifetime under colliding-beam conditions

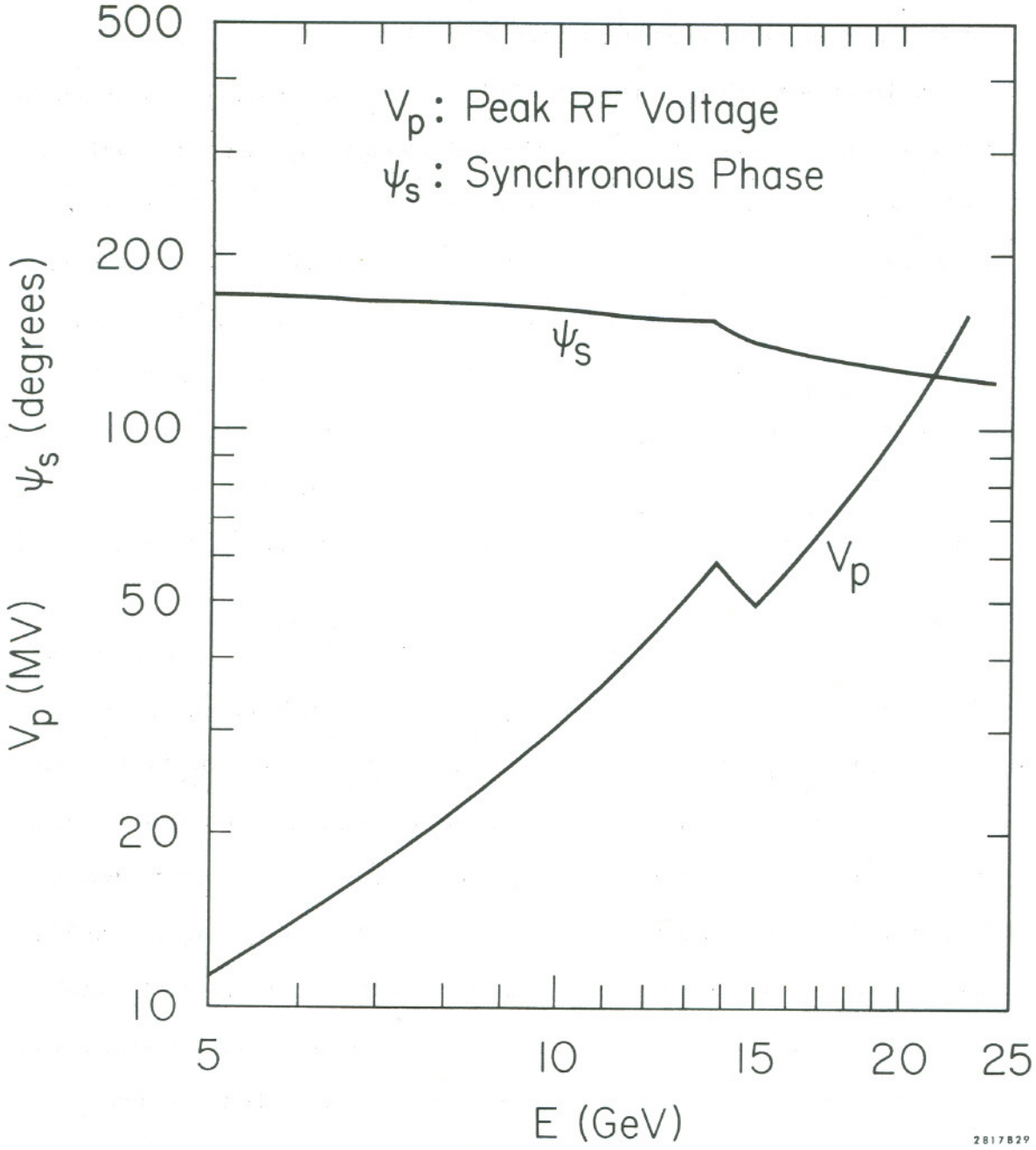

Fig. 53--RF peak voltage and synchronous phase vs energy.

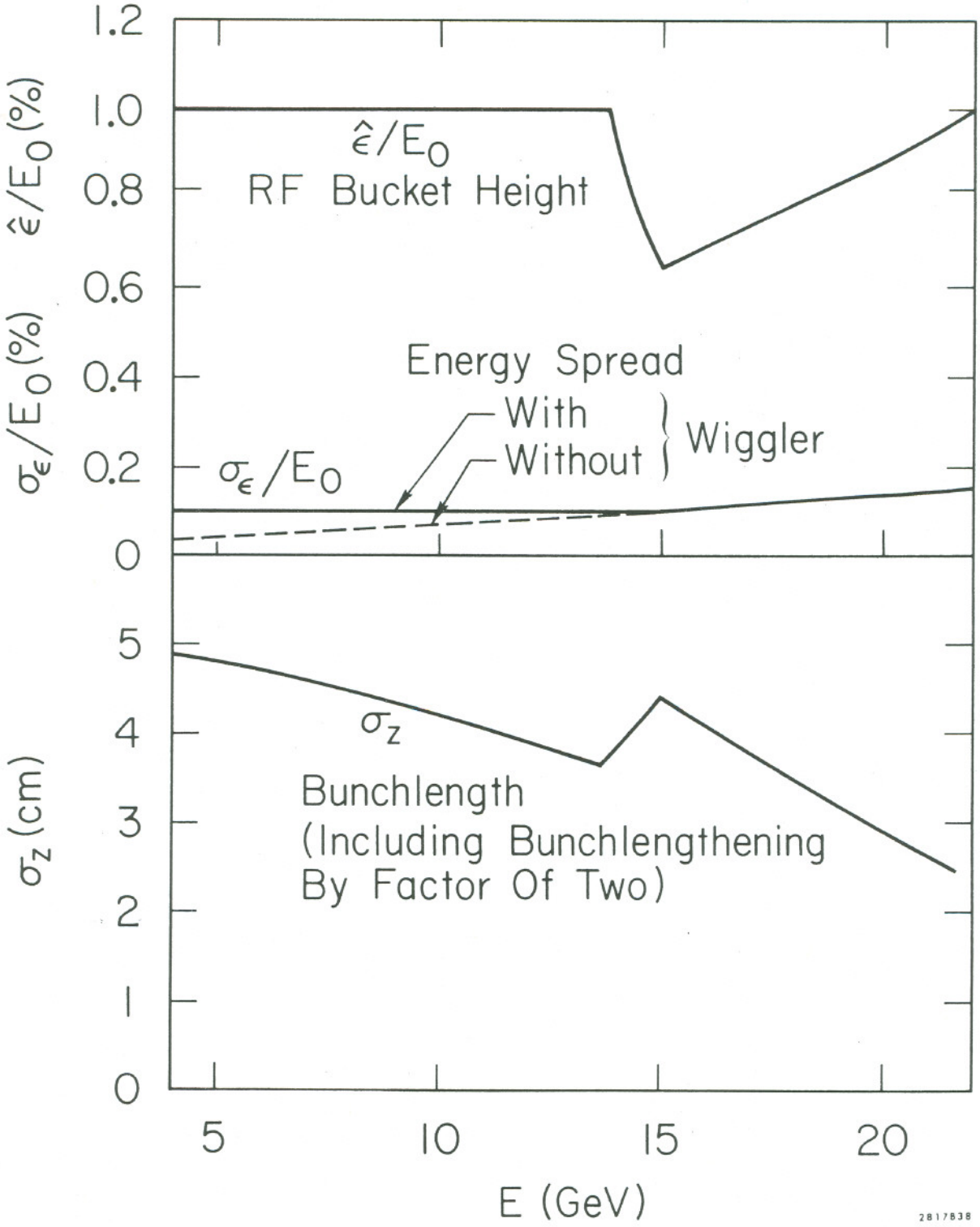

Fig. 54--RF bucket height, energy spread in the beam, and bunch length vs energy.

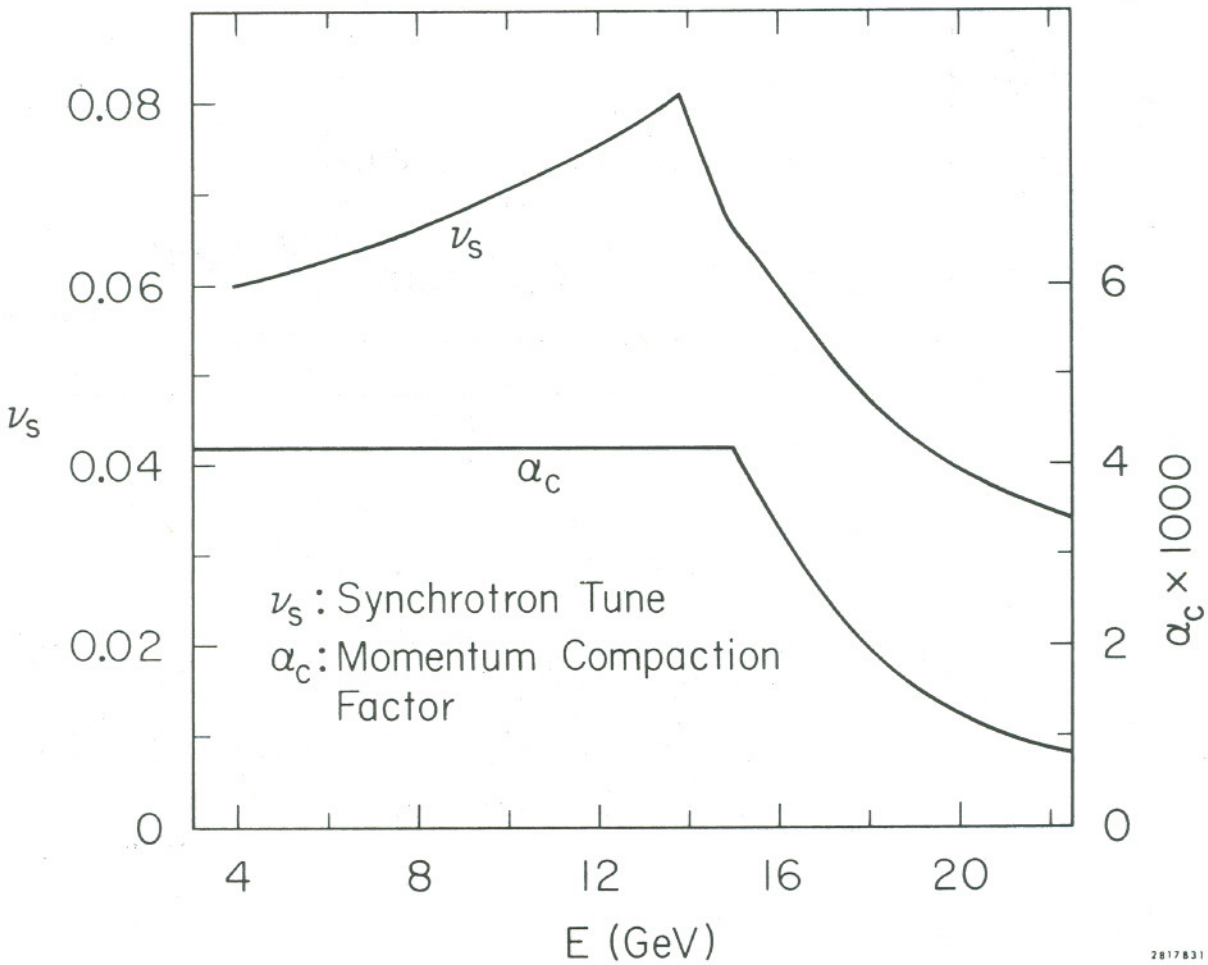

Fig. 55--Synchrotron oscillation tune and momentum compaction factor vs energy.

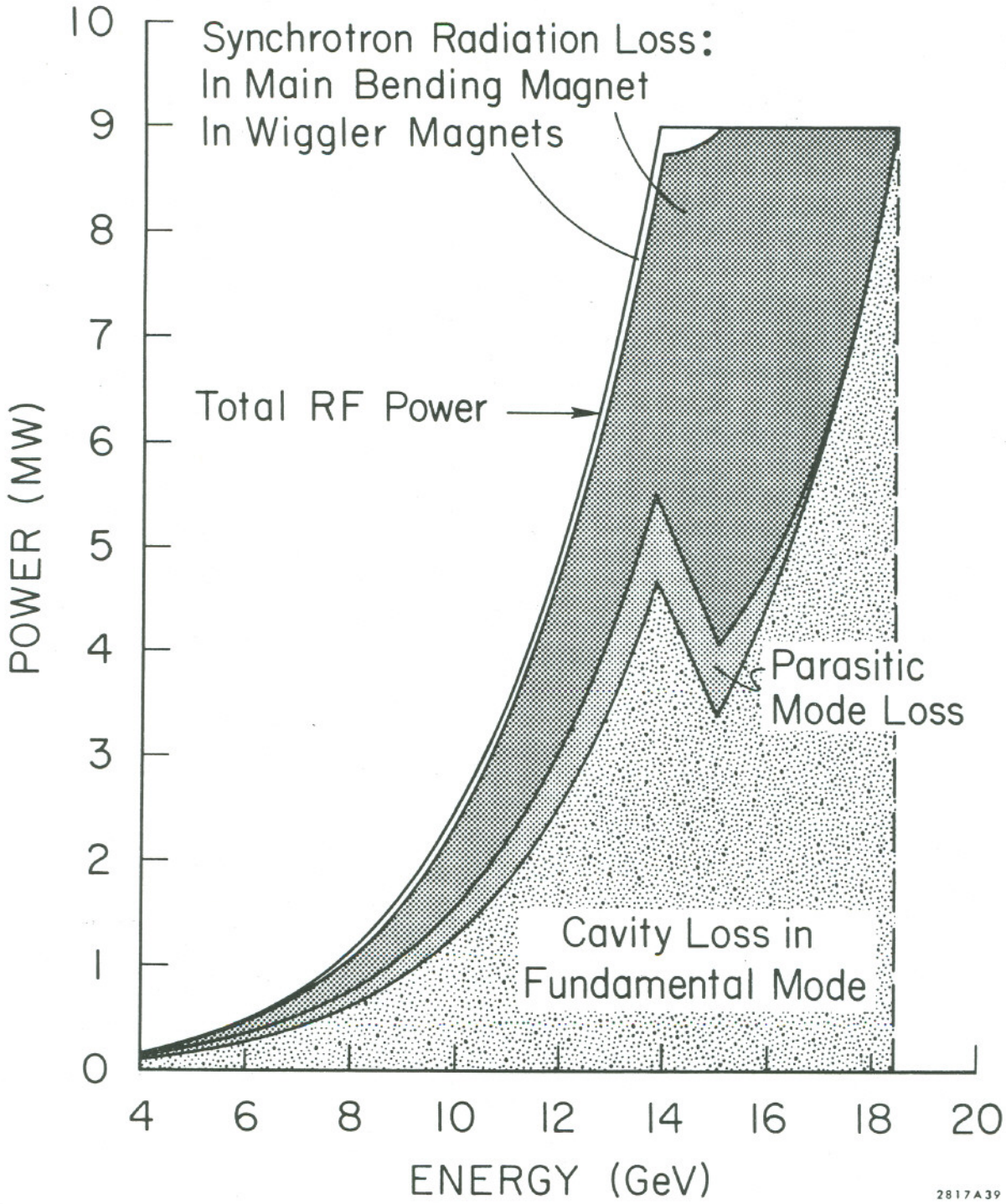

Fig. 56--RF power distribution vs energy.

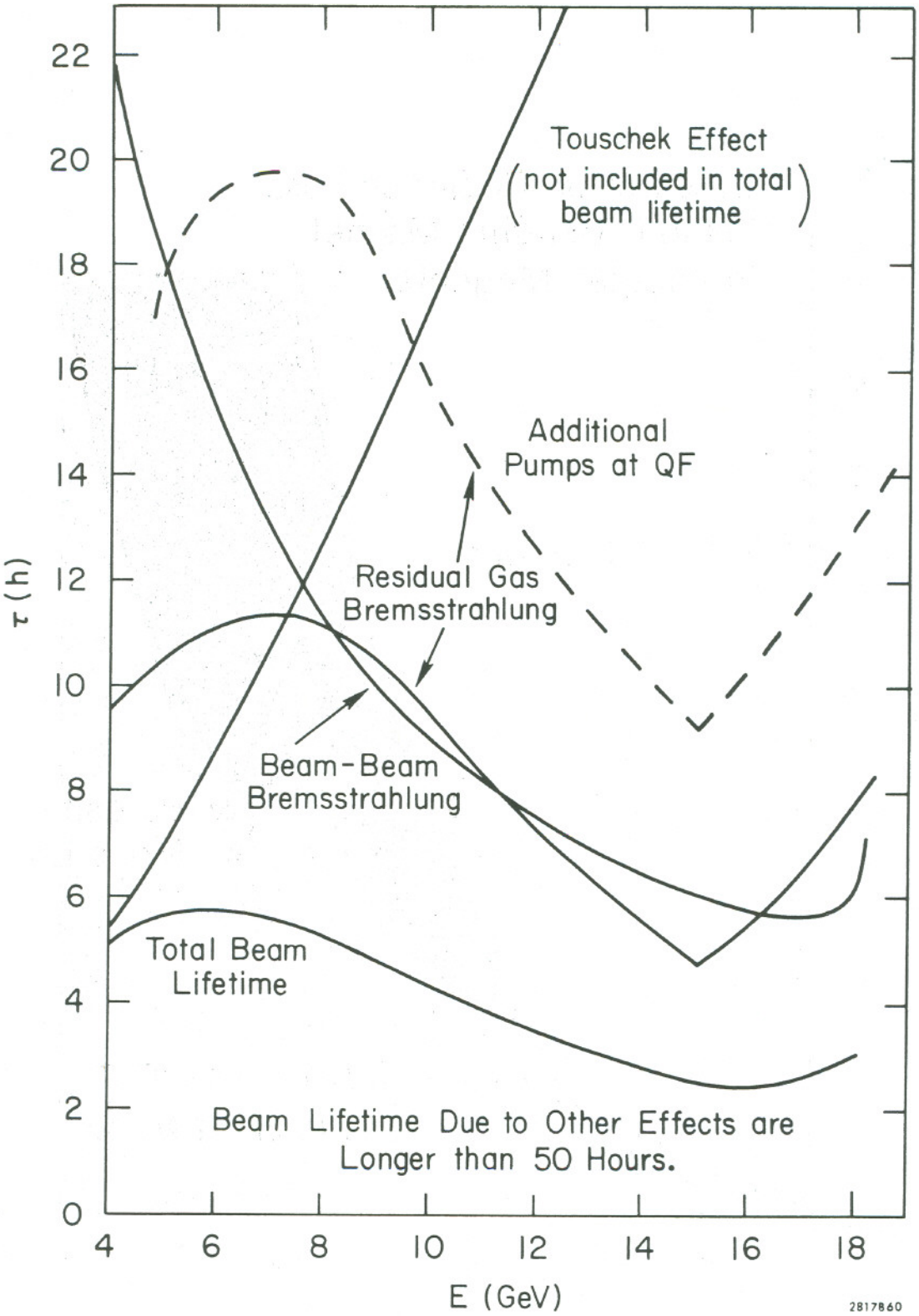

Fig. 57--Beam lifetime vs energy.

is dominated by residual-gas bremsstrahlung and beam-beam bremsstrahlung. The former is independent of the transverse blow-up of the beams in collision. The latter is calculable without knowledge of the details of the blow-up if the values of the stored current and the luminosity are known. By contrast, the intra-beam scattering (Touschek Effect) lifetime is strongly dependent on the blow-up. The Touschek partial lifetime for a single (i.e., non-colliding) beam at natural dimensions is shown for comparison in Fig. 57; however, it is not included in the total beam lifetime calculation because it becomes negligible when the beams collide and blow up. All effects other than residual-gas and beam-beam bremsstrahlung contribute together less than 5% of the total lifetime.

The dashed line in Fig. 57 shows the improvement which could be obtained in the residual-gas bremsstrahlung partial lifetime by adding additional vacuum holding pumps at all QF quadrupole magnets. The potentiality of adding these pumps will be retained as design progresses as a safeguard against unexpectedly high desorption rates and a possible future improvement in average luminosity.

III. PHYSICAL PLANT

A. General Features of the Terrain and Their Effects on Construction Techniques

1. Tunnel Design and Construction

Visualize the PEP ring in plan view as a regular hexagon with broadly rounded corners (see Figs. 1 and 58). In this discussion, the rounded corners will be referred to as arcs and the straight sides will be termed insertions.

The arcs are to consist of two curved sections, each 122 m long and joined in the middle by a short straight section (symmetry insertion) 5.66 m long. The six major insertions are 117 m long with the beam interaction points at their centers.

The ring plane is horizontal and lower than the linear accelerator horizontal plane by 10 m. It is located so that the vertical plane of the accelerator bisects it in a west-to-east direction through two of the arcs, the westernmost being 118 m beyond the end of the accelerator. This arrangement is chosen to allow the two injection beams from the accelerator to be symmetrical.

Since the hexagon comprises twelve major parts, it is convenient to label these parts as Regions 1 through 12 in analogy to a clock's face with Region 1 the northeast arc, Region 2 the northeast insertion and so on around to Region 12 which is the northernmost insertion. Frequent reference to these regions occurs in the material which follows.

The terrain of the site varies in elevation by as much as 30 m. It is highest along the accelerator axis and slopes away to both the north and the south. Consequently, most of the interaction regions will lie in low areas. The centerline of the ring housing (not to be confused with the beam path) as shown in Fig. 59 is to be at an elevation of about 66 m above mean sea level and will pass about 10 m below the floor of the SLAC beam switchyard.

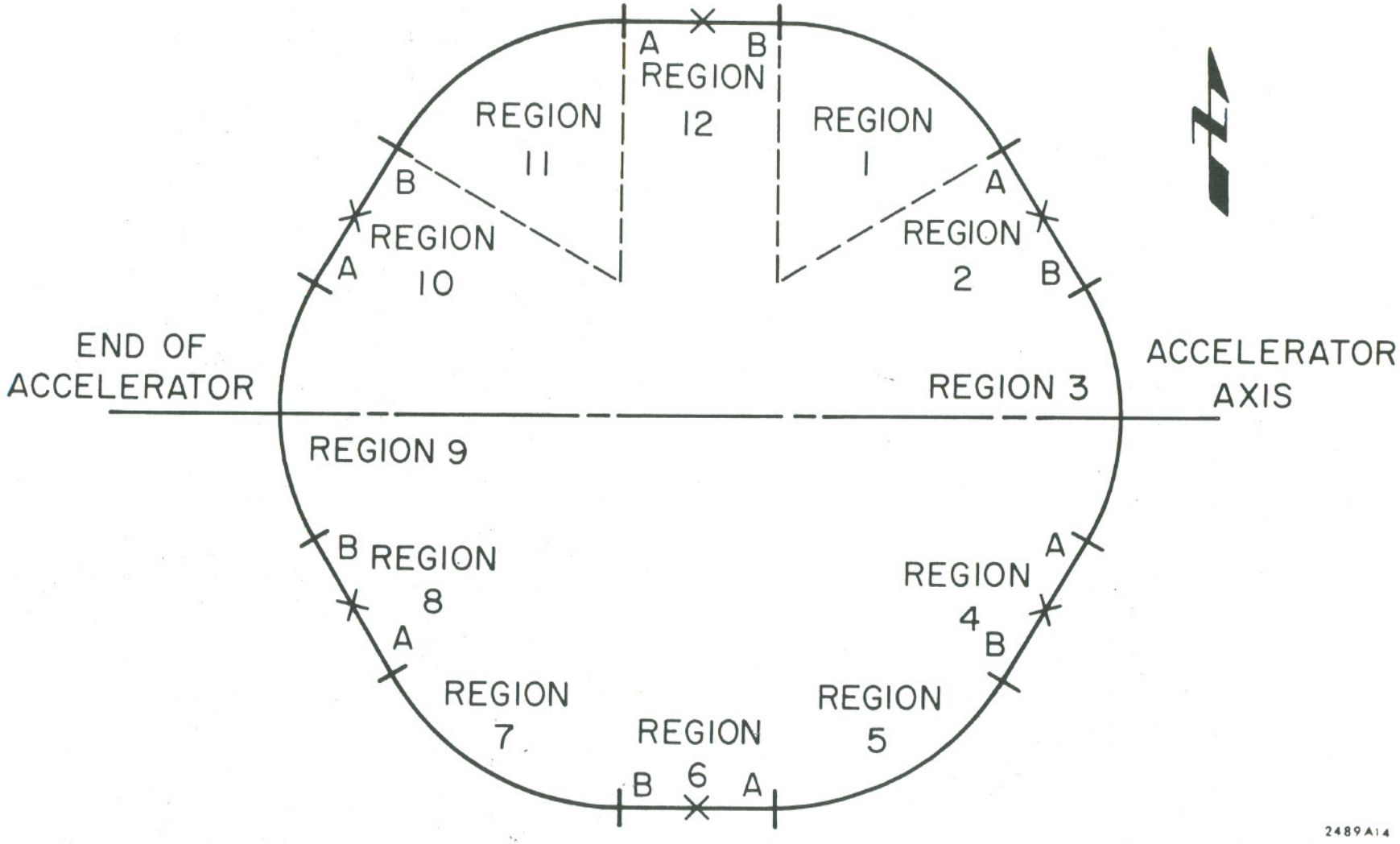

Fig. 58--PEP region numbering system. The accelerator beam is defined to run from west to east with Region 12 on the north side.

0 0 0 0 4 0 2 9 7 8

The prevailing low terrain suggests that the ring housing between Interaction Points 4 and 6, and a short length west of Interaction Point 6 be constructed by cut-and-cover methods. The ring housing in Region 1 may also be of cut-and-cover construction. Elsewhere the ring housing will be constructed by bored tunnel methods. The structures and facilities to be provided for research are described in detail in Chapter IV.

Each of the two injection beam transport tunnels will be joined to the linear accelerator housing at acute angles a short distance downstream from the end of the accelerator. They will branch away and downward, the southern run joining the PEP housing near the junction of Regions 8 and 9 and the northern run near that of Regions 9 and 10. The injection beams themselves will join the storage ring tangentially and from overhead (Fig. 45). Each of the transport tunnels will be about 112 m long. Junctions with the accelerator housing and the ring housing will probably be made by means of large, jacked pipes totalling 45 m in length to minimize jeopardy to existing housings and excessive interruption of regular SLAC operation during construction. The diameter of the injection tunnels will probably be smaller than the diameter of the ring tunnel. This fact together with access conditions suggests construction by hand-mining methods. The structures at junctions with the ring will be of a complicated nature, providing some of the project's most challenging underground construction problems.

The ring tunnel must be large enough to provide space for the electron-positron storage-ring components, cooling system piping and drainage piping, magnet power cables, instrumentation cabling and potential future proton beam hardware, plus suitable aisle space. Present plans call for the e^+-e^- beam components to be suspended from the floor of the tunnel. In the event that a proton ring is added later the e^+-e^- beam will be relocated so as to pass

alternately above and below it, crossing in vertical planes at the interaction points. (See Appendix A.) Provision for a possible future synchrotron radiation experimental facility will also be built into the tunnel. Alternative locations are being evaluated.

Bored tunnel sections will be constructed by soft-ground tunneling methods. Most of the tunnel will be in loosely-consolidated and fine-grained Miocene sandstone. There will be limited areas of uncemented sand which will require especially sturdy initial support. Extensive core-boring and analysis around the periphery of the ring indicates that the tunneled portion of the ring housing will require shield-tunneling methods.

A minimum inside diameter of 3.35 m will be required for the bored tunnels (Fig. 59). However, this dimension, while allowing the necessary space, would require close alignment tolerance of the tunnel centerline; for this reason, a larger tunnel with a more relaxed centerline tolerance might prove less costly.

The finished tunnels will be concrete-lined and painted white for good working light levels and to reduce concrete dusting. Careful concrete-mix design specification and quality control will be exercised, not only to minimize cracking due to dimensional changes caused by unavoidable temperature differences but also to allow for the high sulfate content of the soil and ground water.

Initial support for the tunnels may be provided by steel sets and lagging, rock bolts and spiling, precast concrete sections or shotcrete. The ability to resist the thrust of the shield will be an important determining factor.

In order to suspend beam components from the tunnel roof, special reinforcing will be built into the tunnel's room lining and suspension provisions will be cast in.

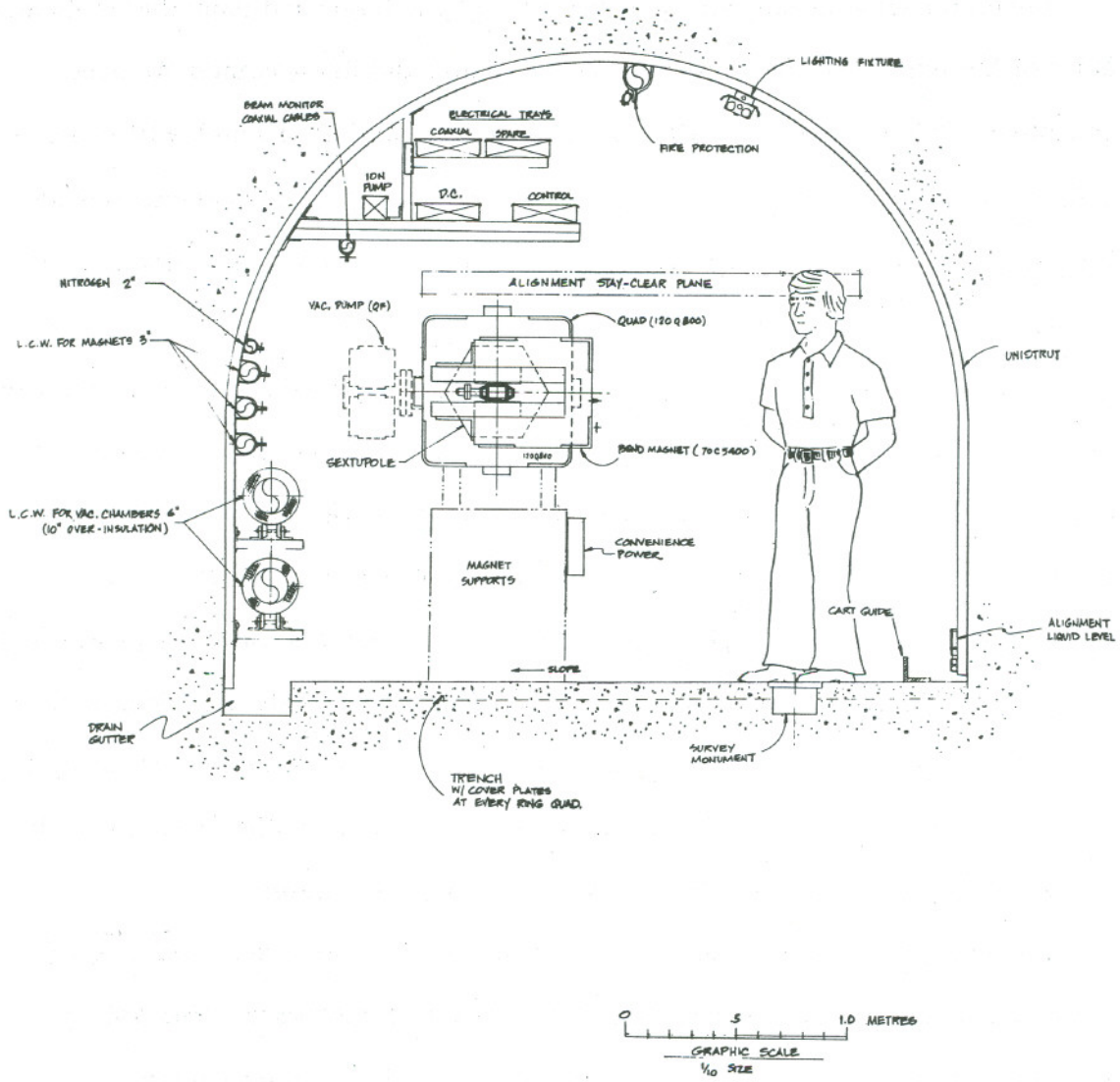

Fig. 59--Tunnel cross section.

To avoid delaying installation and the expense and bother of in-transit warehousing and double-handling, parts of the ring housing will be scheduled for early completion. We will establish three simultaneous tunnel operations, two in the main ring and one in the beam transport tunnels. Scheduling of research-facility construction in the interaction areas will be arranged so that the beginning phase will create portal structures for tunneling. When the tunnels are finished and the portals are no longer needed, the halls will be completed.

2. Roads

About 3.0 km of additional roads will need to be added to the present SLAC road system. Very little heavy earthwork is entailed due to the gently rolling nature of the site. Typical roads will have 20-ft traffic ways with 5-ft shoulders, and maximum grades will be about 8%. Oil-and-rock-chip seal coats will be used over aggregate base courses ranging between 6 and 10 inches in thickness, varying somewhat with subgrade conditions. Permanent surfacing will be done after construction.

3. Earthwork and Erosion Control

Side slopes will be constructed no steeper than 2:1 and will be flatter in areas of prominent visibility. Where space is limited special measures will be taken to enhance appearance. Erosion control surface treatment and early seeding will be done to enable the results to blend into the natural landscape. Adjacent to building areas, ground covers such as ivy, ice plant, etc., will be used not only for appearance but to reduce fire hazards as well. Edges of earthwork sections will be generously rounded to blend into the natural terrain. Any surplus materials will be used in smooth, free-form mounds for sight screening.

During the construction period, temporary silting ponds will be so placed in drainage channels to prevent silt flow into Menlo Park's drainage systems to the north and onto the flat horse-training areas to the south. Sprinkled water will be used as required to reduce dust during construction. Topsoil will be stripped from all areas to be regraded, saved and placed on finished surfaces as part of the erosion control treatment. Material will be hauled from the northern to the southern part of the ring to provide the large quantity of material required by the shielding fills in Region 5. In so doing we will avoid unnecessary excavation.

4. Drainage

High-reliability pumping systems with emergency power provisions will be used to drain the pits of the experimental areas and the lower yard of Region 2. Other yards will be served by gravity pipe systems. Erosion control measures will be taken at drain outlets wherever they are needed. Interceptor ditches, usually asphalt-lined or concrete-lined, will be constructed in peripheral areas around yards to minimize loads on the pumping systems and the storm drains. All ditches, canals and other waterways will be so constructed as to prevent erosion.

5. Landscaping

Throughout most of the construction area, regraded terrain will be treated to assure an early return of the natural grass growths of the site. Around building areas, shrubbery, trees and ground covers will be established early with sight screening a primary consideration.

Groves of eucalyptus, Monterey pine, and other fast growing trees will be used for large stands of sight screening. Drought-resistant plant materials will be used for the most part; however where water is necessary to establish the

plants, temporary pipe systems will be laid on the surface. Limited areas where less drought resistant plants are used will be provided with permanent sprinkler systems.

6. Sanitary Sewers

Sewage from Regions 12 and 2 will flow by gravity systems to SLAC's existing metering station on the Menlo Park Sanitary District system. Regions 4, 6 and 8 will be served by piped systems connecting to an existing sewer on University land which also leads into the Menlo Park system.

7. Surface Buildings

Surface buildings to house instrumentation and control equipment, RF power equipment, toilet facilities, etc., will be located near the interaction areas. RF facilities will be located in Regions 4, 8 and 12, and instrumentation and control housings will be required at all interaction areas. Economical construction will be used but architecture and landscaping will conform to rural aspect of the site. A schematic layout of the surface buildings and utility systems for each interaction region location and for the beam transport lines is shown in Figs. 60 to 66. The internal layout for the RF and instrumentation and control building for Region 8 is shown in Fig. 67.

A large vacuum system assembly building will be required at SLAC's present shop area. It will be of steel construction, conforming to SLAC's present architectural standards.

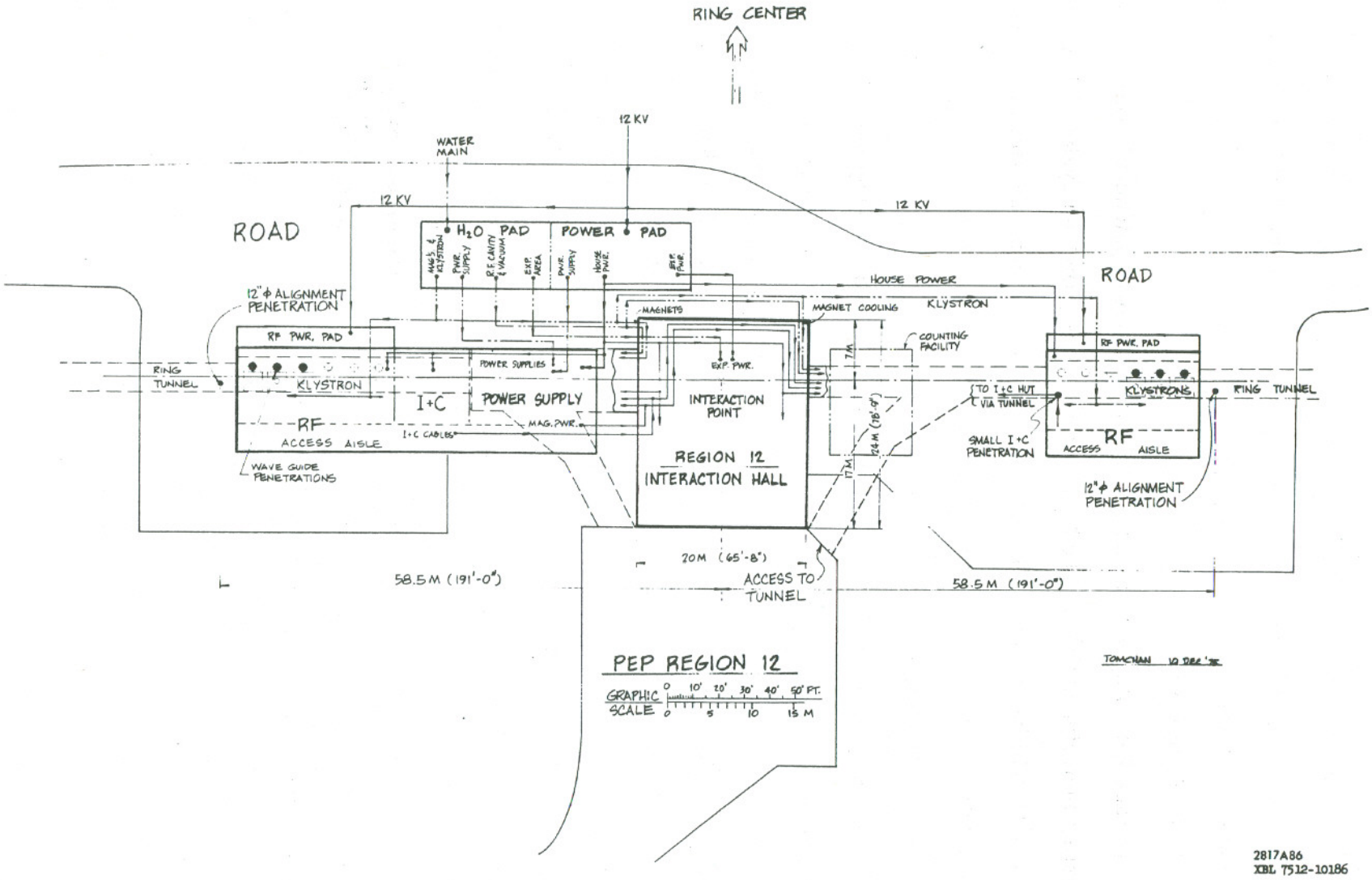

Fig. 60--Region 12 surface buildings and utilities.

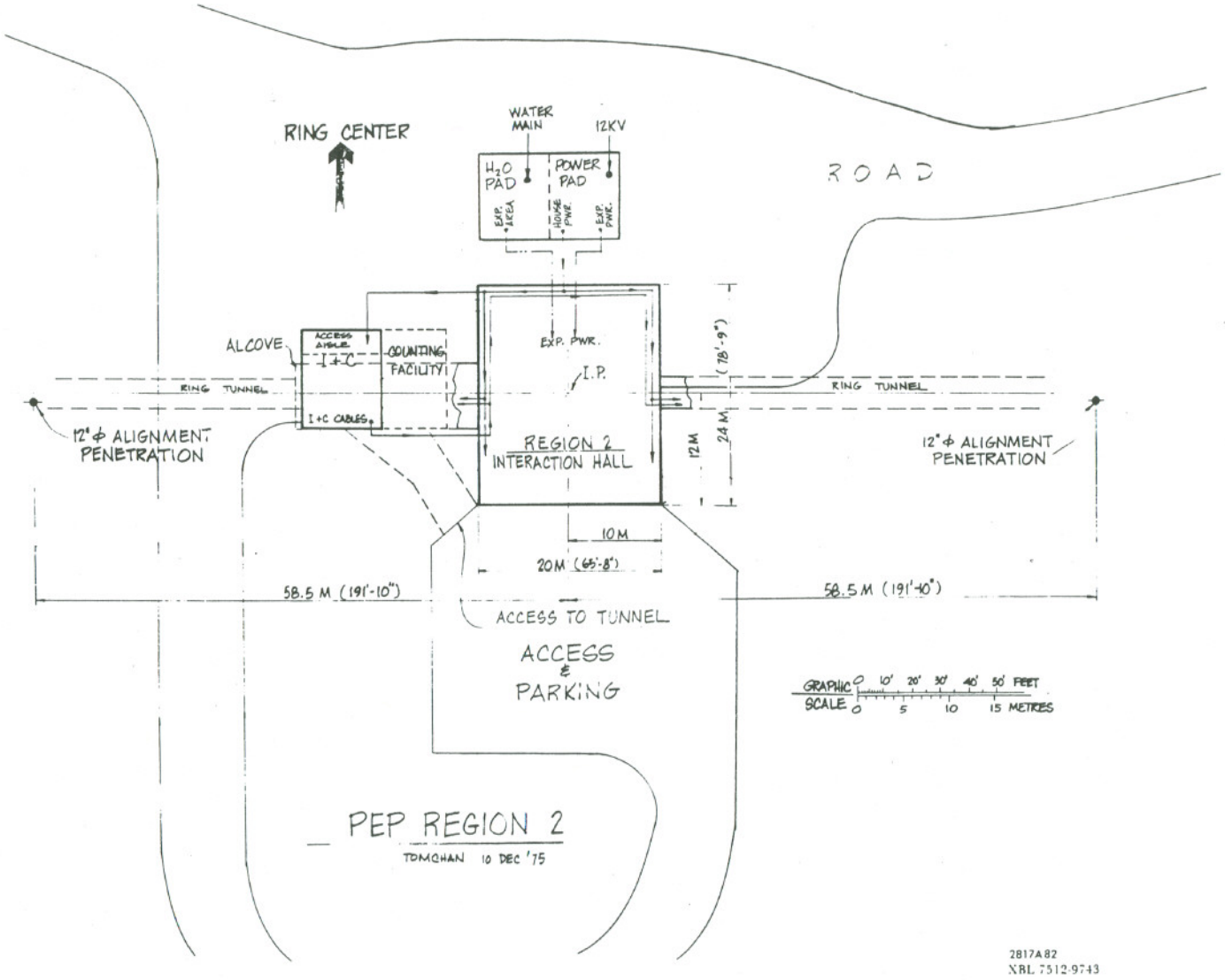

Fig. 61--Region 2 surface buildings and utilities.

0 0 0 0 4 0 2 7 9 8 2

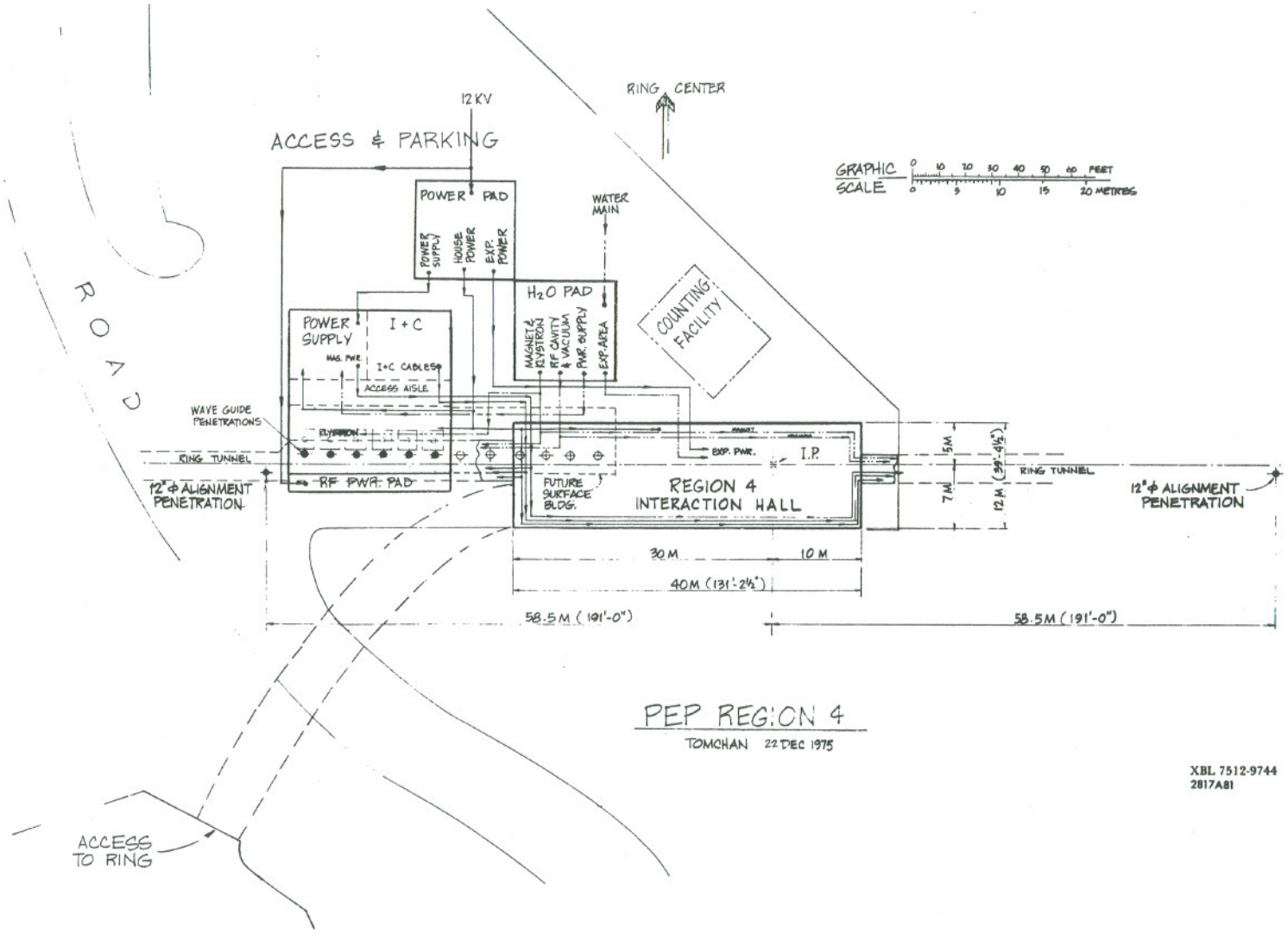

Fig. 62--Region 4 surface buildings and utilities.

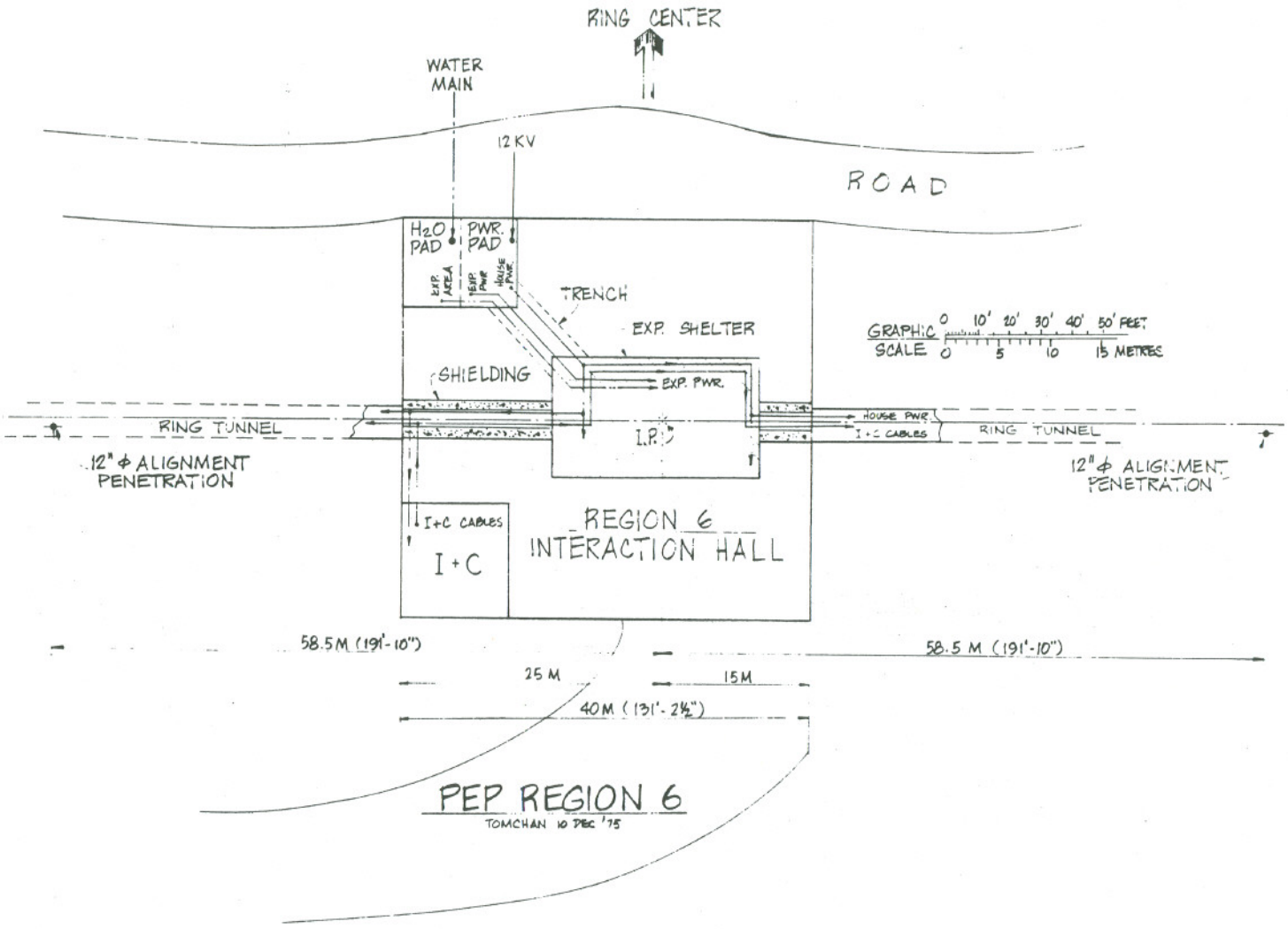

Fig. 63--Region 6 surface buildings and utilities.

0 0 0 0 4 0 2 9 8 3

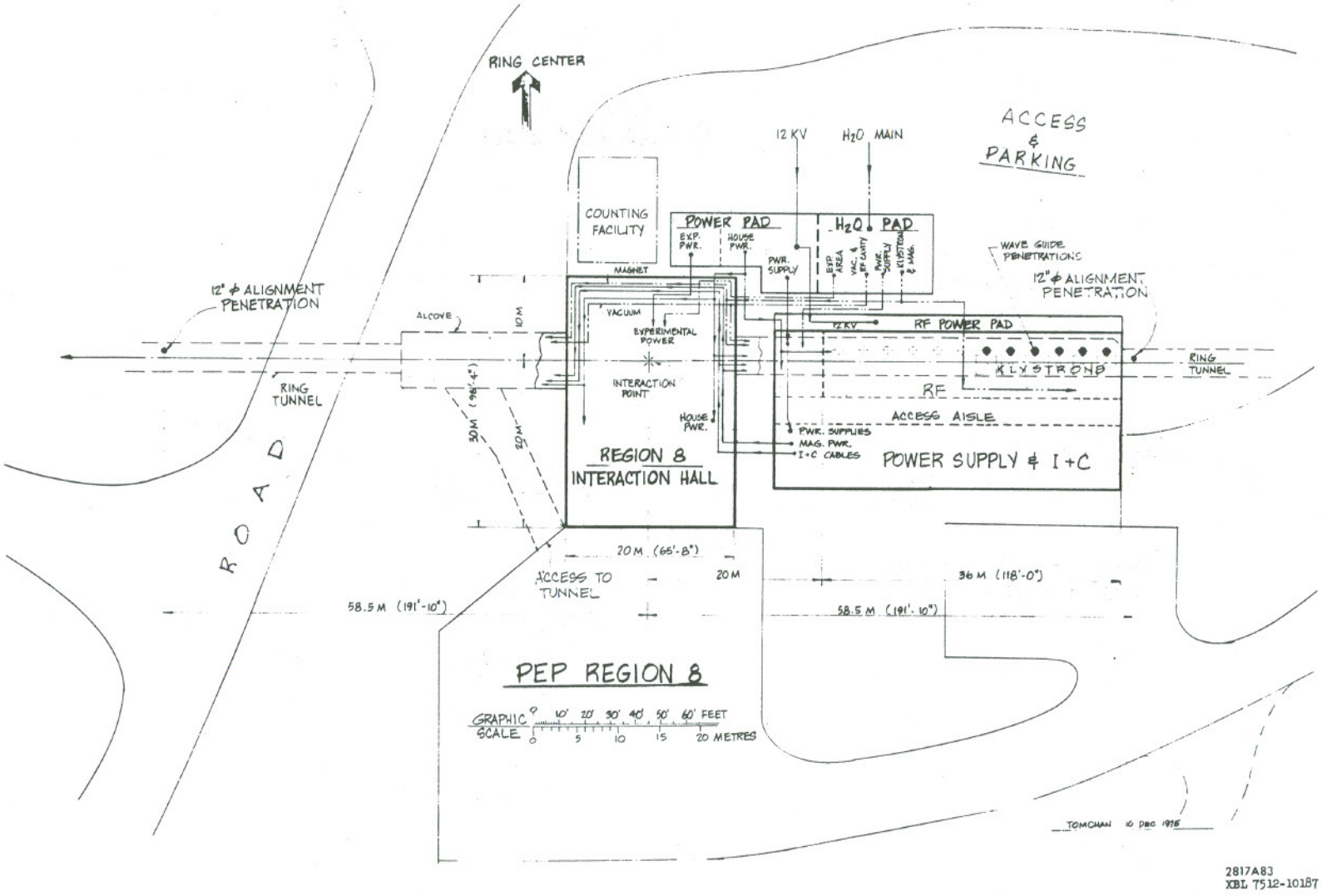

Fig. 64--Region 8 surface buildings and utilities.

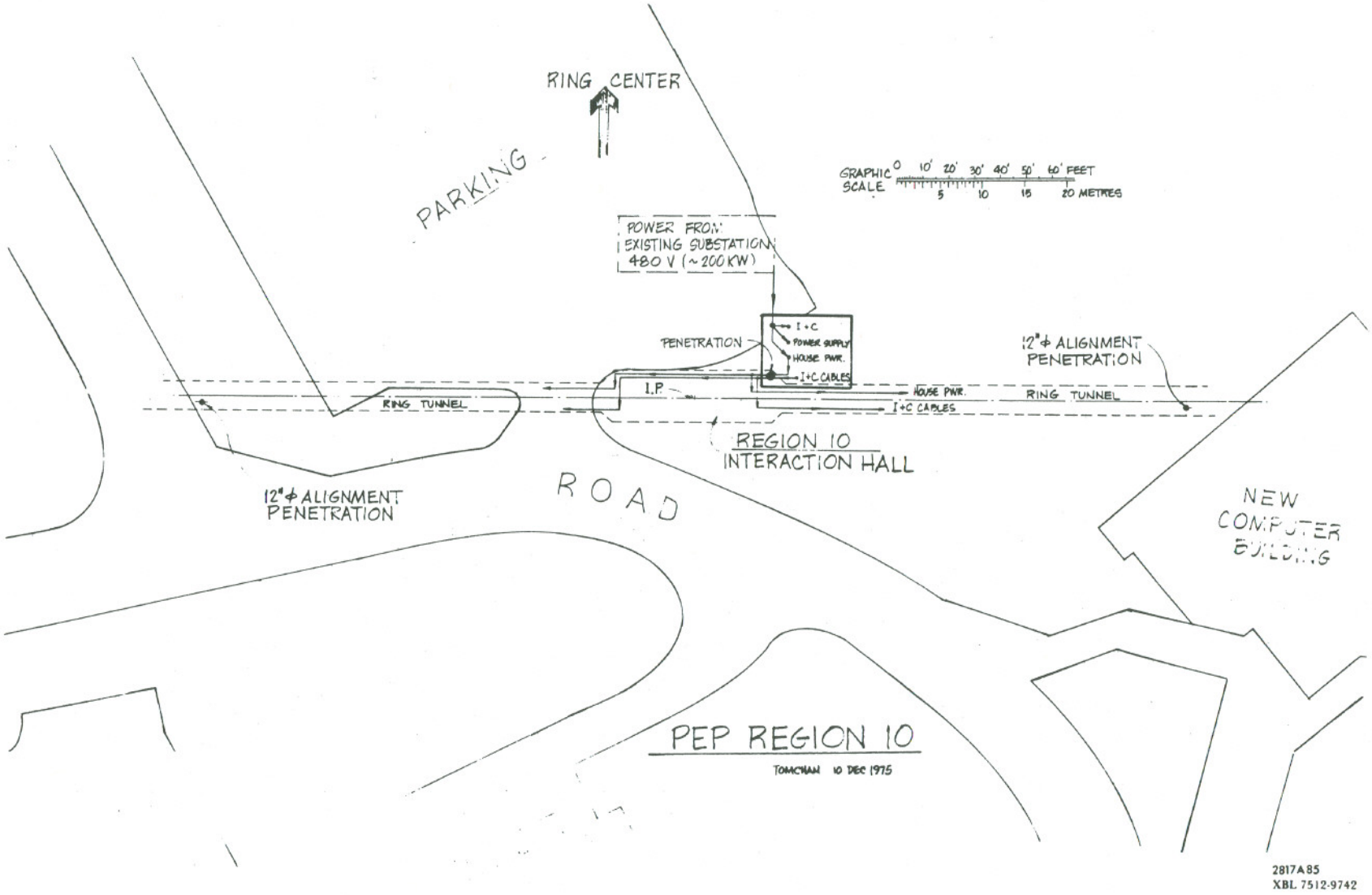

Fig. 65--Region 10 surface buildings and utilities.

0 0 0 0 4 4 0 2 9 8 4

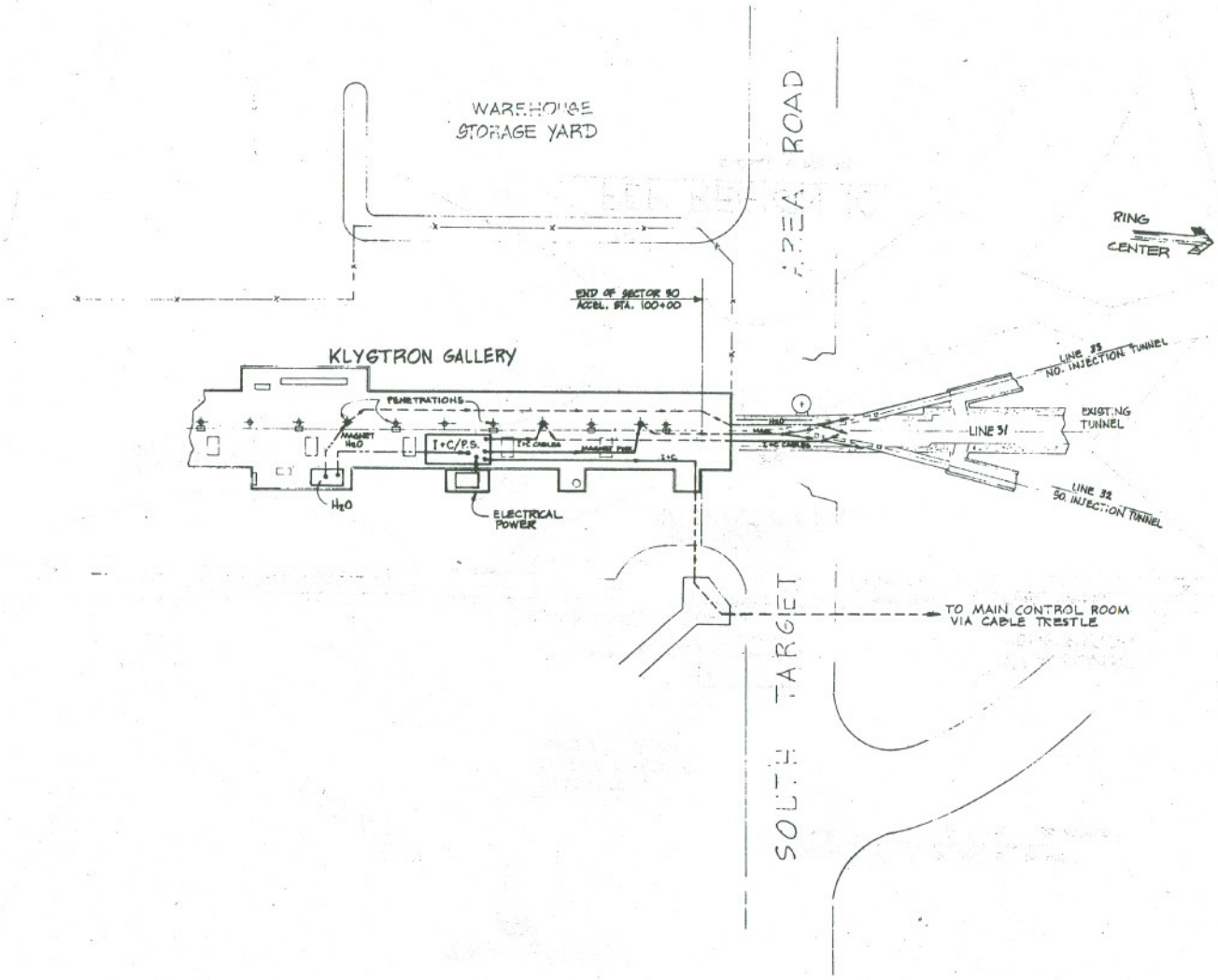

Fig. 66--Sector 30 surface buildings and utilities.

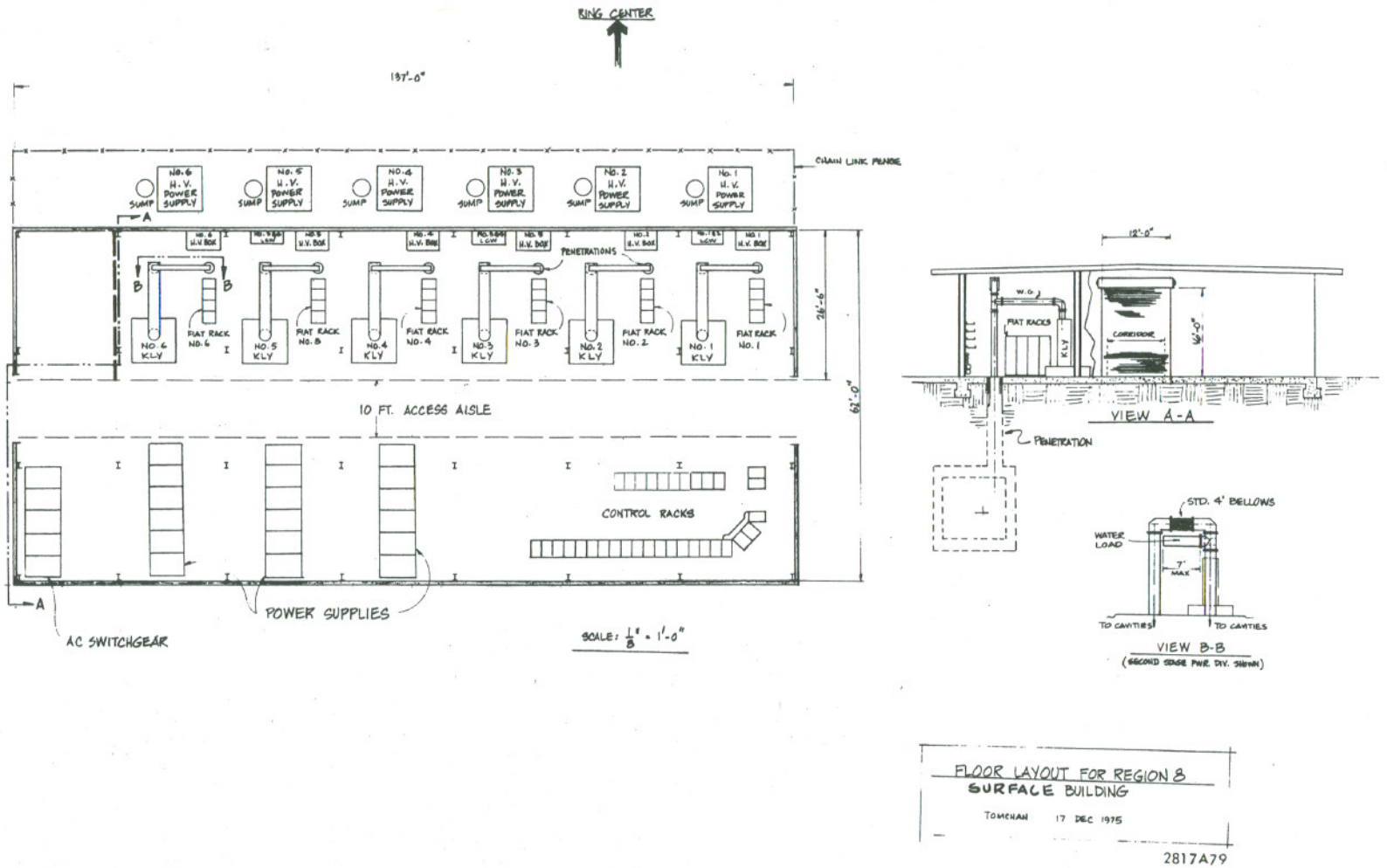

Fig. 67--Floor layout for Region 8 surface buildings.

B. Utilities

1. Electrical Facilities

The maximum electrical power demand for the electron-positron storage ring and experimental apparatus is estimated at 30 MW for the maximum PEP design energy of 18 GeV. This project power demand is based on the regional loads of all PEP components which are compiled in Table XIV. It should be noted, however, that PEP will ordinarily operate at various energies below 18 GeV with varying experimental loads. Therefore the average power utilization will be considerably below the 30 MW maximum demand figure.

Existing SLAC Power System. SLAC presently receives power from two sources:

(1) A 230-kV line with a line capacity of 300 MW. At present a single stepdown main transformer is rated 50/66/83 MVA and the secondary is operating at 12.47 kV with grounded wye.

(2) A standby 60-kV line with a limited line capacity of 18 MW. It is equipped with two 10.7/15.4/18 MVA stepdown transformers, and the secondary is also operating at 12.47 kV with grounded wye.

The 12.47-kV systems from the above two sources are not electrically synchronized in phase; consequently they cannot operate in parallel. Normal operations of the SLAC system are supplied from the 230-kV source with the tie breaker closed and the 60 kV system serving as a standby. (See schematic in upper right corner of Fig. 68.)

PEP Primary Power Loops. Two 12.47-kV underground feeder circuits will be installed in duct banks around the inside of the PEP ring following the trench for the main loop of the water system described in the next section. The two PEP circuits will be fed from two existing Beam Switch Yard (BSY) feeder

TABLE XIV

PEP Power Requirements at 18 GeV (kW)

Region Location	12	2	4	6	8	10	Sector 30	Total Demand by Components	Total[a] Demand to Power Supply
SYSTEM									
1. Magnets and Buses									
Main Dipoles[b]	500		500		500			1890	2224
Q1 and Q2[b]	130		130		130				
Q1-Q2 Trim[c]	10	10	10	10	10	10		60	70
QF's and QD's[c]	280		280		280			840	988
All other Quads[c]					1250			1250	1470
Sextupoles					300			300	353
Wiggler					(180)			0	0
Correction Elements	30	30	30	30	30	30		180	212
Injection Magnets[d]							760	760	895
(Magnet Subtotal)	(950)	(40)	(950)	(40)	(2500)	(40)	(760)	(5280)	(6210)
2. Rf System	3000		3000		3000			9000	15000
3. Experimental Equipment[e]	850	850	850	850	850	~100[f]		4350	5120
4. House Power[g]									
Tunnels	40	40	40	40	40	20[f]	50	270	
Interaction Halls	35	35	35	35	45	10		195	
Surface Buildings	100	60	100	70	110	50[f]	20	520	
MCR					50[f]			50	
(HP Subtotal)	(175)	(135)	(175)	(145)	(245)	(80)	(70)	(1035)	1035
5. Mechanical Utilities									
LCW Systems	400	60	400	60	420	0	150	1490	1490
Cooling Towers					1200			1200	1200
TOTAL	5375	1085	5375	1095	8215	220	980	22345	30055

NOTES:

[a] Projects overall magnet power supply efficiency of 85% and overall rf system's efficiency of 60%.

[b] Dipoles and insertion Quads, Q1Q2, are in series.

[c] Based on 120 mm design for normal cell quads. (The potential 100 mm bore design being studied can provide ~700 kW power reduction.)

[d] For operation at 15 GeV.

[e] Actual demand per area can be 3 × 850 kW with the total power for all areas constrained to 4350 kW.

[f] Assumes power from existing substations.

[g] Power for lights, electronics, cranes, convenience outlets, etc.

2817897

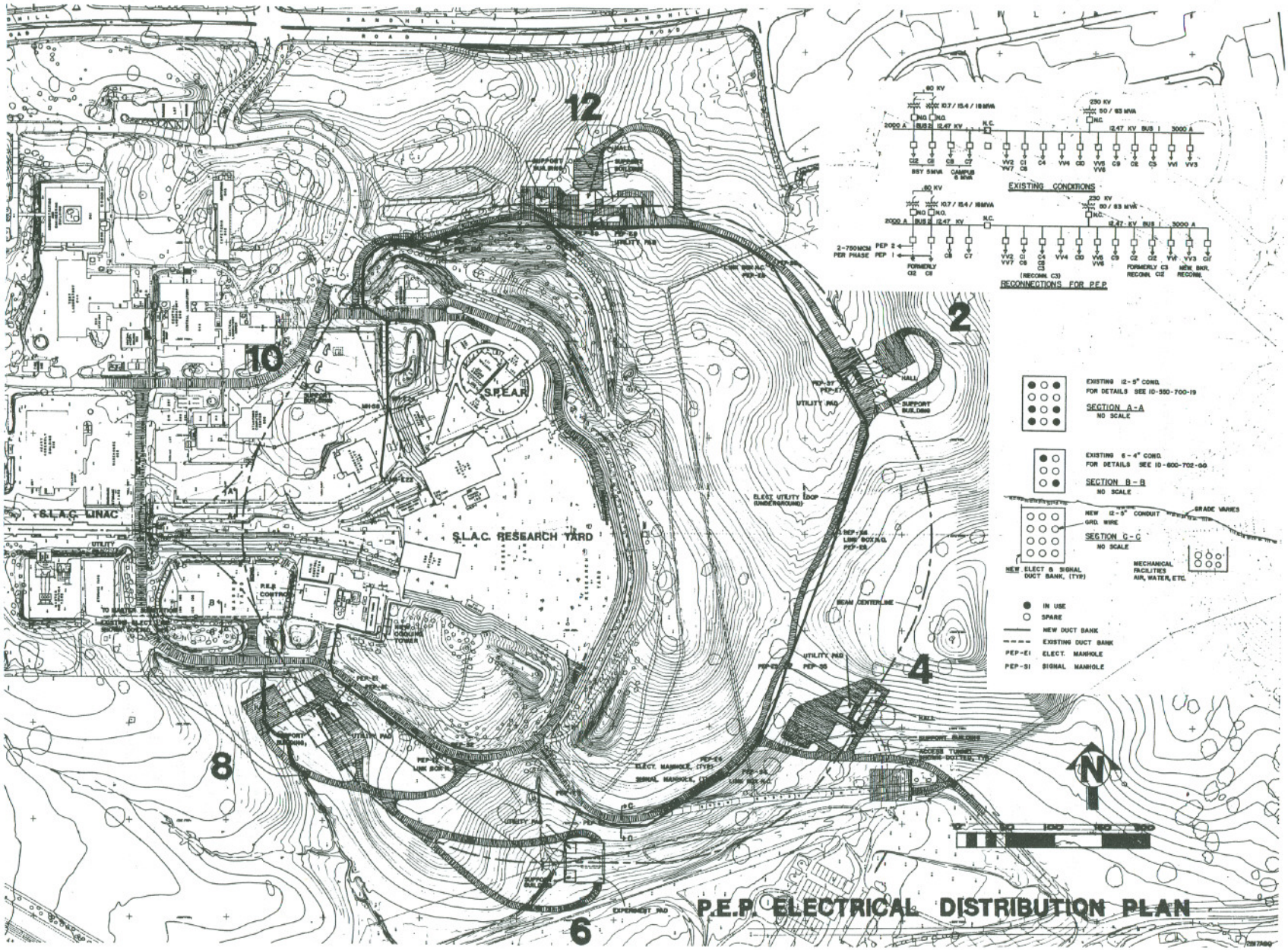

Fig. 68--Electrical research area.

breakers. The presently used BSY circuits will be reconnected to Master Substation Bus No. 1 as indicated in Fig. 68. Some of the existing duct banks (light dashed line in the figure) will be used to connect the PEP loops which are indicated by the heavy dashed lines.

Principal Services. The PEP 12.5-kV main power loop will feed substations at Regions 12, 2, 4, 6, and 8. The major services are summarized in Table XIV and shown schematically in Figs. 60 to 66.

At regions 12, 4, and 8 the 12.5-kV loop will feed the transformer pad and the klystron power supplies adjacent to the rf building. There are six 820-kVA high voltage klystron power supplies at these regions. Each supply will be fed by three 69-kVA single-phase feeder regulators rated 13,800 volts 95 kV BIL with taps for 13,800-12,000 volt operation. To provide the variable voltage requirements for the RF system, these feeder voltage regulators are equipped with 32 steps 5/8 % each to provide ±10% voltage control. To supply all 18 klystron power supplies as now planned, there will be a total of 54 such feeder regulators installed.

The magnet power supplies, house power (including instrumentation and control power, building and tunnel lights) and the pumps for LCW system will be fed via the transformer pads connected to the 12.5 kV-loop at each interaction region. A preliminary arrangement is summarized in Table XV . A portion of the total 5120 kW (from Table XIV) experimental equipment power is supplied within the transformer capabilities indicated (no 480-volt capability was initially available in previous designs). It is expected that additional transformers will be added as required for experimental apparatus and the 12.5-kV feeders will be capable of supplying up to 3 MVA of experimental power at each interaction point.

TABLE XV

PEP Power Requirements (18 GeV) by Area

Region Location	System	Maximum[1] Power Demand (kW)	Approx.[2] Line Requirement KVA	Area Sub-Station Transfers
12 and 4	Magnets	1120	1315	- One 1500 kVA (12.5 kV - 480 V)
	R.F.	5000	5880	- 12.5 kV Step Regulators
	Exp. Equip.	1000	1175	- One 1500 kVA (12.5 kV - 480 V)
	House Power	175	205	One 300 kVA (480-208/120
	Mech. Utilities	400	470	Two 75 kVA (480 - 120)
2 and 6	Magnets	47	55	- One 1500 kVA (12.5 kV - 480 V)
	Exp. Equip	1000	1175	One 300 kVA (480 - 208/120)
	House Power	140	165	Two 75 kVA (480-120)
	Mech. Utilities	60	70	
8	Magnets	2940	3450	- Two 2000 kVA (12.5 kV - 480 V)
	R.F.	5000	5880	- 12.5 kV Step Regulators
	Exp. Equip.	1000	1175	- Two 1500 kVA (12.5 - 480 V)
	House Power	245	290	One 300 kVA (480 - 208/120)
	Mech. Utilities	1620	1900	Two 75 kVA (480 - 120)
10	Magnets	47	55	From Existing Sub-station
	Exp. Equipment	120	140	
	House Power	70	80	
Sector 30	Magnets	895	1050	- One 1500 kVA (12.5 - 480 V)
	House Power	70	80	Two 100 kVA (480-208/120)
	Mech. Utilities	150	175	

(1) Includes power supplies where applicable

(2) Assumes average power factor of .85.

Within the scope of the electrical utility system, the following miscellaneous services are included:

- Temporary construction power
- Emergency lighting in the tunnels and major buildings
- Area lighting at each ring entrance and interaction area
- Emergency power for sump pump and vacuum pumps during electrical outage periods
- Fire-alarm detectors for the support buildings where instruments, computers, and power supplies are housed
- 480 volt motor control centers for LCW pump motors and tunnel exhaust fan motors.

2. Cooling Water Systems and Piped Utilities

The PEP requirements for general mechanical conventional facilities design, construction and installation are outlined briefly below.

Heat Rejection to Cooling Water. Approximately 83% of the electrical input to the storage ring and interaction area detectors will be rejected to cooling water. Machine components will be cooled by closed-loop LCW systems which will in turn reject heat to cooling tower water systems. Heat loads will be as follows:

	Load	MW Heat to Cooling Water
1)	Magnets and Power Supplies	5.5
2)	RF Power, Vacuum Chambers	14.0
3)	Interaction Area Detectors and Power Supplies	4.3
4)	House Power and Mechanical Utilities	2.0
	Total	25.8

Primary Utility Loops. Buildings and tunnels will be served by a number of underground piped utilities. These lines will be looped and located within the ring circumference so that the outer edge of the piping is at least 20 m from the centerline of the tunnel. Primary connections to these pipe loops will be extended to or from the existing SLAC underground piped utility system. A diagram of the main loop is shown in Fig. 69.

Cooling Tower System. The SLAC research area is presently served by a cooling tower with four cells rated at 7.5 MW each. Projected SLAC research loads indicate that Cells No. 1 and No. 2 must remain committed to the SLAC research yard. Cell No. 3 will be reconnected to provide cooling tower water (CTW) for PEP. Cell No. 4 must be kept in service for present purposes, but is lightly loaded. Accelerator Cooling Tower No. 1202 located at Sector 23 can accommodate the PEP injection magnet system load and the Central Shop cooling tower can handle the house power load for auxiliary PEP buildings. The main PEP CTW loop capacity will be 24 MW. Two new PEP cooling tower cells rated at 7.5 MW each will be installed and a new CTW pump basin will be added with three pumps.

RF Cavity and Vacuum Chamber LCW Cooling Systems. The RF cavities and vacuum chambers are of aluminum and must be baked out. For economical considerations, heated water at 458°K and 18 atm pressure should be used. A single portable heater will be used to heat the LCW at the mechanical utility pad at Interaction Regions 4, 8, and 12. The design input to the RF cavities is 9 MW and a maximum of 5.3 MW will be absorbed by stored beams and deposited in the vacuum cooling system via synchrotron radiation; therefore, heat rejection at the cavities will vary from 3.7 MW to about 8.0 MW depending on beam energy.

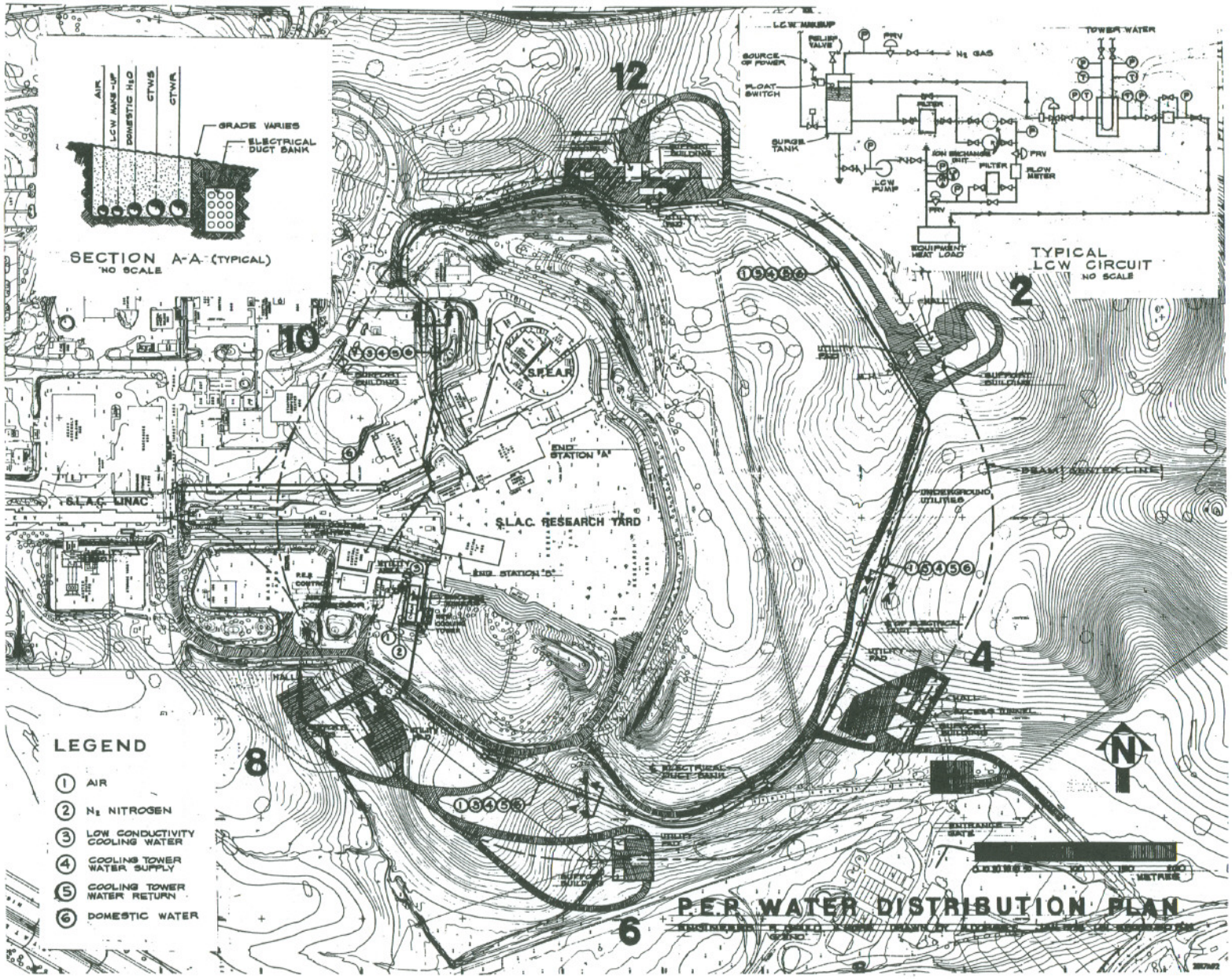

Fig. 69--Cooling tower water system.

0004409 6

Synchrotron radiation with a maximum heat flux of 1.06 MW/m^2 is deposited into and through the aluminum dividing wall between the vacuum wall and LCW cooling passages in the chamber. Since organic materials can plate out in aluminum LCW passages, the RF and vacuum chamber LCW distribution systems will be of stainless steel except for the aluminum vacuum chambers and masks.

Klystron galleries will be located at Regions 12, 4 and 8 around the ring. Cooling water for the RF cavities and vacuum chambers will be supplied from pumps and heat exchangers located near the RF housing as shown in Figs. 60, 62, and 64. The arrangement of the RF cavity and vacuum LCW cooling systems is shown in more detail in PEP Note 133.

Klystron and Ring Magnet LCW Cooling Systems. Klystron LCW cooling passages are of copper, ring bending magnet water-cooled coils are of aluminum and ring quadrupole water-cooled coils are of copper or aluminum. Most LCW piping will be of thinwall stainless steel.

Each klystron, during normal operation and assuming 66% efficiency, will reject 256 kW to LCW and generate 500 kW of RF power output. With no RF power output, all input to a klystron will be removed by its LCW system.

The required LCW supply pressure to main bending magnets and all other LCW-cooled in-ring magnets is 15 atm. The design load for in-ring magnets is 4500 kW and the maximum desirable LCW temperature rise is $20^{\circ}K$. The arrangements of these cooling systems are indicated in PEP Note 133.

Injection Magnet LCW Cooling Systems. The principal injection tunnel equipment to be cooled is the bending magnets, for which the anticipated heat load is 760 kW, and the LCW cooling system design parameters are similar to those for the ring bending magnets. LCW supply pressure will be 18 atm and temperature rise will be $20^{\circ}K$. One cooling system will be used and the heat exchanger and pump will be located at Sector 30 of the linac.

Interaction Area Detector LCW Cooling Systems. There are five major interaction area buildings; each may impose a heat load of up to 850 kW. The system will be designed for expansion to ~2500 kW when required. Optimum detector magnet design requires high LCW friction heat losses and optimum detector design requires spacial stability so that the LCW supply temperature can be controlled. Initially, one LCW system will be installed at Regions 12, 2, 4, 6 and 8. Pressure will be 25 atm and temperature rise through detector magnet coils will be held to 20°K.

Underground Piped Utilities. All underground piped utilities except CTW supply and return loops are extended from existing SLAC systems. CTW supply and return loop pipes will be 10 atm pressure class 150 asbestos cement. A LCW makeup pipe loop will run from the existing SLAC-research-area LCW storage-tank system with a distribution pressure of 7 atm. Domestic water, distributed throughout SLAC at 5 - 6 atm pressure, is used for fire protection and other domestic purposes. It will be run through 10 atm-pressure rated asbestos cement piping under grade around the inside of the PEP ring tunnel.

A medium-pressure nitrogen gas loop will be provided with valved branch lines extending to various PEP loads. The nitrogen loop will be run in the PEP ring tunnels and will be used primarily for operating the pneumatically actuated fast valves of the vacuum system.

The existing SLAC compressed air system distributes clean, dry compressed air at 7 atm pressure. The compressed air loop for PEP will be run through asbestos cement pipe and will be extended to all LCW cooling systems, the PEP cooling tower and all PEP buildings for use in control systems and for other purposes.

A natural gas loop made of two-inch wrapped all-welded steel, extended to the LCW heater stations and to each of the five interaction buildings will be provided.

3. Fire Protection Systems

All areas are classified as Ordinary Hazard, Group I. The sprinkler systems are designed for a coverage of 0.15 gpm/sq ft. The ring is to be divided into twelve zones, each zone with its separate water supply. Six of these zones will supply water to the center of the curved sections of the tunnel. The remaining six will supply water to the interaction areas.

The tunnel sections will be protected by dry-pipe, air-supervised, fusible-link head pre-action sprinkler systems. Ionization type smoke detectors will both alarm and actuate the supply valves to the systems and a manual override will prevent actuation of the supply valves if desired during working hours.

Because of the height of the interaction areas, these will be protected by open head, deluge systems. Both ionization-type smoke detectors and rate-of-rise heat detectors will be used. The smoke detectors will alarm only. The smoke detectors and the heat detectors are interlocked so that signals from both will be required to actuate the deluge valves. A manual override is also provided for these systems.

Surface buildings will be protected by dry-pipe, air-supervised, fusible link head pre-action sprinkler systems. Both ionization-type smoke detectors and rate-of-rise/fixed-temperature detectors will be used. The smoke detectors will alarm only. Signals from both the smoke detectors and the heat detectors will be required to actuate the supply valves.

Fire hydrants capable of delivering 1500 gpm at 20 psi residual pressure will be installed on either side of the interaction areas.

The source of the water for fire protection will be the 10 in. diameter cement-asbestos domestic water pipe which will be installed circumferentially inner-annular to the ring. Domestic services will be connected on the water-main side of the automatic fire protection supply valves.

4. Ventilation

Each curved section of the tunnel will have an exhaust fan located at the midpoint in the ceiling. These fans will provide five air changes per hour and maintain a slightly negative pressure within the tunnel. The air velocity in the tunnel will be very low. In accordance with the recommendations of fire protection engineers, these systems will be maintained in the "on" position during fires to remove smoke, thus assisting fire fighters and minimizing smoke damage to equipment. The air intakes at each end of the curved sections will be provided with smoke detectors which will shut off the fans and close the exhaust duct in order to prevent the drawing of smoke into the tunnels from fires on the outside.

The interaction areas will be provided with both supply and exhaust fans maintaining a slightly positive pressure in the area. The exhaust fans will draw from floor levels in order to remove any heavier-than-air gases which may be used in experiments. Local space heating will be provided as needed.

The surface building will be provided with ventilation and/or space heating depending upon the character of the equipment contained within the building.

C. Shielding Requirements and Provisions

1. Introduction

As was emphasized in Section I, it has been one of the design goals to anticipate the future addition of a proton ring; consequently, the shielding provisions discussed here are aimed at the requirements which will obtain when the proton ring is installed. These requirements are many times more severe than would be necessary for the electron ring alone.

The shielding design of the proton storage ring will be predicated upon the maintenance of a minimum of external radiation levels for all operating conditions. Levels will be below:

(a) 5 millirem per year at any point on the SLAC boundary;

(b) 1.5 rem per year at any point outside the facility shielding;

(c) less than 1 millirem at any point on the SLAC boundary for any single maximum credible accident, i.e., losing the entire beam at the worst point.

The thickness of radiation shielding, the amount of radioactivity induced in accelerator components and surrounding structures and the degree of radiation damage to components and materials depends, to a first approximation, upon the product of energy and intensity of beam losses. The possible sources of beam loss are:

(a) Injection, acceleration and transition losses;

(b) Gas scattering;

(c) Beam instabilities;

(d) Beam scrapers;

(e) Dumping (controlled and accidental).

At the present time, it is possible to give only speculative estimates of the magnitudes of these losses for the proton ring. Somewhat conservative estimates of beam loss are therefore used in this report.

The quality of the stored proton beam will slowly deteriorate with time and it will be necessary to refill the ring at regular intervals. It will be refilled when the luminosity falls significantly, perhaps by a factor of two. It should be noted that a reduction in luminosity need not necessarily result from a corresponding loss of protons from the stored beam, therefore when the ring is to be refilled, the remaining stored beam will be decelerated to an energy of 20 GeV and extracted from the ring into a dump.

The three dominant loss mechanisms are the losses on scrapers, controlled dumping losses and accidental losses. Beam scrapers and dumps will be sited in regions of large overburdens. In other regions, accidental dumping will determine the shielding requirements. Experience at the CERN ISR would indicate that the accidental loss of the entire stored beam will be a rare occurrence.

2. Shielding for Curved Sections

The overhead shielding requirement is determined by the hadron cascade generated in the shield by escaping protons. The minimum overburden planned for the ring tunnel is 5.5 m of earth each (1100 gm cm^{-2}). Calculations based upon extrapolations from experience at the CERN PS show that this overburden plus the added shielding provided by the magnets will permit 50 high-energy dumps at full intensity (3.6×10^{13} protons) without exceeding the radiation limit of 1.5 rem per year at the shield surface. The corresponding dose equivalent at the site boundary, assumed 100 meters distance, would be ~1 millirem.

Muons, produced by the decay of pions and kaons in flight, will be strongly peaked in the forward direction and are not a problem in the vertical plane. It

is possible, however, that they will penetrate the shielding in the horizontal plane at curved sections of the tunnel. For electrons and positrons, the maximum muon energy that may be produced is 18 GeV. In this case, any muons will always be stopped by the combined shielding effects of magnet steel and earth around PEP. In the proton ring, the maximum muon energy would be 200 GeV. In that case, they have sufficient energy to penetrate the lateral shielding in the area of Regions 4 through 7 on the south side of the storage ring. Preliminary estimates indicate that less than 5 millirem would be produced at the site boundary by ten full-intensity beam dumps at the single most sensitive location.

3. Shielding for Experimental Areas

At such time as a proton beam may be introduced into the ring it will be necessary to construct heavier roofs on the halls, adequate to support weight equal to 4 m of earth. This will result in higher, thicker banks at the walls as well as shielding the roof and side walls. Additional personnel protection will be afforded by fencing around roof areas to prevent access when the ring is operating.

The alcoves at the sides of the experimental halls will be covered with earth shielding in depths adequate for an eventual proton beam operation. This will cause most of the areas adjacent to the walls of the halls to be well shielded. Since the housings must be designed to support the anticipated eventual full height of shielding, and since the earth excavated from the tunnel has to be disposed of anyway, there is no extra cost in providing this level of shielding during the initial construction of the electron-positron storage ring.

Portable shielding blocks are expected to be made available from the supplies of the two laboratories.

IV. EXPERIMENTAL AREAS

A. Introduction

The design of the PEP experimental areas reflects the breadth of the expected physics program, the close interaction of experiments and accelerator operations, the diverse topographical features of the site and the determination to build the areas as economically as possible. Solutions of design problems in these areas have involved the work of many physicists and engineers from SLAC and LBL and, through the 1974 and 1975 PEP Summer Studies, of a broad segment of the high-energy-physics community. The entire community is kept informed of design developments through the quarterly PEP NEWS, since the widest exposure and discussion will help to ensure that the areas are to be responsive to prospective users' needs.

B. Characteristics of the PEP Detectors

Crucial to the design of the areas is the wide range of sizes and differing requirements of possible PEP detectors. The most intensive thinking about the detectors thus far took place during the 1974 and 1975 PEP Summer Studies. In each Summer Study, some 60 physicists from U.S. and foreign laboratories and universities worked closely together for a period of four weeks developing detector ideas for e^+-e^- collisions. Divided into various working groups they developed detectors for the following purposes:

(a) QED experiments

(b) Total-cross-section measurements

(c) Combined charged and neutral hadron detection

(d) High-resolution neutral detection

(e) Large-momentum hadrons with particle identification

(f) Weak-interaction experiments with and without polarization measurements in the final state

(g) Searches for new particles

(h) Production and observation with polarized beams

(i) e^+-e^- tagging and observation of two-photon processes.

Table XVI summarizes the main physical characteristics and requirements of 20 detectors developed during the 1974 Summer Study while Table XVII summarizes the requirements of twelve experimental setups designed during the 1975 Summer Study. Figure 70 displays the same information graphically.

The proposed detectors are larger than the present SPEAR detectors, the average length being approximately 11 m and the average width approximately 7 m. Power requirements are modest because many detectors use solid iron magnets or superconducting magnets or no magnets at all. Average floor loadings are not excessive, being approximately 10 tons/m^2. The electronic requirements are typical of large detector systems with hundreds of counters and thousands of wires. While these average properties are useful in getting a sense of scale, the design of the areas must accommodate nearly the whole range of sizes and requirements of all these detector systems.

C. Design Requirements for the Experimental Areas

The design requirements have evolved through the work of the SLAC-LBL Experimental Areas Committees and, most importantly, through the work of the 1974 PEP Summer Study Experimental Areas Group. Briefly stated, the requirements are the following:

(a) Some space (10 to 20 m) transverse to the beam line is needed for setup and repair or modification of experiments. Removal of experiments from the beam line should take a short time, and operation of the machine should be

TABLE XVI

Summary of Experimental Requirements for the 1974 Summer Study Detectors from PEP Note 177

GROUP	EXPT. EQUIP. ±L	±W	±V	WEIGHT TON	CRANE CAPACITY	POWER MW	CABLES Counters	MWPC	COMMENTS
Strange Particles (YAMIN)	5	2	2	200	0	.5	200	$5x10^3$	1) s/c beampipe 2) reverse e^+e^-
All Neutral (DAKIN)	5	2-5	2-5	200	100	.2	1200	?	
Neutral & Charged (GALTIERI)	6	3-5	3-5	190	15	.5	10^3	10^4	s/c magnet
New Particles Non-mag. (CHENG)	2-5	5	3	80	20	.1	100	10^3	
New Particles Split Field (NAUENBERG/LIMON)	5	2	2	40	20	1	200	$2x10^4$	s/c beampipe
New Particles μ-e Detector (BERLEY)	4	4	4	250	40	1			
New Particles Mini Mag. (LITKE)	2-5	2	2	120	20	1	10^3	$2x10^3$	
New Particles Calorimeter (ROSEN)	3	3	3	35	10	.1	800	100	
High Mom. (CRONIN)	6	5	5	300	40	1	600	$5x10^4$	possible rails for side motion
Low Mom. (PEREZ)	5-10	3	3	100	20	1	500	10^4	s/c magnets
Streamer Chamber (MEYER)	7-5	2	4	100	20	1	150	10^3	
σ Total Time Projection Chamber (NYGREN)	6	4	4	100	20	.5	300	$2x10^4$	1) s/c mag. 2) luminosity monitor
σ Total 4π Calorimeter (FELDMAN/HITLIN)	3	3	3	350	20	0	450	500	Vac < 10^{-9}
σ Total "Magic Angle" (LYNCH/SCHWITTERS)	6	2	2	10	0	0	200	$3x10^4$	1) good vac 2) tagging system
$e^+e^- \to \mu^+\mu^-$ (WANDERER)	2-5	2	2	70	20	.2	20	100	1) pol monitor 2) luminosity mon.
$e^+e^- \to \mu\mu/ee$ (YELLIN)	5	2-5	2-5	150	7	.1	200	$3x10^3$	1) pol monitor 2) luminosity mon.
$e^+e^- \to \mu^+\mu^-$ (BUCHHOLZ/STRAUCH)	4	2	2	615	40	.1	200	$4x10^3$	1) luminosity mon. 2) rails for assy.
$e^+e^- \to \mu^+\mu^-$ Uranium Ball (WENZEL)	8 (3)	8	8	13000	30	0	300	10^5	
$e^+e^- \to \mu^+\mu^-$ Iron Tear Drop (STEVENSON)	4.5-10 (3)	4.5	4.5	3000	40	.5	300	10^4	
2γ Tagging (BARBIELLINI)	10	2	2	20	5	.3	400	10^3	collimator before Q2 radius 7 cm

2817895

No.	DETECTOR	ELECTRONICS				
		PHOTOTUBES	MWPC WIRES	DRIFT CHAMBER CHANNELS	CABLES	
					Sig.	HV
1	Parasitic 2γ Tagging	1000	14000		1000	1000
2	General User Magnet (GUM)	20	--	3200	50	50
3	Two-Photon Experiment (⊕ GUM)	300	4000	5000	500	500
4	Neutral Detector (⊕ GUM, ⊕ 2γ tagging)	20	--	600	50	50
5	Crystal Ball with Calorimeter (⊕ 2γ tagging)	1000	--	1500	1000	1000
6	High Momentum I (High-Field Magnet similar to GUM)	400	1000	3000	800	400
7	High Momentum II (Low-Field Magnet)	600	500	5000	600	600
8	General Detector (⊕ 2γ tagging)	300	--	1000 - 5000	300	300
9	Streamer Chamber (⊕ 2γ tagging)	200	50 m^2 delay line	2000	200	200
10	New Particle Search (⊕ 2γ tagging)	340	250	2800	400	400
11	Iron Ball including Longitudinal Polarizer	150	--	1000	300	200
12	Split Iron Ball including Longitudinal Polarizer	200	--	6000	400	200

The ⊕ symbol in the detector column shows what apparatus can be added to the basic detector. Lengths appearing in parentheses are for the two-photon tag which can be used in conjunction with several detectors.

TABLE XVII

Summary of Experimental Requirements for the 1975 Summer Study Detectors
from PEP Note 205

-- continued --

0 0 0 0 4 4 0 2 9 9 5

No.	SIZE/WEIGHT										
	SIZE OF EQUIPMENT (m)			WEIGHT (tons)		SIZE OF LARGEST PIECE (m)			MAGNET		
	±L	±W	±H	Total	Largest Piece	L	W	H	Pwr (MW)	Field (kG)	Vol. (m^3)
1	9.7	1	1	< 1	< 1	1	1	1	--	--	--
2	5.6	4	4	400	30	4	2	2	s/c	15	25
3	9.7	4	4	700	30	4.6	2	0.2	1.7	4.5	13
4	5.6	4	4	200	2	4	3	2	--	--	--
5	3.5 (9.7)	3.5	3.5	630	30	2.5	4	0.3	--	--	--
6	6	4	4	750	30	4	1	0.3	s/c	20	25
7	6	3.6	3.6	350	30	4.5	6	6	s/c	3	240
8	4.7 (9.7)	4	4	300	10	4	2.3	2.3	s/c	15	12
9	4.5 (9.7)	3.5	3.5	1500	30	1	5	5	s/c	15	55
10	3.5 (9.7)	2	2	430	20	0.6	1	1	s/c	20	3
11	9.7	2.2	2.2	150	80 (15)	3.8	4.4	2.2	0.15	18	30
12	9.7	3	3	630	30	9.4	3	0.5	0.2	18	80

TABLE XVII (cont.)

-- continued --

No.	SERVICES										
	SPECIAL GASES			REFRIGERATION			COUNTING ROOMS (m^2)		MONITORS		
	Gas	Vol. (m^3)	P (atm)	T (^oK)	Power (w)	Mass (tons)	Close	Far	Lum.	Pol.	$\gamma\gamma$ Tag.
1	--	--	--	--	--	--	10	10	X	✓	X
2	--	--	--	4	50	2	20	200	✓	X	✓
3	--	--	--	4	30	0.1	10	50	X	✓	X
				Flux Excluder							
4	--	--	--	78	?	200	10	100	✓	✓	✓
5	--	--	--	78	?	100	10	100	✓	✓	✓
6	Pentane Propane	11 75	6 1	4	?	?	10	100	X	X	X
7	Isobutane Pentane	2 19	4 1	4	?	24	10	100	X	✓	X
8	Freon 12	8	4	4	200	?	10	100	✓	✓	✓
9	--	--	--	4	?	?	10	100	✓	X	✓
10	--	--	--	4 78	100 ?	2.5 24	10	100	X	X	✓
11	--	--	--	--	--	--	20	80	✓	✓	X
12	--	--	--	--	--	--	15	100	X	✓	X

TABLE XVII (cont.)

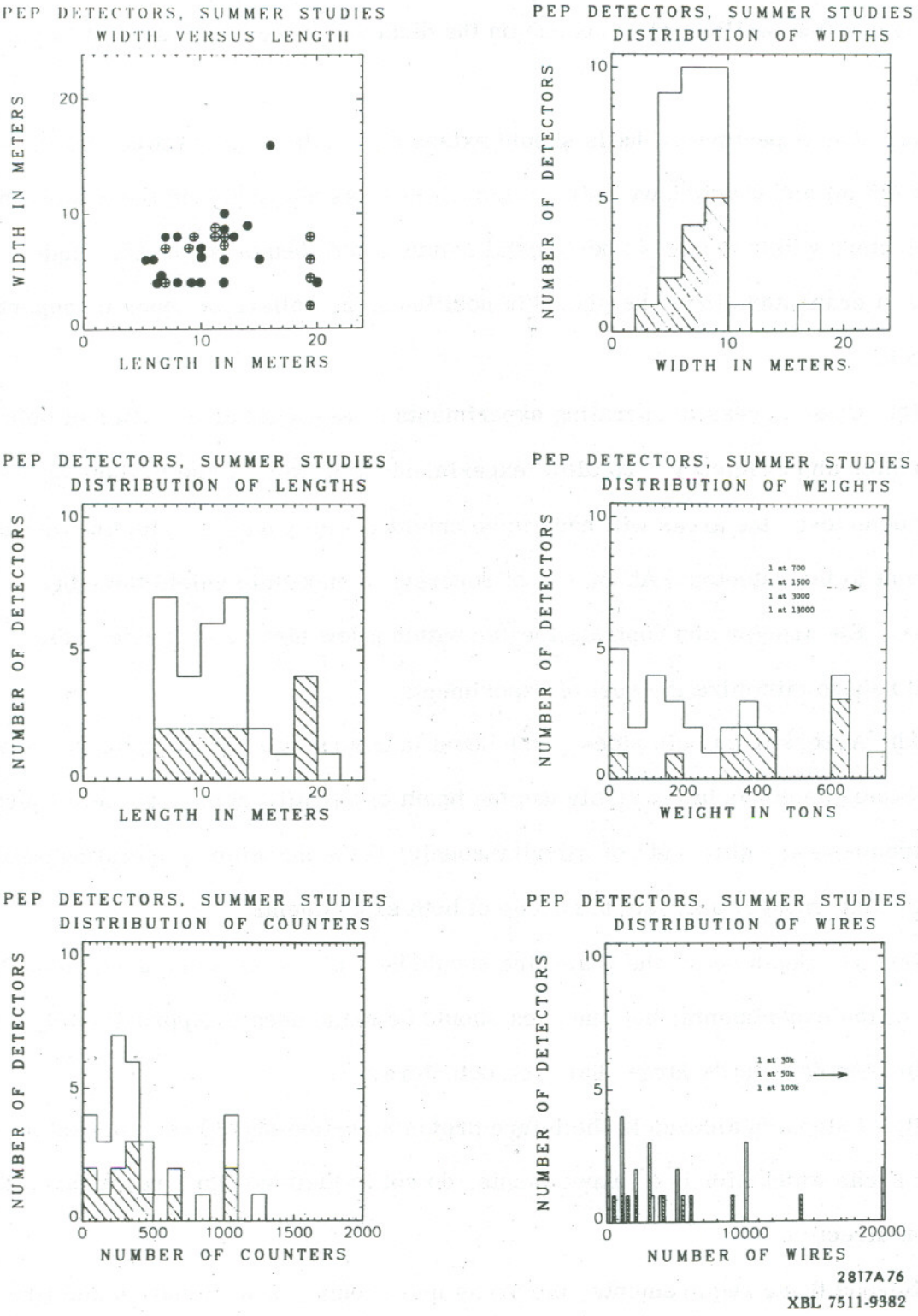

Fig. 70--PEP detectors from the 1974 and 1975 Summer Studies.

able to continue while work proceeds on the detector in the area adjacent to the beam.

(b) The experimental halls should extend the whole length between quadrupoles (20 m) and should have uniform elevation so as not to hinder the movement of detectors within them. Experimental setups could then be assembled under the area crane and simply be placed in position using rollers or other transporting devices.

(c) Close access to operating experiments is essential as a matter of both economics and efficiency. To allow experimenters to work close to their operating detectors, the areas will have to be shielded with portable shielding blocks adjacent to the detector. About 1 m of concrete is enough to shield the stored beams. Electronics and controls located within a few meters of the detector would help to minimize the cost of experiments.

(d) Access from both sides of the beam is desirable in at least some areas. Two experiments could profitably use the beam either alternately, if their energy requirements are different, or simultaneously, if the machine is operating at one energy long enough to satisfy the needs of both experiments.

(e) The depth below the beam line should be 4 m. This would accommodate most of the experiments, but one area should be made deeper (approximately 6 m) to allow for potentially large-diameter detectors.

(f) Extension alcoves in the future proton direction should be provided in those areas which, for e^+e^- experiments, do not in their design already favor the proton direction.

Beyond these requirements, the areas must comply with radiation and fire safety requirements and have the available power, cooling capacity and other utilities necessary for experimental operation.

D. Description of the Experimental Areas

Using the clockwise numbering of regions explained in Section III. A and shown in Fig. 58, we show an elevation cut along the ring in Fig. 71. The topographical variation is an advantage for the varied experimental program we are considering. Each area has strengths and limitations, and together they fit both the land and the varied needs of the program. The basic parameters of the experimental areas are shown in Table XVIII. However, it should be mentioned that the requirement for the crane hook height above the beam line is still being optimized to get the best balance between maximum crane accessibility and allowable cost. Since the land topology favors the clockwise (CW) direction for the future proton beam, alcoves in the CW direction have been included in Areas 12, 2 and 8. They are 20 m long, 7 m wide and 5 m high. Some e^+-e^- experiments will almost certainly need alcoves in any case, and the implementation of Phase II (the 200-GeV proton ring) will require them. Including them now will be less expensive than adding them later. Areas 4 and 6 are extended naturally in the CW proton direction, as described further on.

Some of the special features of each area follow:

(a) Area 12 (Figs. 72 and 73)

This area is located in moderately level terrain with the interaction point approximately 5 m below natural ground elevation. Access to the experimental hall is from a yard located on the outside of the ring and the hall itself is offset laterally from the beam line. This allows the setup of very large apparatus in the 17-m by 20-m area adjacent to the beam. A typical device, and how it might be arranged in the area, is shown in Fig. 74. The most utilitarian means of bringing materials into the experimental hall is through portable loading platforms

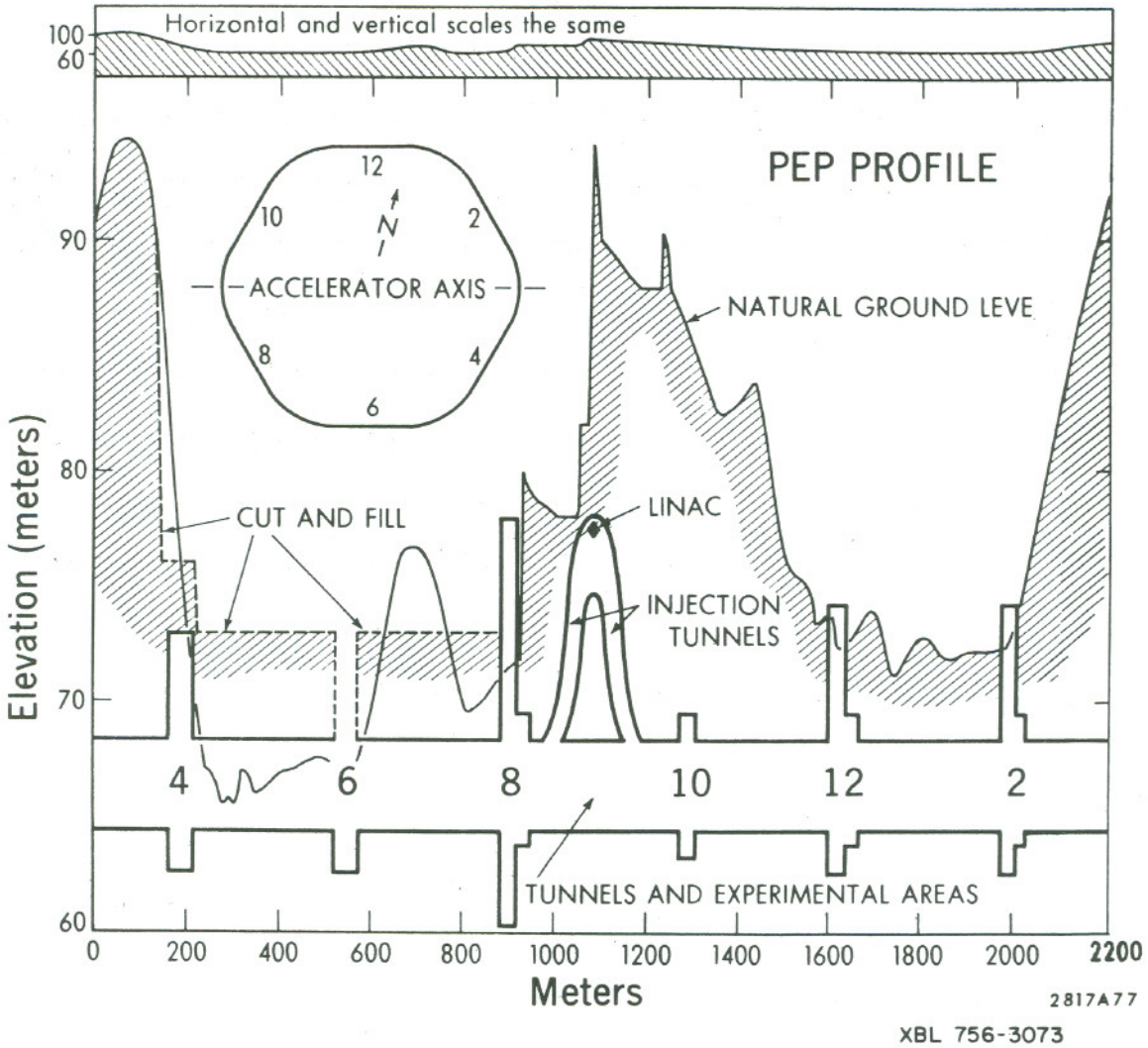

Fig. 71--Topographical profile of the PEP site.

Table XVIII

Specifications for Experimental Areas

Specification	Area 12	2	4	6	8	10
Length (m)						
Clockwise (CW)	10	10	30	25	10	10
Counter Clockwise (CCW)	10	10	10	15	10	10
Width (m)						
Inside	7	12	5	20	10	3.5
Outside	17	12	7	20	20	3.5
Height						
Maximum Crane Hook Clearance above beam	6.0	6.0	5.0		9.0	3
Beam Elevation above floor	4	4	4	4	6	2
Crane (tons)	30	30	30	No	30	No
Nearby Space for Counting House	Yes	Yes	Yes	Yes	Yes	No
Alcove	Yes	Yes	No	No	Yes	No
Length (CW) (m)	20	20			20	
Width ± (m)	3.5	3.5			3.5	
Height + (m)	3	3			3	
Height − (m)	2	2			2	
Power (MW)						
Installed Capacity[a]	3	3	3	3	3	0
Distributed	1	1	1	1	1	0
Loading Access	Outside (yard)	Outside (yard)	Outside (tunnel)	Both (sides)	Outside (yard)	Beam (tunnel)

[a]Available at pad. The total for all areas is 10 MW.

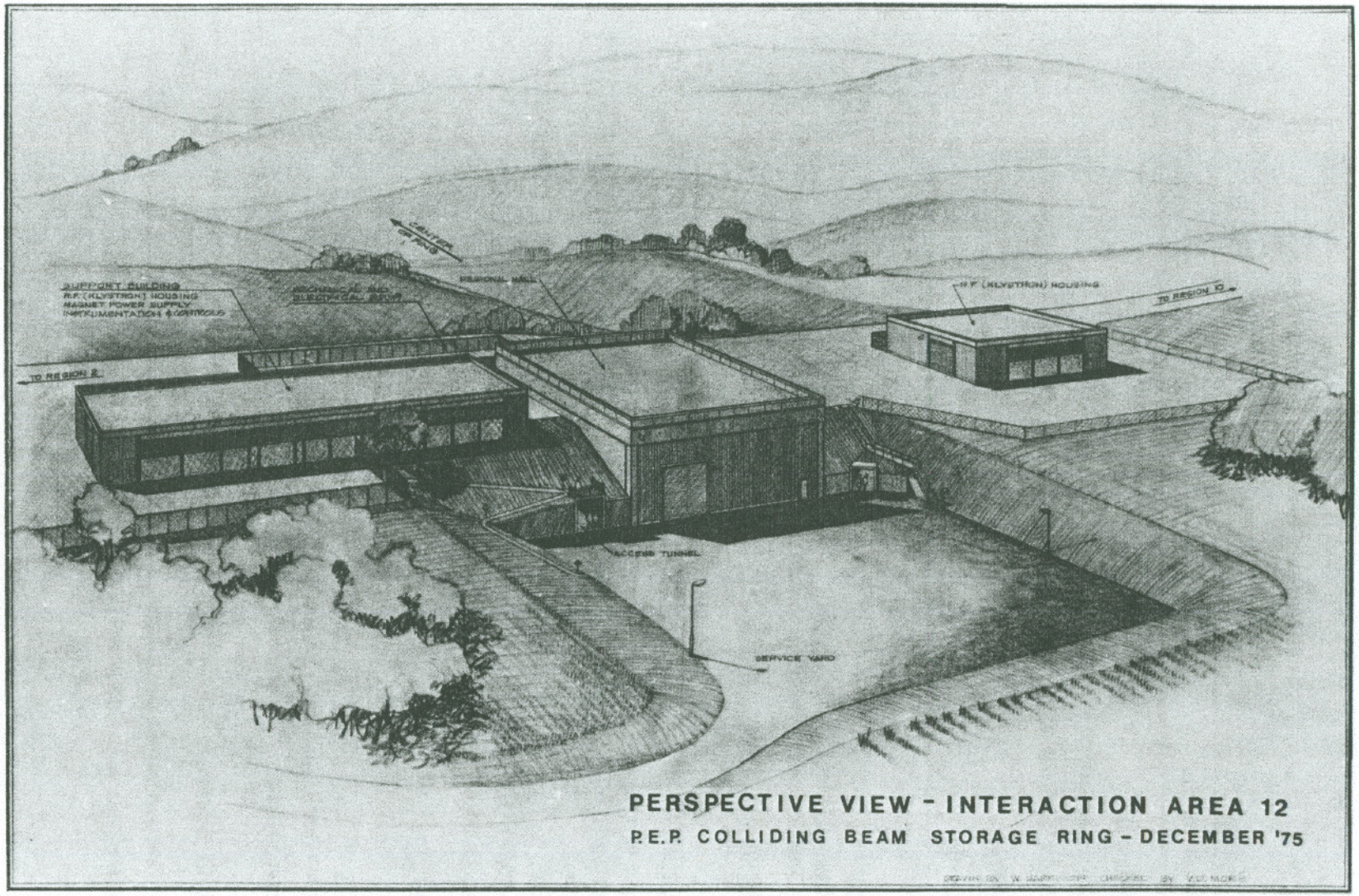

2817A63

Fig. 72--Architectural view of Region 12.

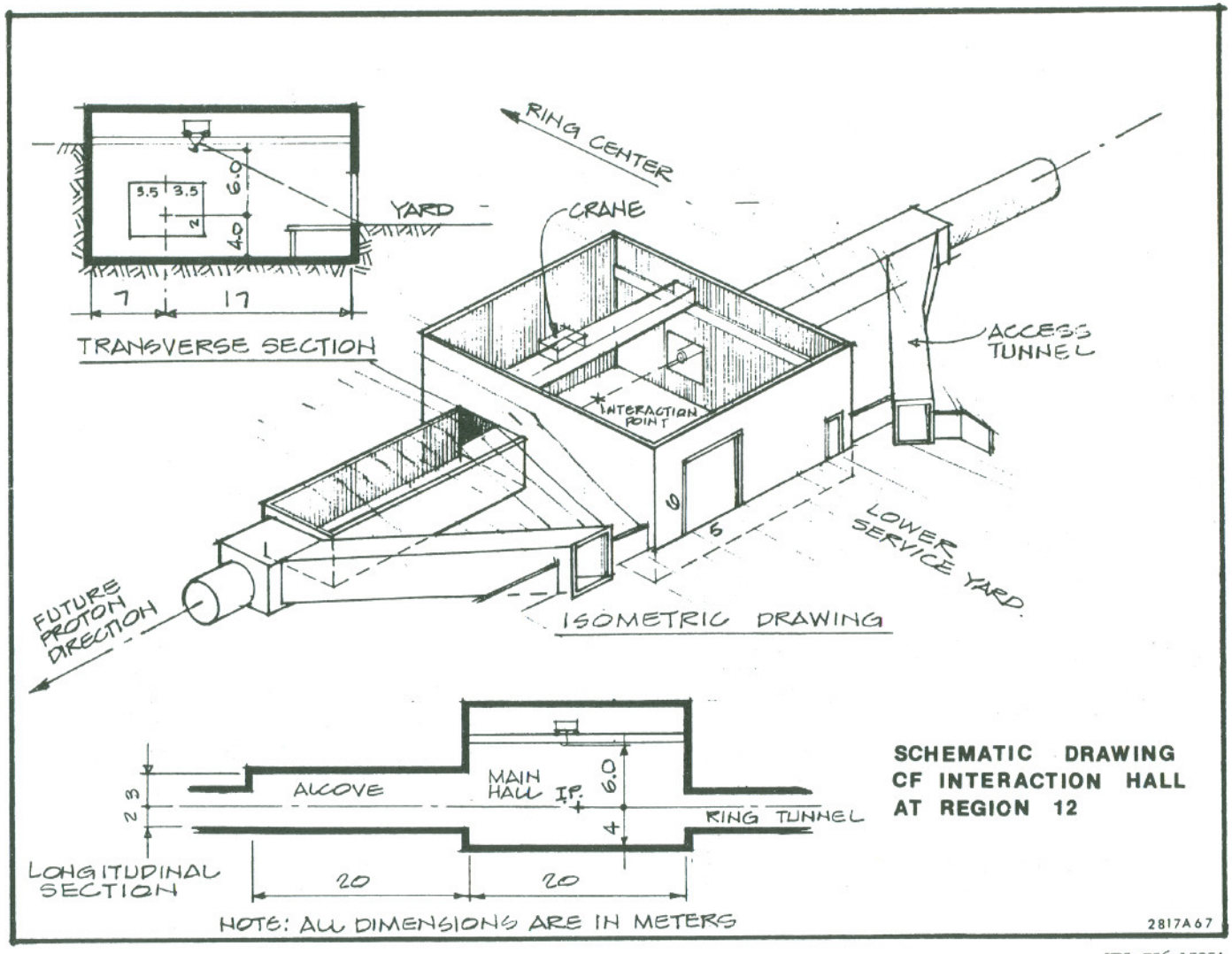

XBL 756-1525A

Fig. 73--Isometric view of Region 12.

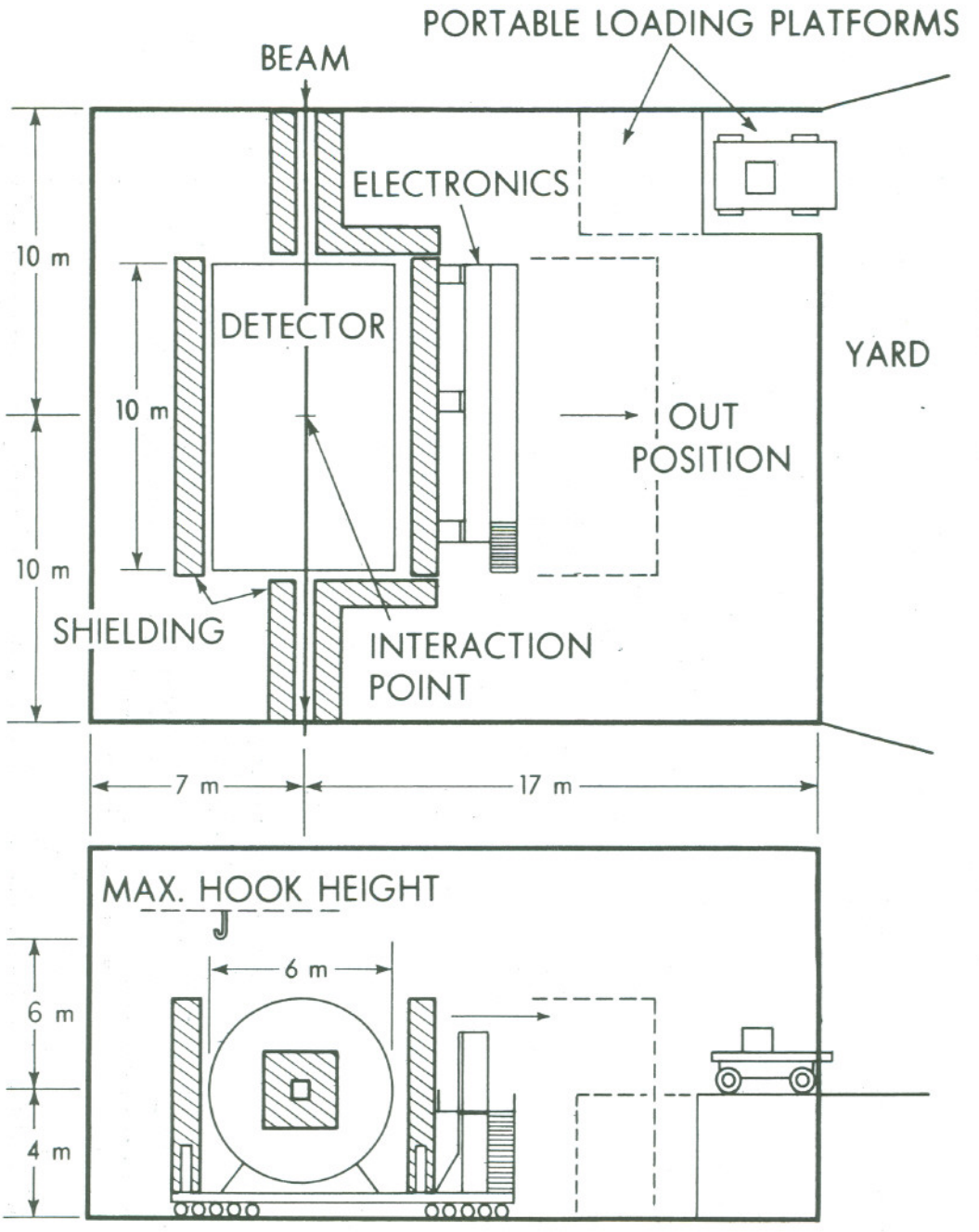

AREA 12: POSSIBLE EXPERIMENTAL SET-UP

2721825
XBL 756-3103

Fig. 74--Possible experimental setup.

placed under crane coverage, as is also shown in Fig. 74. The area has an alcove in the CW direction.

(b) Area 2 (Figs. 75 and 76)

This area is also located in moderate terrain with the interaction point approximately 6 m below the natural land elevation. The experimental hall and yard are similar in dimensions to Area 12, except that the hall will be placed symmetrically 12 m on each side of the beam line. This area will be useful for several modes of operation. For example two compact detectors could alternate position in the beam in a push-pull configuration or two experiments not needing full solid angle coverage could run simultaneously on either side of the beam-line. The area is also useful for one experiment needing large transverse dimensions on both sides of the beamline. The area is extended by an alcove in the CW direction.

(c) Area 4 (Figs. 77 and 78)

Area 4 is on the side of a steep hill with the interaction point approximately 12 m below natural ground elevation. The experimental hall is narrow (12 m) and long (40 m) and is positioned asymmetrically along the beamline, favoring experiments needing length in the CW direction. Access is via a tunnel from an adjacent clear area near grade level. Because the CW direction is already favored, no alcove is included.

An alternative design for this area in being considered. It would involve trading length for width in the hall. The length would be reduced to 20 m and the width increased to 17 m with 12 m towards the outside of the ring.

(d) Area 6 (Figs. 79 and 80)

This area is in the lowest terrain, with the interaction point nearly at natural ground level. Taking advantage of the low terrain and a good sandstone base, the

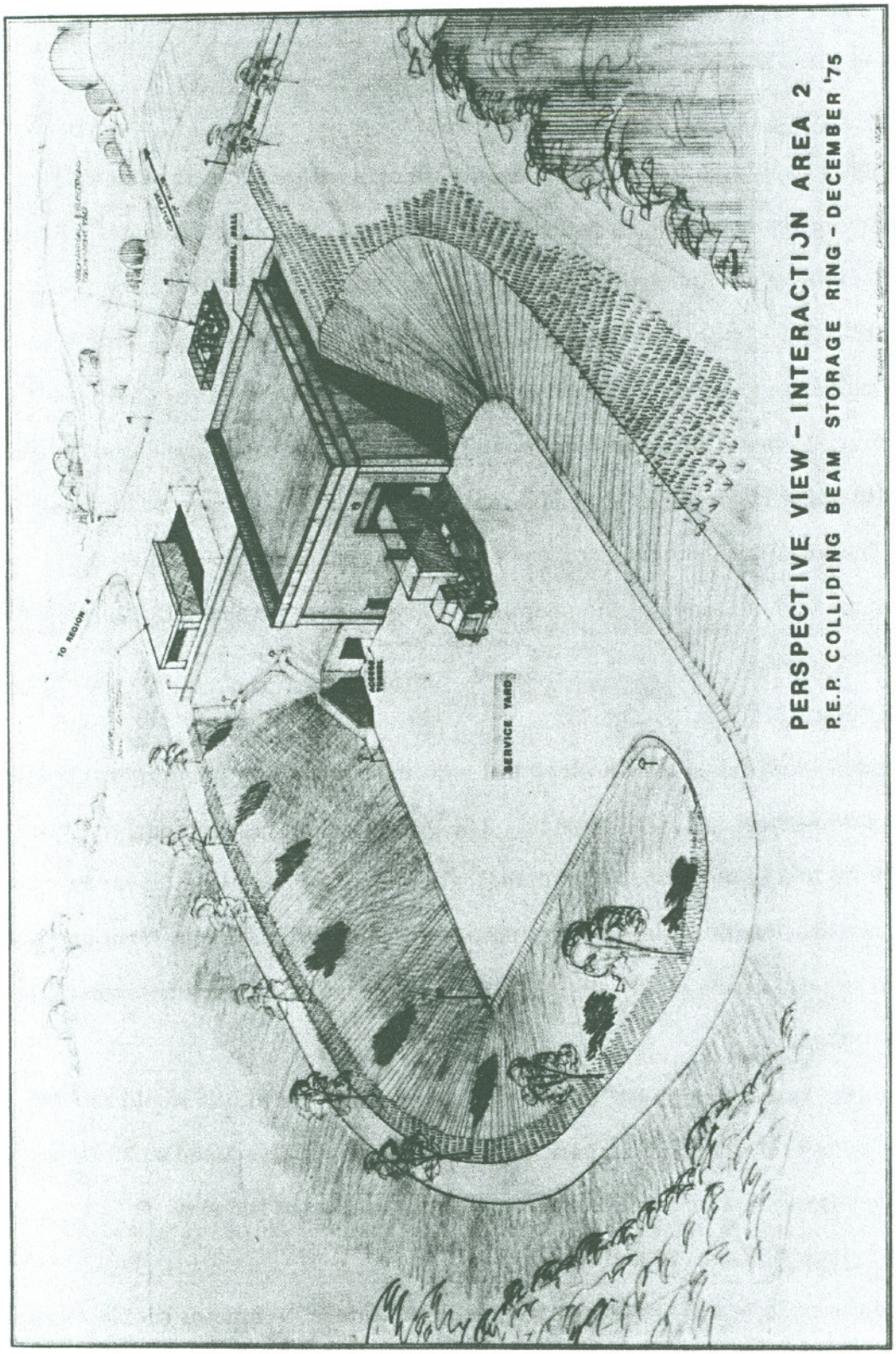

Fig. 75--Architectural view of Region 2.

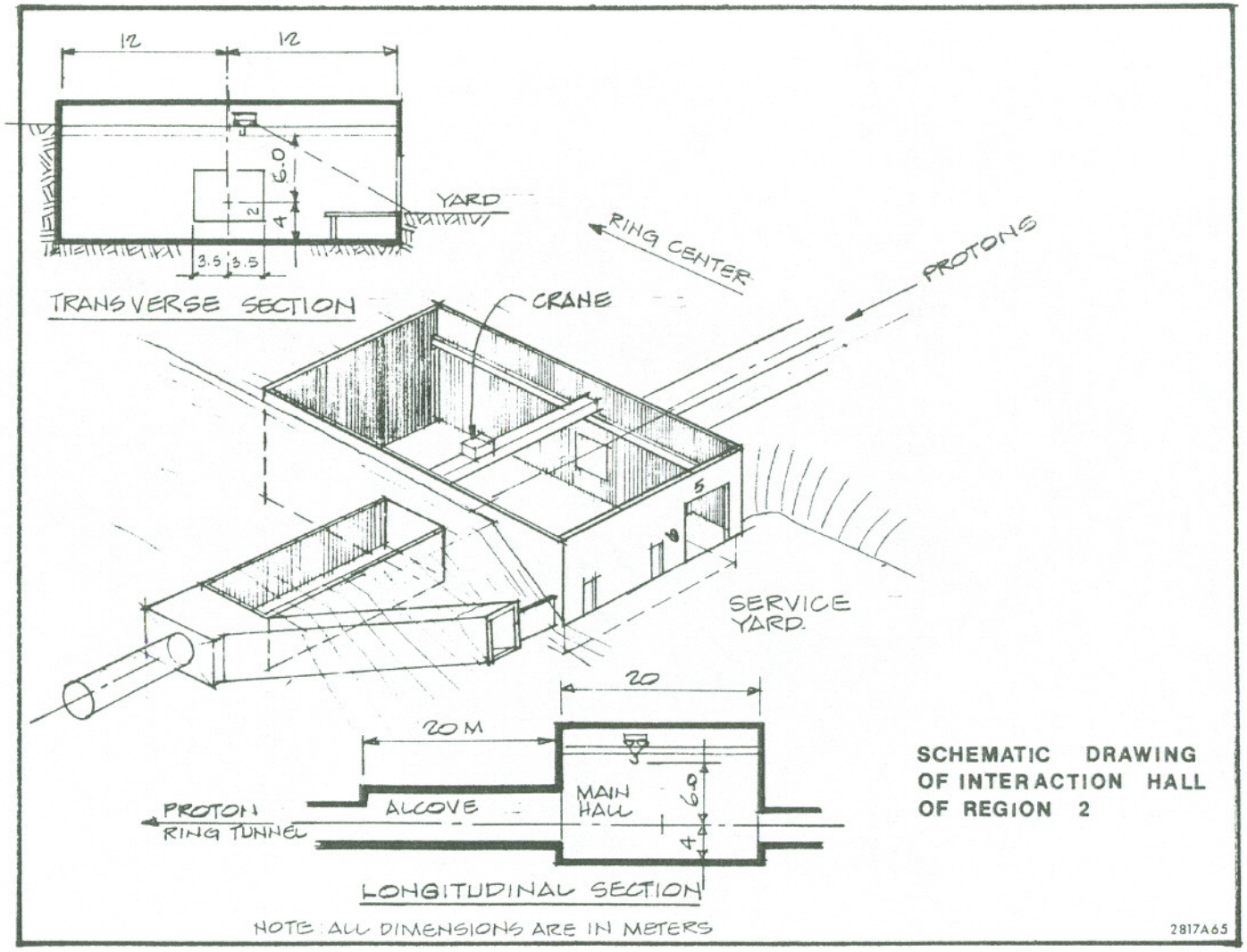

XBL 756-1522A

Fig. 76--Isometric view of Region 2.

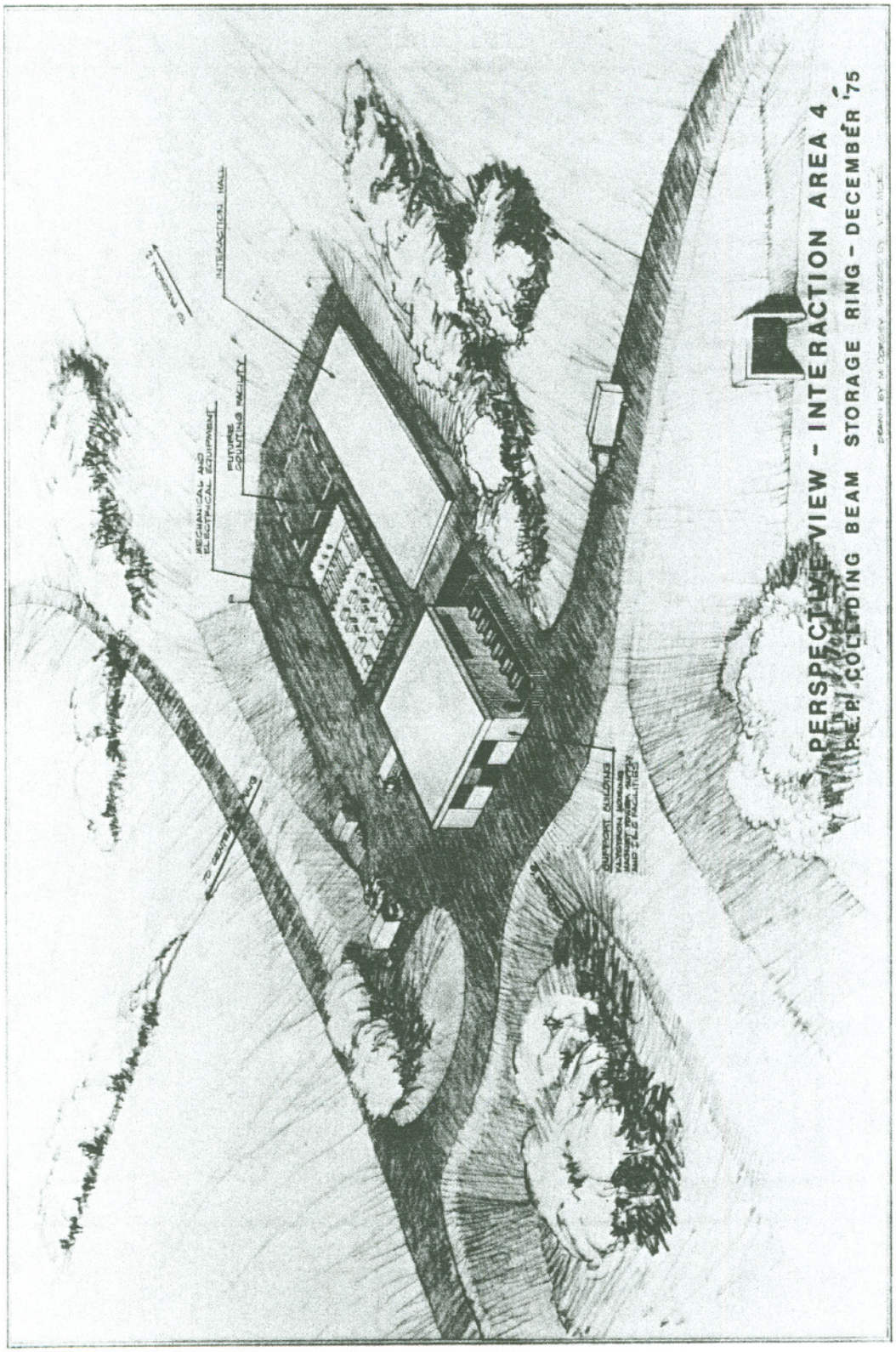

2817A66

Fig. 77--Architectural view of Region 4.

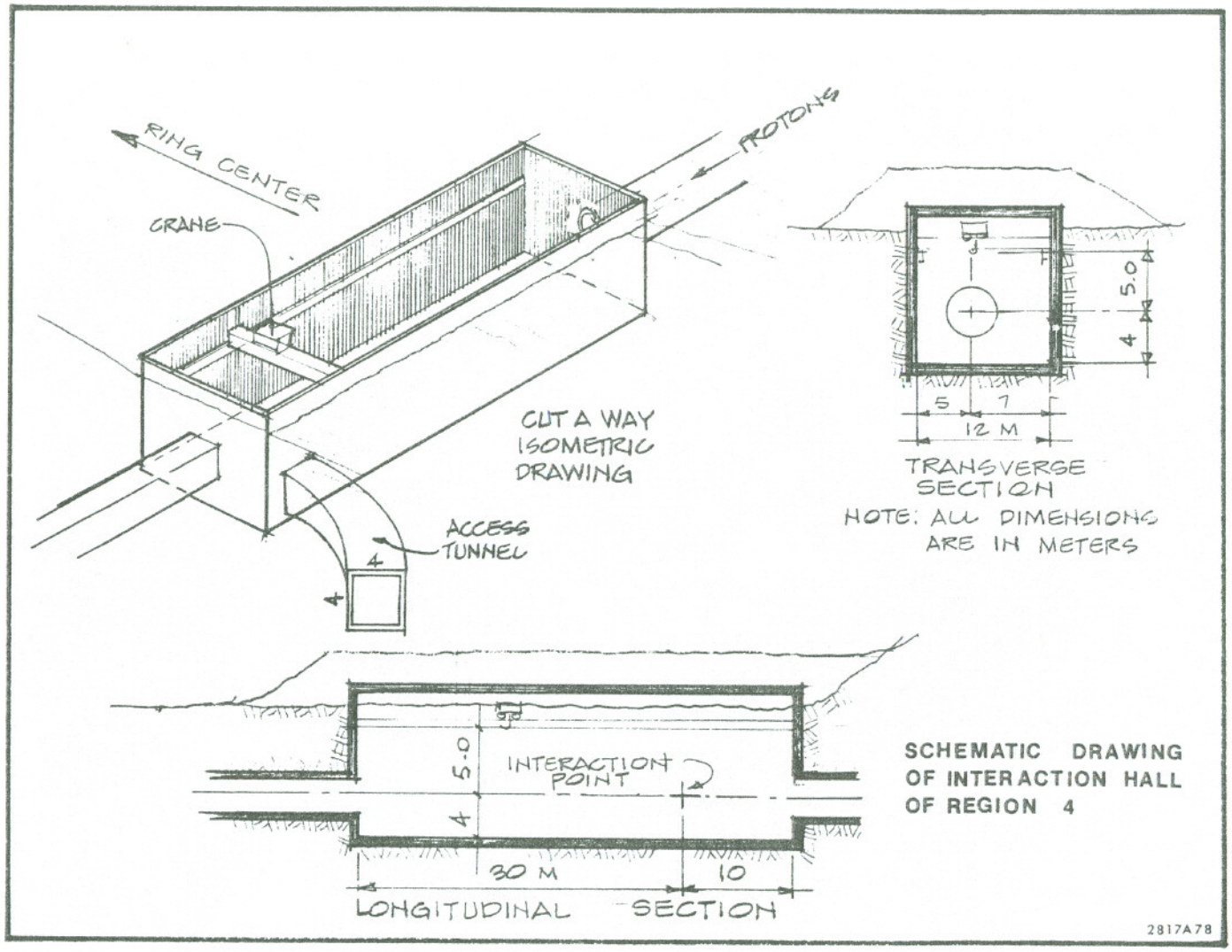

XBL 756-1523A

Fig. 78--Isometric view of Region 4.

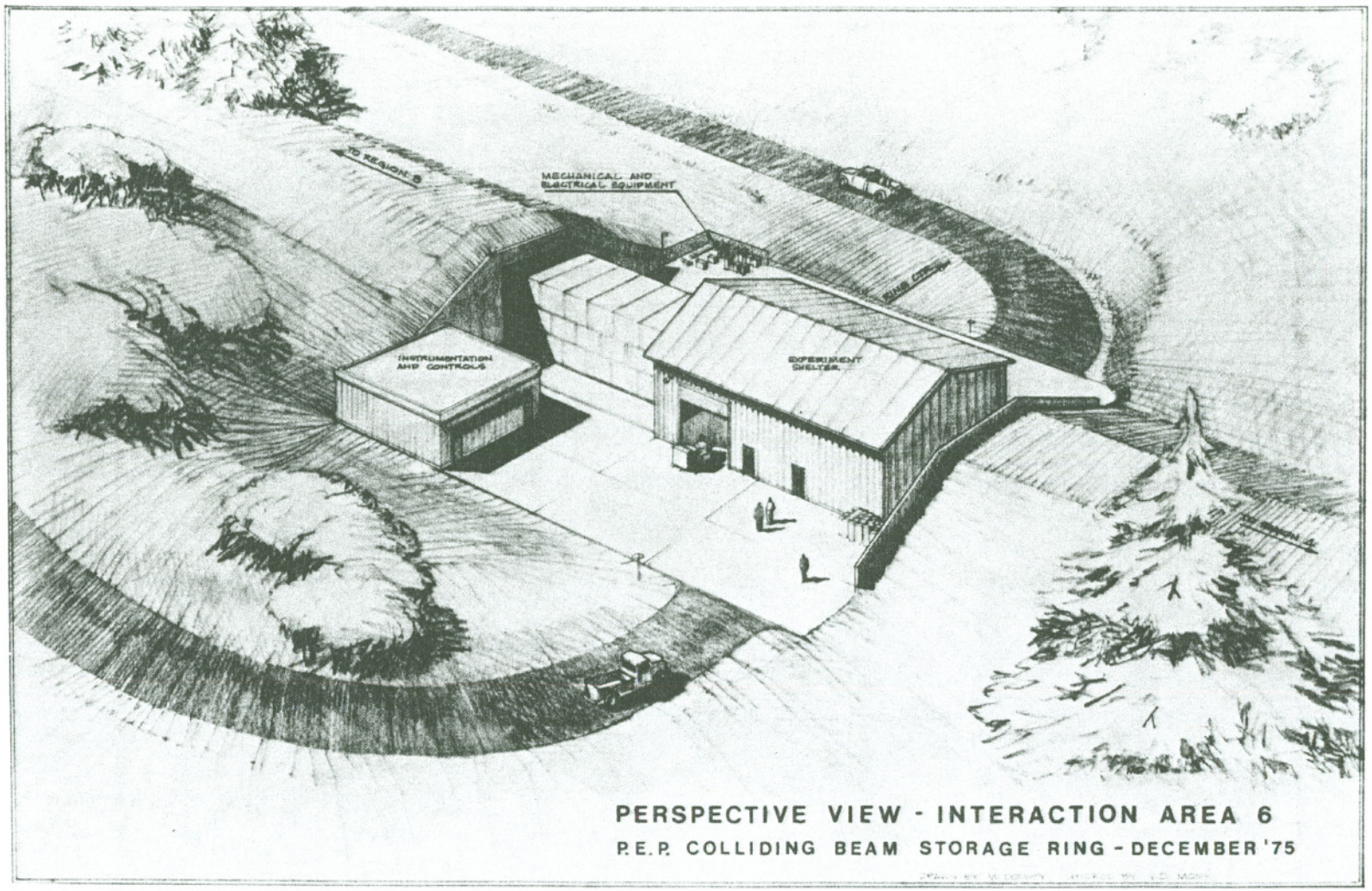

2817A69

Fig. 79--Architectural view of Region 6.

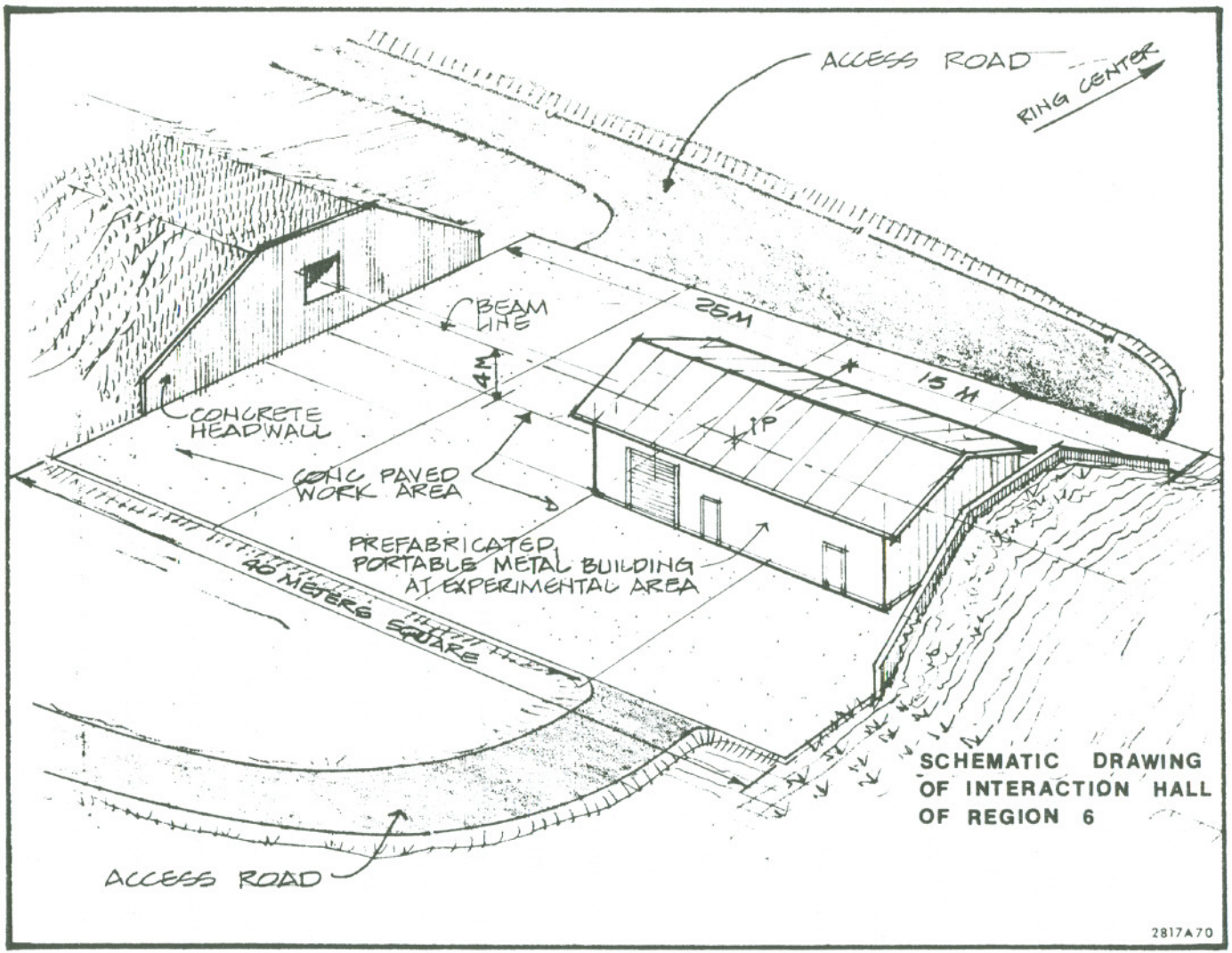

XBL 756-1526A

Fig. 80--Isometric view of Region 6.

proposed area consists of a very large pad (40 m by 40 m) providing great flexibility. Portable cranes, light buildings, portable shielding and ad hoc arrangements will be used to rig and service experiments. The area is offset in the CW direction, and access is possible from both sides of the beam line. The flexibility of this area makes it especially advantageous for future development.

(e) Area 8 (Figs. 81 and 82)

The interaction point in Area 8 is approximately 5 m below natural ground level. The area is similar to Area 12, offset laterally relative to the beam and having an alcove in the CW direction. Its special features are the extra depth below the beam (6 m) and the crane height above the beam line (8 m), both of which will be needed to handle some large experimental devices.

(f) Area 10

This area is deep underground, with the interaction point approximately 20 m below ground level, and its development will be very modest. For a length of 20 m the tunnel will be widened to about 7 m. The area will be devoted primarily to machine physics experiments. For example, anyone who has observed the progress in operating effectiveness in modern accelerators, particularly the ISR and SPEAR, will appreciate the excellent profit which accures to all experiments from the investment of machine time in storage ring improvement studies. Several experiments designed by the Summer Studies would fit in this area, but the apparatus would have to be carried into the area in small pieces.

E. High Luminosity Option

One of the recommendations of the Experimental Areas Group of the 1974 Summer Study was that three areas be developed with perhaps twice the luminosity by reducing the length between quadrupoles to 10 m. Many experiments would fit in this length and would benefit from the increased luminosity. The study of this

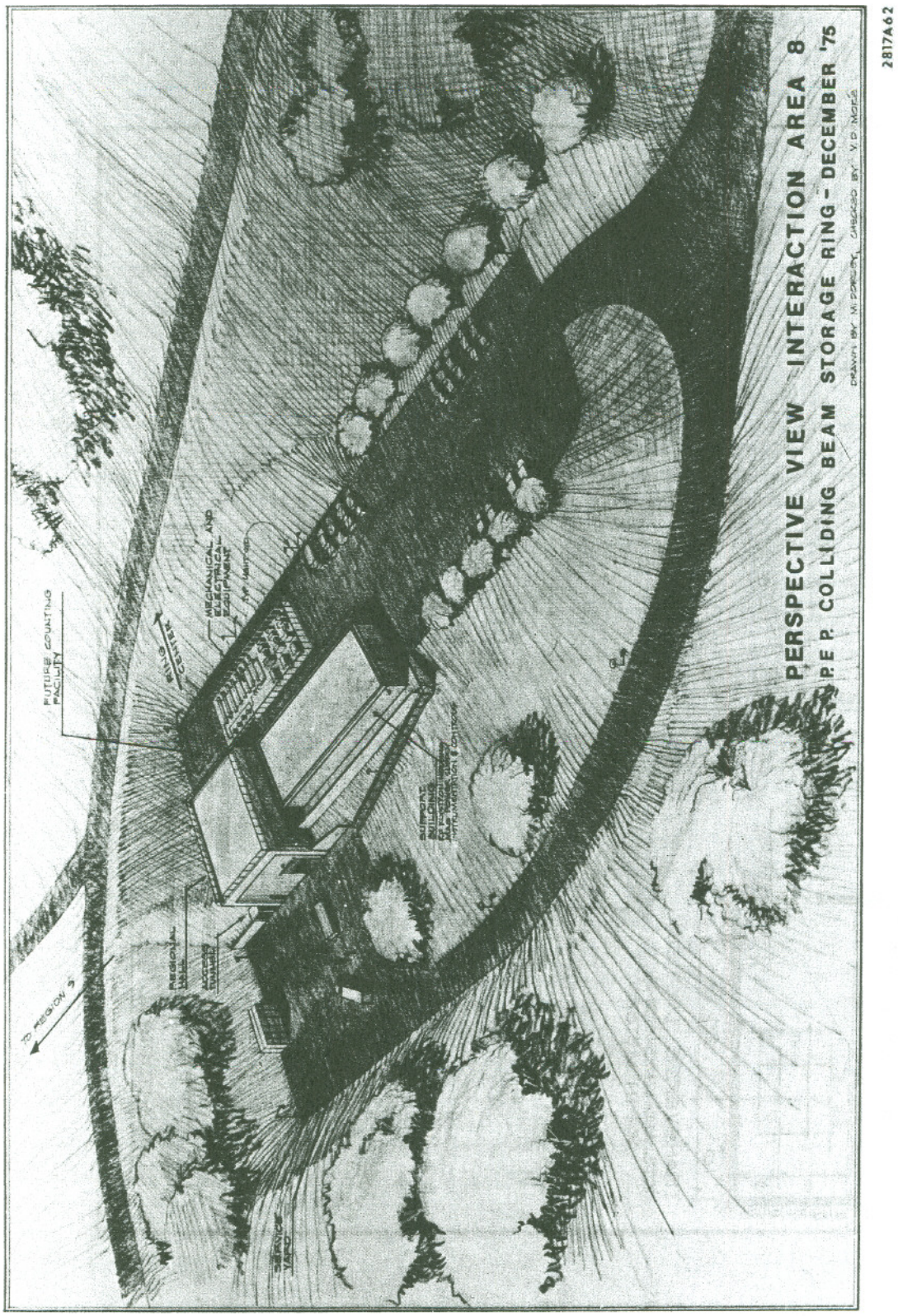

Fig. 81--Architectural view of Region 8.

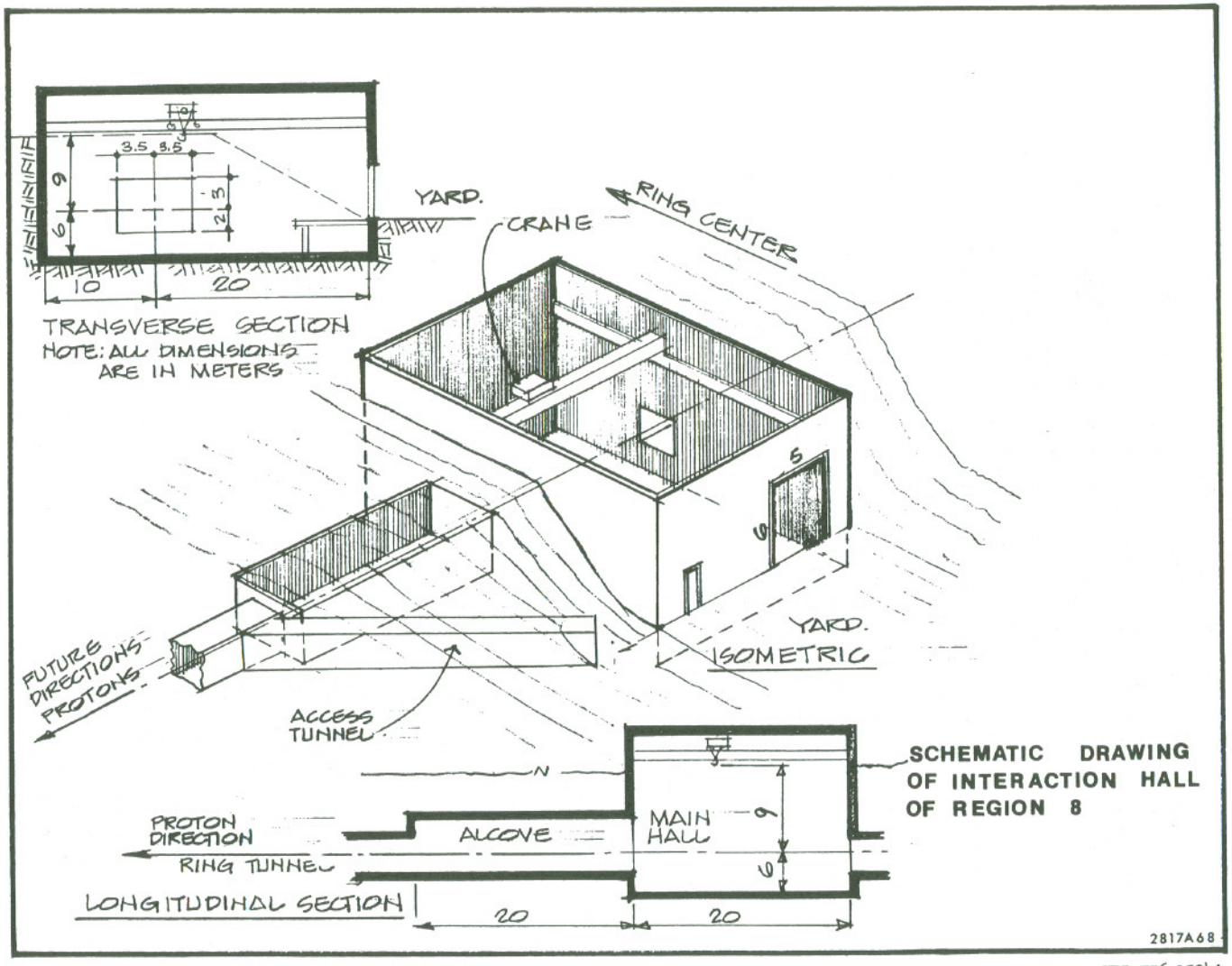

XBL 756-1524A

Fig. 82--Isometric view of Region 8.

high-luminosity option shows that such a program would incur substantial added costs. The increased cost is due to the larger-aperture quadrupoles required, additional power supplies and bus system and greater complexity of controls. This remains, then, as an option which may be added to the machine in the future.

V. COST ESTIMATES AND SCHEDULES

A. Introduction

The estimated cost of the PEP storage-ring facility stated in 1975 dollars is $61.9 million. An additional (Schedule B-9) allowance of $16.1 million is made for labor and materials cost escalation over the four-year construction period. Thus, the grand total estimated cost is $78.0 million.

The relatively small allowance for standard equipment reflects the fact that PEP is being built by already existing laboratories where some standard equipment will be available.

Contingencies are applied at 15% of conventional construction costs and 20% of technical component costs. The latter rate is appropriate in view of the recent and continuing experience in the construction and upgrading of the electron-positron storage ring SPEAR.

The construction schedule shown is based on the following schedule of new obligational authority increments.

	FY76	Transition	FY77	FY78	FY79	FY80
$ Million	2.9	0	25.0	29.9	14.7	5.5

This schedule would permit beam tests to begin in May 1980.

The schedule and the total cost estimate are of course related. If the schedule is stretched out for any reason, the total cost will rise because of escalation and also some loss of efficiency in ED and I work.

B. CONSTRUCTION COST ESTIMATE

($ Thousands)[a]

			Reference Schedule
ED&I		$ 8,425	A
Construction: Conventional Facilities			
Site Work, Structures and Buildings	$14,300		B-1
Water and ac electrical	5,700		B-2
Subtotal Conventional Facilities		$20,000	
Construction: Technical Components			
Magnets	7,425		B-3
Magnet Power Supplies	1,225		B-4
RF System	4,850		B-5
Vacuum System	6,100		B-6
Instrumentation and Control	2,925		B-7
Beam Transport System	1,525		B-8
Subtotal Technical Components		$24,050	
Standard Equipment		75	
TOTAL CONSTRUCTION COSTS		$52,550	
Contingency for ED & I and Construction @ 15% on Conventional Facilities and @ 20% on Technical Components		9,350	
TOTAL		$61,900	
Escalation		16,100	
GRAND TOTAL		$78,000	

[a]Cost estimate in June 1975 dollars. (Assumes $2.9M NOA for FY76 plus transition and 4-year construction schedule.)

C. Cost Schedules

Schedule A: ENGINEERING DESIGN AND INSPECTION

	($ Thousands)	
	Item Cost	Total Cost
Conventional Plant (Sitework, Structures, Water, Electrical and AECM) (16.4% of Construction Cost Estimate of $20,000)	$3,275	
Technical Components (21.4% of Construction Cost Estimate of $24,050)	5,150	
TOTAL		$8,425

Schedule B-1: SITEWORK, STRUCTURES, AND BUILDINGS

Sitework			
Roads (3000 linear meters @ $79.3/linear meter)		$240	
Fencing (2470 linear meters @ $26.3/linear meter)		65	
Drainage		275	
Sanitary sewers		40	
Erosion control		15	
Landscaping		75	
Other (temporary construction, paving, etc.)		185	
			$895
Beam Housing			
Main Ring Tunnels (including IR 10)*		$5,880	
1664 m via underground excavation	$4930		
323 m via cut and cover	$ 950		
Ring access tunnels		405	
Injected beam transport tunnels (including Linac connection)		555	
Injection junctions with Main Ring (including connecting access tunnels)		505	
Ring penetrations (RF, utilities, survey, etc.)		210	
			$7,555

*100 m of bored tunnel included in injection junctions.

-- continued --

Schedule B-1 (cont.)	($ Thousands)	
Interaction Area Structures		
Area 12*	$1,070	
Area 2*	1,130	
Area 4*	1,020	
Area 6	260	
Area 8*	1,470	
Area 10 (included under beam housings)	---	
		4,950
Surface Buildings		
Control Room Building (279 m^2)	90	
Assembly Building (1393 m^2)	320	
RF and I & C Equipment Shelters (9 structures totaling 1672 m^2)	440	
Cleaning Facility Building (149 m^2)	50	
		900
TOTAL Schedule B-1		14,300

*includes cranes - 690K$ total

Schedule B-2: WATER AND ELECTRICAL

	($ Thousands)	
	Item Cost	Total Cost
Cooling Water Distribution System		
Cooling towers and primary distribution	$455	
Ring magnets and klystrons	600	
RF cavities and vacuum	900	
Interaction areas	200	
Injection and beam transport	55	
Other systems (LCW makeup, fire protection, natural gas, temporary utilities, etc.)	590	
		$2,800
ac Electrical Systems		
RF ac services	660	
Water system ac services (cooling tower and services to utility pods)	200	
Ring magnet power supplies	200	
Injection and beam transport power supplies	60	
Primary power distribution (main loop bus and service to breakers)	1,065	
House power (secondary power) (lighting, cranes, and low voltage distribution)	640	
Miscellaneous (emergency, construction, etc.)	75	
		2,900
TOTAL Schedule B-2		$5,700

Schedule B-3: MAGNETS

Bending magnets	$1,990
Quadrupole magnets	2,230
Correction magnets	550
Busing and cooling water	480
Supports	950
Installation, magnetic measurement, alignment	700
Miscellaneous	525
TOTAL Schedule B-3	$7,425

Schedule B-4: MAGNET POWER SUPPLIES

	($ Thousands) Item Cost	Total Cost
Single-Polarity Power Supplies		
Ring	$375	
BT & Inj	380	
		755
Bipolar Power Supplies		
Ring	50	
IR	140	
		190
Installation		
Ring	145	
IR	75	
BT & Inj	60	
		280
TOTAL Schedule B-4		$1,225

Schedule B-5: RF SYSTEM

Klystrons	$1,385	
Klystron power supplies	640	
RF cavities	2,120	
RF monitoring, phasing, and control	460	
Waveguide	245	
		$4,850

Schedule B-6: VACUUM SYSTEM

Ring vacuum	$2,970	
Interaction area vacuum	2,580	
Cleaning tanks and miscellaneous	550	
		$6,100

	($ Thousands)	
	Item Cost	Total Cost
Schedule B-7: INSTRUMENTATION AND CONTROL		
Timing system	$ 70	
Racks, trays, cables, and frames	420	
Interlocks, vacuum, and water	370	
Magnets, power supplies, and electrostatic devices	105	
Beam monitors	610	
Computers and console	1,160	
Video system and communication	190	
		$2,925

Schedule B-8: BEAM TRANSPORT SYSTEM AND INJECTION		
Magnets	$955	
Beam line instrumentation	195	
Vacuum	65	
Inflection components	160	
Installation and miscellaneous	150	
		$1,525

Schedule B-9: ESCALATION FACTORS

	FY76	Transition	FY77	FY78	FY79	FY80
Inflation Assumptions (annualized rate)						
Construction	11%	8%	8%	7%	6%	6%
ED&I	10%	8%	8%	7%	6%	6%

D. Time Schedules

PEP

CONVENTIONAL FACILITIES CONSTRUCTION

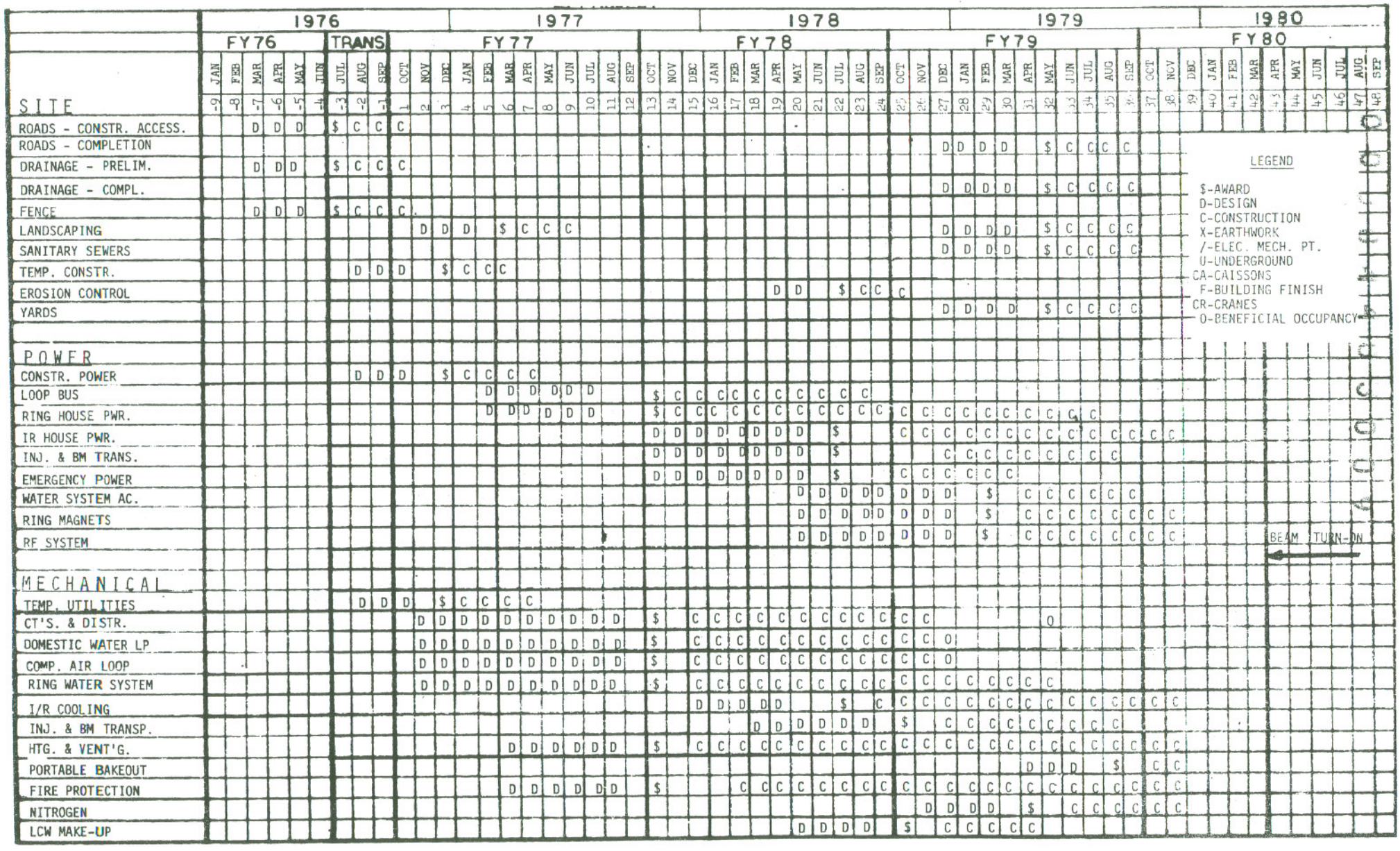

PEP

CONVENTIONAL FACILITIES CONSTRUCTION

	1976												1977												1978												1979												1980									
	FY76						TRANS			FY77												FY78												FY79												FY80									
	JAN	FEB	MAR	APR	MAY	JUN	JUL	AUG	SEP	OCT	NOV	DEC	JAN	FEB	MAR	APR	MAY	JUN	JUL	AUG	SEP	OCT	NOV	DEC	JAN	FEB	MAR	APR	MAY	JUN	JUL	AUG	SEP	OCT	NOV	DEC	JAN	FEB	MAR	APR	MAY	JUN	JUL	AUG	SEP	OCT	NOV	DEC	JAN	FEB	MAR	APR	MAY	JUN	JUL	AUG	SEP
	-9	-8	-7	-6	-5	-4	-3	-2	-1	1	2	3	4	5	6	7	8	9	10	11	12	13	14	15	16	17	18	19	20	21	22	23	24	25	26	27	28	29	30	31	32	33	34	35	36	37	38	39	40	41	42	43	44	45	46	47	48
CUT & COVER (Includes Yard Excavations in I/R Areas for Access Tunnels)																																																										
RGNS 4B, 5								D	D	D	D	D	D	D	D		$	X	X	C	C	C	C				/	/	/	/	0																											
1, 2A, 12B, 12								D	D	D	D	D	D	D	D		$	X	X	C	C	C	C	/	/	/	/	/	0																													
6, (includes I/R								D	D	D	D	D	D	D	D		$	X	X	C	C	C	X				/	/	/	0																												
8A								D	D	D	D	D	D	D	D		$	X	C	C	C	/	/	/	0																																	
8, 8B (includes S. Inj. Junction)								D	D	D	D	D	D	D	D		$	X	X	X	X	C	C	C													/	/	/	/	/	0																
TUNNELS (Includes Penetrations & Shafts)																																																										
RGNS 6B, 7, 8A								D	D	D	D	D	D	D	D	D	D			$			U	U	U	U	/	/	/	/	/	/	0																										
2B, 3, 4A								D	D	D	D	D	D	D	D	D	D			$							U	U	U	U	/	/	/	/	0																								
9								D	D	D	D	D	D	D	D	D	D			$					U	U	U										/	/	/	/	/	0																
10 (includes N. Inj. Jctn. & I/R 10)								D	D	D	D	D	D	D	D	D	D			$								U	U	U	U	U					/	/	/	/	/	0																
11								D	D	D	D	D	D	D	D	D	D			$													U	U	U	U	/	/	/	/	/	0																
ACCESS TUNNELS								D	D	D	D	D	D	D	D	D	D			$			U	U	U	U	/	/	/	U	U		U	U	/	/	/																						
NORTH INJECTION																										D	D	D	D	D		$				U	U	U	U	U	/	/	/	/	0														
SOUTH INJECTION																D	D	D	D	D		$	U	U	U	U	U	/	/	/	/	0																										
INTERACTION REGIONS																																																										
RGN 2													D	D	D	D	D	D	D			$		X	X	CA	CA	CA	CA	X	X			$					F	F	F	F	F	/	/	/	/	0									
4													D	D	D	D	D	D	D			$	CA	CA	CA	CA								$					F	F	F	F	F	/	/	/	/	0									
8													D	D	D	D	D	D	D			$		X	CA	CA	CA	CA	X	X				$			F	F	F	F	F	/	/	/	/	/	0						BEAM				
12													D	D	D	D	D	D	D			$				X	CA	CA	CA	CA	X	X			$			F	F	F	F	F	/	/	/	/	/	0						TURN-ON				
CRANES																																			$			CR	CR	CR	CR	CR	CR	CR	CR	CR	CR										
BUILDINGS																																																										
ASSEMBLY BUILDING			D	D	D	$	C	C	C	C	F	F	0																																													
CLEANING BUILDING			D	D	D	D		$	C	C	C	C	F	0																																													
CONTROL ROOM																D	D	D	D	D		$		C	C	C	C	C	C	0																													
IR - 2 BUILDINGS																															C	C	C	C	C	0																							
IR - 4 BUILDINGS																										C	C	C	C	C	0																												
IR - 6 BUILDINGS																									$					C	C	C	C	C	0																							
IR - 8 BUILDINGS																														C	C	C	C	C	0																							
IR - 10 BUILDINGS																																			C	C	C	C	C	0																			
IR - 12 BUILDINGS																																			C	C	C	C	C	C	0																		
SUMMARY																																																										
SITE & STRUCTURES						$	$	$					$	$	$		$			$		$												$					$				$																
POWER															$							$																		$																			
MECHANICAL															$							$												$										$															

LEGEND

$-AWARD
D-DESIGN
C-CONSTRUCTION
X-EARTHWORK
/-ELEC. MECH. PT.
U-UNDERGROUND
CA-CAISSONS
F-BUILDING FINISH
CR-CRANES
O-BENEFICIAL OCCUPANCY

PEP

TECHNICAL COMPONENTS SCHEDULE

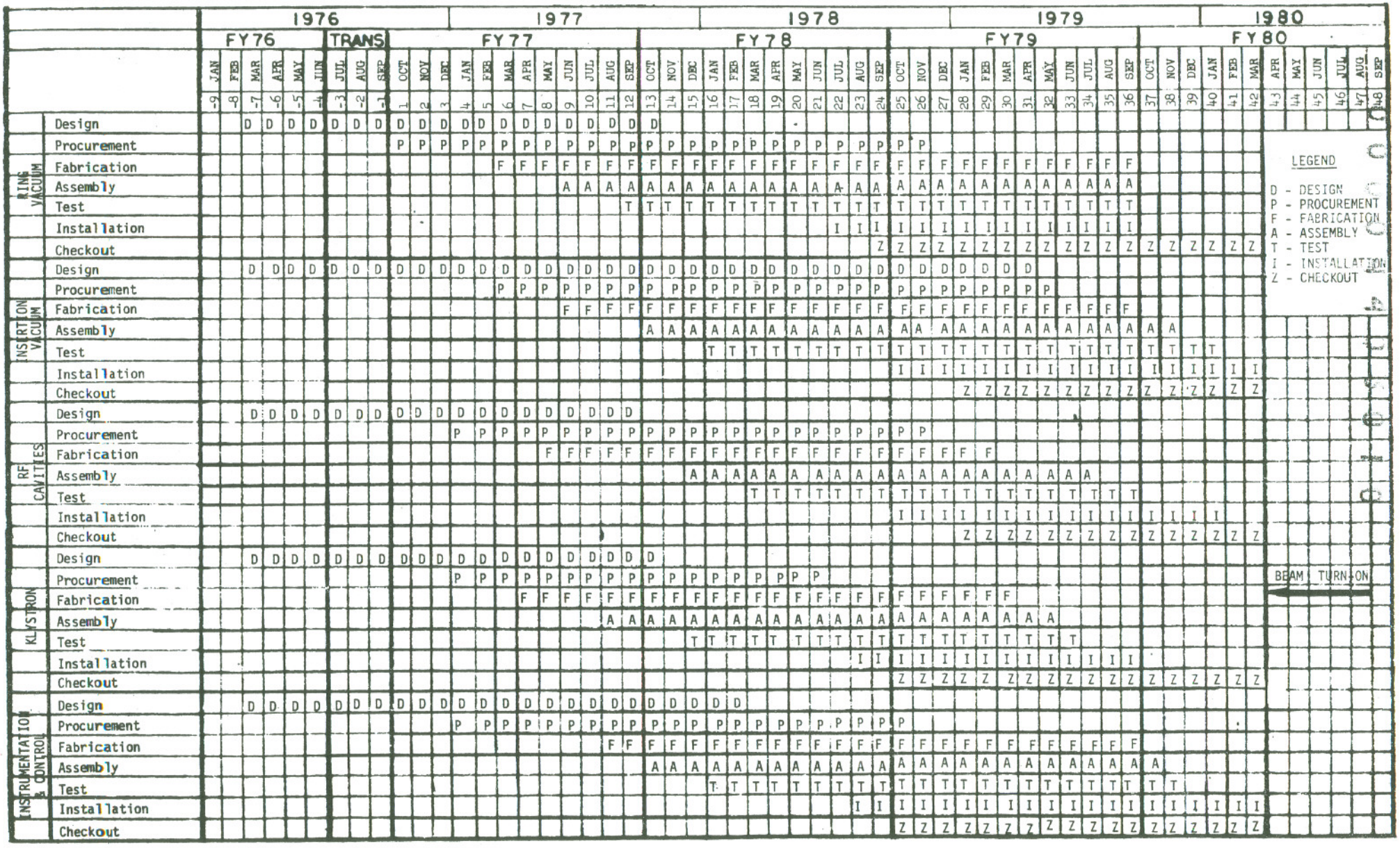

PEP

TECHNICAL COMPONENTS SCHEDULE

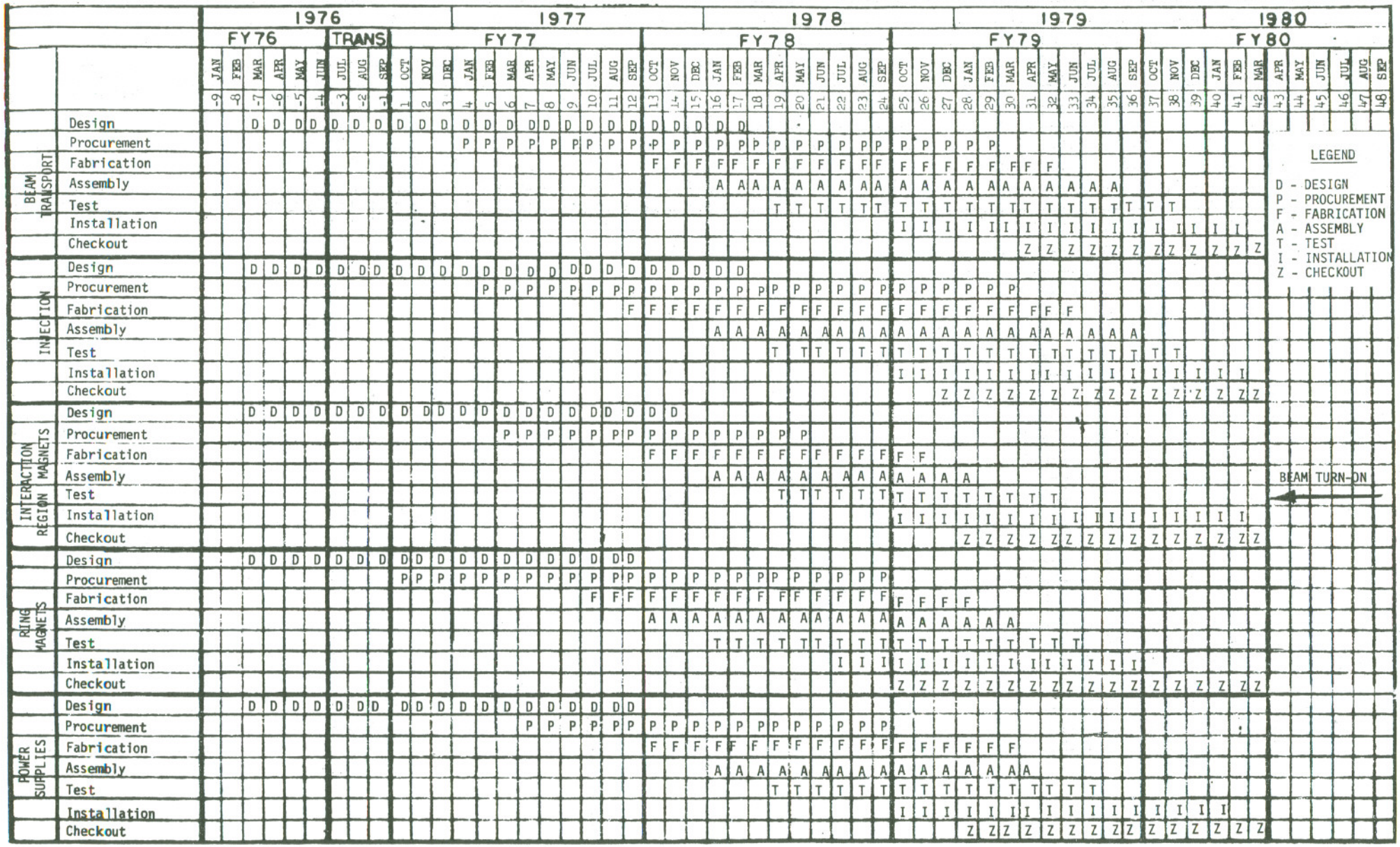

APPENDIX A

THE PROTON-ELECTRON SYSTEM

1. Introduction

Initially the PEP concept[1] included a second ring for achieving ultrahigh-energy collisions of electrons with protons as well as with positrons. In electron-proton collisions, PEP is capable of an extension of the experimental parameters well beyond those of traditional electron machines, i.e., inelastic electron scattering, photoproduction, etc., and in addition it will open the field of weak interactions to practical experimentation with a well understood, well controlled probe—the electron.

This Appendix provides a brief description of a proton-electron system which makes use of the electron-positron ring of this design report. Basically, to obtain electron-proton collisions, a 200-GeV superconducting proton storage ring is incorporated with the 15-GeV electron ring, within the same enclosure. For e-p collisions, the electron energy is set to 15 GeV to maximize luminosity. The center-of-mass energy thus achieved is 110 GeV which is the same energy which would be available with a 6400-GeV beam from a conventional accelerator incident on a stationary hydrogen target. There is no economically feasible way of reaching these energies with a conventional accelerator. The facilities of PEP are designed to allow for this addition creating a total facility of unique capability for particle physics research. Some of the details of this future step, along with the projected parameters, are outlined below.

2. Physics Potential[33]

(a) Deep Inelastic Lepton Scattering $[e^-(e^+)\,p \rightarrow e^-(e^+) + \text{hadrons}]$

Inelastic electron-proton scattering plays an essential and unique role in the investigation of the structure of the hadrons. The known electromagnetic field

generated by the scattered electron interacts locally with the electromagnetic current of the proton and thus can probe the structure of the nucleon at arbitrarily small distances. This local interaction is in sharp contrast to hadron-hadron scattering in which the basic interaction between the particles is more complex. By choosing different energies and angles of the inelastically scattered electron, it is possible to select a wide range of values of the virtual photon's energy (ν) and the square of its mass (q^2), the latter quantity being always negative in electron scattering. In this way, we can study the collisions between a hadronic target and virtual photons having a variety of energies and masses. In particular, experiments can be conducted in the asymptotic region of virtual photon masses large in magnitude compared to a proton mass. This region is not accessible to accelerators using a fixed mass projectile.

Experiments on inelastic scattering at SLAC, with both the mass and energy of the virtual photon large, have yielded profound and unexpected results. These results show that the cross section (or more correctly, the structure functions) do not depend separately on the mass and the energy of the photon, but instead on the combination $\omega = 2\, m\nu/(-q^2)$, where m is the mass of the hadronic target. The quantity ω is called a "scaling variable." This "scaling" behavior has led to major new concepts in our understanding of hadronic structure in terms of a possible substructure within the hadron, namely, point-like constituents (partons). Since the existing hadronic symmetries find their most natural description in terms of fractionally charged quarks, it is natural to try to identify partons with quarks. In the past few years, there is increasing evidence from electromagnetic and weak interactions at high energies to support this identification. Parton/quarks have thus become a familiar construct in particle physics in spite of the fact that they have never been observed as free particles in the laboratory. Scaling finds a

simple explanation through the absorption of the virtual photon by an essentially free parton/quark, provided the parton's charge is point-like and its mass can be neglected in the kinematics.

The range of ν and q^2 has recently been extended with a muon beam at Fermilab from the SLAC domain of $0 < \nu < 20$ GeV, $-37\ \mathrm{GeV}^2 < q^2 < 0$, to a region about 7 times larger, $0 < \nu < 150$ GeV, $-280\ \mathrm{GeV}^2 < q^2 < 0$. The decrease in cross section with q^2 is so rapid that meaningful data are restricted to about $|q^2| < 50\ \mathrm{GeV}^2$, but essentially the full range of ν is explored. The Fermilab data confirm the general features of the observations at SLAC, but show indications of a breakdown of the scaling behavior at the 10 - 20% level. The details of the violation of scaling have not been established as yet, but the trends support the idea of a new, larger mass scale entering the dynamics, rather than a smearing out of the parton's charge.

Before the proton-electron system can be completed, it is expected that considerable additional data on muon scattering will be available from the two experiments planned for installation in the north hall of CERN. The beam feeding these experiments is designed to have an intensity at least 2 orders of magnitude higher than that currently available at Fermilab, and the muon halo predictably will be much less. One of these experiments will explore the validity of scaling through a single arm inelastic scattering over the full kinematic range accessible, and the second experiment will add considerable information on the distribution of hadron fragments associated with such inelastic events.

In the past year the astounding discoveries, first at SPEAR and the AGS and later at SPEAR and DORIS, of a totally unexpected spectroscopy of states of high mass have greatly increased the need for both e^+e^- and $e^{\pm}p$ reactions at PEP. The definitive interpretation of these new states does not exist at present, but it

is apparent that some new degree(s) of freedom in hadronic interactions is (are) being excited at energies above 3 or 4 GeV in the e^+e^- system. PEP Stage 1 (the present design report) is vital for the exploration of these phenomena at higher energies. The physics potential has been discussed in detail in the PEP proposal.[4] The future electron-proton configuration will contribute uniquely in a complementary manner. The apparent mass threshold at about 4 GeV in the annihilation channel may well be the same mass parameter responsible for the scaling violations observed at Fermilab in inelastic muon scattering. If so, the much greater range of virtual photon energy ν and mass squared q^2 of PEP's electron-proton system ($0 < \nu < 6400$ GeV, $-12,000$ GeV$^2 < q^2 < 0$) may show new domains of scaling, followed by regions of failure of scaling, as this and successive mass thresholds are passed.

This picture of domains of scaling as the energy variables are increased is conjectural at the present time. All that one sees now is scaling for a wide range of parameters, with an indication of failure of scaling at the present extremes in these parameters. The PEP e-p addition would make available a much larger kinematic region in the "space-like" region of momentum transfer (q^2), complementing in a most important way the extension of the "time-like" region of q^2 with the PEP e^+e^- system. New hadronic degrees of freedom seen in the direct annihilation channel have consequences in the "crossed channel" of inelastic electron scattering. The data from one type of experiment support and elucidate the data from the other.

As an example, partons were first conceived in the interpretation of inelastic electron scattering and the phenomenon of scaling. They now have proved fruitful in the interpretation of the inclusive spectra of hadrons and of the so-called jet structure in e^+e^- annihilation. This jet structure, only very recently established

at the highest SPEAR energies, has not as yet been found as a prominent feature of the "fragmentation" of very massive virtual photons in inelastic electron scattering. Its existence in e^+e^- annihilation, however, argues strongly for a corresponding phenomenon in inelastic electron scattering, quite apart from any ideas of partons/quarks. Its observation would lend confidence to our basis understanding; its absence would demand a re-assessment of our concepts.

Similarly, the behavior of the ratio R of the total cross section for $e^+e^- \rightarrow$ hadrons to that for $e^+e^- \rightarrow \mu^+\mu^-$, with a plateau at $\sim$ 2.5 from 2 to 3 GeV, a rise and then another plateau at $\sim$ 5 above 4.5 GeV, strongly implies the domains of scaling described above. It is by such study of different aspects of related phenomena that one builds a convincing and interlocking interpretation of fundamental particles.

In addition to the electromagnetic inelastic scattering, it will be possible in PEP e-p experiments to observe the effects caused by a weak neutral current of the type discovered in the recent CERN and FNAL neutrino experiments. The effects of the neutral current would be observable in interference with the electromagnetic current as parity violations, charge conjugation violations, and possibly electromagnetic scaling violations. Since both energy and momentum transfer are easily determined, detailed knowledge as to the nature of these neutral current effects will be possible. This unique very high-energy feature of the PEP facility will yield results bearing on one of the most significant problems in particle physics.

(b) Weak Interactions ($ep \rightarrow \nu_e$ + hadrons)

If the scaling phenomena observed in deep inelastic scattering are assumed to hold also for the weak interactions, as would be implied at least in part by the conserved vector current (CVC) idea, then the Fermi theory implies that the total weak interaction cross section will grow quadratically with center-of-mass energy.

At PEP energies, this has the consequence that the strength of the weak interactions with their inherent violation of parity and strangeness, will be comparable to the electromagnetic interactions. In fact, in the region of the largest momentum transfer accessible with 200-GeV protons and 15-GeV electrons, the scaling hypothesis, together with the point coupling of the 4-fermion theory, predicts that the deep inelastic electromagnetic cross section will be smaller than the weak process cross section.

Present evidence from experiments at Fermilab with neutrinos of energies up to 100 - 200 GeV, corresponding to center-of-mass energies of 15 - 20 GeV, suggests that the total cross sections do rise more or less quadratically with center-of-mass energy over this energy range. The accuracy is not great, however, and there are indications not only of the failure of scaling in certain kinematic regions, but also of new phenomena, perhaps the production of new kinds of particles. At present, these hints are consistent with the idea of a new degree of hadronic freedom being excited at high energies in neutrino interactions, just as in e^+-e^- annihilation. There is as yet no indication of a finite range for the 4-fermion weak interaction implied by the intermediate vector bosons of unified gauge theories of weak and electromagnetic interactions.

Experiments with the electron-proton system of PEP will show either that the weak interaction ceases to be "weak" at high energies or that the Fermi theory in its simple form breaks down. The discovery of a failure in the Fermi theory would in itself be an event of the first magnitude in importance; beyond that one would hope to discover the mechanism of the breakdown.

3. The Total PEP Concept

The "total" PEP configuration would provide a one-of-a-kind facility for high-energy e^--p and e^+-p collisions in addition to e^+-e^- collisions. The

electron-positron system is a straight-forward extrapolation from existing lower energy storage rings, whose properties are fairly well understood. But, there is no present experience with electron-proton storage ring systems, for they don't yet exist, and the technical demands appear more severe.

For the e-p system it is desirable, particularly in view of the weak interaction physics potential, to have the highest possible center-of-mass energy. For the prescribed size of the 15 GeV electron ring, a proton energy of 200 GeV, corresponding to a center-of-mass energy of 110 GeV, can be reached with dipole field strengths of 44 kG, which is reasonably within the capability of superconducting technology. Moreover, superconducting magnets would provide substantial power savings relative to conventional magnet elements.

The proton ring will be added within the same tunnel enclosure. In the present design, the electron ring will be adjusted in elevation, as shown schematically in Fig. 83. The heavier line in the figure represents the proton beam trajectory. The electron orbit, which has almost the same circumference, alternates above and below the proton ring. Short electron and proton bunches counter-rotate synchronously in their respective ring structures and collide in the six interaction regions at the points indicated by the large dots.

Protons will be injected into the superconducting ring at ~5 GeV from a conventional booster synchrotron, accelerated up to 200 GeV, and compressed longitudinally to the desired bunch length before injecting the counter-rotating beam of electrons or positrons in the other ring. The electrons or positrons would be injected from the existing SLAC linac, in the same manner described in Section II. E of this design report.

The possibility exists also for the addition of a second electron ring which would alternate vertically in the opposite sense from the electron structure

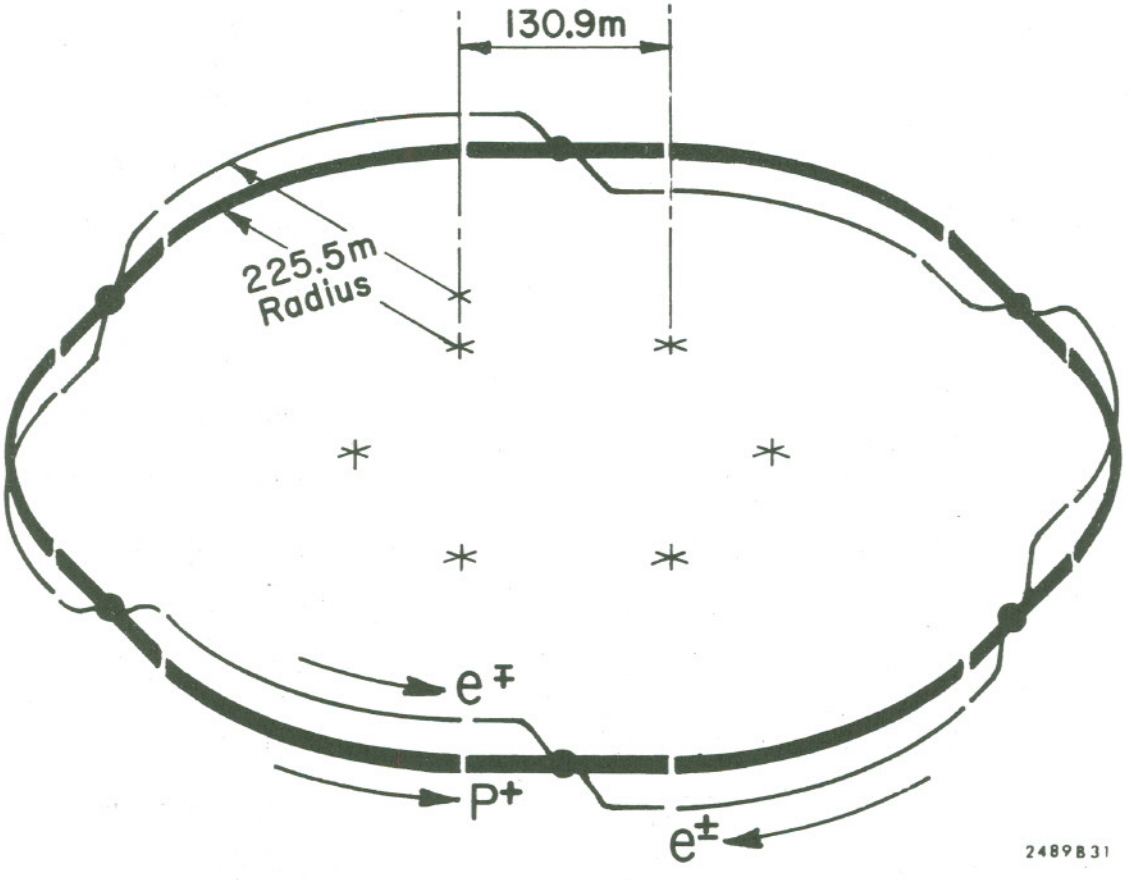

Fig. 83--Schematic view of the PEP electron-proton ring configuration.

shown in Fig. 83. This would provide for e^+-e^+ and e^--e^- collisions, as well as for higher luminosities for the e^+-e^- system at lower energies.

4. Lattice System and Operating Parameters

The proton and electron rings are displaced vertically from each other because the relatively flat beams are more readily separated vertically, and synchronization of electron and proton bunches is simplified. The proton ring will be essentially in a single plane, while the circular sextants of the electron ring will be placed alternately above and below the proton ring. This arrangement makes it easier to eliminate vertical dispersion in the curved sections of the electron ring and at the crossing points, where it would reduce luminosity. Without this alternation, several quadrupoles would be needed between BV1 and BV3 (Fig. 84) to produce a full vertical oscillation of the dispersion vector there. This region could not then be used for synchronization and injection components, chromaticity would increase, and a considerable lengthening of the insertions, would be required.

The insertion region and the neighboring cells of the curved sextants are shown in Fig. 84. The electron and proton bunches collide head-on at the interaction point, and then pass through four common magnets. First is a quadrupole doublet Q1, Q2 that focuses the electrons at the interaction point, but has little effect on the protons. Next is a vertical low-field magnet BVL that permits one to mask the experimental apparatus from the synchrotron radiation emitted in BV1. Magnet BV1 separates the proton and electron orbits vertically. It is followed on the proton line by vertical dipoles BV (4, 5, 6) that bend the protons back to the mid-plane. The quadrupole doublet Q3, Q4 provides a low β focus of the proton beam at the interaction point. Meanwhile the electrons pass through BV2 and are restored to a horizontal plane by BV3.

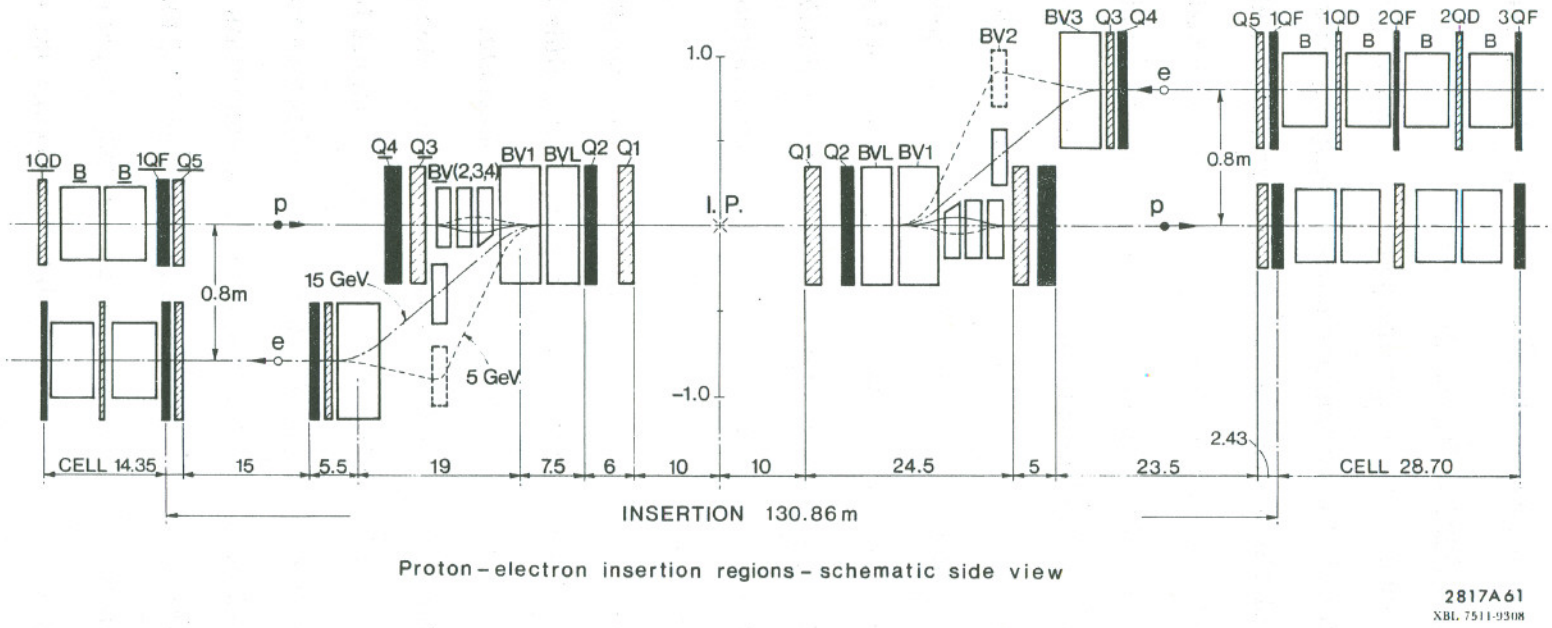

Proton-electron insertion regions - schematic side view

2817A61
XBL 7511-9308

Fig. 84--Schematic side view of insertion and cell structure for the proton-electron system.

Magnet BV2 and the electron beam pipe will be movable to provide synchronization of electron and proton bunches at different proton energies. Following BV3 and the doublet Q3, Q4 is a 15-m clear space for RF cavities and injection components. 1QG is the first quadrupole of the cell-lattice in the sextants. 1QF and the next few quadrupoles in the cells adjacent to the insertion will be independently adjustable. They act together with the insertion quadrupoles to match the beta functions and dispersions between the cells and the interaction point. The corresponding quadrupoles in the proton ring operate in a similar manner.

The cell length of the electron lattice has been shortened relative to the length in the PEP Proposal 4 to 14.35 m. However, the proton cells will remain 28.7 m long due to the more favorable packing. Apart from the vertical shift and removal of the horizontal low field magnets the curved sections of the electron ring are unchanged from the configuration described in this design report. The insertion is changed by shifting 1QG and Q5 farther from the interaction point, adding the doublet Q3, Q4 for fine tuning, and by the addition of the vertical bending magnets.

Apart from the proton ring cell length, the main lattice parameters such as average radius, insertion straight section, interaction area free space, etc. will be the same as that of the electron-positron system in this design report. The length of the free space (19 m) in the interaction region represents a compromise between experimental requirements and orbit considerations. The vertical separation (0.8 m) of the electron and proton structures is sufficient to accommodate the magnets, RF cavities and injection components for both rings. Such a small separation is desired for compatibility with the proposed runnel size and to minimize the power radiated by the electrons in the vertical dipoles.

Table XIX shows a typical set of parameters for operation at (200, 15) GeV and (50, 5) GeV. The variation of luminosity with energy cannot be scaled as readily as for electron-positron collisions, since the properties of proton beams scale differently with energy. Under the approximate constraint that the beam-beam tune shifts should not exceed 0.005 for protons and 0.06 for electrons, and since by present understanding this effect is a performance limitation, the luminosity must decrease with decreasing energy—about a factor of 5 for the above practical range of energies.

The luminosity per crossing at the (200, 15) GeV operating conditions is 7.2×10^{31} cm^{-2} s^{-1}. This is 30% less than the luminosity of 1×10^{32} cm^{-2} s^{-1} shown in the previous PEP proposal.[4] This reduction is caused mainly by the addition of low field magnets shown in Fig. 84 which are used to minimize background due to synchrotron radiation in the experimental areas. In addition, the doublet Q1, Q2 has been unaltered from the stage I configuration in order to retain the full e^+-e^- luminosity capabilities in stage II. Should this capability no longer be required this doublet could be shortened, Q3, and Q4 moved closer to the interaction point and the e-p luminosity would increase. Similarly the luminosity would increase if ways are found to shield the experimental apparatus from synchrotron radiation that allow a shortening of magnet BVL.

The number of protons required (Table XIX) is comparable to the design intensities of FNAL and CERN II. The number of electrons is similar to that required in the single electron-positron ring system. Both beams are divided into a large number of bunches to minimize the beam-beam effects as well as those of high-peak currents.

The proton emittances are conservative, being somewhat larger than those currently achieved in existing high energy proton accelerators; there would be

TABLE XIX

Operating Parameters

		High Energy		Low Energy		
		Proton	Electron	Proton	Electron	
Momentum	p	200	15	50	5	GeV/c
Number of Particles		3.6×10^{13}	0.77×10^{13}	3.6×10^{13}	1.2×10^{13}	
Number of Bunches	n_B	24	24	48	48	
Beam Power Radiated	P	—	5	--	0.2	MW
Luminosity/Crossing	L	7.2×10^{31}		1.7×10^{31}		$cm^{-2}s^{-1}$
Momentum Width - $\left(\frac{\Delta p}{p}\right)_{rms}$	σ_p	.03	0.10	0.120	0.10	%
Bunch Length (rms)	σ_ℓ	0.25	0.05	0.25	0.05	m
Interaction Point						
rms beam width (total)	σ_x^*	0.82	0.65	1.01	0.85	mm
rms beam height	σ_y^*	0.25	0.18	0.50	0.24	mm
β-function horizontal	β_x^*	5.4	2.3	2.03	2.62	m
β-function vertical	β_y^*	2.0	0.68	2.00	1.31	m
dispersion-horizontal	η_x^*	0	0	0	-0.50	m
dispersion-vertical	η_y^*	0	0	0	0	m
Emittances						
horizontal ($\sigma_x\sigma_{x'}$)	ϵ_x	0.125	0.184	0.500	0.184	mm-mrad
vertical ($\sigma_y\sigma_{y'}$)	ϵ_y	0.031	0.046	0.125	0.046	mm-mrad
longitudinal ($\sigma_\ell\sigma_{\beta y}$)	ϵ_ℓ	0.016	1.47[a]	0.016	0.49[a]	m
Beam-Beam Tune Shift						
horizontal	$\Delta\nu_x$	.004	.06	.001	.059	
vertical	$\Delta\nu_y$	.005	.060	.005	.060	
Betatron Function (max)						
horizontal	$\hat{\beta}_x$	520	320	600	150	m
vertical	$\hat{\beta}_y$	600	160	600	100	m
Betatron Tune	$\nu_x=\nu_y$	15.75	18.75	15.75	18.75	
Cells						
length	L_c	28.7	14.35	28.7	14.35	m
dipole field	B_0	4.37	0.303	1.09	0.101	T
quadrupole gradient	$\lvert B_0'\rvert$	56	8.4	14	2.8	T/m
β-function maximum	$\hat{\beta}_c$	48.	26.0	48.	26	m
dispersion maximum	$\hat{\eta}_c$	2.5	1.7	2.5	1.7	m

[a]Includes bunch lengthening factor of 2.

2817894

no advantage in smaller emittances because of the beam-beam effect. The electron emittances are taken as independent of energy; this can be achieved by use of the wiggler system or the variable tune capability of the electron ring lattice.

The proton bunch length is as short as possible, consistent with moderate RF voltage requirements, since high luminosity requires localizing the collisions to the low-β region. In the electron ring, when sufficient RF overvoltage is provided to assure a long quantum lifetime, the natural electron bunch length is quite short enough to achieve the required localization.

The interaction point dispersion is set to zero to avoid potential problems such as magnet ripple effects. As operating experience accumulates, it may be possible to improve the luminosity by going to larger dispersion at the interaction points.

5. Machine Components

The characteristics and parameters projected for some of the principal machine components are described below.

Superconducting Magnet System. For the proton normal-cell structure, 192 dipoles are required, each 5 meters long, operating up to a maximum central field of 44 kG at 200 GeV. There are 84 quadrupoles (1.2 meters long) and 12 quadrupoles (.6 m long) all with a maximum field at the conductor of 38 kG for a maximum required gradient of 50 T/m. For these magnets the required good-field radius is 5.3 and 5.8 cm in the dipoles and quadrupoles respectively. The six insertion regions require, in addition, 24 quadrupoles of length 2.0 m and 24 quadrupoles of length 1.4 m. (The common doublet Q1, Q2 and the vertical bending magnets will be conventional room temperature magnets.) The magnet design[34, 35] incorporates intrinsically stable, fine filament, NbTi

superconductor that is well cooled with liquid helium and rigidly supported, and utilizes a simple compact cryostat-cryogenic transfer system. Operational reliability for large-scale superconducting systems is not yet established. This is one of the major goals of the LBL research and development program and pilot accelerator program (ESCAR).[34-38]

Cross sections of the magnets and their location within the tunnel is shown in Fig. 85. Within the magnets the ultra-high vacuum region is enclosed by a nonmagnetic beam tube, upon which a multi-layered coil is wound. Circular symmetry is used in all inner regions of the magnet for the best possible structural and magnetic properties.

The magnet cryostat is continuous through a half-sextant of the ring with surrounding evacuated thermal insulation, an 80°K temperature shield and finally a room-temperature vessel. Two phase helium at 4.4^{o}K is introduced at the center of a sextant and forced in both directions to the ends of the sextant.[38] The only additional element in the tunnel is the transfer line from the rest of the refrigeration equipment housed above ground. This scheme eliminates interference between refrigeration components and experimental apparatus near the insertion regions.

If the expansion to higher electron energies[16] (i.e., >22 GeV) is required, superconducting quadrupoles and sextupoles would be utilized in the electron ring. Liquid helium could be easily supplied from the proton ring cryosystem.

A summary of the expected heat loads is shown in Table XX. The heat leak at 4.4^{o}K is assumed to be 1.2 W/m, and that from room temperature to 80°K is taken to be 2.5 W/m. Allowance is made for two pairs of electrical leads for the dipoles and six for the quadrupoles. Additional allowance is made for quench leads and beam diagnostic and control equipment. In all, some 600 kW of

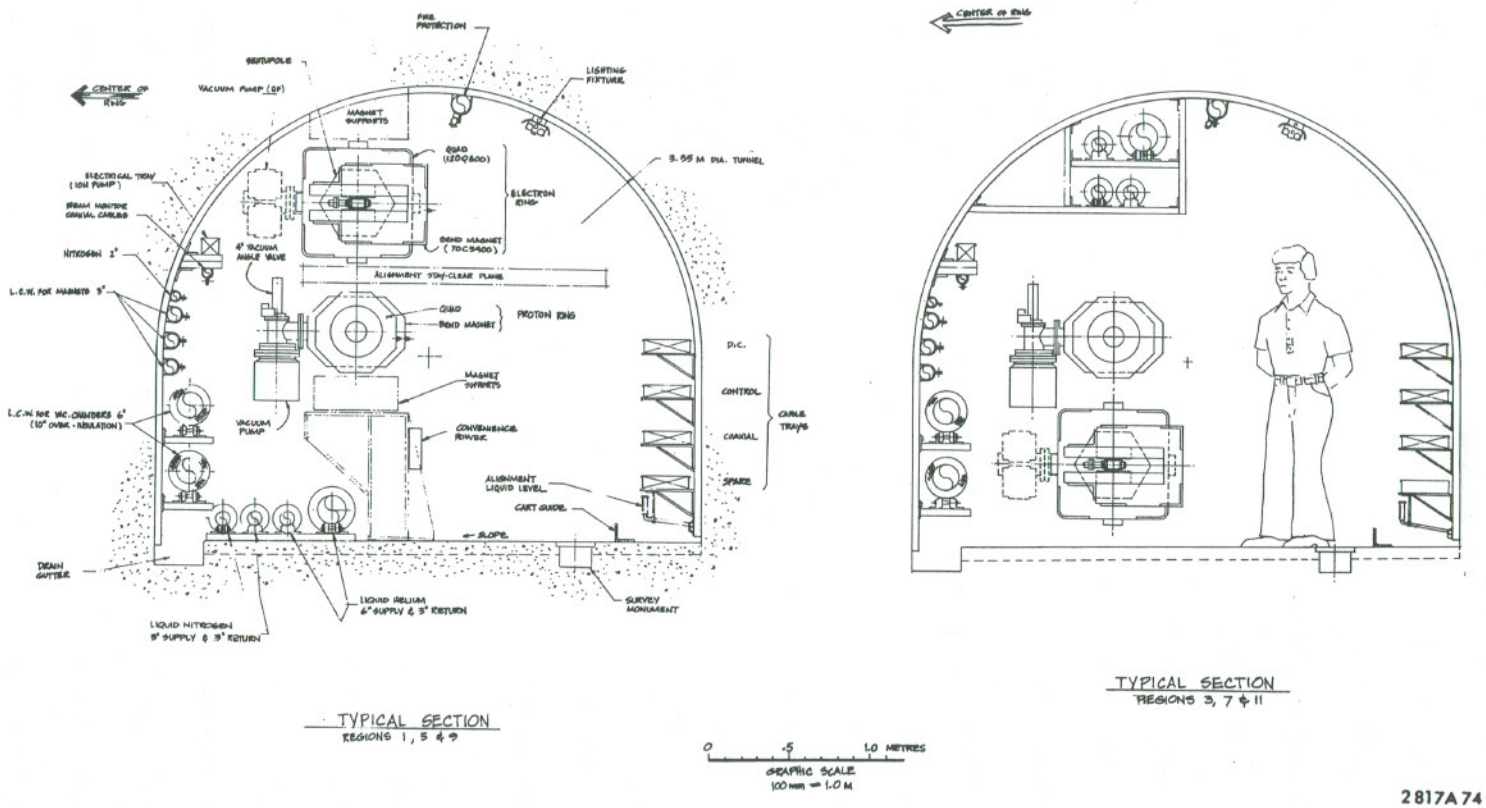

Fig. 85--Tunnel cross sections with electron and proton magnets in alternate arcs of the ring.

installed power capacity will be required for each of the six refrigeration stations. The magnet power supply circuit will parallel the refrigeration system.

Table XX

A breakdown of the 4.4°K refrigeration required for one sixth of the PEP proton ring

Heat Leaks into the Cryostat	420 W
Electrical Lead Losses	220 W
Cryogenic Vacuum Pumps (in the interaction regions)	200 W
Total (steady state load)	840 W
Cooldown Allowance	660 W
Total Installed Refrigeration Required	1500 W

Vacuum System. The residual gas phase density of nitrogen-like molecules should be less than about 3.5×10^5 molecules/cm^3 in order to prevent degradation of the quality of the stored proton beam. This density corresponds to a room temperature gas pressure of 10^{-11} Torr.

In the magnet sections a pressure of 10^{-12} Torr or less can be obtained economically by allowing the vacuum chamber to cool to about 4.5°K, the operating temperature of the superconducting magnets. This temperature provides pumping capacity for all gases except helium, and reduces outgassing of the chamber wall to a negligible rate. The cold bore of the magnet itself could be used as the vacuum chamber if experience with ESCAR demonstrates a high reliability with regard to helium leads from the magnet cryostats. A straightforward analysis of the possibility of beam induced pressure runaway shows this will not be a problem with PEP.

There is no need for a rapid rate of rise of the magnetic field, so eddy current heating will not be a problem, and the vacuum chamber impedance can be made low to suit the requirements of the bunched beam. Because the beam is tightly bunched some image current heating must be anticipated. Vacuum tests for ESCAR show that a temperature rise of the pumping surface up to $5^{o}K$ will not disturb the cryopumping of H_2 if the amount of H_2 on the cryopump is not excessive. This behavior has been verified by measurements at CERN,[39] which show that no change in pressure is observed for temperature differences from 2.5 to $7.0^{o}K$ if the H_2 coverage is less than one monolayer.

The straight insertions contain the accelerating cavities, the injection systems, and the interaction regions with the cross-overs of the electron-positron ring. These elements, the synchrotron radiation, and the requirements of the experimenter will call for a variety of vacuum techniques. Gas loads that could enter from the injection line will be intercepted by a short length of tubular cryopump that is easily cycled. The detailed design of such a pump has already been completed for ESCAR.

Injection, Acceleration, and Bunching. A small 5 GeV synchrotron is visualized as an injector for the superconducting ring. As the intensity and emittance requirements for PEP are not very stringent, there should be no difficulty in providing an economical system.

The present concept for achieving the desired proton bunches is as follows. Each of the 24 bunches is successively loaded from separate booster pulses into existing buckets in the main ring. The bunch lengths are such that they would fit comfortably in buckets at harmonic number 96 (4×24). For a longitudinal emittance of 0.1π m ($6\pi\sigma_{\ell}\sigma_{\beta\gamma}$), the holding voltage would be about 400 keV/turn. This same voltage would be sufficient for an acceleration time of 10 seconds or

more, and the normal damping would produce a bunch length at 200 GeV which would fit a bucket at four times higher frequency (h = 384, f = 52 MHz). At this frequency the voltage would be raised to compress the bunches to the desired length, the final value being ~6 MeV/turn if the emittance is preserved throughout.

The RF structure is visualized as consisting of a number of tubes which would act as drift tubes at the initial frequency, and as half-wave lines at the final frequency. For the system cited above, 17 tubes, occupying a total length of 50 meters, would be utilized with a power consumption of ~2 MW.

In Fig. 84 it is seen that there are twelve straight sections of 24 m length in the proton ring between QA, QB and Q3 and twelve corresponding straight sections in the electron ring. Three sections are used for electron, positron and proton injection. The remaining nine sections are available for electron and proton RF systems, beam disposal systems and diagnostics.

This brief description of components and parameters does not pretend to represent an optimized system nor a comprehensive analysis of the components. It is, rather, a conceptual analysis to confirm that a future e-p system is feasible and compatible with the electron-positron system which is the subject of this design report. Numerous orbit dynamics questions, both single-particle and collective still remain, which require further study. Most of all, substantial development in super-conducting technology is needed to produce reliable operational systems.

APPENDIX B

SUMMARY OF SOIL STUDIES TO DATE

In the summer of 1973, when engineering studies for a large, colliding-beam storage ring started in earnest, soil studies were begun to determine the nature of earth materials where tunneling might be undertaken. The initial ring concept, a 2100-m oval, was investigated by drilling seventeen test holes with a truck-mounted 15-cm auger drill rig. These holes were roughly logged to determine the general nature of the site's materials, but no laboratory testing was undertaken to determine engineering characteristics. The drilling indicated a heterogeneous, unsystematic arrangement of gravels, sand, clay, claystone and shale in the upper levels, with sandstone occurring at depths 6 to 20 m below the surface.

In an effort to determine systematic arrangement of the site's sedimentary deposits, the 1973 drilling program was followed by seismic refraction geophysical surveys.[40] Such surveys, by measuring velocities of seismic waves at varying depths, can indicate densities and competence of subterranean formations and can provide some indication of the speed of tunnel advances. The survey indicated that upper levels have relatively low compressional wave velocities between 360 and 540 m per second. These are in desiccated adobe and sandy clay. Underneath these surface materials, wave velocities varied from 700 to 1000 m per second in fine-grained sandstone, shale and clay with gravel. These velocities, comparable to earlier refraction studies of SLAC materials, indicate materials having bearing values of at least 20,000 kilograms per sq. m. Structures below these materials showed wave velocities in excess of 1500 m per second. Thus, the refraction surveys, as might be expected, indicated increasing competence of materials with depth.

In 1974, five more deep holes were drilled in order to determine the nature of materials at key points where the ring (by now conceived as hexagonally shaped) was anticipated to be located. No unusual differences from those of the earlier samplings were disclosed by these borings.

The geologic composition of the SLAC site consists of materials of three geologic ages: Eocene, Miocene and Pliocene-Pleistocene. SLAC's original construction had disclosed that Eocene formations could be troublesome, sometimes being composed of expansive clays, shales and siltstones. Miocene formations, although younger than the Eocene, are more dependable, being composed generally of fine-grained, loosely-consolidated sandstones having excellent engineering characteristics. Little contact with Pliocene-Pleistocene formations occurred in the original construction.[41, 42, 43]

Subdivision developments immediately north of the PEP site in Menlo Park have experienced serious construction problems caused by highly-expansive Eocene clays. In that area, such clays are generally overlain by adobe soils. Areas of Regions 12, 1 and 2 of PEP's ring (Fig. 1 of the design report) are likewise overlain with expansive adobes. In that same PEP area, a 1967 geological report[43] postulated a Pliocene-Pleistocene formation which could create engineering problems for construction. Because of this, a detailed geologic, soils-mechanics study of Regions 12, 1 and 2 was undertaken in the summer of 1975.[44] Trenching, drilling and materials testing was done in order to ascertain accurately the geologic structure and engineering characteristics of soils and rock. It was found that the Eocene formations so troublesome to the north do not extend into PEP's construction area, and that expansion characteristics of the claystones found should not create serious difficulties. That same summer, an interim report of the general geological structure of the entire PEP site was made.[45]

A test-drilling program continues, with extensive materials testing along the perimeter of the PEP ring. This program should provide the information necessary to determine methods and design of tunnels as well as basic design of the interaction area research halls.

APPENDIX C

COOPERATIVE BASIC AGREEMENT

BETWEEN

THE BOARD OF TRUSTEES OF THE LELAND STANFORD JUNIOR UNIVERSITY

AND

THE REGENTS OF THE UNIVERSITY OF CALIFORNIA

This Cooperative Basic Agreement is entered into effective this 25th day of February, 1974, by and between the BOARD OF TRUSTEES OF THE LELAND STANFORD JUNIOR UNIVERSITY (hereinafter called "Stanford") and THE REGENTS OF THE UNIVERSITY OF CALIFORNIA (hereinafter called "UC").

RECITALS

I. INTRODUCTION

A. The Ernest Orlando Lawrence Berkeley Laboratory (LBL) is a National Laboratory operated by UC under contract W-7405-ENG-48 with the U.S. Atomic Energy Commission (AEC). The Director of LBL reports to the President of UC. The Stanford Linear Accelerator Center (SLAC) is a National Facility for High Energy Physics Research operated by Stanford under contract AT(04-3)-515 with the AEC. The Director of SLAC reports to the President of Stanford.

B. For several years LBL and SLAC have been collaborating in the study of a novel high-energy particle accelerator system consisting of a ring containing counter-rotating persistent beams of electrons and positrons, and a second intersecting ring containing a persistent rotating beam of protons. Collision between these beams will permit studies of elementary particles at higher energy, and therefore in finer detail than ever before.

C. The concept of the system, called PEP for "proton-electron-positron," has been developed to the point where design and construction of an accelerator can take place. It appears desirable to accomplish the realization of this concept in stages. The first stage will consist of a single ring of approximately 300 meter radius able to contain counter-rotating beams of electrons and positrons with energies up to 15 GeV at full interaction rate. These particles will be injected into the ring by the existing linear accelerator at SLAC. Provision will be made in the construction of PEP to maintain full compatibility with the later addition of a superconducting proton ring for protons of energies up to about 200 GeV and/or a second electron ring to provide for collision of electrons with electrons and positrons with positrons. Provision will also be made for the future installation of experimental facilities for the full PEP Project. Meanwhile, the single ring will comprise a unique tool for conducting experiments involving electron-positron collisions, and by itself will be the basis for a front line experimental program for many years. For ease of reference, the term "PEP Project" as used hereafter in this Agreement means the design, construction and operation of the PEP accelerator system as finally funded, built, and operated.

D. In consideration of the foregoing facts, and being keenly aware of the potentialities of the PEP Project for advancing mankind's knowledge of the constitution and nature of matter, and in appreciation that the task is of such challenge as to warrant the marshalling of the combined

resources and talents of Stanford and UC, with a consequent sense of the historical importance of this act the parties hereto enter into this Cooperative Basic Agreement.

AGREEMENTS

II. CONSTRUCTION PROPOSAL

A. It is agreed that LBL and SLAC will collaborate in the preparation of a construction proposal to be submitted to the Atomic Energy Commission for commencement of construction in Federal fiscal year 1976 of a high energy electron-positron ring to be constructed at SLAC and to be operated jointly by SLAC and LBL as a national physics facility as described in Articles III. and IV. of this agreement. Provision will be made in the construction of PEP to maintain full compatibility with the later addition of a superconducting proton ring for protons of energies up to about 200 GeV and/or a second electron ring to provide for collision of electrons with electrons and positrons with positrons. Provision will also be made for the future installation of experimental facilities for the full PEP Project.

B. The technical and scientific justification for this construction proposal will be based specifically on the electron-positron colliding beam device. The parties agree that both scientific interest and current technical knowledge are such as to justify the construction of an electron-positron storage ring in its own right; they also emphasize that the scientific goals of the full PEP Project provide good reasons to include in the design those features essential to permit realization of the full PEP Project in the future.

C. As contained in the "5-year Budget Assumption" for 1976-1980 which was submitted by LBL and SLAC on November 13, 1973 to the AEC, the construction cost of the first stage of the PEP Project is estimated to be between $50 and $60 million.

III. MANAGEMENT PLAN

A. It is agreed that the goal of the project management is a true collaboration between LBL and SLAC. the PEP Project will have a senior scientific and technical staff drawn in a balanced way from the two Laboratories. These persons, while working on the PEP Project, will remain employees of their respective Laboratories. In particular the Project Director and Deputy Director will be appointed by the Directors of LBL and SLAC so that one comes from each Laboratory. The Project Director will report to the Directors of LBL and SLAC.

B. The two Laboratory Directors will be advised in relation to the project by a single PEP Program Committee (PPC) having a majority of non-SLAC, non-LBL members. This Committee will be appointed jointly by the Directors of the Laboratories. This Committee shall advise the Directors on all major phases of the PEP Project such as experimental facilities construction, and storage ring modification projects. Such projects shall go forward only after authorization by both Laboratory Directors, irrespective of the source of funding. The Committee shall meet as often as required but not less frequently than twice each year.

Cooperative Basic Agreement Stanford/UC

C. It is intended that the PEP Project will be operated as a National Physics Facility. Steps are in progress to involve the national high-energy-physics community in planning for the physics utilization as well as in setting up appropriate advisory mechanisms. In particular, it is agreed that an Experimental Program Committee (EPC) will be constituted to review experimental proposals under procedures designed to assure equitable access to the entire high-energy physics community. Detailed scheduling decisions and coordination of PEP Project experiments with SLAC operations shall be made under SLAC procedures.

D. The Presidents of Stanford and UC will be advised of the status of the PEP Project through, respectively, the Directors of SLAC and LBL. In addition, the Scientific Policy Committee (SPC) of SLAC, advisory to the President of Stanford University, and the Scientific Educational Advisory Committee (SEAC), advisory to the President of the University of California, will schedule joint meetings when deemed advisable if it is believed that further advice on scientific policy governing the conduct of the PEP Project should be made available to the Presidents of the collaborating universities and, through them, as appropriate, to the Atomic Energy Commission.

E. Stanford and UC may enter into modifications of this agreement or into agreements implementing this agreement as may be necessary to carry out the PEP Project.

IV. MANPOWER AND FISCAL ARRANGEMENTS

A. Preconstruction research and development work is now under way at both Laboratories, supported by the operating funds of each institution under the financial plans of their contracts with AEC.

B. The construction proposal described in Article II. A. will set forth the scope and estimated costs of major elements and components of the design and construction phase of the first stage of the PEP Project.

C. It is agreed that Stanford and UC shall seek to have the construction of the first stage of the PEP Project performed by Stanford under a contract between Stanford and the Atomic Energy Commission. Requests to the Atomic Energy Commission for construction directives to proceed with stages of the construction of the PEP Project shall be approved by both Laboratory Directors. It is agreed that the health and strength of the technical high-energy support efforts as well as of the research programs of the two Laboratories must be maintained, and this goal will be used as a guide in determining how the personnel and facilities of each Laboratory are to support the design, preparation of specifications, and construction of the PEP Project.

D. After completion of construction to the satisfaction of both Laboratory Directors, SLAC and LBL will participate in the operation of the PEP Facility as follows:

Cooperative Basic Agreement Stanford/UC

1. SLAC will be responsible under the terms of Article III. for managing and coordinating accelerator operations. Funding support for accelerator operations will be through the SLAC operating contract with AEC.

2. The operation of each experimental facility built with SLAC and/or LBL funds shall be the responsibility of SLAC or LBL and shall be supported with their operating funds in the manner most advantageous to the conduct of the national high-energy physics program.

3. During the operational phase of PEP, accelerator research and development and facilities research and development pertaining to PEP, as well as preconstruction work for the full PEP, will be supported by the two Laboratories, using their operation funds.

4. Experimental facilities construction and PEP storage ring modification projects may be supported separately or jointly in accordance with funding provided to LBL and SLAC.

5. The Laboratories will participate in the physics research program of the PEP Project using operating funds from their separate contracts in a manner similar to that of other laboratories or universities performing research at the PEP National Physics Facility.

V. SETTLEMENT OF DISAGREEMENTS

Should the two Laboratory Directors be unable to agree on a substantive issue relating to this Agreement, it shall be referred to the Presidents of Stanford and UC for resolution.

VI. TERM AND TERMINATION

This Agreement shall continue in force from year to year from date of execution; provided, however:

A. Should Federal or other funding not be obligated for the construction of the PEP Project by June 30, 1980, this Agreement shall terminate.

B. This Agreement shall continue so long as Federal or other funding is provided for the operation of SLAC and LBL and for the construction and operation of the PEP Project.

IN WITNESS WHEREOF, the parties hereto have executed this Agreement as of the date first above written.

THE REGENTS OF THE
UNIVERSITY OF CALIFORNIA

By: _____
Charles J. Hitch
President, University of California

By: _____
Marjorie J. Woolman
Secretary

By: _____
Dean A. Watkins
Chairman

THE BOARD OF TRUSTEES
OF THE LELAND STANFORD
JUNIOR UNIVERSITY

By: _____
Richard W. Lyman
President, Stanford University

ASSISTANT SECRETARY OF THE REGENTS
OF THE UNIVERSITY OF CALIFORNIA

APPENDIX D

PEP Reports

PEP Note #	Title	Author(s)
1	A High-Energy Proton-Electron-Positron Colliding Beam System	C. Pellegrini, J. Rees, B. Richter, M. Schwartz, D. Möhl and A. Sessler
2	A Model for a High Energy Proton-Electron-Positron Colliding Beam System: SPEAR plus a Proton Ring	D. Möhl and A. Sessler
3	Inelastic Electron-Proton Scattering with SPEAR plus a Proton Ring	M. L. Stevenson
4	(PEP Note #4 was a piece of the Isabelle report)	
5	Feasibility Study for a 15-GeV Electron-Positron Storage Ring	S. Berman, S. Drell, J. Rees, B. Richter
6	Electromagnetic Backgrounds and Photon Tagging	M. Davier and A. Odian
7	How Much Free Space Can We Provide for Experimental Apparatus?	P. Morton and J. Rees
8	On the Use of Isabelle in a PEP System and Other Related Topics	D. Möhl and A. Sessler
9	Proposed NAL Photoproduction Experiments and Some Comparisons with PEP Capabilities	S. M. Flatté
10	A Question of Duty Cycle	S. M. Flatté
11	Angular Distributions for Hadrons Produced in PEP Electroproduction Experiments	F. J. Gilman
12	PEP Kinematics - Deep Inelastic Scattering -- Two Exclusive Reactions as Examples	G. Goldhaber
13	Brookhaven HEDG Meeting of December 10, 1971	J. Rees
14	Check on the Equivalent Radiator for PEP	A. Odian
15	Radiative Processes in Electron-Proton Collisions at PEP	S. J. Brodsky

PEP Note #	Title	Author(s)
16	The Kinematics and Possible Dynamics of Inelastic Lepton Scattering in PEP (15 GeV electrons on 70 GeV protons)	M. L. Stevenson
17	PEP Kinematics -- Additional Remarks on the Reaction of the Type $ep \rightarrow e'\rho N$	G. Goldhaber
18	PEP Parameters	D. Möhl
19	Limitation of the Transition Energy in Large e-p Colliding Beam Facilities	H. Wiedemann
20	On the Calculation of Luminosity for Electron-Proton Colliding Beam	L. Smith
21	High Voltage Rf Systems for the PEP Rings	M. Allen and J. Rees
22	The Self-Destructive Behavior of Stored Electron Beams: The Disease Patterns, Symptoms and Cures	A. Sessler
23	PEP Model One -- A Machine Design Example	A. Garren
24	Conceptual Design of a Hybrid Detector for Electron Physics at Isabelle and PEP: Solenoid + Quantameter + Hadrometer (Calorimeter)	M. L. Stevenson
25	Further Consideration of the Rf System for PEP	M. A. Allen
26	Multiple Coulomb Scattering and Multiple Gas Bremsstrahlung at SPEAR	J. E. Augustin
27	A Correction to Formulas Computing the Touschek Lifetime in Storage Rings	H. Wiedemann
28	Strongly Turbulent Collective Motion and the Anomalous Size of Stored Particle Beams	A. Sessler
29	Variable Proton Momentum at PEP	R. O. Bangerter
30	Noise in Proton Accelerators	E. Hartwig, V. K. Neil, R. K. Cooper
31	PEP Lattice Design	R. Bangerter, A. Garren, P. Morton and J. Rees

PEP Note #	Title	Author(s)
32	Use of the Electron Ring for Protons in the PEP System	A. Garren and T. Elioff
33	Proton-Electron-Positron Design Study	The LBL/SLAC Storage Ring Study Group
34	PEP Model Five: An Update of PEP Parameters	A. Garren
35		
36	Notes on PEP "Bull Session" of March 1-2, 1973	
37	Beam Loading in High-Energy Storage Rings	P. B. Wilson
38	PEP Model Six	A. Garren
39	Scaling of FODO-CELL Parameters	H. Wiedemann
40	Closed Orbit Beam-Beam Effect for Crossing Beams	M. Month and A. G. Ruggiero
41	Space-Charge Effects at Transition Energy: An Attempt to Scale from the CPS to PEP-6 and Other Machines	D. Möhl
42	The Excitation of Non-linear Resonances by a Displaced Elliptical Beam	E. Keil
43	Bunch Lengthening and Widening Effects Due to the Combination of Rf Noise and the Presence of Inductive Wall Elements	G. H. Rees
44	The Beam-Beam Limit in SPEAR as a Single Resonance Effect	A. G. Ruggiero
45	Bunch Lengthening	F. J. Sacherer
46	Proton Beam Enlargement by Gas Scattering	H. Wiedemann
47	Synchrotron Radiation Integrals for PEP-6	R. H. Helm
48	Enlargement of the Electron Beam Cross-Section in a Storage Ring Due to an Oscillating Synchrotron Radiation Damping Time Constant	H. Wiedemann

PEP Note #	Title	Author(s)
49	Transverse Bunch-Bunch Instability in PEP (Resistive Wall)	A. G. Ruggiero
50		
51	Aspects of PEP as Compared to EPIC	G. H. Rees
52	Calculation of Resonance Effects Due to a Localized Gaussian Charge Distribution	A. G. Ruggiero and L. Smith
53	Equilibrium Energy Distribution in a Non-linear Potential Well in the Presence of Quantum Fluctuations	H. G. Hereward
54	The Head-Tail Effect in PEP	A. G. Ruggiero
55	Interaction of a Coasting Beam and a Bunched Beam with Frequency Slip	M. Month and A. G. Ruggiero
56	Some Possible Causes of Bunch Shape Distortion in SPEAR	H. G. Hereward
57	Possibility of Observing Turbulence in SPEAR	H. G. Hereward
58	e-p Luminosity for Different Energies in PEP	H. Wiedemann
59	Diffusion-like Blow-up in Asynchronous Bunched Beam Collisions	E. Keil
60	A Negative Momentum-Compaction Lattice	R. H. Helm
61	Magnet Insertion Code (MAGIC)	W. W. Lee, L. C. Teng, M. J. Lee
62	PEP with Crossing Angle	R. Chasman, A. Garren, and M. Month
63	Longitudinal Beam-Beam Effect in Head-on Collisions	J. E. Augustin
64	Behaviour of a Stochastic Non-linear System Excited by an External Harmonic Force	J. R. LeDuff
65	Diffusion on a Single Non-linear Resonance in the Case of e-p Collisions	J. R. LeDuff

PEP Note #	Title	Author(s)
66	Storage Ring Experiments	T. Elioff, H. Hereward, J. M. Paterson, H. Wiedemann
67	Influence of the Touschek Effect on Life-time Measurements in SPEAR	H. G. Hereward
68	The Use of Rf-knockout to Measure Synchrotron Oscillation Frequencies and Energy Spread	D. Möhl, P. L. Morton
69	Preliminary Design of a 15-GeV Electron-Positron Variable-Tune Storage Ring	J. Rees, B. Richter
70	Superconducting Dipoles and Quadrupoles for the PEP Accelerating-Storage Ring	M. A. Green
71	Properties of Bunch Lengthening Effect Observed on Existing e^+-e^- Storage Rings	J. LeDuff
72	Incoherent Beam-Beam Effect: A Computer Simulation	A. Renieri
73		
74		
75	Comments on Obtaining Longitudinally Polarized Beams in e^+-e^- Storage Rings	R. F. Schwitters
76	Neutron Shielding for PEP	J. B. McCaslin and R. H. Thomas
77	Detection of Proton Beam Jet in 15 x 200 GeV PEP	A. Garren,,J. Kadyk
78	Double Thin-lens Approximation for Preliminary PEPSI8 Lattice Design	R. Helm and M. J. Lee
79	PEP Parameters	B. Richter
80	Typical PEP Condigurations and the Resulting Beam-Stay-Clear Requirements	R. Helm, M. Lee, A. Lisin, P. Morton

PEP Note #	Title	Author(s)
81	Transverse Diffusion of Proton Beams Due to Noise	P. Channell
82	Proton Losses from PEP	R. H. Thomas
83	Muon Shielding for PEP	T. M. Jenkins, R. H. Thomas
84	PEP Inflection	G. E. Fischer
85	A Few Thoughts Regarding Beam Cavity Mode Excitation in PEP	G. Loew et al.
86	Proton-Electron-Positron: PEP	Lloyd Smith
87	A Method for Producing Long Beam Polarization at PEP	R. Schwitters, B. Richter
88	Synchrotron Radiation Absorbing Surfaces	J. Jurow and N. Dean
89	Higher-Order Modes in SPEAR II Cavities	M. Allen
90	Energy Loss to Parasitic Modes of the Accelerating Cavities	M. Sands
91	Concerning the Density Distribution and Associated Fields	J. Laslett
92	Parasitic Cavity Losses in SPEAR-2	M. Sands
93	Examples of Weak-Beam/Strong-Beam Computation Formed by Use of the Program "WEAK 8" with Graphic Output	J. Laslett
94	An Example of the Use of Program "WEAK 9"	J. Laslett
95	A Bench Measurement of the Energy Loss of a Stored Beam to a Cavity	M. Sands and J. Rees
96	The PEP Electron-Positron Ring -- PEP Stage I	J. Rees
97	Rf Systems for High-Energy e^-e^+ Storage Rings	M. A. Allen and P. B. Wilson
98	Preliminary Design Considerations for the Stage I PEP Lattice	R. H. Helm and M. J. Lee
99	Beam Enlargement by Mismatching the Energy-Dispersion Function	R. H. Helm, M. J. Lee and J. M. Paterson

PEP Note #	Title	Author(s)
100	Beam Loading in High-Energy Storage Rings	P. B. Wilson
101	Stored Current Capability of the PEP Rf System	P. B. Wilson
102	Comparison of Two Configurations for Intersection Regions	W. A. Wenzel
103	Measurement of Higher-Order Mode Losses in SPEAR II by Shift in Synchrotron Phase and Increase in Net Cavity Power	M. A. Allen, J. M. Paterson, P. B. Wilson
104	Alternative Theories of the Non-Linear Negative Mass Instability	Paul J. Channell
105	Physical Picture of the Electromagnetic Fields between Two Infinite Conducting Plates Produced by a Point Charge Moving at the Speed of Light	A. W. Chao, P. L. Morton
106	Shielding Requirements for Radiation Produced by 15-GeV Stored Electrons	T. M. Jenkins, J. B. McCaslin, R. H. Thomas
107	PEP Experimental Areas -- Winter 1975	W. A. Wenzel
108	The PEP Electron-Positron Ring -- an Update	LBL-SLAC Joint Study Group
109	The Radiation Dose to the Tunnel Linings and the Production of Nitric Acid and Ozone from PEP Synchrotron Radiation	W. R. Nelson
110	Higher Order Multipole Magnet Tolerances	A. W. Chao, P. L. Morton, M. J. Lee
111	Control of Closed Orbit Deviation Due to Synchrotron Radiation	M. J. Lee, P. L. Morton, J. R. Rees and B. Richter
112		K. Bane and P. Wilson
113	The PEP Injection System	K. L. Brown, R. T. Avery J. M. Peterson
114	Vacuum System for the Stanford-LBL Storage Ring (PEP)	D. Bostic, U. Cummings, N. Dean, D. Jeong, J. Jurow
115	Beam Energy Loss to Parasitic Modes in SPEAR II	M. A. Allen, J. M. Paterson J. R. Rees, P. B. Wilson

PEP Note #	Title	Author(s)
116	Background Estimates for PEP	F. Martin
117	Implications of Shorter Cells in PEP	H. Wiedemann
118	Parasitic Loss of a Gaussian Bunch in a Closed Cavity	A. W. Chao
119	Differential Energy Loss for a Particle in a Square Pulse of Charge Traveling between Infinite Conducting Plates	A. W. Chao, P. L. Morton
120	Design of an Electrode System for Beam Tranverse Excitation	J.-L. Pellegrin
121	The Behavior of Betatron Oscillation in the Vicinity of Half Integral Structure Resonances	E. Keil
122	Beam Induced Transit Time Signals at SPEAR	R. McConnell
123	Stored Current in PEP at 125, 200 and 358 MHz	P. B. Wilson
124	High Performance Magnet Power Supply Optimization	T. Jackson
125	Control of Beam-Size and Polarization Time in PEP	J. M. Paterson, J. R. Rees, H. Wiedemann
126	Bunch Lengthening and Bucket Distortion Due to Cavities	E. Keil
127	PEP Initial Design -- Injection Transfer Line Coordinates	R. T. Avery
128	PEP Ring Coordinates -- Configuration E	R. Avery, T. Chan
129	On the Horizontal Shape of an Electron Bunch	A. Chao
130	Stationary Solution of the Fokker-Planck Equation for Linearly Coupled Motion in an Electron Storage Ring	A.W. Chao, M.J. Lee
131	Transient Particle Distribution for Linearly Coupled Motion in an Electron Storage Ring	A.W. Chao, M.J. Lee

PEP NOTE #	Title	Author(s)
132	Evaluation of the Field Quality of the Prototype PEP Cell Quadrupole Magnet	A.W. Chao, M.J. Lee, P.L. Morton
133	PEP Cooling Water Systems and Underground Piped Utilities Design Criteria Report	F. Hall, D. Robbins
134	Some Up-to-date Additions to MAGIC for PEP Deisgn Studies	M. Lee, A. King
135	Closed Orbit Distortions due to Survey and Alignment Errors in PEP I	Dick Sah
136	Particle Distribution and Beam Lifetime with Vacuum Chamber Walls	A. W. Chao
137	1974 Summer Study	
138	Introductory Remarks	K. Strauch
139	The PEP Electron-Positron Ring	J. Rees
140	Event Rates to be Expected at PEP	B. Richter
141	Report of the Study Group for the Measurement of the Total Cross Section for e^+e^- Hadrons	G. Abrams, G. Feldman, D. Hitlin, H. Lynch, D. Nygren, R. Schwitters, B. Shen
142	Non-magnetic Detector for Measuring σ_T and Charged Multiplicities in e^+e^- Annihilation	H. Lynch, R. Schwitters
143	Precise Measurement of the Total Cross Section	G. Feldman, D. Hitlin
144	The Time-projection Chamber -- A New 4π Detector for Charged Particles	D. Nygren
145	Contribution of the Two-photon Annihilation Process in the Measurement of σ_T at PEP	B. Shen
146	Detection of High-momentum Hadrons	G. Buschhorn, D. Coyne, J. Cronin, J. Klems, C. Morehouse, M. Strovink
147	Heavy Hadrons -- Group Report	G. Barbiellini, C. Buchanan, B. Cork, J. Dakin, H. Lynch, J. Marx, J. Perez-y-Jorba, P. Yamin

PEP NOTE #	Title	Author(s)
148	Large-solid-angle Detector for Charged and Neutral Particles -- Group Report	A. Barbaro-Galtieri, J. Kadyk, T. Mast, J. Nelson, A. Odian, D. Yount
149	The Detection of Low-energy Charged Particles with Particle Identification Up to 3.5 GeV/c	J. Perez-y-Jorba
150	Study of a Multi-hadron Facility for PEP Based on Toroidal Field Magnets	P. Spillantini
151	A Streamer Chamber Detector for PEP	G. Buschhorn, H. Meyer, A. Odian, D. Yount
152	Comments on the Simultaneous Measurement of Charged and Neutral Components of Multihadron Events	P. Yamin
153	Some Design Considerations for a Large Solid Angle Charged Plus Neutrals Detector for e^+e^- Storage Ring	T. Mast, J. Nelson
154	Report on Neutral Particle Detectors and Q.E.D. -- Group Report	E. Bloom, F. Bulos, G. Buschhorn, J. Dakin, E. B. Hughes, T. Mast, J. Nelson, A. Odian, C. Prescott, S. Yellin, D. Yount
155	Properties of Some Photon Detectors	E. Bloom, F. Bulos, G. Buschhorn, D. Cheng, J. Dakin, E. B. Hughes, T. Mast, J. Nelson, A. Odian, C. Prescott, S. Yellin, D. Yount
156	Liquid Argon Gamma Ray Detector -- Variations of the Willis Chamber	A. Odian
157	Report of the Weak Interactions/EM Final States Group	D. Buchholtz, D. Cline, P. Limon, A. Litke, C. Prescott, L. Resvanis, L. Stevenson, K. Strauch, L. Sulak, P. Wanderer, W. Wenzel, S. Yellin
158	Tests of μ-e Universality for Weak Neutral Currents at PEP	D. Cline, L. Resvanis

PEP NOTE #	Title	Author(s)
159	A Compact Magnetic Detector for μ^+-μ^- Asymmetry Measurements and Longitudinal Polarization Utilization at PEP	U. Camerini, D. Cline J. Learned, P. Wanderer, L. Resvanis
160	A Suggested Detector	S. Yellin
161	Study of the Reaction $e^+e^- \rightarrow \mu^+\mu^-$ with an Iron Solenoid Spectrometer	K. Strauch
162	Solenoid Spectrometers for $e^+e^- \rightarrow \mu^+\mu^-$ and Other Final States	W. Wenzel
163	Direct Measurement of Muon Polarization in $e^+e^- \rightarrow \mu^+\mu^-$	P. Limon, M. L. Stevenson, W. Wenzel
164	Strange Particle Experiments at PEP	D. Hitlin, J. Marx, P. Yamin
165	Parity Violating Momentum Correlations as a Means of Observing Weak Interactions in $e^+e^- \rightarrow$ Hadrons	J. Klems
166	Polarization Group Coordinators' Summary	D. Buchholz, G. Manning, F. Martin, C. Morehouse, C. Prescott, L. Resvanis, G. Shapiro, H. Steiner, R. Schwitters, K. Strauch, W. Taner, P. Wanderer, W. Wenzel
167	Control of Direction of Beam Polarization	R. Schwitters
168	Note on Longitudinal Beam Polarization	W. Wenzel
169	Resonance Method to Produce a Polarization Asymmetry in Electron-Positron Storage Rings	W. Toner
170	Two Methods to Measure the $e^{\pm}$ Polarization at PEP	U. Camarini, D. Cline, J. Learned, A. Mann, L. Resvanis, P. Wanderer
171	A Pulsed Polarization Monitor for PEP	C. Prescott
172	A First Look at a Polarimeter for EPIC or PEP	W. Toner
173	An Alternate Way of Measuring Beam Polarization at an e^+e^- Colliding Beam Facility	D. Buchholz, G. Manning, C. Prescott
174	New Particle Searches at PEP	D. Berley, F. Bulos, D. Cheng, B. Cork, P. Limon, A. Litke, U. Nauenberg, J. Rosen, B. Shen, L. Sulak, J. Trefil, F. Winkelmann

PEP NOTE #	Title	Author(s)
175	Colliding γ Beams: Two-photon Processes and Tagging	G. Barbiellini, G. Ringland B. Shen, W. Toner, W. Vernon
176	Background Sources at PEP	H. Lynch, R. Schwitters, W. Toner
177	Report of the Experimental Areas Group	D. Berley, D. Coyne, J. Cronin, G. Feldman, D. Hitlin, P. Innocenti, J. Kadyk, G. Manning, F. Martin, U. Nauenberg, B. Richter, R. Schwitters, M. Stevenson, K. Strauch, M. Strovink, R. Taylor, P. Wanderer, W. Wenzel
178	1975 PEP Summer Study	
179	An Experimenter's View of PEP	J. M. Paterson
180	Comparison of Jet and Phase Space Models at E_{cm} = 30 GeV	G. Hanson, P. Oddone
181	Report of the Polarization Group	W. Ford, K. Kondo, F. Martin, G. Manning, D. Miller, C. Prescott
182	Measurement of Weak Interaction Contributions to $e^+e^- \rightarrow \mu^+\mu^-$ Using Longitudinal Polarization of the e^+ and e^- Beams	G. Manning
183	A Beam Pipe for Polarization Experiments	F. Martin
184	A System for Obtaining Longitudinal Beam Polarization at PEP with Vertical Dipoles Located Outside of the Interaction Region	A. Garren, J. Kadyk
185	Summary of the Weak Interactions Group	A. Benvenuti, W. Ford, D. Hitlin, K. Kondo, G. Manning, R. Morse, T. Rhoades, A. Sessoms, L. Stevenson, K. Strauch, A. Zallo
186	Iron Ball Mark II	W. T. Ford
187	EM-Weak Interference in $e^+e^- \rightarrow \mu^+\mu^-$ Scattering	R. Morse

PEP NOTE #	Title	Author(s)
188	Weak-Electromagnetic Interference Effects in $e^+e^- \rightarrow \mu^+\mu^-$ Hadrons	D. Hitlin, A. Sessoms
189	A General Users Magnet Design	F. Lobkowicz, U. Becker, K. Berkelman, M. A. Green, E. Groves, K. Halbach, J. Kadyk, N. Mistry, A. Sessoms, M. Strovink
190	Use of Discrete Coils in Axial Field Spectrometers	J.D. Taylor, W.A. Wenzel
191	The Study of Neutral Particles	W. Bartel, F. Bulos, A. Eisner, G. Hanson, D. Hitlin, U. Koetz, R. Kotthaus, D. Luke, M. Marshak, T. Mast, J. Matthews, C. Peck, K. Strauch, D. Yount
192	The Crystal Ball at PEP	W. Bartel, F. Bulos, D. Luke, C. Peck, K. Strauch
193	A Liquid Argon Neutrals Detector (LAND) for PEP	A. Eisner, G. Hanson, D. Hitlin, U. Koetz, M. Marshak, T. Mast, J. Matthews, C. Peck, D. Yount
194	Resolving Overlapping Gammas in a Modular Neutrals Detector	F. Bulos
195	Report of the General Purpose Detector Group	A. Barbaro-Galtieri, W. Bartel, F. Bulos, R. Cool, G. Hanson, U. Koetz, R. Kotthaus, S. Loken, D. Luke, A. Rothenberg
196	Considerations for a General Flexible Detector	F. Bulos
197	The Streamer Chamber as a General Detector	G. Barbiellini, R. Kotthaus S. Poucher, A. Seidl, F. Villa, D. Yount
198	A Time Projection Chamber	D. Nygren
199	Comparison of Time Projection and Drift Chamber Detectors	J.A.J. Matthews, A. Rothenberg

PEP NOTE #	Title	Author(s)
200	Mark II Magnetic Detector for SPEAR	R. R. Larsen
201	Detection of High Momentum Particles with Identification of the Final State	U. Becker, R. Cashmore, E. Groves, L. Keller, S. Loken, C. Morehouse, S. Poucher, M. Strovink
202	Use of Microchannel Electron Multipliers in High Energy Physics	P. Lecomte, V. Perez-Mendez
203	Photon-photon Physics	G. Barbiellini, A. Benvenuti, K. Berkelman, A. Courau, F. Foster, K.-W. Lai, F. Lobkowicz, J. Matthews, N. Mistry, T. Rhoades
204	Report of the New Particle Group	A. Carroll, B. Cox, A. Eisner, K.-W. Lai, F. Lobkowicz, M. Marchak, J. Marx, J. Matthews, N. Mistry, C. Morehouse, J. Poucher, R. Rothenberg, A. Seidl, D. Yount
205	Report of the Experimental Areas Group	A. Carroll, B. Case, D. Coyne, F. Foster, F. Lobkowicz, F. Martin, C. Morehouse, P. Oddone, C. Prescott, L. Keller, G. Manning
206	Geotechnical Investigation of the PEP Site	R. S. Gould
207		
208		
209		
210		
211	Status Report: Plans for PEP Survey and Alignment	R. Sah

APPENDIX E

REFERENCES

1. C. Pellegrini et al., Proc. 8th Int. Conf. on High Energy Accelerators CERN 1971 (European Org. for Nuclear Research, Geneva, 1971), p. 153.
2. T. Elioff, IEEE Trans. Nucl. Sci. NS-20, No. 3, 1039 (1973).
3. R. Bangerter et al., IEEE Trans. Nucl. Sci. NS-20, No. 3, 786 (1973).
4. A Proposal for a Positron-Electron Colliding-Beam Storage-Ring Project (PEP), Report Nos. LBL-2688 and SLAC-171 (April 1974).
5. J.-E. Augustin et al., Phys. Rev. Letters 33, 1406 (1974).
6. J. J. Aubert et al., Phys. Rev. Letters 33, 1404 (1974).
7. G. S. Abrams et al., Phys. Rev. Letters 33, 1453 (1974).
8. J.-E. Augustin et al., Phys. Rev. Letters 34, 764 (1975).
9. G. J. Feldman et al., Phys. Rev. Letters 35, 821 (1975).
10. W. Tanenbaum et al., SLAC-PUB-1644 (1975) (to be published).
11. W. Braunschweig et al., Phys. Letters 57B, 407 (1975).
12. K. L. Brown, D. C. Carey, C. H. Iselin, F. Rothacker, SLAC-91, Rev. 1 (1974).
13. A. A. Garren, A. S. Kenny, LBL Internal Note, 1968 (unpublished).
14. A. S. King, M. J. Lee, W. W. Lee, SLAC-183 (1975).
15. R. H. Helm, M. J. Lee, Proc. 9th Int. Conf. on High Energy Accelerators, Stanford, 2-7 May 1974 (Stanford Linear Accelerator Center, Stanford, California, 1974), p. 622.
16. H. Wiedemann, Proc. 9th Int. Conf. on High Energy Accelerators, Stanford, 1974 (Stanford, 1974), p. 629, or PEP-117 (March 1975) (unpublished).
17. J. M. Paterson, J. R. Rees, H. Wiedemann, PEP-124 (July 1975) (unpublished).

18. R. Schwitters, SPEAR Note 159 (April 1973) (unpublished).

19. A. W. Chao, M. J. Lee, P. L. Morton, IEEE Trans. Nucl. Sci. NS-22, No. 3, 1878 (1975).

20. H. DeStaebler, SLAC-TN-74-13 (August 1974).

21. W. R. Nelson, G. T. Warren, R. L. Ford, PEP-109 (March 1975) (unpublished).

22. E. Keil, PEP-126 (August 1975) (unpublished).

23. See, for example, M. A. Allen and P. B. Wilson, Proc. 1972 Proton Linear Accelerator Conf., Los Alamos, N. Mex., 10-13 Oct 1972 (USAEC TIC, Oak Ridge, Tenn., 1972), p. 279.

24. M. A. Allen and R. A. McConnell, IEEE Trans. Nucl. Sci. NS-20, No. 3, 373 (1973).

25. M. A. Allen et al., IEEE Trans. Nucl. Sci. NS-22, No. 3, 1269 (1975).

26. E. A. Knapp, B. C. Knapp, and J. M. Potter, Rev. Sci. Instrum. 39, 979 (1968).

27. F. Amman, IEEE Trans. Nucl. Sci. NS-20, No. 3, 858 (1973).

28. E. Keil et al., "Beam Cavity Interaction in Electron Storage Rings," SLAC-PUB-1580 (1975). To be published in Nucl. Instrum. Meth.
A. W. Chao, PEP Note 118 (April 1975) (unpublished).

29. M. A. Allen, J. M. Paterson, J. R. Rees, and P. B. Wilson, IEEE Trans. Nucl. Sci. NS-22, No. 3, 1838 (1975).

30. P. B. Wilson, PEP-123 (July 1975) (unpublished).

31. U. Cummings et al., J. Vac. Sci. Technol. 8, 348 (1971).

32. C. R. Carman and J.-L. Pellegrin, Nucl. Instrum. Methods 113, 423 (1973).

33. LBL-SLAC Study Group, Report Nos. LBL-750 and SLAC-136 (April 1972).

34. W. Gilbert, R. Meuser, and F. Toby, Proc. 4th Int. Conf. on Magnet Technology, Brookhaven, 1972 (NTIF CONF-720908).

35. W. Gilbert, LBL-2418 (Nov 1973).

36. R. Avery et al., Proc. 9th Int. Conf. on High Energy Accelerators, Stanford, 1974 (Stanford, 1974), p. 179, and LBL-2603 (May 1974).

37. T. Elioff et al., LBL-3078 (Sep 1974).

38. R. Byrns et al., LBL-3387 (Nov 1974).

39. C. Benvenuti, private communication (unpublished).

40. John A. Blume & Assoc., "Final Report on Reconnaissance Geophysical Survey, 300 Meter Radius Storage Ring," private communication (Sep 1973).

41. Dames & Moore and Frank W. Atchley, "Soils and Geological Investigations for Proposed Linear Electron Accelerator - Sand Hill Site" (Nov 1960).

42. Aetron-Blum-Atkinson Report No. ABA 88, "Geological Site Investigation for Stanford Linear Accelerator Center" (March 1965).

43. B. M. Page and L. L. Tabor, "Chaotic Structure and Decollement in Cenozoic Rocks near Stanford University," Geol. Soc. Am. Bull. 78, 1 (Jan 1967).

44. Earth Sciences Associates, "Geotechnical Site Investigations of Regions 11, 12, 1, 2, and 3 - Positron-Electron Project" (July 1975).

45. L. L. Tabor, "Interim Geological Report on the PEP Site" (Oct 1975).

APPENDIX F

STORAGE RING PARAMETERS

Main Storage Ring Parameters

Nominal maximum energy	18	GeV
Minimum energy	4	GeV
Maximum current per beam (at 15 GeV)	92	ma
Design luminosity per interaction region		
Maximum luminosity at 15 GeV	1×10^{32}	$cm^{-2}sec^{-1}$
Below 15 GeV	$10^{32}(E/15)^2$	$cm^{-2}sec^{-1}$
At 18 GeV	1.5×10^{31}	$cm^{-2}sec^{-1}$
Beam lifetime	2.5 to 5.7	h
Number of interaction regions	6	
Available free length for experimental setup	19.0	m
Circumference	2200.0002	m
Symmetry	sixfold	
Average radius	350.1409	m
Largest diameter	710.8429	m
Smallest diameter	677.7638	m
Average radius with normal periodic cells	219.9240	m
Magnetic radius	165.5177	m
Bending magnet filling factor in cells	75	%
Length of interaction straight section (IP to center of Q3)	58.54335	m
Length of bend section (center of Q3 to center of 9QF)	121.96000	m
Length of symmetry straight section (center of 9QF to center of sextant)	2.83000	m
Orbital frequency	136.2693	kHz

Lattice Parameters for Standard Configurations Used for Operation with Wiggler Magnets from below 5 GeV to up to 15 GeV

Focusing structure in bend section	F-O-D-O	
Total number of cells	96	
Number of normal cells		
Mechanically identical	72	
Electrically identical	48	
Number of matching cells	24	
Length of normal cell	14.35	m
Length of matching cell at symmetry point	14.90	m
Length of matching cell at interaction straight section	20.96	m

	Beam dynamics function values in		
	Normal cell	Matching cell	Interaction straight section
Maximum betatron function:			
β_x(m)	26.5	33.5	190
β_y(m)	33.1	32.3	530
Maximum eta function:			
η_x(m)	1.81	1.98	1.15
η_y(m)	0	0	0

Phase advance per normal cell	$\psi_x = 47^o$ $\psi_y = 36^o$
Betatron oscillation tunes	$\nu_x = 18.77$ $\nu_y = 19.26$
Synchrotron oscillation tune	$\nu_s = 0.064$
Momentum compaction factor	$\alpha_c = 0.00415$

Transverse acceptance of the storage ring for ideal orbit and on-momentum particles

$A_x = 30\ \pi$ mrad mm

$A_y = 14\ \pi$ mrad mm

Maximum energy spread acceptance relative to beam energy	≥ 1.4	%
Horizontal beam emittance	$\sigma_x^2/\beta_x = 0.231\ \pi$	mrad mm
Natural energy spread	$\sigma_\varepsilon/E_0 = \pm 0.100$	%
Transverse damping time	$\tau_x = \tau_y = 8.2$	msec
Uncorrected chromaticity ($\delta = \Delta p/p_0$)		
	$\xi_x = \Delta\nu_x/\delta = -34.0$	
	$\xi_y = \Delta\nu_y/\delta = -100.3$	
Variation of damping partition number with energy	$\Delta J/\delta = 462$	

Beam dynamics parameters at interaction point:

Betatron function	$\beta_x^* = 3.707$	m
	$\beta_y^* = 0.184$	m
Eta function	$\eta_x^* = -0.653$	m
	$\eta_y^* = 0$	m
Crossing angle	$\chi = 0$	
Maximum beam-beam tune shift	$\Delta\nu_x = \Delta\nu_y = 0.06$	
Optimum coupling	$\kappa = 0.27$	

PEP Main Ring Bend Parameters

Magnet Designation	70C5400	
Number of Magnets	192	
Field @ 18 GeV	0.3625	T
$\int B d\ell$ @ 18 GeV	1.957	T-m
Pole Width	0.21	m
Gap Height	70	mm
Core Length	5.33	m
Magnetic Length	5.40	m
Width of Useful Field (0.1%)	100	mm
Lamination Height	0.496	m
Lamination Width	0.53	m
Packing Factor (min)	96	%
Core Weight	8580	kg
Amp Turns per Pole @ 18 GeV	10409	A-turns
Turns per Pole	16	
Pancakes per Pole	1	
Conductor Cross Section	65 x 9	mm^2
Cooling Hole Diameter	2 @ 5	mm
Conductor Cross-Sectional Area	546	mm^2
Current @ 18 GeV	650.6	A
Inductance	19.6	mH
Resistance @ 40^oC	17.9	mΩ
Power @ 18 GeV	7.58	kW
Voltage Drop @ 18 GeV	11.6	V
Stored Energy @ 18 GeV	4.15	kJ
Coil Weight	242	kg
Number of Water Circuits	2	
Water Flow Rate	9.45×10^{-5}	m^3/sec
Water Pressure Drop	1.38	MPa
Temperature Rise	19	^oC

PEP Standard Quadrupole Parameters (18 GeV)

(Low Impedance Design)

Magnet Designation	120Q640	
Nominal Peak Gradient	20	T/m
Gradient	12.61	T/m
Pole Tip Field	0.757	T
Gradient Length Product	8.07	T
Inscribed Radius	60	mm
Minimum Gap	34.4	mm
Core Length	0.580	m
Magnetic Length	0.64	m
Width of Useful Field	120	mm
Laminate Height	365	mm
Laminate Width	402	mm
Packing Factor (min)	96%	
Core Weight	1700	kg
Amp Turns per Pole	18062	A-turns
Turns per Pole	12	
Pancakes per Pole	1	
Conductor Cross Section	9×72	mm^2
Cooling Hole(s) Diameter	2 @ 5	mm
Conductor Cross-sectional Area	609	mm^2
Current	1505	A
Current Density	2.47	A/mm^2
Inductance	5.14	mH
Resistance @ $40^{\circ}C$	4.47	$m\Omega$
Power	10.1	kW
Voltage Drop	6.73	V
Stored Energy	5.82	kJ
Aluminum Weight	150	kg
Number of Water Circuits	1	
Temperature Rise	35.4	$^{\circ}C$
Water Flow Rate	6.85×10^{-5}	m^3/sec
Water Pressure Drop	1.034	MPa

PEP Standard Quadrupole Parameters (18 GeV)
(High-impedance Design)

Magnet Designation		120Q750	120Q1000	120Q380
Used for		QF, QD, 2QF, 3QF, 8QF, 8QD, 1QD	Q3, 1QF	9QF
Number of Magnets		180	24	12
Nominal Peak Gradient	T/m	20	20	20
Operating Gradient	T/m	10.76	10.76	10.76
Pole Tip Field @ Operating Gradient	T	0.646	0.646	0.646
Gradient Length Product	T	8.07	10.76	4.09
Inscribed Radius	mm	60	60	60
Minimum Gap	mm	34.4	34.4	34.4
Core Length	m	0.690	0.940	0.32
Magnetic Length	m	0.750	1.00	0.38
Width of Useful Field	mm	120	120	120
Lamination Height	mm	340	340	340
Lamination Width	mm	378	378	378
Packing Factor (min)	%	96	96	96
Core Weight	kg	1700	2316	788
Amp Turns per Pole	A-turns	15412	15412	15412
Turns per Pole		57	57	57
Pancakes per Pole		1	1	1
Conductor Cross Section	mm^2	12.7 sq.	12.7 sq.	12.7 sq.
Cooling Hole Diameter	mm	6.3	6.3	6.3
Conductor Cross-Sectional Area	mm^2	121.3	121.3	121.3
Current	A	270.4	270.4	270.4
Current Density	A/mm^2	2.23	2.23	2.23
Inductance	mH	56.4	75.2	28.6
Resistance @ 40^oC	mΩ	112	140	68.4
Power @ 18 GeV	kW	8.17	10.2	5.0
Voltage Drop @ 18 GeV	V	30.2	37.9	18.5
Stored Energy	kJ	2.06	2.74	1.04
Aluminum Weight	kg	150	187.5	91.6
Number of Water Circuits		2	4	2
Temperature Rise	^oC	24.6	10.2	11.4
Water Flow Rate	$10^{-5}m^3/sec$	7.95	18.4	10.5
Water Pressure Drop	MPa	1.034	1.034	1.034

PEP Insertion Region Quadrupole Parameters

Magnet Designation		160Q2000 (Q1)	160Q1500 (Q2)
Number of Quadrupoles		12	12
Rated Gradient	T/m	6.6 (±0.4)	6.6 (±0.4)
Rated Pole-tip Field @ 18 GeV	T	0.53 (±0.03)	0.53 (±0.03)
Inscribed Aperture Radius	mm	80	80
Minimum Gap Between Poles	mm	53	53
Core Length	m	1.95	1.45
Magnetic Length	m	2.0	1.5
Useful Field Width ($\Delta B/B \leq 10^{-4}$)	mm	168	168
Turns per Pole		26 (16)	26 (16)
Rated Current	A	660 (±65)	660 (±65)
Current @ 15 GeV	A	542 (-16)	542 (+9)
Current @ 18 GeV	A	651 (-5)	651 (+22)
Coil Sections per Pole		2 (1)	2 (1)
Conductor Cross Section	mm^2	23 x 20 (6.5 x 6.5)	23 x 20 (6.5 x 6.5)
Cooling Hole Diameter	mm	6.5 (3.5)	6.5 (3.5)
Conductor Area	mm^2	426 (32)	426 (32)
Rated Current Density @ 18 GeV	A/mm^2	1.54 (2.0)	1.54 (2.0)
Resistance @ 40^oC	mΩ	36.5 (260)	29.1 (200)
Rated Voltage (max.)	V	24.1 (16.9)	19.2 (13.0)
Rated Power (max.)	kW	15.9 (1.1)	12.7 (0.9)
Stored Energy @ 18 GeV	kJ	9 (∿0)	7 (∿0)
Inductance @ 18 GeV	mH	42 (16)	32 (12)
Core Weight	kg	9000	6700
Aluminum Coil Weight	kg	594	474
Number of Water Circuits		4 (2)	4 (2)
Water Temperature Rise	^oC	20	20
Water Flow Rate	m^3/sec	1.90×10^{-4} (1.3×10^{-5})	1.52×10^{-4} (1.0×10^{-5})
Water Pressure Drop	MPa	0.82 (0.60)	0.46 (0.30)

Values in parentheses are for auxiliary windings.

PEP Standard Sextupole Parameters

Magnet Designation	140S250	
Number of Sextupoles	162	
Peak Design Gradient	15.0	T/m
Design Gradient at Pole Tip	7.91	T/m
Pole Tip Field @ Design Gradient	0.277	T
Inscribed Radius	70	mm
Core Length	0.20	m
Magnetic Length	0.25	m
Weight of Iron	205	kg
Amp Turns per Pole	5655	A-turns
Turns per Pole	49	
Design Current	115	A
Conductor Size (square copper)	5.8 x 5.8	mm^2
Conductor Area	24.7	mm^2
Current Density	4.7	A/mm^2
Resistance @ 40^oC	91.6	mΩ
Power	1.22	kW
Number of Water Circuits	2	
Temperature Rise	9	^oC
Water Flow Rate	$1.6 \times 10^{-5} m^3/sec$	
Water Pressure Drop	1.03	MPa

PEP Wiggler Magnet

Magnet Designation	50H1200	
Number of Magnets	9	
Peak Field	2	T
$\int B d\ell$ @ 2T	2.40	T-m
Gap Height	50	mm
Pole Width	240	mm
Core Length	1.15	m
Magnetic Length	1.20	m
Width of Useful Field ($\Delta B/B < 0.1\%$)	130	mm
Magnet Height	500	mm
Magnet Width	960	mm
Core Weight	3360	kg
Amp Turns per Pole @ 2T	44210	A-turns
Turns per Pole	96	
Pancakes per Pole	3	
Conductor Cross Section (sq. aluminum)	12.7 x 12.7	mm^2
Cooling Hole Diameter	6.3	mm
Conductor Cross-Sectional Area	121.3	mm^2
Current @ 2T	460.5	A
Inductance	968	mH
Resistance @ 40^oC	184	mΩ
Power @ 2T	39.1	kW
Voltage Drop	84.7	V
Stored Energy	102.7	kJ
Coil Weight	123.4	kg
Number of Water Circuits	6	
Water Flow Rate	3.26×10^{-4}	m^3/sec
Water Pressure Drop	1.38	mPa
Temperature Rise	28.8	^oC

Low Field Bend Magnet

Magnet designation	70C2000	
Number of magnets	24	
Field @ 18 GeV	240	G
$\int B d\ell$ @ 18 GeV	480	G-m
Pole width	0.19	m
Gap height	0.07	m
Core length	1.93	m
Magnetic length	2.0	m
Width of the useful field	.080	m
Amp-turns/pole @ 18 GeV	690	A-turns
Turns/pole	23	
Conductor cross section	26.7	mm^2
Cooling	Air	
Current @ 18 GeV	30	A
Resistance	0.172	Ω
Power @ 18 GeV	154	W
Voltage drop	5.13	V

PEP Magnet Power Supplies

Ring and Injection Choppers

Magnet Circuits	Total Power Required (kW)	No. of 600V dc Choppers	Current Rating (A)	Locations	No. of Magnets per Circuit
B+Q1+Q2	1850	6	700	4, 8, 12	192+12+12
Q3	134	1	300	8	12
1QF	185	1	300	8	12
1QD	114	1	300	8	12
2QF	252	1	300	8	12
3QF	196	1	300	8	12
QF	430	3	300	4, 8, 12	48
QD	420	3	300	4, 8, 12	72
8QF	130	1	300	8	12
8QD	116	1	300	8	12
9QF	99	1	300	8	12
Wigglers	180	1	700	8	9
SD	53	1	300	8	48
SF	26	1	300	8	48
H1	160	1	200	Sector 30	15
H9S	80	1	200	Sector 30	8
H9N	80	1	200	Sector 30	8
Q1S	36	1	100	Sector 30	9
Q1N	36	1	100	Sector 30	9
Q18S	28	1	100	Sector 30	7
Q18N	28	1	100	Sector 30	7

Magnet	Total Power	No. of Circuits	Rating (V/A)	Location
Ring Corrective Elements (not choppers)				
Special Sextupoles	60	5		8
Q1, Q2 Trims	48	24	± 30/100	2, 4, 6, 8, 10, 12
Steering Coils (transitions)	160	48	± 30/100	2, 4, 6, 8, 10, 12
Steering Coils (arcs)	30	96	± 30/10	2, 4, 6, 8, 10, 12
Low Field Bends	7	24	± 30/10	2, 4, 6, 8, 10, 12
Rotated Quad	20	2	± 120/100	8
Remaining Injection Supply Requirements (not choppers)				
Q6N, S thru Q17N, S	64	16	+ 50/100	Sector 30
Bumps	40	8	+ 50/100	Sector 30
Trim T1	3	1	± 50/100	Sector 30
Vertical Bends	36	3	+ 120/100	Sector 30
Trims T2S, N thru T18S, N	12	10	± 120/10	Sector 30
V and H Steering	29	24	± 120/10	Sector 30

Rf Parameters (15 GeV)

Orbital frequency	136.2693	kHz
Radiofrequency	353.21016	MHz
Harmonic number ($2^5 \times 3^4$)	2592	
Momentum compaction factor	0.00417	
Synchrotron radiation loss per turn	27.056	MeV
Energy loss into parasitic modes per turn[1]	3.7	MeV
Peak rf voltage	48.8	MV
Quantum lifetime	50	h
Circulating current per beam	92	mA
Particles per beam	4.22×10^{12}	
Synchrotron radiation power per beam	2.5	MW
Total active length of accelerating structure	38.2	m
Total shunt impedance	715	MΩ
Number of accelerator sections	18	
Number of cavities per accelerator section	5	
Fundamental mode dissipation per cavity	36.7	kW
Power loss to parasitic modes[1]	0.7	MW
Total available rf power	9.0	MW
Number of vacuum pumps (500 ℓ/sec) per accelerator section	3	
Number of klystrons	18	
Klystron beam voltage	62	kV
Klystron beam current	11.5	A
Klystron beam power	713	kW
Klystron drive power	15W	
Klystron output power	500	kW
Klystron efficiency	70	%
Maximum energy, limited by rf system		
9 MW, 38.2-m accelerating structure	18.4	GeV
9 MW, 76.4-m accelerating structure	20.5	GeV
9 MW, 152.8-m accelerating structure	22.8	GeV
Bunch length (theoretical, without bunch lengthening)	$\sigma_e = 2.3$	cm
Total rf bucket height relative to beam energy	≥ 1.4	%

[1]Estimated for a bunch length of 4.5 cm and a parasitic-mode-loss impedance of 40 MΩ.

Vacuum System

1. Vacuum Components in One Bend Arc

Average pressure	2.2×10^{-8}	Torr
Desorption due to synchrotron radiation at 15 GeV	10^{-5}	Torr ℓ/sec/ma
Total pumping speed	27,400	ℓ/sec
Number of distribution pumps	32	
Pumping speed of distribution pumps	800	ℓ/sec
Number of holding pumps	18	
Pumping speed of holding pumps	100	ℓ/sec
Material for bend chamber	Al 6061-T4	
Length of bend chamber	13.92	m
Number of bend chambers	32	
Material for instrument module	304 Stainless Steel/Copper	
Length of instrument module	0.43	m
Number of instrument modules	18	
Number of isolation valves	4	
Number of ion gauges	4	
In situ bake-out temperature (hot water, 18 atm)	185	^{o}C

2. Vacuum Components in One Interaction Straight Section

Average pressure	5×10^{-9}	Torr
Total pumping speed per straight section	4400	ℓ/sec
Number of pumps (pumps at rf cavities not included)	20	
Pumping speed per pump	220	ℓ/sec
Number of fast valves	2	
Number of isolation valves	2	
Material for vacuum chamber	304 Stainless Steel	
Number of ion gauges	8	
In situ bake-out temperature	200	^{o}C max.

3. General Vacuum Components

Number of roughing pumps (portable units)	6
Quadrupole residual gas analyzer	3
Temperature-monitoring system with 100 thermocouples (movable unit)	1

Injection System

Injector accelerator	SLAC	
SLAC beam parameters for injection into PEP		
Energy	4 to 15	GeV
Momentum width	±0.5	%
Emittance		
Positrons	0.2π x (15 GeV/E)	mm-mrad
Electrons	0.02π x (15 GeV/E)	mm-mrad
Pulse length	1	nsec
Particles per pulse		
Positrons	1.3×10^8	
Electrons	1.3×10^9	
Repetition rate	up to 360	pps
Injection time	4 to 10	min.

Injection System Magnet Parameters

1. Pulsed Switching Magnet (29PM1)

Maximum field	3.3	kG
Effective length	0.96	m
Bend angle (15 GeV)	6.3	mr
Clear aperture	± 12.5	mm
Wave form	Single 600-Hz sinusoid	
Repetition rate	360	Hz
Peak voltage	3.8	kV
Peak current	420	A
Average power	3	kW
Weight	725	kg
Number required	1	

2. Splitter Iron-Septum Magnet (29B1)

Maximum field	10.9	kG
Effective length	3.0	m
Bend angle (15 GeV)	65	mr (3.75^{o})
Gap height	30	mm
Clear aperture		
Vertical	$\pm$ 12.5	mm
Horizontal	$\pm$115	mm
Ampere-turns	34,000	A-t, d.c.
Power	22	kW
Weight	9,000	kg
Number required	1	

3. Horizontal Bend Magnets (28B2 to 28B16; 30B2 to 30B16)

Maximum field	12.6	kG
Effective length	2.6	m
Bend angle (15 GeV)	65	mr (3.75^{o})
Gap height	30	mm
Clear aperture		
Vertical	$\pm$ 12.5	mm
Horizontal	$\pm$ 25	mm
Ampere-turns	32,000	A-t, d.c.
Power	12	kW
Weight	2,700	kg
Number required	30	

4. Quadrupoles (28Q1 to 28Q23; 30Q1 to 30Q23)

Maximum gradient	3.0	kG/cm
Effective length	0.4	m
Inscribed radius	30	mm
Clear aperture	25.0	mm radius
Ampere-turns per pole	12,000	A-t, d.c.
Power	7.9	kW, max.
Weight	225	kg
Number required	46	

5. Vertical Bend Magnets (28B17, 30B17)

Maximum field	7.3	kG
Effective length	3.0	m
Bend angle	44	mr (2.5^{o})
Gap height	45	mm
Clear aperture		
Horizontal	± 20	mm
Vertical	± 35	mm
Ampere-turns	28,000	A-t, d.c.
Power	10	kW
Weight	2,250	kg
Number required	2	

6. Injection Iron-Septum Magnets (28B18, 30B18)

Maximum field	7.3	kG
Effective length	3.0	m
Bend angle (15 GeV)	44	mr (2.5^{o})
Gap height	35	mm
Clear Aperture		
Horizontal	± 12.5	mm
Vertical	± 25	mm
Ampere-turns	21,500	A-t,d.c.
Power	8.2	kW
Weight	2,250	kg
Number required	2	

7. Pulsed Kicker Magnets (28PM1 to 28PM3; 30PM1 to 30PM3)

Maximum field	∿ 0.6	kG
Effective length	1.0	m (28PM1 & 28PM3)
	2.0	m (30PM1 & 30PM3)
Clear aperture		
Vertical	∿ ± 40	mm
Horizontal	∿ ± 40 - ± 80	mm
Wave form	Half-sinusoid, damped, 3 μs long	
Peak Voltage	12 - 19	kV
Peak current	10 - 15	kA
Repetition rate	360	Hz
Number required	6	

8. d.c. Bump Magnets (28A1 to 28A4; 30A1 to 30A4)

Maximum field	4.7	kG
Effective length	0.5	m
Gap height	140	mm
Clear aperture		
Vertical	± 25 - ± 40	mm
Horizontal	± 50 - ± 80	mm
Ampere-turns	23 - 50	kA-t
Power	2 - 5	kW (max.)
Weight	∿ 225	kg
Number required	8	

PEP Power Requirements at 18 GeV (kW)

Region Location	12	2	4	6	8	10	Sector 30	Total Demand by Components	Total[a] Demand to Power Supply
SYSTEM									
1. Magnets and Buses									
Main Dipoles[b]	500		500		500			1890	2224
Q1 and Q2[b]	130		130		130				
Q1-Q2 Trim[c]	10	10	10	10	10	10		60	70
QF's and QD's[c]	280		280		280			840	988
All other Quads[c]					1250			1250	1470
Sextupoles					300			300	353
Wiggler					(180)			0	0
Correction Elements	30	30	30	30	30	30		180	212
Injection Magnets[d]							760	760	895
(Magnet Subtotal)	(950)	(40)	(950)	(40)	(2500)	(40)	(760)	(5280)	(6210)
2. Rf System	3000		3000		3000			9000	15000
3. Experimental Equipment[e]	850	850	850	850	850	~100[f]		4350	5120
4. House Power[g]									
Tunnels	40	40	40	40	40	20[f]	50	270	
Interaction Halls	35	35	35	35	45	10		195	
Surface Buildings	100	60	100	70	110	50[f]	20	520	
MCR					50[f]			50	
(HP Subtotal)	(175)	(135)	(175)	(145)	(245)	(80)	(70)	(1035)	1035
5. Mechanical Utilities									
LCW Systems	400	60	400	60	420	0	150	1490	1490
Cooling Towers					1200			1200	1200
TOTAL	5375	1085	5375	1095	8215	220	980	22345	30055

NOTES:

[a] Projects overall magnet power supply efficiency of 85% and overall rf system's efficiency of 60%.

[b] Dipoles and insertion Quads, Q1Q2, are in series.

[c] Based on 120 mm design for normal cell quads. (The potential 100 mm bore design being studied can provide ~700 kW power reduction.)

[d] For operation at 15 GeV.

[e] Actual demand per area can be 3 × 850 kW with the total power for all areas constrained to 4350 kW.

[f] Assumes power from existing substations.

[g] Power for lights, electronics, cranes, convenience outlets, etc.

PEP Power Requirements (18 GeV) by Area

Region Location	System	Maximum[1] Power Demand (kW)	Approx.[2] Line Requirement KVA	Area Sub-Station Transfers
12 and 4	Magnets	1120	1315	- One 1500 kVA (12.5 kV - 480 V)
	R.F.	5000	5880	- 12.5 kV Step Regulators
	Exp. Equip.	1000	1175	- One 1500 kVA (12.5 kV - 480 V)
	House Power	175	205	One 300 kVA (480-208/120
	Mech. Utilities	400	470	Two 75 kVA (480 - 120)
2 and 6	Magnets	47	55	- One 1500 kVA (12.5 kV - 480 V)
	Exp. Equip	1000	1175	One 300 kVA (480 - 208/120)
	House Power	140	165	Two 75 kVA (480-120)
	Mech. Utilities	60	70	
8	Magnets	2940	3450	- Two 2000 kVA (12.5 kV - 480 V)
	R.F.	5000	5880	- 12.5 kV Step Regulators
	Exp. Equip.	1000	1175	- Two 1500 kVA (12.5 - 480 V)
	House Power	245	290	One 300 kVA (480 - 208/120)
	Mech. Utilities	1620	1900	Two 75 kVA (480 - 120)
10	Magnets	47	55	From Existing Sub-station
	Exp. Equipment	120	140	
	House Power	70	80	
Sector 30	Magnets	895	1050	- One 1500 kVA (12.5 - 480 V)
	House Power	70	80	Two 100 kVA (480-208/120)
	Mech. Utilities	150	175	

(1) Includes power supplies where applicable

(2) Assumes average power factor of .85.